



Universidad
Complutense
Madrid



GRAN
TELESCOPIO
CANARIAS
GTC

MEGARA Preliminary Design. Science Case

GTC Code: EXT/UCM/1715-R

Code: TEC/MEG/024

Issue: 2.A

Date: 01/02/2012

Pages: 207



Authors:	<p>MEGARA Science Team+: Africa Castillo Morales, Alfonso Aguerri, Antonio Cava, Artemio Herrero, Ata Sarajedini, Carmen Eliche Moral, Carmen Sánchez Contreras, Casiana Muñoz-Tuñón, Daniel Rosa, David Barrado y Navascues, Divakara Mayya, Elena Terlevich, Emanuele Bertone, Enrique Pérez Montero, Esperanza Carrasco, Esteban González Guardia, Fernando Serena, Francisco Manuel Sánchez Moreno, Guillermo Tenorio Tagle, Ignacio Trujillo, Jaime Zamorano, Jesús Gallego, Jorge Iglesias, Jorge Jiménez Vicente, José M. Vilchez, José Miguel Rodríguez Espinosa, José Guichard, Jorge Sánchez Almeida, Lino Rodríguez Merino, Lucía Rodríguez, Manuel Peimbert, María Luisa García Vargas, Mercedes Mollá, Miguel Chávez, Miriam García, Mónica Rodríguez, Nicolás Cardiel, Nuria Huélamo, Olga Vega, Pablo G. Pérez-González, Patricia Sánchez Blázquez, Rafael Guzmán, Raffaella Anna Marino, Raquel Cedazo, Roberto Terlevich, Sebastián Sánchez, Sergio Pascual, Sergio Simón, Sergiy Silich, Silvia Torres-Peimbert, Victor Villar, Yiannis Tsamis.</p> <p>Armando Gil de Paz, Principal Investigator</p> <p>María Luisa García Vargas, Project Manager</p> <p>Ana Pérez Calpena, System Engineer</p>
Revised by:	María Luisa García Vargas
Approved by:	<p>Armando Gil de Paz, Principal Investigator</p> <p>María Luisa García Vargas, Project Manager</p>



Distribution List:

Name	Affiliation	Date
René Rutten	GRANTECAN	01/02/2012
Armando Gil de Paz	UCM	01/02/2012
María Luisa García Vargas	FRACTAL	01/02/2012
Ana Pérez Calpena	FRACTAL	01/02/2012
MEGARA Science Team		01/02/2012
MEGARA Instrument Team		01/02/2012

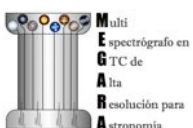


Acronyms:

2MASS	Two Micron All Sky Survey
ACS	Advanced Camera for Surveys
ADC	Atmospheric-Dispersion Corrector
AEGIS	All-wavelength Extended Groth strip International Survey
AGB	Asymptotic Giant Branch
AGN	Active Galactic Nucleus
AIV	Assembly, Integration and Verification
ALMA	Atacama Large Milimeter Array
AOI	Angle of Incidence
AR	Anti-Reflection (coatings)
BCD	Blue Compact Dwarf galaxy
BH	Black Hole
CALIFA	Calar Alto Legacy Integral Field Area Survey
CCD	Charge Coupled Device
CDR	Critical Design Review
CEL	Collisionally-Excited Line
CMD	Color Magnitude Diagram
COSMOS	Cosmological Evolution Survey
CPU	Central Processing Unit
CSC	Compact Stellar Cluster
CSE	CircumStellar Envelope
DAS	Data Acquisition System
DEEP	Deep Evolutionary Exploratory Probe
DEEP2	Deep Extragalactic Evolutionary Probe (phase 2)
DEIMOS	DEep Imaging Multi-Object Spectrograph
DLA	Damped Ly Alpha Systems

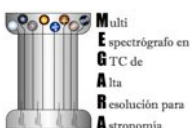


DRP	Data Reduction Pipeline
DSS	Digitized Sky Survey
EB	Error Budget
EED	Enclosed Energy Diameter
EER	Enclosed Energy Radius
EGS	Extended Groth Strip
ETC	Exposure Time Calculator
F-C	Folded-Cassegrain
FIR	Far InfraRed
FLAMES	Fibre Large Array Multi Element Spectrograph on the VLT
FOV	Field Of View
FRD	Focal Ratio Degradation
FUV	Far Ultraviolet
FWHM	Full Width at Half Maximum
FWZI	Full Width at Zero Intensity
GALEX	Galaxy Evolution Explorer
GC	Globular Cluster
GLORIA	Global Robotic Telescope Intelligent Array
GMOS	Gemini Multi-Object Spectrograph
GOODS	Great Observatories Origins Deep Survey
GP	Green Pea (galaxy)
GTC	Gran Telescopio Canarias
GTM	Gran Telescopio Milimétrico
HLS	Herschel Lensing Array
HR	High-Resolution (VPHs)
HRD	Hertzprung-Russell Diagram
HST	Hubble Space Telescope
IFU	Integral Field Unit





IGM	Inter-Galactic Medium
IR	InfraRed
IRAC	InfraRed Array Camera
ISM	Inter-Stellar Medium
LBV	Luminous Blue Variable
LCB	Large Compact Bundle
LCU	Local Control Unit
LDSS	Low Dispersion Survey Spectrograph
LIRG	Luminous InfraRed Galaxy
LOS	Line Of Sight
LR	Low-Resolution (VPHs)
MB	Massive Blue (star)
MEDUSA	MEGARA Distant-Universe Spectroscopic Analysis
MEGADES	MEGARA Galaxy Disks Evolution Survey
MEGARA	Multi Espectrógrafo en GTC de Alta Resolución para Astronomía
MHD	Magneto-HydroDynamics
MILES	Medium-resolution Isaac Newton Telescope Library of Empirical Spectra
MIR	Mid InfraRed
MOS	Multi-Object Spectrograph
MR	Mid-Resolution (VPHs)
MS	Main Sequence
MW	Milky Way
NDWFS	NOAO Deep Wide-Field Survey
NDWFS	NOAO Deep Wide-Field Survey
NIRSOS	Near-infrared atlas of SO-Sa galaxies
NUV	Near Ultraviolet
OPMS	Observing Program Management Subsystem
ORL	Optical Recombination Line





OS	Order-Sorting (filter)
PACS	Photodetector Array Camera and Spectrometer on the Herschel Space Observatory
PAU	Physics of the Accelerating Universe (project)
PDR	Preliminary Design Review
PN	Planetary Nebula
PPN	Pre-Planetary Nebula
PSF	Point Spread Function
RC	Red Clump
RC3	Third Reference Catalog of Bright Galaxies
RGB	Red Giant Branch
RL	Recombination Line
RMS	Root Mean Square
ROC	Radius of Curvature
RS	Re-pressurizing Shocks
S4G	Spitzer Survey of Stellar Structure in Galaxies
SAURON	Spectrographic Areal Unit for Research on Optical Nebulae
SCB	Small Compact Bundle
SDSS	Sloan Digital Sky Survey
SED	Spectral Energy Distribution
SFC	Smaller Fiber Core
SFE	Star Formation Efficiency
SFH	Star Formation History
SFR	Star Formation Rate
SGW	Super Galactic Wind
SHARDS	Survey for High-z Absorption Red and Dead Sources
SINGS	Spitzer Infrared Nearby Galaxies Survey
SMBH	Super Massive Black Hole



SMC	Small Magellanic Cloud
SN	Super Nova
SP	Stellar Population
SPIRE	Spectral and Photometric Imaging Receiver on the Herschel Space Observatory
SpUDS	Spitzer Ultra Deep Survey
SQ	Stephan's Quintet
SSC	Super Stellar Cluster
sSFR	Specific Star Formation Rate
SSP	Single Stellar Population
STIS	Space Telescope Imaging Spectrograph
SXDS	Subaru/XMM-Newton Deep Survey
SXDS	Subaru/XMM-Newton Deep Survey
TBA	To Be Assigned
TBC	To Be Confirmed
TBD	To Be Done
TBU	To Be Updated
TIR	Total Internal Reflection
ToI	Target of Interest
TRGB	Tip of the Red Giant Branch
UCM	Universidad Complutense de Madrid
UDF	(Hubble) Ultra-Deep Field
UDS	Ultra Deep Survey
UF	University of Florida
UKIDSS	UKIRT Infrared Deep Sky Survey
UKIRT	United Kingdom Infra-Red Telescope
ULIRG	Ultra Luminous InfraRed Galaxy
UPM	Universidad Politécnica de Madrid



UV	UltraViolet
UVES	Ultraviolet and Visual Echelle Spectrograph on the VLT
VIMOS	Visible MultiObject Spectrograph
VLT	Very Large Telescope
VPH	Volume Phase Holographic (grating)
WBS	Work Breakdown Structure
WISE	Wide-field Infrared Survey Explorer
WP	Work Package
WR	Wolf-Rayet (star)
XMM	X-ray Multi-Mirror Mission
XSL	X-shooter Spectral Library
Λ CDM	Λ Cold Dark Matter (model)

**Change Control**

Issue	Date	Section	Page	Change description
1.A	17/10/2011	All	All	First issue
1.B	25/01/2012	All	All	Second issue
2.A	01/02/2012	All	All	Final version for PDR delivery

Reference Documents

N°	Document Name	Code
R.1	MEGARA Preliminary Design. Folded-Cass Optics	TEC/MEG/026
R.2	MEGARA: Fiber MOS Prototype: design, manufacturing and tests	TEC/MEG/021
R.3	MEGARA Preliminary Design. Pseudo-slit discussion	TEC/MEG/056
R.4	MEGARA Preliminary Design: Spectrograph Optics	TEC/MEG/058
R.5	Spectrograph Mechanics: Design upgrades from conceptual design	TEC/MEG/043
R.6	MEGARA Preliminary Design. Cryostat	TEC/MEG/028
R.7	MEGARA Preliminary Design. Detector and DAS	TEC/MEG/051
R.8	MEGARA Conceptual Design. Science Case	TEC/MEG/010
R.9	MEGARA. PSF simulations: Spectral Resolution and Cross-talk effects	TEC/MEG/076
R.10	MEGARA. Alternatives Trade-off study	TEC/MEG/044
R.11	MEGARA. Preliminary Design. Instrument Overview	TEC/MEG/059
R.12	MEGARA. Observing Modes	TEC/MEG/005

Reference Documents (GTC codes)

N°	Document Name	Code
R.1	MEGARA Preliminary Design. Folded-Cass Optics	EXT/UCM/1729-R
R.2	MEGARA: Fiber MOS Prototype: design, manufacturing and tests	EXT/UCM/1724-R
R.3	MEGARA Preliminary Design. Pseudo-slit discussion	EXT/UCM/1731-R
R.4	MEGARA Preliminary Design: Spectrograph Optics	EXT/UCM/1742-R
R.5	Spectrograph Mechanics: Design upgrades from conceptual design	EXT/UCM/1733-R
R.6	MEGARA Preliminary Design. Cryostat	EXT/UCM/1744-R
R.7	MEGARA Preliminary Design. Detector and DAS	EXT/UCM/1737-R
R.8	MEGARA Conceptual Design. Science Case	No code
R.9	MEGARA. PSF simulations: Spectral Resolution and Cross-talk effects	EXT/UCM/1808-R
R.10	MEGARA. Alternatives Trade-off study	EXT/UCM/1734-R
R.11	MEGARA. Preliminary Design. Instrument Overview	EXT/UCM/1778-R
R.12	MEGARA. Observing Modes	EXT/UCM/1714-R

**INDEX**

1. SUMMARY	17
1.1 Design changes with respect to the Conceptual Design.....	17
2. SCIENTIFIC DRIVERS OVERVIEW.....	21
2.1 Science Team interests.....	21
2.2 Galactic and extragalactic nebulae: The need for the MEGARA IFU	22
2.2.1 Nearby galaxies (beyond the Local Group)	23
2.2.2 Planetary Nebulae: from the Asymptotic Giant Branch to the Planetary Nebulae stage. 24	
2.2.2.1 <i>Nebular shaping and acceleration beyond the AGB: early evolution of PNe.....</i>	<i>24</i>
2.2.2.2 <i>Chemical abundances in PNs and HII regions.....</i>	<i>25</i>
2.2.3 UV resonant-line emission from the high-redshift IGM.....	26
2.2.4 Arcs and highly-magnified distant galaxies in clusters	26
2.3 Point-source science	27
2.3.1 Stellar astronomy	28
2.3.1.1 <i>Solar analogous in Galactic open clusters.....</i>	<i>28</i>
2.3.1.2 <i>Formation of low-mass stars in stellar clusters.....</i>	<i>29</i>
2.3.2 Local Group galaxies	29
2.3.3 Distant galaxies	30
2.3.3.1 <i>Intermediate-redshift BCDs.....</i>	<i>31</i>
2.3.3.2 <i>Clump-cluster, peas and starburst galaxies</i>	<i>31</i>
2.3.3.3 <i>High-redshift proto-clusters</i>	<i>32</i>
2.4 E-Science	33
2.5 MEGARA Early Science	33
3. MEGARA SCIENCE.....	34
3.1 MEGADES: MEGARA Galaxy Disks Evolution Survey.....	34
3.1.1 Motivation.....	34
3.1.1.1 <i>Secular evolution of disks: the inside-out scenario</i>	<i>35</i>



3.1.1.2	<i>Secular evolution of disks: stellar migration</i>	37
3.1.1.3	<i>Secular evolution of disks: galaxy-to-galaxy variations</i>	41
3.1.1.4	<i>Secular evolution of disks: satellite accretion and minor mergers</i>	42
3.1.1.5	<i>Secular evolution of disks: spatial distribution of metals in galaxy disks</i>	45
3.1.1.6	<i>Secular evolution of disks: starburst activity</i>	48
3.1.1.7	<i>Secular evolution of disks: green-valley galaxies and AGN activity</i>	54
3.1.1.8	<i>Massive stars in Local Group galaxies</i>	57
3.1.1.8.1	Advanced stages of massive star evolution	58
3.1.2	Objectives	60
3.1.3	Methodology	63
3.1.3.1	<i>Determining the role of secular processes: beyond inside-out formation</i>	63
3.1.3.1.1	Stellar kinematics.....	63
3.1.3.1.2	Spectral indices	67
3.1.3.1.3	Chemical abundances	70
3.1.3.2	<i>Mapping the spatial distribution of metals in galaxy disks</i>	72
3.1.3.2.1	Chemical abundances and abundance ratios.....	72
3.1.3.2.2	Radial abundance gradients	74
3.1.3.2.3	Metals distribution in galaxies traced in 2D	75
3.1.3.2.4	Long-standing questions on the determination of chemical abundances	76
3.1.3.3	<i>Determining the role of minor mergers</i>	79
3.1.3.4	<i>Determining the role of starburst activity</i>	81
3.1.3.4.1	M82-like Super Galactic Winds	81
3.1.3.4.2	Neutral Galactic Winds.....	81
3.1.3.4.3	Direct observation of massive-star feedback	83
3.1.3.5	<i>Determining the role of nuclear activity</i>	83
3.1.3.6	<i>Studying the evolution of massive stars in external galaxies</i>	85
3.1.4	Sample.....	87
3.1.4.1	<i>Local Group disk galaxies</i>	87



3.1.4.1.1	The Local Group spiral galaxy M33	87
3.1.4.1.2	The Local Group galaxy IC 1613	89
3.1.4.2	<i>Nearby galaxies (beyond the Local Group)</i>	90
3.1.4.2.1	S4G survey.....	90
3.1.4.2.2	The MEGADES-S4G sample	91
3.1.4.3	<i>Additional MEGADES targets</i>	103
3.1.4.3.1	M82	103
3.1.4.3.2	ULIRGs.....	103
3.1.5	Observations	104
3.1.5.1	<i>Local Group galaxy M33</i>	106
3.1.5.1.1	Disk RGB-stars chemical abundances and kinematics.....	106
3.1.5.1.2	Disk light-weighted star formation and chemical histories	110
3.1.5.1.3	Disk massive-blue-stars chemical abundances and kinematics	110
3.1.5.1.4	Ionized-gas metal abundance diagnostics.....	111
3.1.5.1.5	Massive blue stars in the Local Group.....	112
3.1.5.2	<i>Nearby galaxies (beyond the Local Group): The MEGADES-S4G sample</i>	117
3.1.5.2.1	Strategy	117
3.1.5.2.2	Analysis tools.....	119
3.1.5.2.3	Observing time: kinematics, stellar populations and metallicity of disks	120
3.1.5.2.4	Observing time: inner disks, stellar populations and dynamics.....	123
3.1.5.2.5	Observing time: (neutral) galactic winds.....	124
3.1.5.2.6	Observing time: nuclear activity.....	125
3.1.5.3	<i>Additional MEGADES targets</i>	126
3.1.5.3.1	M82	126
3.1.5.3.2	ULIRGS	127
3.2	Galactic Planetary Nebulae.....	129
3.2.1	Nebular shaping and acceleration beyond the AGB phase.....	129
3.2.1.1	<i>Scientific motivation and objectives</i>	129



3.2.1.2	<i>Strategy: observations and analysis planned</i>	133
3.2.2	Chemical abundances in PNs and HII regions	135
3.2.2.1	<i>Scientific motivation and objectives</i>	135
3.2.2.2	<i>Strategy: observations and analysis planned</i>	141
3.3	MEDUSA: MEGARA Distant-Universe Spectroscopic Analysis	143
3.3.1	Scientific motivation and objectives	143
3.3.2	Strategy of the MEDUSA Cosmological surveys	144
3.3.3	The nature and evolution of Green Pea galaxies	146
3.3.4	Star Formation Feedback in Massive systems at different redshifts	148
3.3.4.1	<i>Scientific motivation</i>	148
3.3.4.2	<i>Objectives</i>	149
3.3.4.3	<i>Sample and observing strategy</i>	150
3.3.4.4	<i>Serendipity project</i>	152
3.3.5	On the formation redshift of dwarf galaxies. Properties and star formation histories of low-mass galaxies	154
3.3.5.1	<i>Introduction: Scientific rationale</i>	154
3.3.5.2	<i>Proposed MEGARA observations</i>	154
3.3.5.3	<i>Feasibility study and observational strategy</i>	157
3.3.6	Galaxy over-densities at high-redshift	160
3.3.6.1	<i>Scientific motivation</i>	160
3.3.6.2	<i>Objective</i>	163
3.3.7	Analyzing the faintest and/or most distant SFGs using gravitational lenses	167
3.3.7.1	<i>Scientific motivation</i>	167
3.3.7.2	<i>Objective</i>	170
3.4	Stellar astronomy with MEGARA	172
3.4.1	Chromospheric activity and age of solar analogs in open clusters	172
3.4.1.1	<i>Introduction</i>	172
3.4.1.2	<i>Solar analogs</i>	172



3.4.1.3	<i>Observing proposal</i>	174
3.4.1.4	<i>Observations</i>	176
3.4.1.5	<i>Stellar atmospheric parameters</i>	177
3.4.2	Low-mass star formation in ESO Gaia stellar clusters	178
3.4.2.1	<i>Introduction: Star Formation and the low-mass end</i>	178
3.4.2.1.1	The Gaia mission	179
3.4.2.1.2	The ESO-Gaia survey	180
3.4.2.2	<i>Objectives</i>	181
3.4.2.3	<i>Methodology</i>	181
3.4.2.3.1	Chemical abundances	181
3.4.2.3.2	Ages	181
3.4.2.4	<i>Sample</i>	182
1.1.1.4.1	Stellar Associations in the Gould Belt.....	183
1.1.1.4.2	Perseus Arm.....	184
1.1.1.5	<i>Observations</i>	184
4.	MEGARA EARLY SCIENCE / TARGETS OF INTEREST.....	185
4.1	NGC 604.....	186
4.2	M81187	
4.3	Stephan's quintet: A galaxy-scale shock in a group of galaxies.....	188
4.4	NGC 7027: a multipolar PN in the making.	189
4.5	Einstein ring LRG 3-757	190
5.	BIBLIOGRAPHY	191



(Page intentionally left blank)



1. SUMMARY

This document describes the applications envisioned by the MEGARA Science Team for the scientific exploitation of the MEGARA instrument in its different modes and configurations. Such applications led to the definition of the instrument requirements and therefore drive the design of MEGARA. These requirements encompass those of the "Instrument 1" listed in the "*Announcement of Opportunity for new instrumentation for the Gran Telescopio Canarias*" issued by GRANTECAN on September 14th 2009. See document R.11 for a description of the instrument requirements.

In summary, MEGARA is designed to satisfy the needs a broad and heterogeneous astronomical community interested in the study of a variety of astronomical objects at intermediate-to-high spectral resolutions ($R=5,000-20,000$) in the optical window of the electromagnetic spectrum. The broad nature of our Science Team has led to establish the need of having both an Integral Field Unit (IFU) and a Multi-Objects Spectrograph (MOS) mode in MEGARA. The necessity of having these two observing modes has led to propose two concepts that are extensively discussed elsewhere in this Preliminary Design: MEGARA-Basic, where only one spectrograph is available and these two modes are to be used alternatively, and MEGARA-Advanced, where they could be used simultaneously. Our baseline for the Preliminary Design in terms of scientific exploitation is MEGARA-Advanced although such baseline will never jeopardize the feasibility neither have any impact on the cost or risks associated to the MEGARA-Basic concept.

In this regard, we will discuss throughout this document the impact on each scientific program of having one or the other concept available at GTC. The impact of potential de-scoping alternatives to MEGARA-Basic on the scientific capabilities of MEGARA will be also discussed throughout this document. These alternatives include the removal of the SCB and the optical-red mid-resolution (MR) VPHs from the budget and management plan of the instrument.

1.1 Design changes with respect to the Conceptual Design

As part of the "Alternatives Trade-off study" review (one of the PDR milestones), a discussion between GRANTECAN and the MEGARA team took place where both parts shared their views on the meaning and scope of the requirements specified in the "*Announcement of Opportunity for new instrumentation for the Gran Telescopio Canarias*". As a consequence of this discussion the MEGARA team decided to incorporate a number of changes in the design of the MEGARA focal plane and the pupil elements, compared to those presented in the Conceptual Design.

These changes include (i) the design of a set of four additional medium-resolution ($R\sim 11,000$) VPHs in the optical red and (ii) the addition of an IFU fiber bundle (Small Compact Bundle or SCB) based on $70\mu\text{m}$ -core fibers (see "Alternative 1" in R.10) that yields an improved spatial and spectral resolution but a reduced FOV and degraded PSF sampling compared to those given by the IFU bundle based on $100\mu\text{m}$ -core fibers (now called Large Compact Bundle or LCB). See Table 1.1 for a comparison between the parameters of the two IFU bundles. These additions allow MEGARA to cover the full optical window with a spectral resolution of $R\geq 11,000$ ($R\geq 14,400$ for the SCB).

Throughout this document and for each scientific application making use of the MEGARA IFU mode we will perform a trade-off analysis of the pros and cons of using either the SCB or LCB.



Parameter		IFU Modes		MOS Mode
		Large Compact Bundle	Small Compact Bundle	Dispersed Bundle
Spaxel size		0.685 arcsec	0.480 arcsec	0.685 arcsec
Field of View		14 x 12 arcsec ²	10 x 8 arcsec ²	3.5 x 3.5 arcmin ²
FWHM (1D)		3.5 pix	2.7 pix	3.5 pix
Resolving Power (R_{FWHM})	LR VPHs	6,250	8,100	6,250
	MR VPHs	11,000	14,400	11,000
	HR VPHs	19,100	24,700	19,100

Table 1.1: Main characteristics of the MEGARA LCB and SCB IFUs and the Dispersed bundle (MOS). Throughout this document we will refer to R_{FWHM} as resolving power, spectral resolution or simply R , indistinctly. Note that in most design documents these terms will refer to the EED80 resolution element ($\Delta\lambda$) instead, which is roughly 10% larger than the FWHM.

In addition to these changes, the MEGARA Science Team also introduced modifications to the layout of the robotic positioners presented in the instrument Conceptual Design. These modifications include (i) the addition of a total of 6 robotic positioners that would fill the gap between the MEGARA SCB and LCB IFUs and the other 94 robotic positioners already included in the Conceptual Design^{1,2} and (ii) the use of 8 of the robotic positioners in the outer edge of the instrument FOV for measuring the sky background simultaneously with the observation with the LCB. The $8 \times 7 = 56$ fibers associated to these positioners will be evenly distributed along the pseudo-slit of the LCB IFU. In Figure 1.1 we show the layout of the instrument focal plane as it is presented for its Preliminary Design Review.

¹ This gap was intentionally left empty in the Conceptual Design, as it was the space occupied by the Sparse Bundle in the MEGARA-Full concept, now considered out of the scope of the instrument.

² Note that this requirement is also consequence of one of the comments of the external evaluators to the "Alternatives Trade-off Study".

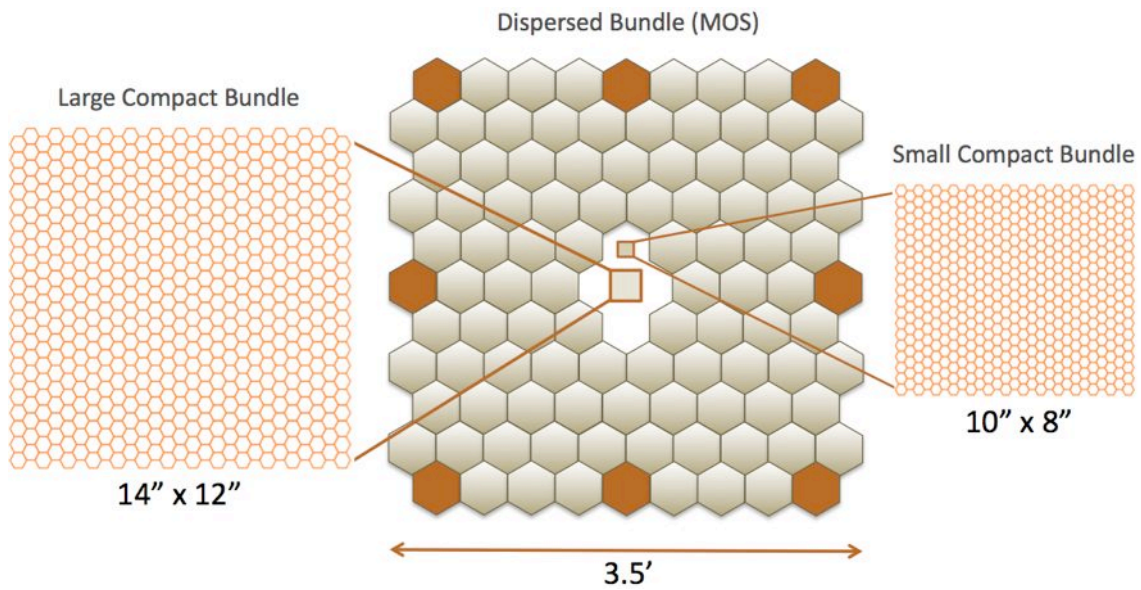


Figure 1.1: Layout of the Large Compact (LCB), Small Compact (SCB) and Dispersed bundles (MOS). The fiber bundles to be used for sky subtraction simultaneously with the LCB observations are shown as orange filled hexagons.

Finally, all these modifications plus a refinement of the scientific requirements imposed by the MEGARA Science Team led to some changes in the design of the VPHs used in MEGARA. These changes, except for the case of the four new MR VPHs in the red, are relatively minor. In Table 1.2 we show the spectral setups (at PDR level) of MEGARA.

VPH Name	Setup	R_{FWHM}	$\lambda_1-\lambda_2$ (Å)	λ_c (Å)	$\Delta\lambda_{FWHM}$ @ λ_c (Å)	Δv_{FWHM} (km s ⁻¹)	Rec. Disp. (Å pix ⁻¹)
VPH405-LR	LR-U	6,251	3,670 - 4,402	4,051	0.648	48	0.185
VPH480-LR	LR-B	6,251	4,348 - 5,216	4,800	0.768	48	0.219
VPH570-LR	LR-V	6,250	5,164-6,194	5,700	0.912	48	0.261
VPH675-LR	LR-R	6,249	6,115-7,334	6,749	1.080	48	0.309
VPH865-LR	LR-I	6,248	7,836 - 9,399	8,650	1.384	48	0.396
VPH410-MR	MR-U	11,069	3,890 - 4,309	4,104	0.370	27	0.106
VPH443-MR	MR-UB	11,067	4,200 - 4,652	4,431	0.400	27	0.114
VPH481-MR	MR-B	11,067	4,562 - 5,054	4,814	0.435	27	0.124
VPH521-MR	MR-G	11,065	4,941 - 5,472	5,213	0.471	27	0.135



VPH567-MR	MR-V	11,065	5,371 - 5,950	5,667	0.512	27	0.146
VPH617-MR	MR-VR	11,064	5,847 - 6,477	6,170	0.558	27	0.159
VPH712-MR	MR-R	11,064	6,744-7,470	7,115	0.643	27	0.184
VPH777-MR	MR-I	11,063	7,362-8,154	7,767	0.702	27	0.201
VPH926-MR	MR-Z	11,062	8,778-9,723	9,262	0.837	27	0.239
VPH665-HR	HR-R	19,079	6,450-6,841	6,646	0.348	16	0.099
VPH863-HR	HR-I	19,079	8,379-8,887	8,634	0.452	16	0.129

Table 1.2: MEGARA VPH setups. The resolution, $R_{FWHM} = \lambda / \Delta\lambda_{FWHM}$, is derived from the FWHM ($\Delta\lambda_{FWHM}$) of the 1D spectra and the case of the LCB IFU and MOS modes.

The impact (mainly benefits) of the changes described in this section on the scientific applications of MEGARA are considered and discussed extensively throughout this document.



2. SCIENTIFIC DRIVERS OVERVIEW

2.1 Science Team interests

In this section we provide a brief summary of the scientific objectives that have driven the Preliminary Design of MEGARA, as put together and agreed by the MEGARA Science Team. The detailed MEGARA science cases are exhaustively described in Section 3.

The scientific interests of the MEGARA Science Team can be grouped in two categories, (1) the study of Galactic and extragalactic nebulae and (2) the study of point sources (or close to point sources) with intermediate-to-high projected densities on the sky. Among the former our interests include the study of Planetary Nebulae (including pre- and young PNe), nearby galaxies, and the high-redshift IGM and among the latter the study of Galactic open stellar clusters, resolved stellar populations in Local Group galaxies, intermediate-redshift dwarf and starburst galaxies, and high-redshift cluster galaxies.

The MEGARA Science Team encompasses researchers with a broad range of scientific interests belonging to institutions of all members of the GTC community (Spain, Mexico and UF). This guarantees that, as a facility instrument, MEGARA will also successfully serve to the interests of the entire astronomical communities of the GTC Consortium members. In Figure 2.1 below we show a diagram that summarizes the main lines of research of the MEGARA Science Team and the corresponding team members with interest in each of these topics.

Our team includes experts from most research areas in Astronomy, both Galactic and extragalactic, except for the study of the Sun and Solar System objects.

What is common to all our scientific interests is the need for an intermediate-to-high spectral resolution, in the range $R \sim 5,000-20,000$. In some of the cases above this need is a mere consequence of velocity resolution (kinematics) but in many cases is given by the need of reducing line blending, either directly when lines from different elements ought to be measured in stars or *via* a reduction in the degeneracy of the properties of composite stellar populations.

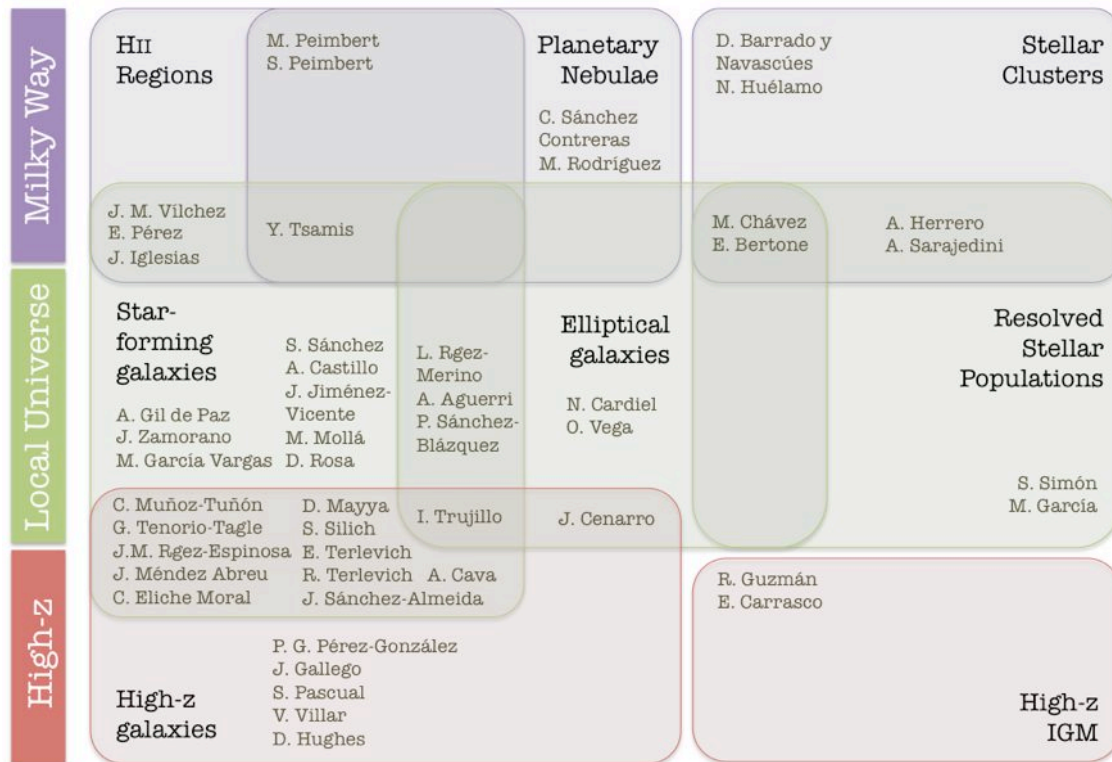


Figure 2.1: Areas of main scientific interest of the MEGARA Science Team. We note that these include most of the areas of research in Astronomy (excluding the study of the Sun and the Solar System). The main interest of the UPM group (F.M. Sánchez Moreno, R. Cedazo, E. González, F. Serena) is e-Science with focus in Astronomy, which, as a general discipline, shares interests with all of the above (see Section 2.4).

2.2 Galactic and extragalactic nebulae: The need for the MEGARA IFU

In the case of the study of nebulae, it has now become clear that the use of a bi-dimensional spectrometer is critical to obtain precise answers to the problems that these fields (either in its Galactic or extragalactic version) are facing. While the use of a Fabry-Pérot type of instrument might be a good choice in this regard should someone be only interested in single emission-line kinematics *and* if a precise flux calibration across the entire line profile is not required, the use of a Integral Field Unit (IFU) has certainly shown to be a more reliable approach, especially if one is interested on more than one single spectral feature or on absorption features (see e.g. the SAURON project).

It is because of this that early in the design process of MEGARA it became obvious the need for an IFU that would yield the required spectral resolution ($R=5,000-20,000$). Although some of the science cases originally planned by the MEGARA Science Team (see R.2) require of an IFU with a FOV significantly larger ($\sim 1 \times 1$ arcmin²) than that included in the current MEGARA design (14×12 arcsec² in the case of the LCB), we still should be able to achieve our objectives by (1) targeting objects of smaller angular size (more distant and/or physically smaller) and (2) by fast-mapping extended targets. We note the reader that during the design process of MEGARA we have always prioritized throughput, which, along with the large light-gathering power of GTC and an optimized Control system should allow mapping relatively extended targets with high efficiency.

The main interests of the MEGARA Science Team regarding the study of nebular objects are:



2.2.1 Nearby galaxies (beyond the Local Group)

We aim to study the evolution of galaxy disks through the analysis of their velocity ellipsoids and the 2D spatial distribution of spectral indices and chemical abundances. This goal constitutes the core of MEGADES, the *MEGARA Galaxy Disks Evolution Survey*. As extensively discussed in Section 3.1.1 this analysis is fundamental to disentangle the roles of the secular processes involved in the shaping the present-day properties of disks, i.e. in-situ star formation, stellar migration and satellite accretion and (minor-)merging among others. In addition to the study of the unresolved stellar populations in galaxy disks outlined here, MEGADES will also include the detailed single-star spectroscopic analysis of the Local Group galaxies M33 and IC 1613 (see Section 3.1.4.1).

Furthermore, MEGADES will also be used to study the interplay between the massive-star formation and the interstellar medium and its consequences on the further evolution of actively star-forming galaxies (positive vs. negative star-formation feedback) through the analysis of galactic winds both in line emission ($H\alpha$ primarily) and in absorption lines (NaI D, KI) arising from cool ISM associated to the galactic-wind material. We will make use of the observations proposed within MEGADES to address some of the most fundamental problems on the analysis of the chemical properties of galaxies, including the long-standing problem of the abundance discrepancies and the potential identification and analysis of chemo-dynamical phenomena (i.e. kinematical components of the ISM with distinct chemical enrichment).

In order to be as much efficient as possible and given the current budget constrains (which limit the number of MEGARA spectrographs to unity and, therefore, the FOV of the MEGARA IFU to 14×12 arcsec²) we will target galaxies which can be scanned along the major and minor axes in just a few IFU pointings. These galaxies, with an apparent size comparable to the MEGARA MOS FOV, will be also observed (simultaneously in the case of the MEGARA-Advanced configuration) with the set of robotic positioners placed on individual HII regions with the objective of measuring metal-abundance radial and 2D distributions. Galaxies included in the S4G survey (Sheth et al. 2010), a diameter- and volume-limited sample of galaxies within 40 Mpc, will be used as targets for this program.

With regard to the spatial resolution, a sampling close to that of the typical seeing in La Palma, as that provided by the LCB, is good enough for most scientific applications described above. Only in the case of the study galactic winds in relatively distant galaxies and in Galactic Planetary Nebulae, the improved spatial and spectral resolutions of the SCB could be beneficial.

In terms of the resolving power, the study of the stellar velocity ellipsoid and ionized-gas kinematics (including chemo-dynamical phenomena) requires of resolutions in the range $R=6,000-20,000$ (depending on the properties -e.g. mass and inclination- of the target under analysis). The determination of the 2D spatial distribution of spectral indices and chemical abundances both require of a wide wavelength coverage (in the lower number of spectral setups possible) while a spectral resolution of $R \sim 5,000$ would suffice. Such a spectral resolution would also take advantage of state-of-the-art spectral libraries (e.g. the X-shooter Stellar Library or XSL; Cheng et al. 2011) when analyzing spectral indices throughout the disks of our targets.



2.2.2 Planetary Nebulae: from the Asymptotic Giant Branch to the Planetary Nebulae stage

The process (or processes) that lead to Planetary Nebula (PN) formation out of the winds of Asymptotic Giant Branch (AGB) stars are complex and poorly known. In this proposal, we focus on two of the biggest challenges in the study of these latest stages of the stellar evolution of intermediate mass (solar-type) stars: understanding 1) nebular shaping and acceleration beyond the AGB and 2) chemical enrichment. Our twofold approach highlights the power of MEGARA to carry out different but complementary studies of nebular objects, on the one hand, characterization of the spatio-kinematic structure and, on the other hand, ionized-gas diagnostics with spatial resolution.

2.2.2.1 *Nebular shaping and acceleration beyond the AGB: early evolution of PNe*

One of the aims of our studies of PNs and pre-PNs (i.e. objects that have recently left the AGB phase) with MEGARA is to make progress in our understanding of the nebular shaping process, which is believed to be driven by the interaction between collimated, fast (i.e. jet-like) winds ejected during the late-AGB or early post-AGB stages and the slow, largely spherical envelopes formed during the previous AGB phase as a result of a heavy mass-loss process. We will use MEGARA for a detailed characterization of the morphology and velocity structure of a sample of objects displaying diverse morphologies and spanning a range of evolutionary stages (from early post-AGBs, PPNs, and PNs). Special emphasis will be made on the study of sources with post-AGB ejections currently active and sculpting the AGB circumstellar envelopes (CSEs).

The FOV required for the MEGARA IFU is simply given by the size of the vast majority of young PN and PPNs known to date (5-20 arcsec, see e.g. Sahai et al. 2007; Sahai et al. 2011). We anticipate that no more than three pointings with the SCB mode (FOV~10"x8") are required and, in many cases, the targets can be accommodated in one pointing. Since both spatial and spectral resolution are required for a comprehensive study of the spatio-kinematic structure of the different nebular components typically present in these objects (such as shocked elongated lobes, axial knots, arc-like features, etc), the SCB will be the preferential observational configuration used. Resolving the kinematical structure imprinted by the interaction of the fast post-AGB wind on the AGB CSE requires high spectral resolutions; we will use the HR-R VPH for a resolution of $R\sim 25,000$ around the $H\alpha$ line, which is an excellent tracer of the atomic and ionized gas component in these objects. Also, full spectral coverage at lower resolutions ($R\sim 6,000-10,000$, using the LR and MR VPHs) is desired for a proper characterization of the physical conditions in the nebulae derived from emission line diagnostic ratios.

The main features in the emission line profiles to be analyzed are the broad wings, observed to reach FWZIs~1,000-2,000 km/s in a number of PPNs/PNs, and the blue-shifted, absorption features observed in the HI Balmer profiles of some PPNs – the latter P-cygni like profiles are probably produced by intervening cooler gas associated to pristine post-AGB winds. The simultaneous access to, e.g., $H\alpha$, $[SII]\lambda\lambda 6717, 6731\text{\AA}$ and $[NII]\lambda\lambda 6548, 6584\text{\AA}$ lines (with the LR, MR and even HR VPHs) is a clear benefit of the use of an IFU compared with what would be obtained from Fabry-Pérot observations alone.



2.2.2.2 *Chemical abundances in PNs and HII regions*

We aim at characterizing the emission-line spectra of evolved (fully photo-ionized) PN. Such a study would allow us not only to determine the chemical abundances of their envelopes but also to tackle fundamental open questions about the physical properties of the ionized gas. Major open questions include:

What is the origin of the discrepancy between the oxygen abundances implied by recombination lines and collisionally-excited lines?

As a related question, which lines provide the most reliable abundances and what method should be used to calculate the metallicity of the gas?

How do the best estimates of chemical abundances in PN compare with those derived for the present-day interstellar medium located in HII regions? and how do they compare with those that have been derived for intermediate-mass stars?

The disagreement between the abundances implied by recombination lines and collisionally excited transitions of heavy elements in HII regions and PNs is one of the main open questions in the study of ionized nebulae. This discrepancy not only introduces an uncertainty of at least a factor of 2 in our abundance determinations but also might provide clues on processes that are crucial to our understanding of galactic chemical evolution. A related issue on which we need more information concerns the temperature structure of real objects and whether it can be reproduced with photoionization models, since the assumed temperature structure affects significantly the abundances derived with collisionally excited lines.

MEGARA on GTC can provide for nearby nebulae spectral maps with enough spectral resolution and wavelength coverage to address these topics by studying variations, both spatially and from object to object, in the abundance discrepancy and in the temperatures implied by different diagnostics. For some PNs, MEGARA will also provide integrated fluxes, which will allow a direct comparison with spectral diagnostics and emission lines from other wavelength regimes, such as the UV, radio, and the IR.

We intend to obtain deep spectra with spectral resolutions around or above $R=5,000$ of specific regions of a sample of nearby PNs. These observations will allow us to carry out a detailed analysis of the chemical abundances of most elements found in PNs using both temperature-sensitive collisionally-excited transitions and recombination lines. In order to address some of the questions listed above, this study will be extended by including the observation of specific individual Galactic HII regions. Here the need for a FOV as wide as possible makes of the IFU LCB the observing mode of choice.



2.2.3 UV resonant-line emission from the high-redshift IGM

According to state-of-the-art models of the evolution of the meta-galactic UV radiation field at high-redshift, an instrument such as MEGARA in combination with GTC could allow, for the first time, detecting emission from red-shifted UV resonant lines such as OVI1033 Å, CIV1550 Å, Ly α that arise in the high- z IGM. This is particularly feasible if we use statistical filament stacking techniques but even direct imaging detections are possible (depending on the model parameters adopted for the evolution of the radiation field at high redshift).

This kind of pioneering work requires of a FOV comparable to the extension of the features to be analyzed (filaments, Ly α -blobs). Thus, depending on the model parameters and the redshift range explored, maps of a few to tens of pointings should be needed to disentangle the 3D structure of the high- z IGM line emission. A good blue sensitivity at $\lambda \sim 5000$ Å and spectral resolution (not worse than $R \sim 5,000$) are a must in this case. This is due to the necessity of resolving the 3D structure of the IGM in velocity, to differentiate the effects of bulk motions from those of radiative transfer in these resonance lines and to improve sky subtraction (see e.g. Martin et al. 2010). The need for an accurate sky subtraction and for covering a large FOV both point towards the LCB as mode to be used.

Despite the remarkable impact that such experiment would have, we, the MEGARA Science Team, have decided that the uncertainties in the actual intensity of the high- z meta-galactic UV radiation field justifies pursuing this project only as part of parallel observations with the MEGARA IFU; i.e. when primary MOS observations are carried out with MEGARA-Advanced.

2.2.4 Arcs and highly-magnified distant galaxies in clusters

In addition to the study of the high-redshift IGM another application of the MEGARA IFU for the study of the high-redshift Universe envisioned by our Science Team is the 2D spectroscopy of far-infrared (Herschel) selected sources in regions of high-magnification in intermediate-redshift clusters. These sources are being identified thanks to the *Herschel Lensing Survey* (PI: E. Egami), a *Herschel Open Time Key Programme* devoted to the observation with the PACS and SPIRE instruments that reaches 5 mJy at 100 μ m and 10 mJy at 250 μ m in a total of 40 clusters. The faint continuum emission and relatively large projected size in the sky of some of these sources (arclets in most cases) make necessary the use of an IFU in order to identify them and for spectroscopically measuring their redshifts. Indeed, in many cases the position of the optical counterpart of the IR-bright galaxy is not known (it is extremely faint in the continuum), so only using an IFU with an exceptional covering factor such as MEGARA we can target the area with high magnification and try to recover spectroscopic data from the arc. Moreover, the magnification produced by the cluster can be used to explore the faintest regime in all the science topics introduced in this section. For example, MEGARA observations of nearby clusters with known Herschel arcs could also target (with the positioners, taking advantage of the high multiplexing of MEGARA) candidates for faint green peas at intermediate- or even high- z , since they may count with a significant magnification from the cluster (or weak-, medium-lensing from individual galaxies in the field). Also in this case we aim to use the LCB as it provides a wider field of view and a better sky subtraction than the SCB.

2.3 Point-source science

The other major area of scientific interest within our team refers to the study of point sources (or marginally-resolved sources from the ground). This includes the study of Galactic open clusters, individual stars in Local Group galaxies and very distant galaxies. Except in the case of the study of the RGB population in Local Group galaxies, where the use of a wide-field IFU could still provide a significant advantage at some galactocentric distances (<7 Mpc in the case of M33), in the remaining cases the surface densities range between a fraction to a few sources per arcmin². For such science applications the possibility of having a relatively high multiplexed ($\sim 100x$) MOS mode within the non-vignetted FOV of the Folded Cass focus of GTC is ideal. In Figure 2.2 we show the maximum field density reachable with the Multi-Object Spectrograph (MOS) mode proposed for MEGARA compared with other instruments³. Clearly, the MEGARA MOS is the best instrument for performing spectroscopic observations of moderate-to-highly crowded fields, such as Galactic stellar clusters, resolved stars in Local Group galaxies, ultra-deep cosmological fields (e.g. UDF) or distant galaxy clusters.

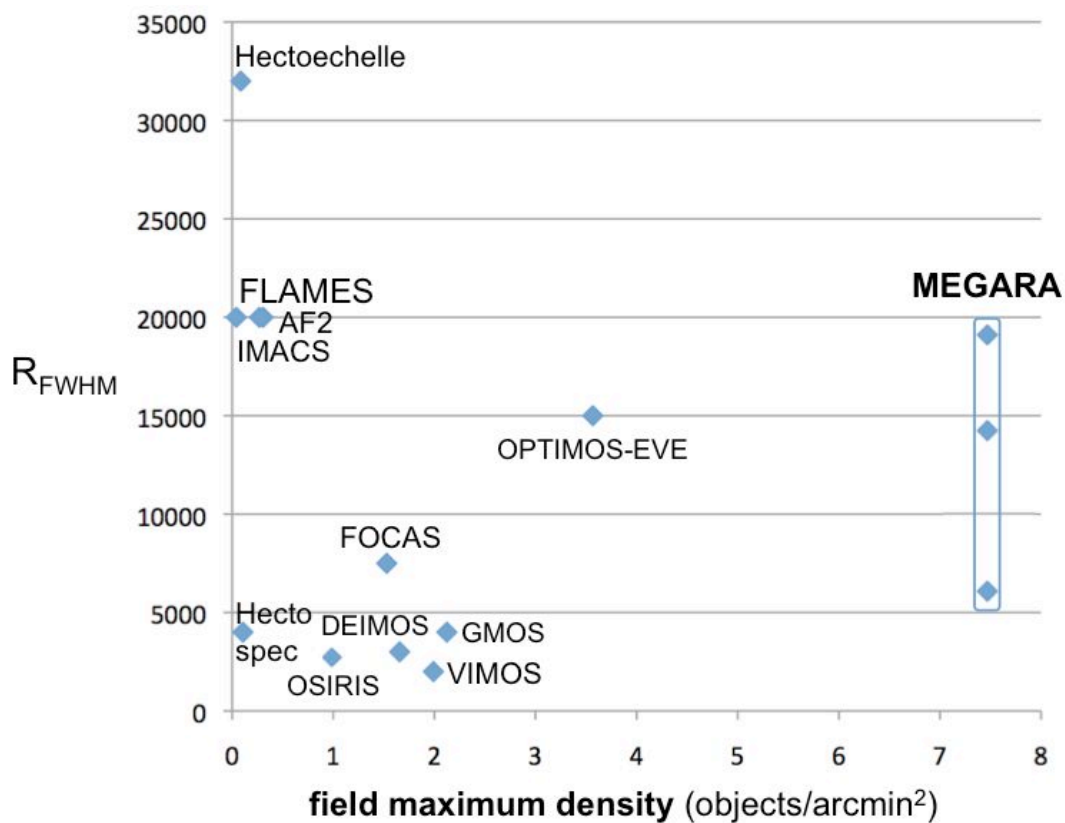


Figure 2.2: Spectral resolution versus maximum density of objects for different multi-object spectrographs (MOS) already built or planned. For the sake of comparison we also show the different resolutions and maximum density reachable with MEGARA.

³ The reader is referred to the Exposure Time Calculator Users Guide for a similar comparison in terms of instrument throughput.



Given the fact that GTC lacks an ADC at least a total field covered by each MOS positioner should be no less than 2 arcsec. This is achieved in our case by using 7 hexagonally packed lenslets covering 0.685 arcsec each (~ 2.1 arcsec in diameter total). In order to highlight the need for having such configuration in the case of the MEGARA MOS mode we note that at $R \sim 11,000$ in the blue the differential refraction across the entire wavelength range simultaneously covered at this resolution ($\sim 500 \text{ \AA}$) at an airmass of 1.8 is ~ 0.7 arcsec, i.e. comparable to the size of each individual spaxel in the MEGARA MOS (0.685 arcsec), with effects being noticeable at an airmass of 1.30 already. Moreover, as the targets in the some of the studies described above are marginally resolved from the ground under good seeing conditions, the use of small mini-bundles of 7 spaxels each (instead of single fibers) provides a way to recover some (rather limited though) spatial information. Given that the lenslets used for the robotic positioners that patrol the outer $3.5 \times 3.5 \text{ arcmin}^2$ are identical to those used in the LCB IFU these can also nicely used for a precise sky background subtraction during the observations of relatively extended nebular objects. Since this would be true only in the case that both the LCB IFU and the MOS components could be used simultaneously as intended in MEGARA-Advanced, we have also devoted a set of eight positioners for simultaneous sky-background determination when observing with the LCB IFU. The fibers associated to these positioners would be evenly distributed along the LCB pseudo-slit for a further improvement in the sky-background determination.

Below we include a summary of the main interests of the MEGARA Science Team related to the study of (or close to) point sources:

2.3.1 Stellar astronomy

The characteristics of the MEGARA MOS are optimal for the analysis of the properties of stars in Galactic open clusters, especially at Galactocentric distances beyond which the apparent size of the clusters matches the MEGARA MOS field of view (at and beyond ~ 2 kpc). Among the MEGARA Science Team there is interest in two different aspects regarding the study of the stellar content of Galactic open clusters that refer to the characterization of (i) solar analogs and (ii) low-mass stars.

2.3.1.1 *Solar analogous in Galactic open clusters*

The objective of this study is to re-calibrate the activity-sensitive Ca H+K index with the stellar age for an extended sample of solar analogs in stellar open clusters. Once properly calibrated this relation could be applied to field stars and, in particular, to specific solar-type stars showing IR excesses or possibly hosting planetary systems. We will also make use of the measurements of spectral indices to be obtained from the MEGARA observations proposed for the determination of the effective temperature and gravity. This study is done in the context of the characterization of solar analogs candidates for the future search of Sun-Earth-like planetary systems.



2.3.1.2 *Formation of low-mass stars in stellar clusters*

This project intends to study of properties of very low mass stars (and brown dwarfs) in young stellar associations from a holistic perspective. First, within the Gould Belt (the Local Bubble, a structure few hundred parsec across), then, moving farther away, to the galactic anticenter and the Perseus Arm (beyond 2 kpc). The goal is to put star formation in a galactic perspective and to include the effects of both metallicity and environment.

Specifically, we will study the low-mass star formation in the Gould Belt by carrying out a complete census of three clusters in this region (NGC1333+IC348, NGC7160, IC4665). This study will also include the derivation of stellar properties such as accretion along with the characterization of the lowest (planetary-)mass objects. It will then be extended to a sample of a few clusters in the Perseus Arm (including the complex formed by W3-W4 and W5) with the aim of exploring these properties in a completely different environment within the Galaxy.

We will first characterize a sample of photometrically-selected stars in all these clusters using medium-resolution spectroscopy ($R \sim 6,000$) covering $H\alpha$, $\text{Li } \lambda 6708\text{\AA}$, $\text{NaI } \lambda 8200\text{\AA}$, CaT (LR-R and LR-I) and then, once their membership is confirmed and their spectral types derived, we will obtain high-resolution spectroscopy ($R \sim 19,000$) in the $H\alpha$ (including also the $\text{Li } \lambda 6708\text{\AA}$ line) and CaT regions to identify activity and accreting related phenomena along with accurate radial velocities.

This project is carried out in the context of the Gaia mission and its supporting (and follow-up) observing programs, including the ESO-Gaia (FLAMES) ESO Large Programme. In this regard, MEGARA will provide the needed multiplexing for observing some of the stellar clusters to be observed with Gaia but, where the high stellar density, prevents its observation with FLAMES at VLT.

2.3.2 Local Group galaxies

Two are the objectives of the spectroscopic characterization of the resolved stellar population in star-forming Local Group galaxies.

First, we aim at characterizing the massive blue star population in the late-type Local Group star-forming galaxies M33 (the Triangulum galaxy) and IC1613 from intermediate-to-high-resolution spectroscopy in the blue range of the optical spectrum ($R \sim 11,000$) and in the $H\alpha$ region ($R \sim 19,000$). These observations will allow us to study of the role played by stellar rotation in the surface abundance enrichment of massive stars and characterize their mass loss rates at a wider range of metal abundances than previously accomplished, from $1.3Z_{\odot}$ (in the central parts of M33) to $0.04Z_{\odot}$ (IC1613).

Secondly, we will study the RGB population in the disk of M33 using intermediate spectral resolution ($R \sim 6,000$) in the CaT region. From there measurements we will derive both the single-star velocity ellipsoid and the disk metal-abundance gradient. Observations in the CaT at high-resolution ($R \sim 19,000$) will be also performed in order to self-calibrate the low-resolution metal-abundance estimates and in cases where the velocity dispersion (σ) is expected to be low. This study will be done as a function of galactocentric distance, which, again, should allow us to disentangle among others the effects in-situ star formation, stellar migration, and satellite accretion on the evolution of



disks, as these various mechanisms leave a distinct imprint in the velocity pattern of individual stars at different radii.

The fact that both objectives can be accomplished using common targets ensures an optimal use of the MEGARA MOS mode. Since both M33 and IC1613 are far more extended than the flat, non-vignetted Folded-Cass focal plane of GTC a series of a few MOS pointings will be obtained. In the case of the M33 these will be arranged along both the major and minor axes (see Figure 2.3), following a similar pattern that for the more distant S4G galaxies (see Section 3.1.5.2).

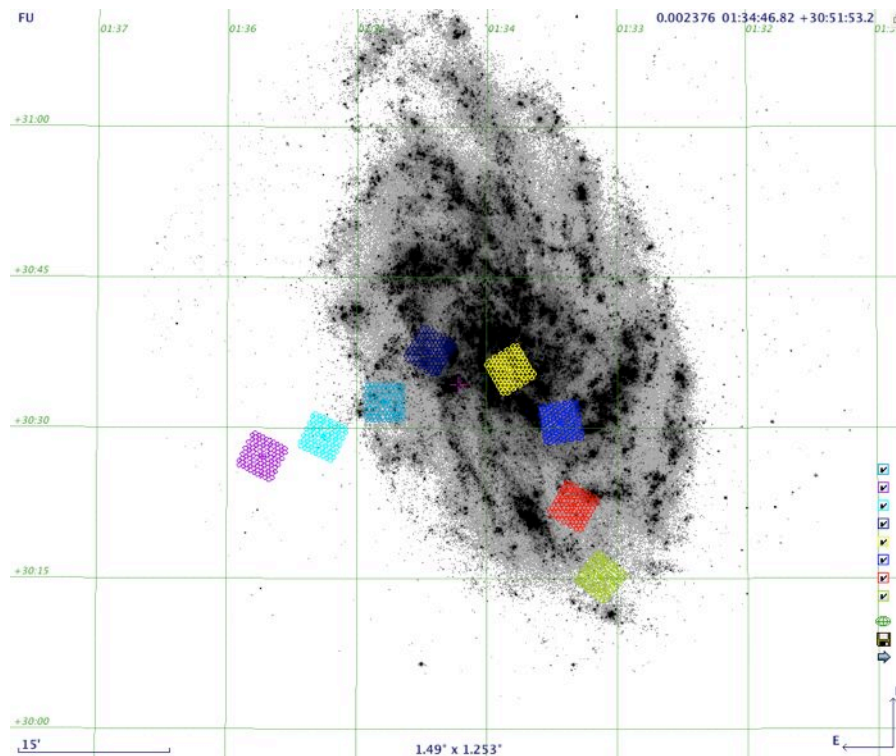


Figure 2.3: Layout of the proposed MEGARA MOS fields on the disk of M33. All except one pointing (in cyan) coincide in position, field-of-view (FOV) and orientation with observations obtained with ACS/HST in at least two bands, F606W and F814W. These will be used to identify potential spectroscopic blends.

2.3.3 Distant galaxies

There are multiple interests within the MEGARA Science Team regarding the study of high-redshift galaxies: Intermediate-redshift Blue Compact Dwarf (BCD), clump-cluster, peas and starburst galaxies and high-redshift proto-clusters. In order to address all these topics with maximum efficiency a MOS with the capability of observing a relatively large number of objects within a small patch of the sky (density ≥ 1 arcmin⁻²) is required. The high number densities of sources accessible with the MEGARA MOS will allow pursuing many of these goals as part of a common observing program (see Section 3.3).



2.3.3.1 *Intermediate-redshift BCDs*

Very little is known on the properties of distant dwarf galaxies. This situation is particularly critical in the range $0.4 < z < 1.3$ since this is the epoch (1) when cosmic SFR density started to decline, (2) the overall galaxy population moved from highly active systems to the current Hubble sequence; and (3) when expansion accelerates. Our main goal here is to take advantage of the good multiplexing ($\sim 100\times$) and optimization for high-number density fields of the MEGARA MOS to carry out an extensive spectroscopic survey of these numerous, but faint dwarf systems between $0.4 < z < 1.3$ (in conjunction with the other studies on Cosmological fields described in Section 3.3). Among the different types of dwarf galaxies we will target BCD candidates as these are expected to show high equivalent widths in emission and central surface brightnesses (Gil de Paz et al. 2003; Gil de Paz et al. 2005).

The goals are to (1) confirm their nature as intermediate-redshift BCDs, (2) determine their dynamical masses (from their emission-line widths), (3) identify those galaxies with galactic winds and (4) analyze their physical properties when possible.

This study requires of intermediate spectral resolutions ($R \sim 6,000$) in order to properly determine dynamical masses for such low-mass systems. Significantly higher resolutions are not advisable as they will imply a large number of spectral setups to cover the emission from the $[\text{OII}]\lambda\lambda 3726, 3729 \text{ \AA}$ doublet in the entire redshift range of exploration ($0.4 < z < 1.3$).

2.3.3.2 *Clump-cluster, peas and starburst galaxies*

Large and massive clumps of star formation have been detected in more than half of the resolved $z > 1$ galaxies in the Hubble UDF (see Elmegreen et al. 2005). These star-forming entities are found in galaxies at all distances in the range $0.07 < z < 5$. They have sizes of about 2 kpc and masses often larger than $10^8 M_{\odot}$. They are so luminous that dominate the appearance of their host galaxies at optical wavelengths. Massive clumps like these are found in galaxies with a variety of different morphologies, from somewhat normal compact galaxies (ellipticals?), spirals, and irregulars, to types not observed locally, including chain galaxies and their face-on counterparts, clump-cluster galaxies (see Elmegreen et al. 2005).

These observations have an interpretation within the framework of the evolution of galaxies, where clump-cluster galaxies are considered as examples of star-forming disks at their earliest stage, and maybe also initial seeds for spiral galaxies and, through mergers, spheroids as well (Elmegreen & Elmegreen 2005; 2006, 2007; Bournaud, Elmegreen, & Elmegreen 2007). In order to model and understand the various feedback mechanisms at these early stages of galaxy disks evolution (see e.g. Tenorio-Tagle et al. 2007, 2010; Silich et al. 2010 and references therein), it is important to determine the kinematics and physical state of the gas in the clumps.

The basic questions to answer here are: do the clumps show ionized-gas features? Do they show signs of negative feedback (e.g., shells, chimneys, winds)? Are they coeval star formation events or the result of continuous star formation? Are there cases of positive star-formation feedback? The main goal of this program is to determine the physical properties of star-forming clumps for galaxies



at different redshifts selected from a Cosmological field such as COSMOS.

We plan to obtain spectroscopy for a large subsample of a few hundreds (~300-400) candidate clump cluster galaxies using MEGARA at GTC. We will use the LR VPHs with $R=6,000$ in order to detect one or several of the most relevant emission lines expected to be present in these galaxies so to perform a basic spectral analysis.

In addition, for a small subsample (half dozen at different redshifts) of well positioned objects in redshift space (as confirmed by the LR observations described above), we aim at obtaining integral-field high-resolution spectroscopy in order to resolve spectroscopically ($\sigma\sim 5-7$ km/s) and spatially (~ 1 kpc/resolution element) the line emission for the most massive clumps present in the galaxies of the sample. The resolved emission line profiles of the star-forming clumps in this galaxy will be analyzed looking for the presence of a single or a double component in the velocity space that will give us important insights on the hydrodynamical state of this object. In addition, by spatially resolving the different clumps using integral field spectroscopy we will obtain information on possible spatial differences where positive/negative feedback takes place. We will use the MEGARA SCB IFU (10×8 arcsec²) with either the HR-R *or* HR-I VPHs depending on redshift, in this case.

2.3.3.3 *High-redshift proto-clusters*

Another objective for which the high number density of objects simultaneously observable with MEGARA MOS is best suited is the identification and characterization of high-redshift proto-clusters of galaxies. Recent studies on the evolution of the properties of galaxies in clusters at $z\sim 1$ have shown (1) that red galaxies still prefer denser environments up to this redshift (Elbaz et al. 2007) and (2) that there are also more bright blue galaxies in over-densities than in the Local Universe (Cooper et al. 2008). However, this has been limited to $z\sim 1$ due to the lack until quite recently of photometric surveys that would allow covering fields large enough to identify the sparse population of high-redshift over-densities (<10 deg⁻²; Eisenhardt et al. 2008) with enough depth. Thanks to the new generation of photometric surveys (e.g. COSMOS, NDWFS, SXDS) some high-redshift over-densities (or proto-clusters) are now being found.

The objective of this program is to spectroscopically confirm high-redshift ($z>1$) over-density candidates extracted from our own photometric database (RAINBOW; Pérez-González et al. 2008a; Barro et al. 2011). The proto-cluster candidates will be observed in the red for $z<1.5$ and in the blue for $z>1.5$, both at intermediate spectral resolutions ($R\sim 6,000$). This intermediate spectral resolution, similar to that of DEEP2 but higher than most spectroscopic surveys, will allow (1) optimizing the detection of the [OII] $\lambda\lambda 3726,3729\text{\AA}$ doublet in between the OH forest and (2) measuring velocity widths (and dynamical masses) down to $\Delta v\sim 50$ km s⁻¹.



2.4 E-Science

Research in astronomy poses two main challenges: 1) the immensity of the sky and 2) the huge amount of astronomical data being gathered. In fact, astronomers are nowadays facing great difficulty in finding the resources to analyze the increasing flood that modern astronomy instruments generate - insufficient computing power, insufficiently powerful software tools, and even insufficient human resources. In order to meet these challenges, an increasing number of astronomical projects have begun to try to foster citizen participation to help analyse data by using collaborative Internet applications (the so-called Web 2.0).

This is context of the GLORIA project, a EU/FP7-funded initiative of the UPM members of the MEGARA Science Team, that aims to build the first open access world wide network of robotic telescopes to serve citizens from around the world for free, but competing for observing time. This means that, users must prove their capabilities in order to get observing time. The principle of this open access network will be *“the more you produce the more observing time you get”*. Calculation of the productivity of a user will be measured automatically thanks to the collaboration of the rest of the users of the network. Hence GLORIA (which stands for **G**LObal **R**obotic telescope **I**ntelligent **A**rray) is indeed an *“Intelligent Array”* and it bases its intelligence in its community. Like most Web 2.0 projects, GLORIA implements a reputation-based scoring system to reward user contributions, driven by parameters such as the quality of the gathered and processed images, number of hours invested in the observations, etc, as well as the votes granted by the rest of the community.

This project will be conducted in the period 2012 - 2014 and by the end of 2013 it will be operational for commissioning. At the end of 2014 the consortium will produce a standard for adding new telescopes and experiments to this network. Whether part of the observing time from any European large telescope (such as VLT, VISTA, etc.), or even GTC, could be eventually be incorporated to GLORIA is still TBD.

2.5 MEGARA Early Science

In order to generate a quick scientific return from MEGARA, the MEGARA Science Team has identified a series of targets and very specific science topics (some of them included in the major science goals of the team, others not) that aim to pursue at the beginning of the scientific exploitation of MEGARA (what we call MEGARA Early Science). These so-called Targets of Interest (ToIs) and the corresponding scientific objectives to be addressed are described in Section 4. The objective of these programs will be also to demonstrate the potential of MEGARA and also to publicize to the GTC community the different capabilities of the instrument. Finally, these observations should serve to fine-tune future observing programs in terms of both exposure time and spectral configurations to be used.

3. MEGARA SCIENCE

3.1 MEGADES: MEGARA Galaxy Disks Evolution Survey

3.1.1 Motivation

While the basic aspects of stellar evolution are relatively well understood since last century, the basics of galaxy evolution are still of intense debate and disagreement within the astronomical community. This is basically a consequence of the fact that the typical distance between galaxies relative to their own size is much lower than in the case of stars, so the vast majority of galaxies (even those in the field) have not evolved in perfect isolation for their entire life, especially at early epochs, where the Universe as a whole was much denser than it is today. In addition, some "internal secular" processes that take place in galaxies are actually episodic and might have actually being triggered by the interaction with the environment, such as nuclear activity or very active star formation. Although these mechanisms are considered to be secular (according to the definition of secularity used by Kormendy & Kennicutt 2004) they leave a marked and highly unpredictable imprint on the subsequent evolution of these objects, which contribute to differentiate the evolution of galaxies one from another. In Figure 3.1 we show a diagram that lists and relate the different mechanisms, internal and external, secular and non-secular that play a role on shaping the properties of current-day galaxies.

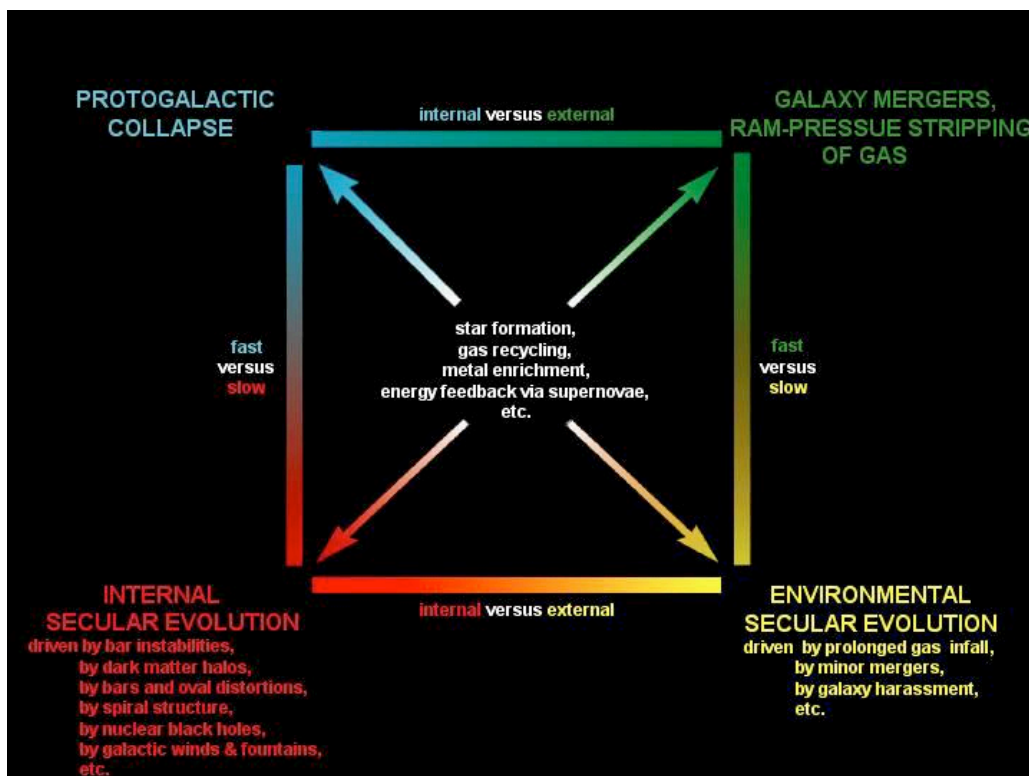


Figure 3.1: Diagram by Kormendy & Kennicutt (2004) where the different mechanisms shaping the current-day properties of galaxies, along with the connection between them, are listed.



As the relative contribution of all these mechanisms is difficult to establish, either in individual galaxies or in the galaxy population as a whole, the evolution of galaxies is in many aspects still a puzzle.

One of the main scientific goals of the MEGARA Science Team is to contribute to start putting together some of the pieces of that puzzle. In particular, we aim to understand how secular processes; both internal, such as stellar migration, nuclear activity or starbursts, and external, e.g. gas in-fall, satellite accretion and minor mergers, shape the spectro-photometric, chemical and kinematical properties of present-day disks.

3.1.1.1 *Secular evolution of disks: the inside-out scenario*

As we have commented above, the evolution of galaxies is a complex process as many are the mechanisms that might alter their present-day photometric, chemical, and kinematical properties: monolithic collapse, major and minor mergers, bars, rings, density waves, stellar diffusion, gas in-fall, and, in the case of galaxies in clusters, also ram pressure stripping and galaxy harassment (see Figure 3.1 above). Despite this rather discouraging scenario, in the case of the formation of the disks in galaxies a picture has emerged in recent years that attempts to explain most of their observational properties: During the first several Gyr of history ($z > 1$) and possibly following some level of monolithic collapse the evolution of disk galaxies is dominated by frequent (mostly minor) mergers, which lead to the formation of what it is known as the thick-disk component. After that period the frequency of mergers decreases and the disk becomes dynamically cooler allowing for the formation of the so-called thin-disk component. During the evolution of the thin disk (at $z < 1$) the high angular momentum of the gas in the outer parts of the disks results in a delayed gas in-fall and star formation activity in these regions compared to the inner disk. This is known as the *inside-out* formation scenario for galaxy disks.

Although initially proposed to explain the G-dwarfs metallicity distribution of stars in the Milky Way (Lacey & Fall 1985; Matteucci & Francois 1989), this scenario is also a key prediction of the Λ CDM paradigm of galaxy formation. As an example, in Figure 3.2 we show the evolution of a massive disk galaxy simulated by Samland & Gerhard (2003). Their three-dimensional model follows the chemo-dynamical evolution of this galaxy in a Λ CDM universe.

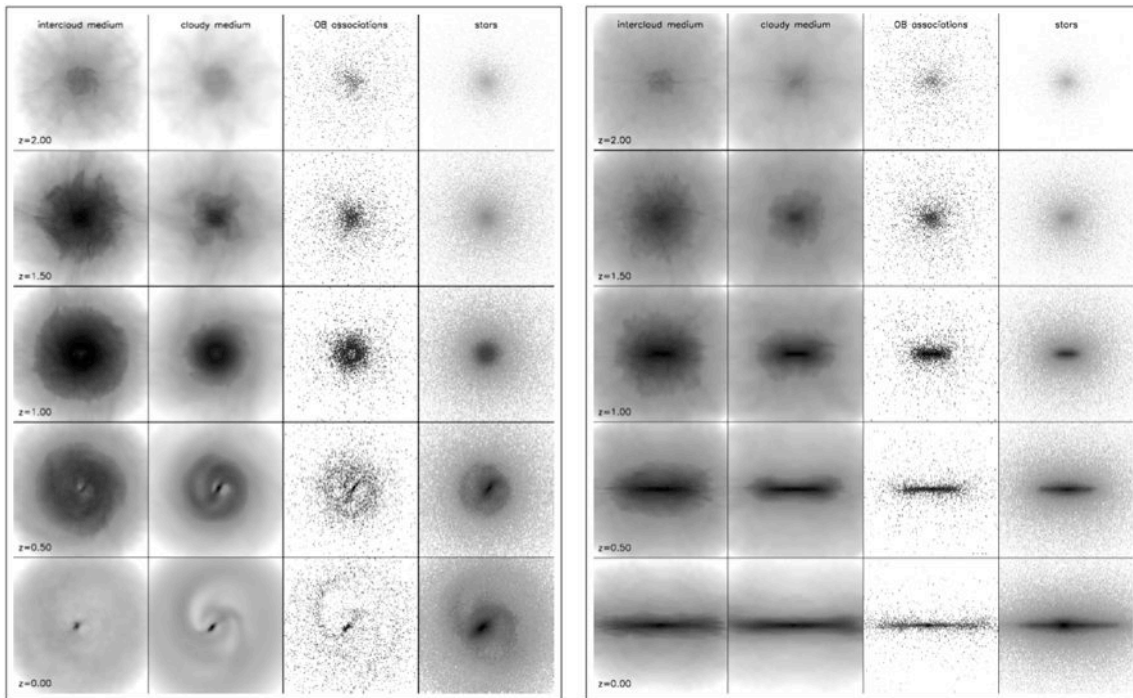


Figure 3.2: Results of the dynamical simulations of Samland & Gerhard (2003), showing the inside-out evolution of a massive disk-like galaxy, viewed face-on (left) and edge-on (right). Each column shows the evolution with redshift of the spatial distribution of ionized gas, the cloudy medium, the associations of young OB stars and the total stellar surface density.

The dissipation and collapse of the gas clearly takes place in an inside-out fashion. First, the stellar halo is formed early through a rapid collapse at $z > 1.5$. Between $z = 1.5$ and $z = 1$ a thick disk appears. Later, the bulk of the star formation takes place mainly in the thin disk. The progressive flattening of the gas component and the OB associations nicely illustrates this. Due to its larger angular momentum gas in the outer disk collapses on longer timescales than in the central regions. As a result, the distribution of newly born stars not only gets vertically flatter, but also more radially extended as star formation shifts outwards.

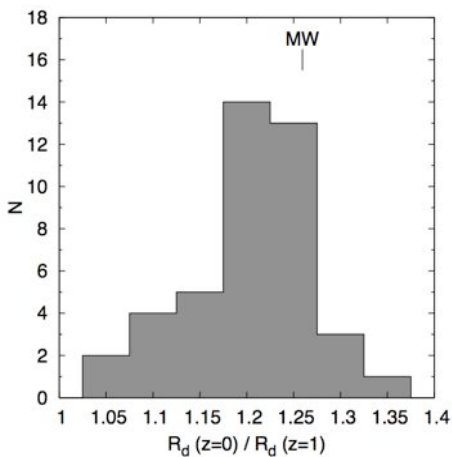


Figure 3.3: Histogram showing the relative growth of nearby disks between $z = 1$ and $z = 0$. These show a median growth of $\sim 25\%$ (Muñoz-Mateos et al. 2011). Results obtained from the fitting of multi- λ radial surface-brightness profiles of the SINGS sample (Kennicutt et al. 2003) to the predictions of the disk models of Boissier & Prantzos (1999). These models assume a gas in-fall parameterized by the total mass of the galaxy halo and its specific angular momentum.



Although the theoretical predictions of the *inside-out* scenario in the case of external galaxies were formulated some time ago now (e.g. Boissier & Prantzos 1999, Mollá et al. 1999), it has been only recently that inside-out growth of galaxy disks has been quantified observationally. The color, dust-to-gas ratio, and metallicity gradients in nearby galaxies (Muñoz-Mateos et al. 2007, 2009ab, 2010; Zaritsky et al. 1994) and the weak dependence of the mass-size relation with redshift (Trujillo et al. 2004, 2006) are both in broad agreement with the predictions of the inside-out scenario for the evolution of disks. Quantitatively speaking, both types of studies yield an increase of $\sim 25\%$ in size between disks at $z \sim 1$ and at present (see Figure 3.3).

While the inside-out scenario has served to successfully reproduce many of the observational properties of galaxy disks, mainly coarse properties, such as color and metallicity gradients, and restricted to a specific radial range within galaxies, there is cumulative evidence that such scenario cannot predict neither the details of these properties (in terms of spatial resolution, chemical abundances and certainly kinematics) nor even coarse properties across the entire face of the disks. In this regard, significant departures from the predictions are found in many objects both in the inner and very outer parts.

Below we describe some of the internal secular mechanisms that could be responsible for departures in the observational properties of the disks compared with the predictions of the inside-out scenario.

3.1.1.2 *Secular evolution of disks: stellar migration*

The availability of large imaging datasets on nearby galaxies at all wavelengths from the UV to the FIR (mainly from GALEX, SDSS, 2MASS, Spitzer) have recently led to a significant progress in the study of nearby disk galaxies. In addition to the possibility of inferring the radial-dependence of the history of star formation in numerous systems, the unprecedented quality and depth of these datasets have allowed to reach the outer edges of disks, where the predictions of the simple *inside-out* model outlined above could face its most severe challenges.

In this regard, the analysis of a large sample of spiral disks observed as part of the Sloan Digital Sky Survey (SDSS) by Bakos et al. (2008) have revealed U-shaped color profiles near the position where the galaxy surface brightness decreases abruptly (Figure 3.4). This work demonstrated that while in the inner disk the profiles show the expected bluing towards the outer regions, this trend reverses as we move beyond the break in surface brightness. Yoachim et al. (2010) have recently confirmed these results using radial profiles in spectroscopic indices using IFU observations of the nearby disk galaxy NGC 6155.

Other recent results that challenge the standard predictions of the inside-out scenario refer to the metallicity gradients in the outer parts of disks. The inside-out scenario predicts a roughly constant negative gradient throughout the entire galaxy disk. The analysis of the outer disks of M33, NGC 300, or M83 among others, however, indicate a flattening or even a reversal in the metal abundance gradient (either of the stars or the ionized gas) that cannot be explained by a simple inside-out growth model (Mendes de Oliveira et al. 2004; Barker et al. 2007; Vlajic et al. 2009; Bresolin et al. 2009; see Figure 3.5).

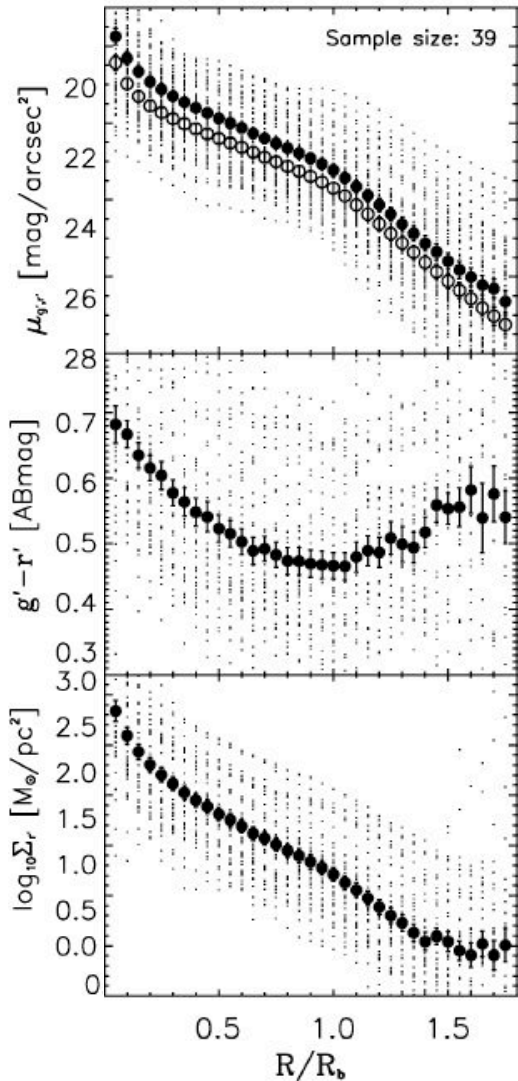


Figure 3.4: Surface-brightness (top), color (center), and stellar mass density (bottom) radial profiles of nearby galaxies observed as part of SDSS (Bakos et al. 2008). Only galaxies showing a down-bending) in their surface brightness profiles are shown here.

Figure 3.5: Metallicity gradient from the analysis of the single-star CMDs in NGC 300 (Vlajic et al. 2009).

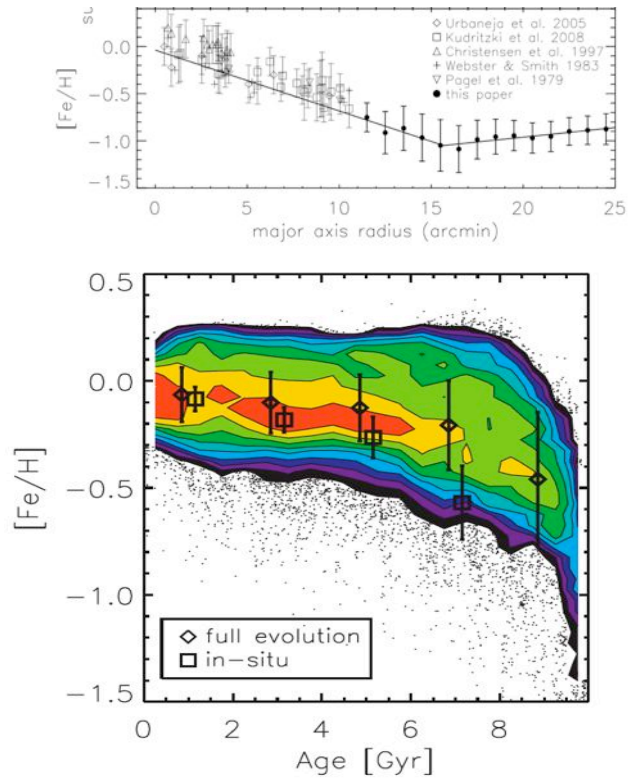


Figure 3.6: Age-metallicity distribution of stars in the Solar neighborhood color coded by the density of stars. The open boxes and the corresponding errors bars represent the mean values and dispersion in $[Fe/H]$ for a given age considering only stars formed in-situ, while the open diamonds and their errors bars correspond to the values obtained with the full N-body simulations of Roskar et al. (2008).

In our own Milky Way, the simple *inside-out* scenario has also failed to explain the shape of the age-metallicity distribution of stars in the Solar neighborhood, the dispersion in age predicted at a given metal abundance being significantly narrower than that observed (see Figure 3.6).

In summary, three are the main observational evidence that challenge the picture of an evolution based exclusively on the inside-out scenario: (1) the behavior of the color profiles in the outer regions of disks, (2) the flattening of the metallicity gradients, (3) and the dispersion in the age-metallicity distribution of stars in the Milky Way. The possible explanations that have been put forward up to now are based on the predictions of different flavors of state-of-the-art high-resolution N-body simulations of disks. Regarding the presence of departures in the inner regions of disks we refer the reader to Sections 3.1.1.3 and 3.1.1.4.



Predictions from idealized N-body simulations of galaxy disks

The N-body simulations by Roskar et al. (2008) predict a drop in SFR and stellar density in the outer regions of the disks with the presence of stars beyond this break being exclusively due to stellar migration. According to this model, as we move further out beyond the break we find progressively older stars, which have been migrating for a longer period of time, leading to a positive age and color gradient in these regions. This is in nice agreement with the observational results from Bakos et al. (2008). Noteworthy, these models are also able to reproduce the dispersion of the age-metallicity distribution of stars in a Milky-Way-like disk (see Figure 3.6).

In the case of the Roskar et al. model stellar migration is mainly due to a mechanism known as *churning*: Sellwood & Binney (2002) demonstrated that a star just outside (inside) the corotation radius can be caught in the spiral arm resonance and transported inward (outward) while preserving the circularity of its orbit. They also showed that transient spiral arms are at peak strength only for long enough to produce a single crossing from one side of the corotation to the other for each star. As a consequence, a large number of stars are scattered away from their birth radii. In the particular case of the Milky Way recent works suggest a high frequency of transient spiral arms (Baba et al. 2009). The frequency of the transient spiral arms in external galaxies is thought to be a sensitive function of the disk-mass fraction given that both the arm-interarm contrast and the magnitude of the potential fluctuation generated by a given contrast increase with the disk-mass fraction (Sellwood & Binney 2002).

Figure 3.7 shows the dramatic impact that stellar migration has on the *effective* Star Formation History of disks (compared to the *in-situ* SFH). If these predictions are confirmed for the bulk of the population of disks our current ideas on the chemical, spectro-photometric, and kinematical evolution of spiral galaxies, which have been traditionally based on the assumption of negligible radial mixing, should be revised.

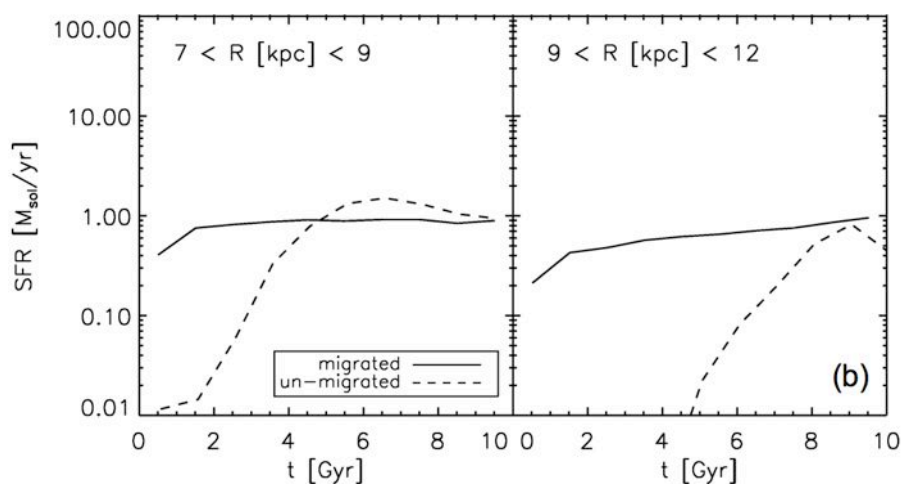


Figure 3.7: Comparison between the Star Formation History of the galaxy disk simulated by Roskar et al. (2008) with (solid-line) and without stellar migration (dashed line) at the approximate galactocentric distance of the Sun (left) and in the outer regions of the disk (right).

Note that the simulation of Roskar et al. (2008) was performed under idealized conditions, where the disk grows *by construction* in an inside-out fashion and where star formation is



virtually suppressed beyond the position of the break in the galaxy surface brightness profile. Hence, the stars beyond the break in their model must have migrated there. While these controlled, high resolution simulations are necessary to study many of dynamical processes having place on the disk, it is also important to compare these predictions with those obtained in a fully cosmological context, where hot and cold modes of gas accretion and the effects of mergers and interactions are included.

Predictions from fully cosmological N-body simulations of individual galaxy disks:

On the other hand, there are now available in the literature a few fully cosmological, high-resolution, N-body simulations of individual disks such as those carried out by Sánchez-Blázquez et al. (2009) and Martínez-Serrano et al. (2009).

In the case of the disk simulated by Sánchez-Blázquez et al. (2009) the reddening in the outermost regions of the surface brightness profiles is due to a sharp decrease in the SFR in these regions associated to a decrease in volume gas density likely induced by the warping of the HI disk. This model also shows a down-bending in the galaxy (blue) surface brightness profiles at the position of this star formation threshold. Although not responsible for the shape of the color profiles, migration also accounts for a large fraction of the stars beyond this break (up to $\sim 60\%$) and minimizes the magnitude of the break in the stellar mass density profile. Given the high mass of the disk simulated in this work, the main mechanism responsible for stellar migration in this case is *heating*. Through this mechanism the spiral structure (transient or long-lived arms) and molecular clouds can gradually heat stellar disks, moving stars towards more inclined and eccentric orbits and changing the overall angular momentum distribution of the disk. Stars that are on eccentric orbits are at different radii at different phases of their orbits and, therefore, tend to naturally produce some radial mixing. However, the radial excursions due to this mechanism are not sufficient to explain the flat age-metallicity relation in the solar neighborhood (Sellwood & Binney 2002). Typical radial variations for a population of stars with a radial velocity dispersion σ_r are $\Delta R \approx \sqrt{2}\sigma_r/k$, where k is the epicyclic frequency; for the old stars in the Milky Way the maximum value for the excursions near the Sun is $\approx 1-1.5$ kpc. In more massive and hotter disks, such as the one simulated in Sánchez-Blázquez et al. (2009), the average length of these excursions is ~ 3 kpc.

Other effect besides radial stellar migration that is associated with the *heating* of a galaxy disk is an overall increase in σ_z (the vertical component of the stellar velocity dispersion) as stars are moved towards more inclined orbits. This would be noticeable when comparing the σ_z values (or line-of-sight velocity dispersion in face-on disks) of stars of different ages (Lacey 1991).

Although, as Sánchez-Blázquez et al. (2009) themselves pointed out, *heating* is likely the main mechanism responsible for stellar migration in their simulated disk, *churning* and angular momentum transfer induced by merger-driven gas inflows might also playing a role (Young et al. 2007). Disentangling the relative contribution of these mechanisms to the net radial migration of stars in galaxy disks is challenging but should be addressed.

All these results show that in order to advance in our understanding of the evolution of disks it is mandatory that we determine the actual role of stellar migration (and the mechanism(s) responsible for it) and compare its effects to those due to the time evolution in the position of

the threshold of star formation. In Section 3.1.3.1 we will discuss how MEGARA will allow us (1) to quantify stellar migration and the mechanism(s) that drives it and (2) to determine what leads the observational properties (colors and metal abundances) of galaxy disks beyond the star formation threshold: migration or evolution in its position with redshift.

3.1.1.3 Secular evolution of disks: galaxy-to-galaxy variations

Until recently very few observational data had been put forward to test the predictions of the inside-out scenario of the formation of galaxy disks, except in the case of the Milky-Way disk. The few observational tests carried out so far in external galaxies have been focused on the analysis of individual objects. Muñoz-Mateos et al. (2007) studied for the first time a large sample (161 objects) of disk galaxies in the context of the inside-out scenario of disk formation. This work showed that in the *inner* disks, where one would expect a negative gradient in color (or equivalently in age or specific SFR; sSFR) even when significant migration could be present, galaxies show a large dispersion in sSFR gradient with many galaxies showing null or even negative sSFR gradients (or equivalently positive color gradients; see Figure 3.8).

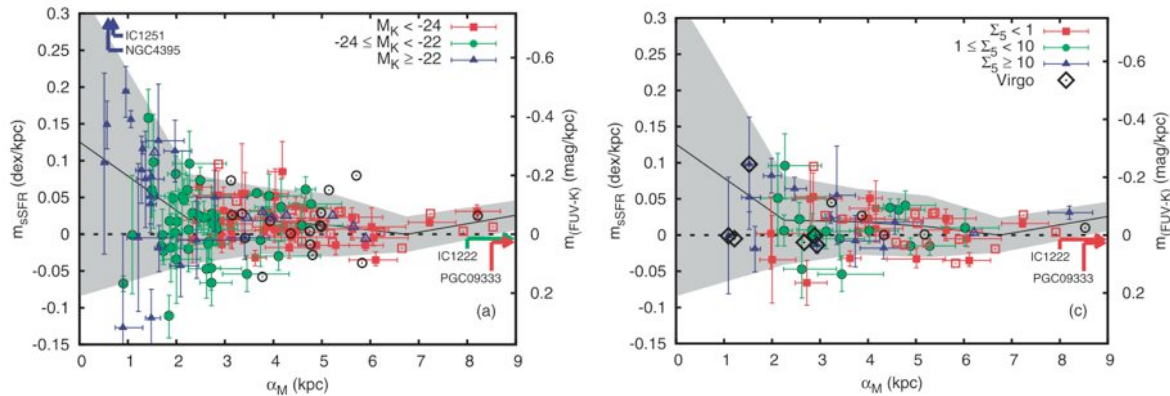


Figure 3.8: Left: Specific SFR gradients in a sample of nearby spiral disks. Positive values of m_{sSFR} mean inside-out formation while negative values correspond to galaxies growing outside-in (shrinking). Symbols are coded by K-band luminosity. Right: The same with the galaxies coded by the environmental density parameter Σ_5 (Muñoz-Mateos et al. 2007).

While some of the dispersion in the sSFR gradient could be due to intrinsic differences in the mass or specific angular momentum of the dark matter halo where the galaxy resides (Muñoz-Mateos et al. 2010), negative sSFR gradients cannot be explained within the *inside-out* scenario of disk formation. In this regard, it is worth mentioning that in the N-body simulations by Sommer-Larsen et al. (2003) some of the disks modeled seem to have formed from *outside-in*, i.e. they would show negative sSFR gradients.

In the case of the few cluster disk galaxies observed and analyzed so far in this context, the reversal in the color and sSFR gradients has been interpreted as due to ram pressure stripping



that effectively removes the gas from the outer parts of the disks and reduces the SFR in these regions, which then become redder (Boselli et al. 2006). However, except for these few Virgo cluster galaxies included in the Muñoz-Mateos et al. (2007), which show slightly negative sSFR gradients, no dependence with the environment was found using either the projected local density, estimated using the Σ_5 parameter (Balogh et al. 2004), or the projected distance to the nearest neighbor with mass larger than 0.2 times the mass of the galaxy itself. As we comment below, satellite accretion and, in some cases, minor mergers are mechanisms that might also mimic the properties of an outside-in formation in a disk, including the possibility of showing negative sSFR gradients.

3.1.1.4 *Secular evolution of disks: satellite accretion and minor mergers*

One of the aspects of the evolution of galaxies that is obviously beyond the reach of the inside-out scenario for the formation of disks is the relevance (in terms of stellar mass or surface brightness) and final location of stars that were originally formed in orbiting or merging satellites. The Λ CMD paradigm for the evolution of the dark matter halos in the Universe predicts the existence of large numbers of low-mass halos orbiting present-day massive galaxies. Although the exact number of these halos is still matter of intense debate (see e.g. Koposov et al. 2009) there are certainly numerous known dwarf satellites around galaxies like our own Milky Way. While, according to state-of-the-art N-body simulations, averaged over a long period of time these satellite accretion events and minor mergers (with or without stars or gas) are likely to lead to an inside-out disk growth, they should leave a specific imprint on some of the observational properties of disks, both in their inner regions and in their outskirts⁴.

Minor-merger remnants

The light distribution and kinematics of disks contain a wealth of information on the recent history of disk galaxies. These properties have revealed numerous structures associated to these regions, including distinct inner disks, stellar (or gaseous) rings, dust lanes, nuclear spirals, and nested bars (Scorza & van den Bosch 1998, Moiseev et al. 2004). In particular, inner disks are frequent components in S0-Sab galaxies. Erwin & Sparke (2002) found kiloparsec-scale inner disks in $\sim 20\%$ of a sample of barred S0-Sa galaxies, and Peletier et al. (2007) have detected them in almost all Sa-Sab's in a sub-sample of the SAURON survey. Moreover, the majority of lenticulars exhibits fast-rotating, disk-like cores, instead of slow-rotating bulges (Cappellari et al. 2007). Being these inner, kinematically-cold components so common in the centers of early-type disk galaxies, it is still unknown how they are formed.

Numerical simulations have shown that several internal secular processes can form inner disks, such as gas inflow through a bar, bar dilution, and star formation in rings that shrink in radius towards the galaxy center with time (Combes et al. 1992, Norman 1996, Englmaier & Shlosman 2004). However, bar evolution alone is insufficient to explain the mass concentrations hosted by the bulges of early-type galaxies (Debattista et al. 2006). Recently, N-body models have shown that secular evolution can be induced externally to the galaxy too. Minor mergers can

⁴ We differentiate between satellite accretion and minor mergers simply based of the timescale of the event.

structurally transform a Sb or Sc galaxy into a S0, generating inner disks and rings in the remnant at the same time through the coupling of the satellite disruption with the evolution driven by transient spirals and bars induced by the merger (these later processes are commonly ascribed to internal secular evolution, see Eliche-Moral et al. 2006, 2011, 2012; Figure 3.9).

The noticeable capability of minor mergers in triggering secular evolution in galaxy disks derived from numerical simulations and the high number of these events observed (Lotz et al. 2011) both point out towards minor mergers playing major role in the formation of inner disks and rings in early-type galaxies. However, the role of minor mergers in the generation of these dynamically-cold inner substructures is still unknown. It is worth noting that this is a critical issue also because the formation mechanism of the inner disks is likely responsible for the growth of galactic bulges as well.

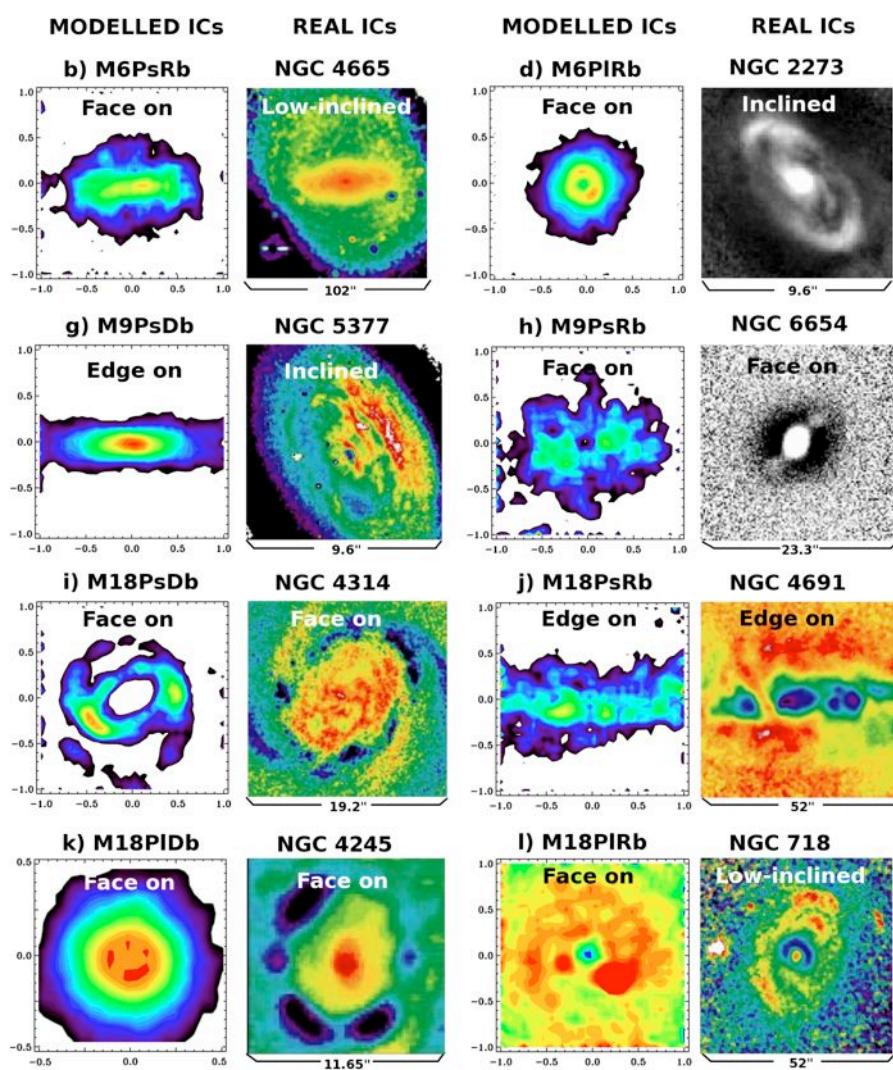


Figure 3.9: Comparison of some inner rings and disks formed in the minor merger simulations by Eliche-Moral et al. (2011) to some structures with similar morphologies detected in some early-type galaxies (1st and 3rd columns and 2nd and 4th columns, respectively). Colored maps of real galaxies correspond to B–R or V–I color maps of the galaxies by Erwin & Sparke (2003), while the grey-scale maps represent unsharp masks in V, R or H bands by the same authors.

Satellite bombardment

When a disk has been exposed to the bombardment from relatively massive subhalos signatures of those events are expected, either in the morphology (Kazantzidis et al. 2008; see Figure 3.10), e.g. the Monoceros Ring in our own Milky Way, or in the stellar kinematics (Kazantzidis et al. 2009; see Figure 3.11). In particular, as shown in Figure 3.11, the bombardment of disks yields a clear increase in σ_z in the outer parts of disks, which can be measured if the spectral resolution (in σ) is better than $\sim 10\%$ the galaxy circular velocity.

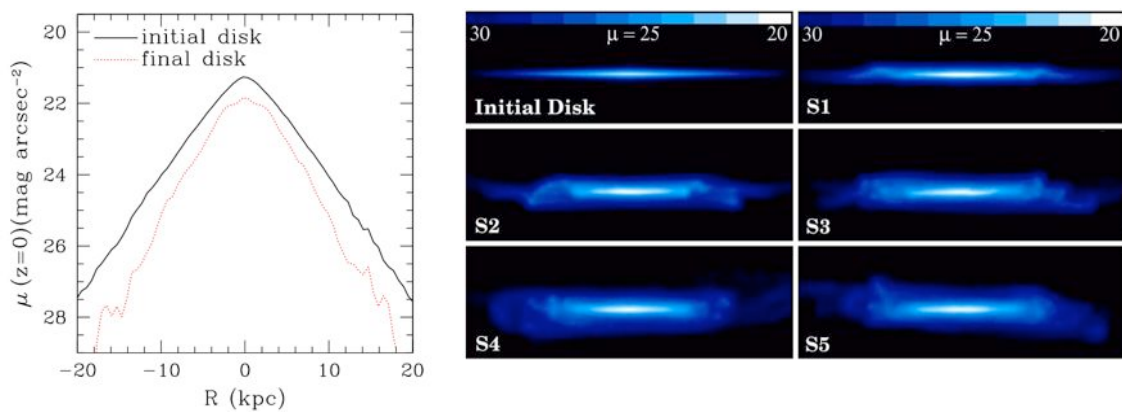


Figure 3.10: Evidence for disk flaring in the simulated disk after several consecutive passages of a satellite (Kazantzidis et al. 2008). Left: Edge-on surface brightness profiles of the stellar disk as a function of projected radius. Right: Edge-on view of the 3D simulations.

While this increase in the different components of the velocity ellipsoid (mainly in σ_z) in the outer parts of the disks with relatively massive orbiting satellites is primarily due to the heating of the stars already in the disks, stars from the satellites themselves can also be accreted, leading to a change in the properties of the outer disks that also compete with the effects of migration and *in-situ* star formation. These stars would also inherit the distinct kinematics of the galaxy halo (see Casertano et al. 1990) and well-differentiated chemical abundances and abundance ratios. In this latter regard, the results of Cooper et al. (2010) indicate that the stars accreted from orbiting satellites should yield flat or negative metallicity gradients, opposite to the effects expected from stellar migration.

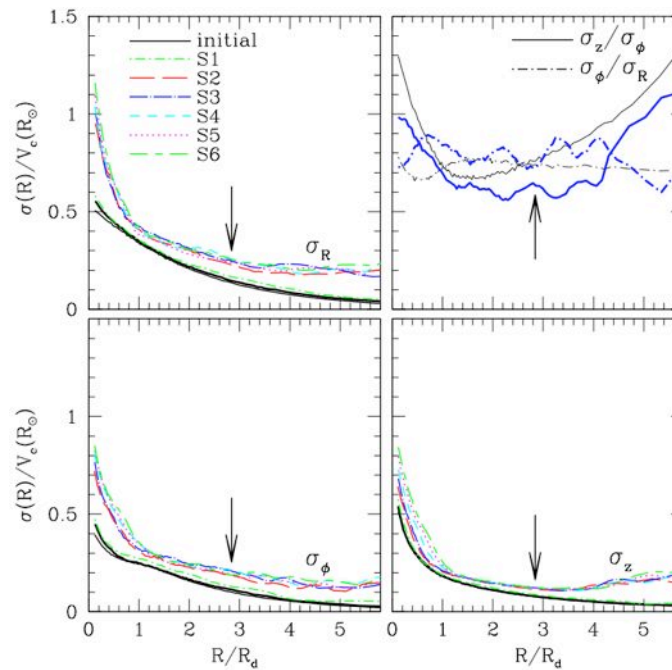


Figure 3.11: Velocity dispersion profiles of the disk simulated by Kazantzidis et al. (2009) as a function of projected radius in units of the radial scale length of the initial disk. Color lines represent the profiles after each consecutive satellite passage. Note the raise in σ_z in the outer parts of the disk. In the upper right panel the velocity dispersion ratios σ_z/σ_ϕ (solid lines) and σ_ϕ/σ_R (dot-dashed lines) are shown for the initial (thin lines) and final (thick lines) disk. Bombardment heats the thin galactic disk considerably in all three directions and causes its velocity ellipsoid to become more anisotropic.

3.1.1.5 Secular evolution of disks: spatial distribution of metals in galaxy disks.

One of the first observables used to validate the predictions of the inside-out scenario was the spatial distribution of metals across galaxy disks. As commented above, this scenario was initially proposed to explain the G-dwarfs metallicity distribution of stars in the Milky Way (Lacey & Fall 1985; Matteucci & Francois 1989) and has been confronted since then with numerous measurements of metallicity gradients in the disks of nearby galaxies (Zaritsky et al 1994; Pilyugin, Vilchez & Contini 2004. Moustakas et al. 2010; see Figure 3.12).

In general, the metallicity distribution in galaxies constitutes a basic record to determine the role played by secular evolution processes in galaxy evolution as each of the processes listed in Figure 3.1 is expected to spatially distribute the metals, mainly radially but also at smaller physical scales, in a different way. The study of the 2D metallicity distribution in galaxy disks also provides us with clues to analyze the efficiency of chemical enrichment, to test the prescriptions of stellar nucleosynthesis as well as the degree of gaseous mixing and metal dissemination in the interstellar medium. Therefore, by measuring the abundance of metals in galaxy disks with spatial resolution MEGADES will provide fundamental information not only on the processes shaping the evolution of disks but also on the physics of the interstellar medium.



HII regions as metallicity tracers

When massive stars are formed they ionize their surrounding gas producing the observed large variety of morphologies of ionized-gas (or HII) regions, as well as their characteristic emission line spectra. Giant HII regions in spiral and irregular galaxies have been observed for long time now, with spectroscopy of these objects obtained by some pioneering works as early as the 1940's (e.g. Aller 1942). Subsequent seminal work on spectroscopy of extragalactic HII regions was carried out by Smith (1975), Shields and coworkers (e.g. Shields and Searle 1978, McCall et al 1985), Kwitter and Aller (1981) and by Pagel and collaborators in the 80-90's (e.g. Pagel et al 1979, 1980; Vilchez et al 1988; Diaz et al 1991), among others. Thus spectroscopy of giant HII regions in galaxies has remained an essential tool for the determination of the metallicity of the (ionized) ISM (Zaritsky et al 1994; Vilchez and Iglesias-Paramo 1998; Esteban 2002; Bresolin et al 2005; Bresolin et al 2010 among others). The knowledge of ISM abundances and their variations across disk galaxies is a key ingredient for the study of the chemical evolution; among other things because they can be determined much further away than single-star abundances and it is not affected by the severe degeneracies associated to the determination of stellar abundances from the spectra of unresolved stellar populations.

During the last years a considerable amount of work has been carried out obtaining and refining gas-phase element abundances and abundance gradients in galaxies. It is now well known that spiral galaxies typically present a negative radial gradient of chemical composition, with the highest abundance values localized towards their centers, reaching between solar and two times solar values, in agreement with the broad predictions of the inside-out scenario of galaxy disk evolution in this regard (see e.g. Boissier et al. 2003). This points to the gas in-fall as the main (but not only, as we will show later) process shaping the chemical evolution of disks.

On the other hand, irregulars and dwarf galaxies in general do not show measurable abundance gradients, suggesting a substantial degree of chemical homogeneity for the composition of their ISM.

The amount of work on abundances and gradients in relatively nearby spiral galaxies has been increasing over the last years. Moreover, recent works have recently derived metal-abundance distributions for an increasing number of distant galaxies allowing cosmic chemical evolution of galaxies to be studied (e.g. Erb et al. 2006; Mannucci et al. 2009; Jones et al. 2010). This, in principle, could allow us to investigate the epoch where other process beyond secular gas-infall (e.g. major mergers or monolithic collapse) could dominate the early evolution of disks. Thus, these recent findings suggest that $z > 2$ galaxies could have formed their disks during an inside-out process combined with important amounts of gas inflow in their very initial phases (cf. Jones et al. 2010; Cresci et al. 2010).

Despite this remarkable progress, measurements of 2D metal abundances, gradients and central metallicities are still scarce, even in the case of nearby galaxies. MEGARA will arrive most timely to attack this problem, extending to larger and more distant samples the methodology applied to giant extragalactic HII regions. As part of MEGADES we aim (1) to expand the range of parameters of the galaxies where metallicity distributions have been measured, (2) to explore the well-known abundance discrepancies by analyzing in detail a number of very nearby

systems, and (3) to analyze the impact of chemo-dynamical effects on the abundance determinations. All these objectives are part of the ultimate goal of using the ionized-gas abundances as a testimony of the processes that contribute to the evolution (chemical in this case) of galaxy disks.

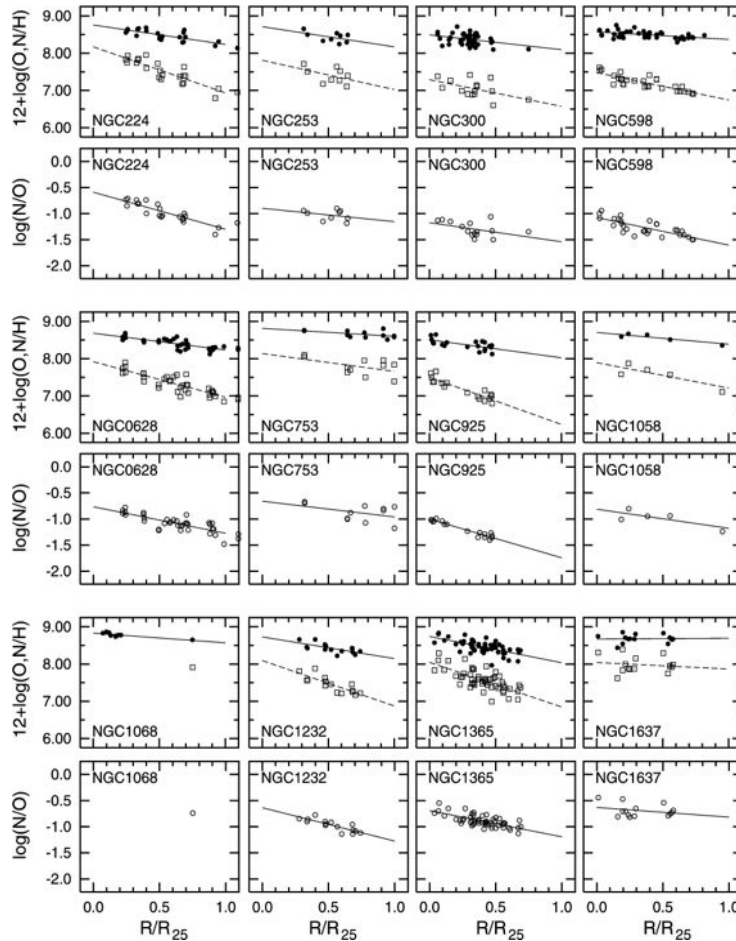


Figure 3.12: Examples of radial abundance gradients of oxygen and nitrogen, and corresponding N/O ratio, versus galaxy radius, normalized to the galaxy radius at the $\mu_B=25$ mag arcsec $^{-2}$ isophote, derived for a sample of spiral galaxies. Adapted from Pilyugin, Vilchez & Contini (2004).

Massive stars as metallicity tracers

A- and B-type supergiants are visually the brightest stars, permitting their detailed spectroscopic analysis at distances well beyond the Local Group. The spectra of these stars display features belonging to a large number of elements: B supergiants show lines of C, N, O, Si, Mg, and Ca, and A supergiants add Na, Fe, Ni, Ti to the list. Therefore, we can use these stars to study the chemical composition of very nearby galaxies with unprecedented accuracy and spatial resolution. Therefore, this kind of analysis is complementary to that to be carried out on extragalactic HII regions that we described above.



Metal enrichment: ISM homogeneity and chemical mixing

It is now well known that the interplay between massive stars, sources of new metals, and the dust and gas surrounding star clusters, presents a very rich phenomenology and a complex structure in star forming regions.

In this context, the identification of the mechanisms giving rise to the mixing of the new metals into the ISM in galaxies still is a matter of great debate. This is a critical aspect of the chemical enrichment process in galaxies that needs to be addressed. In this regard, detailed 2D studies of HII regions in nearby galaxies are much needed. This study will be a fundamental piece of work for our understanding of the process of chemical enrichment of the interstellar medium in galaxies. Although there are few theoretical models for the dissemination and mixing of newly synthesized metals into the ISM (Tenorio-Tagle 1996; de Avillez et al. 2002) they are not necessarily consistent; thus there is an urgent need for strong observational constraints on this issue, and MEGARA can contribute to this important niche in the near future.

3.1.1.6 Secular evolution of disks: starburst activity

As commented above, the interplay between the stars and the surrounding ISM in regions of massive star formation has a profound impact on the chemical evolution of disks. More dramatically, in cases of very active massive star formation even the rate of formation of subsequent generation of stars might be affected by such interaction, either promoting (positive feedback) or quenching star formation (negative feedback).

Bursts of star formation or starburst are events where hundreds of solar masses per year are transformed into stars. Some of them end up expelling enriched material, processed during the starburst, to the intergalactic medium via the so-called Super Galactic Winds (SGW). Indeed, observations have shown that superwinds are found in a wide variety of actively star-forming galaxies (Marlowe et al. 1995, Rossa & Dettmar 2003, Heckman et al. 1990, Martin 2005). Although the timescale for these events is much smaller than a Hubble time their impact on the host galaxies makes them an essential phenomena in the study of galaxy evolution, and thus, in the evolution of the Universe. SGWs are in fact considered as the principal mechanism responsible for the presence of metals in the intergalactic medium (Veilleux et al 2005). In spite of their importance for galaxy evolution, the nature of SGWs is still unclear. Question such as which conditions trigger them, how energetic are they, what mass, momentum, energy, and metals do they transport, still lack a clear answer.

M82-like Super Galactic Winds

From the observational point of view, the nearby galaxy M82 has provided us with possibly the best example of SGW in the Local Universe. The characteristic kpc-size biconical and filamentary structures typical of SGW expanding perpendicular to the host galaxy are clearly seen. They are thought to be the result of mechanical energy released into the interstellar medium by a nuclear starburst. Besides, spectroscopy shows that SGWs are characterized by extended emission in H α and other emission lines with several kinematic distinct components

that reveal velocities from hundreds up to a few thousand kilometers per second.

From the theoretical point of view, the extended structure associated to SGWs has been modeled using 2D hydrodynamical calculations (e.g. Tomisaka & Ikeuchi 1988). In these calculations, biconical structures may develop once the starburst has generated a remnant that exceeds the dimensions of the galaxy disk, causing it to blowout. However, the predicted X-ray luminosity is more than 3 times lower than observed (Strickland & Stevens 2000) and also, the predicted complex filamentary structure at large distances from the galactic disk is in clear contrast with the H α filamentary structure in M82. New models (Tenorio-Tagle & Muñoz-Tuñon, 1997, 1998) taking into account the infall of material into the center of the starburst are obtaining more realistic solutions.

Space-based HST observations revealed that often a burst of stars shows up in the form of a very compact and luminous cluster, the superstar clusters (SSCs). However, all calculations in the literature modeled SGWs as being produced by a single central cluster that spans tens of parsecs. More recent 2D hydrodynamic models (Tenorio-Tagle et al 2003, Silich et al. 2003, Silich et al. 2004, Tenorio-Tagle et al. 2005) have shown that the interaction of the winds produced by neighboring SSCs, give rise to the filamentary structure observed in M82 (see Figure 3.13). Besides, as a result of the interaction between the winds the material is funneled in an auto collimated way, towards the intergalactic medium.

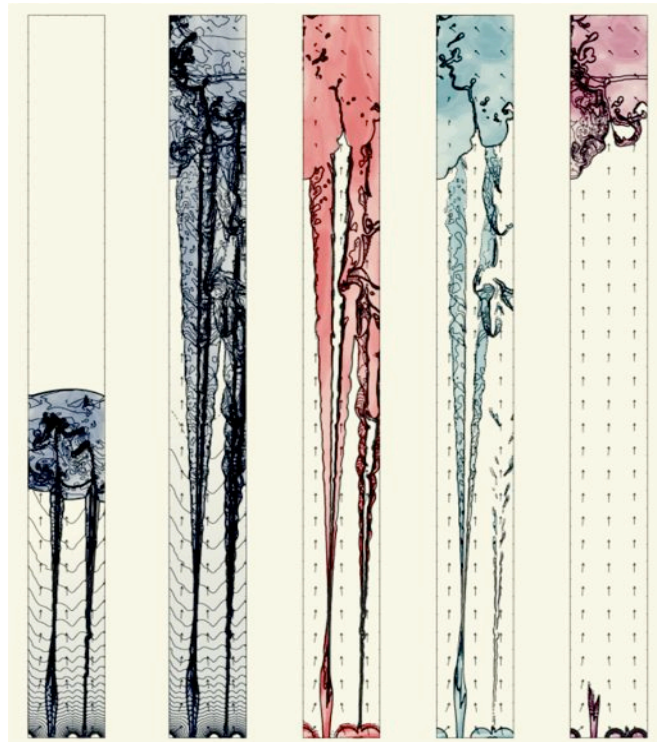


Figure 3.13: Hydrodynamical calculation of free expanding Super Galactic winds for three SSCs ($M = 10^6 M_{\odot}$) separated 30 and 60 pc from the central one and with a metallicity $Z=10Z_{\odot}$. The size of the panel is 100pc x 1 kpc. The filaments are emitting in H α and soft X-rays but in hard X-rays we only see the zone around the SSCs base (Tenorio-Tagle et al. 2003, Tenorio-Tagle & Muñoz Tuñon 2005).



In parallel, Melo et al. (2005) analyzed HST images in H α measuring the properties of a well selected catalog of SSCs in M82. From this result, it becomes clear that the number of filaments is clearly smaller than the number of SSCs, indicating that nearby SSCs combine their mechanical energy to act as a single source. In spite of this work, data to characterize the physical properties (kinematics, extinction, and ionization structure) of the filamentary structure is still lacking. Due to the extended, irregular, and clumpy nature of the starburst regions, this can be hardly achieved with traditional long-slit spectroscopy. MEGARA, thanks to its combination of Integral Field Unit and MOS capabilities, is perfectly suited for such study.

Neutral Galactic Winds

Classically, two have been the approaches used for the analysis of the properties of Galactic Winds in galaxies:

(i) Searches for extra-planar gas in galaxies have been carried out in the hot or warm phases through X-ray (e.g. Dahlem et al. 1998) or optical emission lines (e.g. Lehnert & Heckman 1996) respectively. In order to distinguish the faint wind emission from the background galaxy light, this approach has been preferably carried out in highly inclined galaxies where dense winds are easily detected. Although very useful information on the spatial distribution of the wind (biconical, egg-shaped, etc.), and its potential sources of energy are obtained in this way, most kinematical information is lost. The M82-like SGWs described above, by construction, have been all studied in this way (see also the case of NGC 3079).

(ii) An alternative approach is to look for interstellar absorption lines to probe the outflowing gas. Most useful interstellar lines (SiII and CII but also OVI) lie in the UV region of the spectrum (or in the optical at high redshift), limiting their use in nearby galaxies to space observations but a few are found at rest-frame optical wavelengths (Na I and K I) and can be explored from the ground. This approach has several advantages: it is less prone to the high-density bias, and provides information on the kinematics of the outflow. This approach favors detection of winds in galaxies with low inclination, and probes a cooler phase of the ISM (e.g. Heckman et al. 2000). However, as spectral information is obtained from long-slit observations, this approach does not provide much spatial information of the structure of wind. Traditionally, the most energetic starbursts have been studied in this way.

Recently, by means of IFU observations, Jiménez-Vicente et al. (2007) have found the existence of a strong wind in the nuclear region of NGC 4321. This is a canonical giant spiral galaxy, previously assumed to be fairly quiescent with no nuclear activity and only a moderate SFR in the nuclear regions. Therefore, a galactic outflow of this magnitude was not expected in this galaxy. This and other nearby galaxies have later been proved to host some low-luminosity AGN activity that was missed by standard optical diagnostics (see Saytapal et al. 2008). These findings suggest that Galactic Winds could be more frequent than previously thought.

Our work in Jiménez-Vicente et al. (2007) and Castillo-Morales et al. (2007) also showed that a non-negligible fraction of the wind might be able to escape the galaxy. In order to carry out this work, we had to separate the stellar and interstellar contribution to the Na I D lines on each fiber (Figure 3.14). This allowed us to show, for the first time, that regions where the stellar and interstellar components of Na I D dominate do coexist in the same galaxy. The use of integral

field spectroscopy and a careful data analysis were critical in this discovery. In this way, we have been able to produce the first maps of the distribution and kinematics of the absorbers (see Figure 3.15) in the Galactic Wind of a nearby galaxy. We have also been able to detect the ionized component of the wind (in $H\alpha$, NII and SII) and to separate it from the underlying gas in the galactic disk (Figure 3.15), giving place to an unprecedented global view of several phases in the outflow.

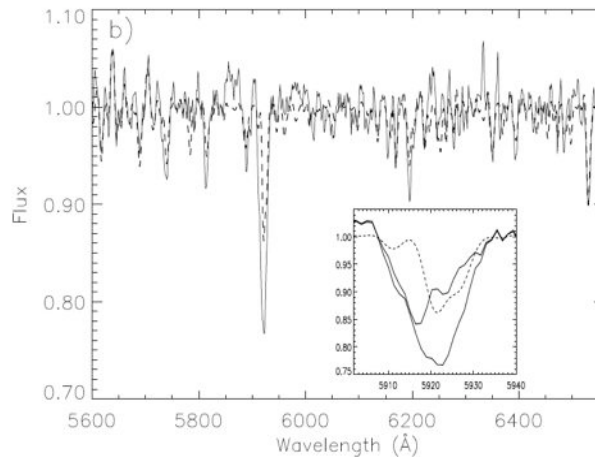


Figure 3.14: Nuclear spectrum of NGC 4321 obtained with WHT-INTEGRAL SB3 fiber bundle with the stellar template plotted on top as a dashed line. The inner panel shows in detail the fit to the Na I absorption doublet (dashed line) and the residuals (thick solid line).

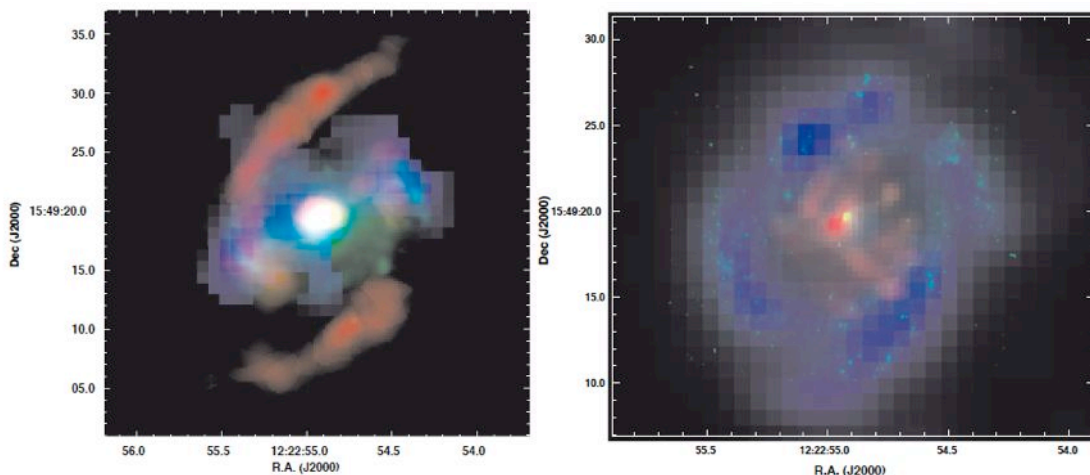


Figure 3.15: The wind in the nuclear region of NGC 4321. (Left): Composite RGB image of the equivalent width of the interstellar Na I doublet (blue), K band image (green) and CO intensity map (red). Intensities are arbitrarily scaled. (Right): Composite RGB image of $H\alpha$ intensity of the wind component (red), HST/ACS F555W (green) and $H\alpha$ intensity from the underlying galaxy disk (blue). Intensities are arbitrarily scaled.



Massive-star feedback

In order to understand the physics of Galactic Winds of any kind it is critical that we have a perfect understanding of how the winds arising from massive stars interact with the surrounding interstellar medium. One of the most conspicuous manifestations of such interaction is the occurrence of ionized hydrogen bubbles around these stars. Although complex processes of ionization and hydrodynamics are involved, the basic concept is that the spherically symmetric wind of a massive star sweeps up the surrounding medium (Weaver et al. 1977). The combined effect of the winds and SN explosions from massive stars commonly result in the formation of superbubbles. Some examples of these superbubbles in Local Group galaxies are NGC 346/N66 in the SMC (Gouliermis et al. 2008), the 30Dor complex (Walborn et al. 2002), NGC 3603 in our own Galaxy (Brandner et al. 2000), to name a few. These superbubbles can lead to a galactic-scale wind (or SGW) in those cases where Rayleigh-Taylor instabilities efficiently break out the superbubble and let the hot metal-rich gas inside to escape (Tenorio-Tagle et al. 2003). Thus, as the first step towards the formation of a SGW, superbubbles and even the mere interaction of individual massive stars ought to be addressed before the role of SGW on the spectro-photometrical and chemical evolution of galaxies could be fully understood.

Within MEGADES we are particularly interested in the Local Group magellanic irregular IC 1613, whose metallicity is significantly smaller than the SMC (0.04 to 0.2 Z_{\odot} , Talent et al. 1980; Peimbert et al. 1988; Tautvaišienė et al. 2007). From the analysis of the blue massive star population of IC 1613 we can study the winds of its OB stars and their interplay with the ISM in a very-low-metallicity regime, and use the results as a proxy for the very-metal poor early Universe.

The stellar component in IC 1613 extends about 16.5 arcmin from its centre (Bernard et al. 2007), but the young population concentrates in the central 9×9 arcmin². The largest, most massive OB associations are found in the NE lobe of the galaxy (García et al. 2010a; Borissova et al. 2004) where giant HII shells are seen (Meaburn et al. 1988; Valdez-Gutiérrez et al. 2001; Lozinskaya et al. 2003). At the distance of IC 1613, blue massive stars can only be studied efficiently using 8-10m class telescopes with multi-object spectroscopic capabilities. Few spectroscopic works based on VLT data have presented reliable spectral classification or stellar parameters for blue massive stars in IC 1613 (Bresolin et al. 2007, Herrero et al. 2010, García et al. 2010b). However, they are limited by the instrumental configuration and cannot study properly the higher concentration of blue stars at the centre of IC 1613 superbubbles. Consequently, while the structure and dynamics of ionized and neutral hydrogen has been thoroughly studied, the stellar side is poorly known (including whether or not it hosts a disk) and the source of mechanical energy, which carved the structures, is still a matter of debate.

Meaburn et al. (1988) studied the intricate distribution and kinematics of HII in the bubble region of IC1613. They calculated that the stellar content suffices to explain the hydrogen ionization, but the power of their stellar winds cannot drive its expansion, so they proposed a multiple supernovae (SN) scenario as the likely origin of the bubbles. However, only one supernova remnant has been detected in IC1613 (Dodorico et al. 1980) although it is possible that older (fainter) remnants cannot be detected at its distance. On the other hand, Meaburn et al. 1988 inferred spectral types for the stars from photometric colors, then used calibrations of



stellar wind power with spectral type from the 1980's, and assumed the electron density of the nebula.

The problem was revisited more recently by Valdez-Gutiérrez et al. (2001) and Lozinskaya et al. (2003), who concluded that the combined mechanical energy of the winds of the OB associations at the centres of the bubbles can account for their formation in most cases. The SN explanation was not totally discarded as Valdez-Gutiérrez et al. (2001) pointed out that the mechanical energy of the expanding shells amounts to 80% of a SN explosion. While the instrumental set-up (Fabry-Perot interferometry) used to measure gas velocities meant considerable improvement with respect to Meaburn et al.'s work, the study of the stellar populations was still based on photometry or very-low resolution spectra. Moreover, none of these works takes into account that the wind power of the metal-poor IC 1613 stars [$12 + \log(O/H) = 7.9$; Bresolin et al. 2007] is smaller than for solar-metallicity stars, as the wind of OB stars is driven by the absorption of radiation by the transitions of metallic ions. Accurate stellar and wind parameters of the stellar content from quantitative spectroscopic analysis are crucial to make proper calculations.

To make things more interesting, chains of potentially very massive stars are found in the intersection of several giant HII shells of IC 1613. The picture complicates further when HI is considered, which interacts with ionized hydrogen at the chains of stars (Lozinskaya et al. 2003). Lozinskaya et al. (2002) suggested that the shocks produced in the collision of the giant HI and HII shells can trigger star formation, and that the stellar concentrations on HII rims are the most active star-forming loci of IC 1613. Note also that the projected morphology of GS1 and its radial velocity measurements are consistent with two lobes of a tilted bipolar structure, aligned in our line of sight (Meaburn et al. 1988; Lozinskaya et al. 2003), which resembles the projected view of the biconical outflow in M82, a SGW driven by an ensemble of SSCs (Tenorio-Tagle et al. 2007).

Hence, the debate is opened: Do stars at the center of IC 1613's bubbles drive their expansion? Or, was the formation of these stars induced by the collision of the else how-produced HII structures, or the collision of these with neutral hydrogen? A detailed spectroscopic analysis is needed to decide if massive stars can propel the expansion. The proposed observations will help to disentangle the on-going physical processes in IC 1613: the radial velocities of the stars will help to a better picture of the dynamics of the field, and the determination of the stellar wind parameters will confirm or discard that the central stars alone can propel the bubble.

In addition to the study of IC 1613 we will also study similar phenomena in M33 as part of the observations of a number of fields described in Section 3.1.5.1.5. This will allow us to increase the range of properties where the interaction between massive stars and their environment could be analyzed in detail. Finally, as part of the MEGARA Early Science observations (see Section 4) and with the same goal in mind we will also observe M33's most massive star-formation complex, the HII region NGC 604.

3.1.1.7 *Secular evolution of disks: green-valley galaxies and AGN activity*

Although the existence of two well defined population of galaxies (ellipticas and spirals, blue cloud and red sequence) it is know for many decades already it has been only recently that the existence of a bimodality in their properties has been proved statistically (Kauffman et al. 2003; see Figure 3.16). In this regard many are the questions that such distribution in the properties of galaxies have posed: why do galaxies tend to be either “red and dead” or blue and star forming, and in particular, what is happening to galaxies in the intermediate “green valley” of the color-magnitude diagram?

In order to come close to answering these questions, major observational and theoretical efforts have been recently put together. In this regard, it has now become clear that spatially-resolved information, spectroscopy if possible, for a large sample of galaxies, is essential for this endeavour. This will be one of the objectives of MEGARA as part of the MEGADES survey.

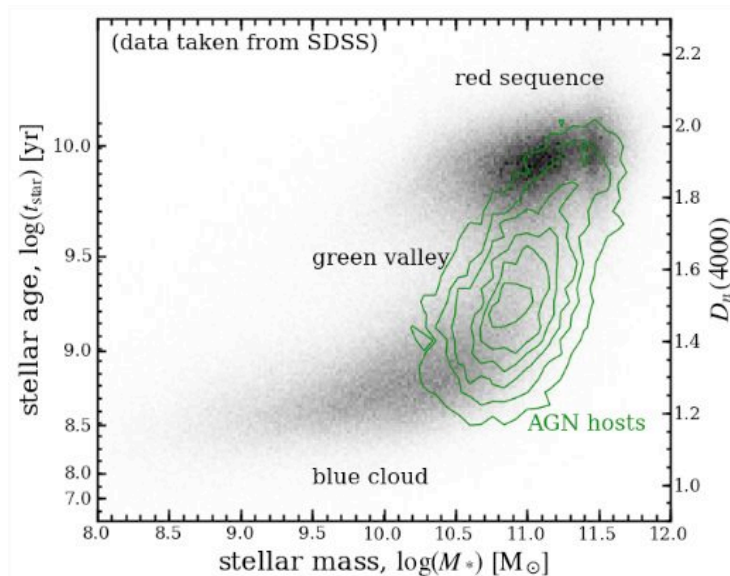


Figure 3.16: D_{4000} vs. stellar mass distribution for the galaxies in the SDSS survey. The contours indicate the density distribution of AGN hosts, clearly located in the intermediate “green valley” region.

MEGARA should allow us (1) to understand the nature of the observed bimodality in the properties of galaxies and (2) to distinguish among the different evolutionary scenarios proposed between star-forming/blue/late-type galaxies and gas-dry/red/early-type ones.

In the core of this bimodality is the fact that the bulk of the population of massive galaxies appear red and dead at present time. This quenching of star-formation in these massive galaxies is one of the most poorly understood yet fundamental aspects of galaxy evolution. It should involve both a “switching-off” of the star formation and a morphological transformation in order (1) to reconcile the predicted and observed massive end of the galaxy luminosity function, (2) to understand why during this cosmological time (from $z \sim 1$ to the present time), most of the stars are formed in late-type (blue-cloud) galaxies (e.g., Wolf et al. 2005), but the mass is accumulated in early-type (red-sequence) ones (e.g., McIntosh et al. 2005) and (3) to reproduce the observed ratio of red-sequence to blue-cloud galaxies at different cosmological times.

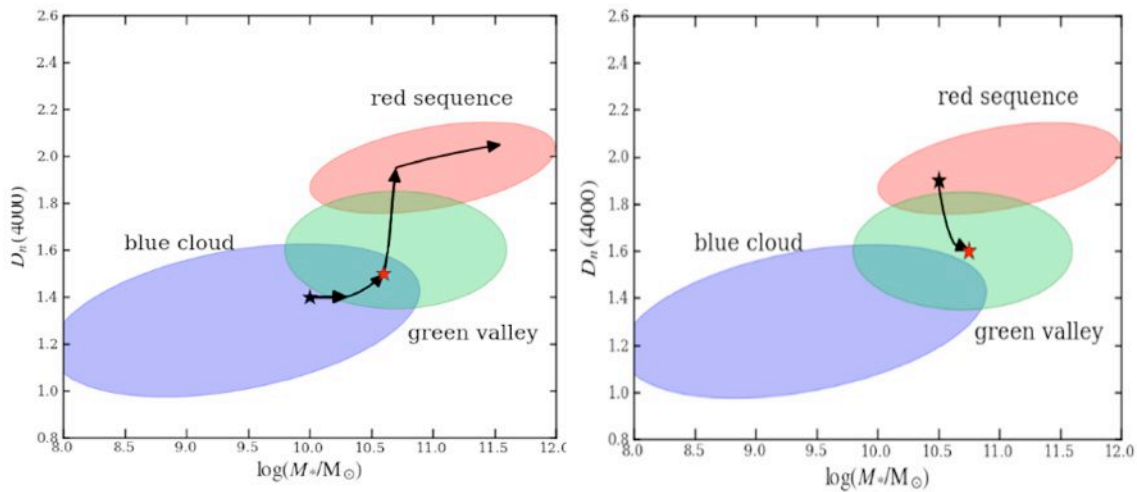


Figure 3.17: Two different proposed scenarios to explain the link between AGN activity and the evolution within the Color-Magnitude diagram. The left panel shows the proposed AGN-merger-Early type evolution, while the right panel shows the E-type-reyouth evolution.

Standard explanations invoke galaxy mergers which can drive inflows of cold gas that fuel central starbursts and AGNs (e.g., Hopkins et al., 2008). The gas is then consumed by the starburst, and subsequent outflows from the AGN (and the starburst itself) can heat (and expel) the remaining gas, quenching star formation and switching off the nuclear activity. The cosmological co-evolution of the black-hole/bulge masses (eg., Cisternas et al. 2011) and the location of the AGN hosts in the so-called transition “green valley” region of the CM-diagram (e.g., Kauffman et al. 2003; Sánchez et al. 2004) both support this scenario. Although the effects that should lead to the evolution from the blue cloud to the red sequence are expected to take place in a relatively short timescale this mechanism is still considered as a secular process even if it is triggered by a non-secular process such a major merger event (see Kormendy & Kennicutt 2004).

However, observations have struggled to test the details of this “self-regulated” hypothesis. On one hand there is a lack of direct evidence of the relation between the merging processes and the AGN activity in general. This may be related to the differences in the time-scale associated with both processes. On the other hand, there are some puzzle examples of apparently “quenched” galaxies that does not fit with this scenario. One example is the significant population of bar-dominated (face-on) disk galaxies on (or above) the red-sequence observed at different redshifts (e.g, Masters et al. 2010; Bundy et al. 2010): How can a merger shut star formation off without destroying the disk? Do these galaxies host an active nucleus? Could they fit within the standard explanations at all? The observations designed by the MEGARA Science Team as part of the MEGADES survey should provide fundamental clues to solve some of these questions. This will be possible thanks to both the sample size and the depth and resolution, both spatial and spectral, of the observations proposed.

Three complementary scenarios have been proposed: (a) Disks are re-grown in gas-rich mergers before quenching completes, perhaps during the starburst phase (e.g., Robertson et al. 2006); (b) Quenching may also be driven by “starvation” in average high-density environments (e.g., Bekki 2009); (c) Star-formation is suppressed by internal structural changes (e.g., “morphological quenching”; Martig et al. 2009). Integrated quantities cannot distinguish between a truncated disk model in which SFH has gradually ended over ~ 2 Gyr (scenario b & c), and a 2-component model in which a central starburst ($\sim 20\%$ by mass) lead to a rapid quenching (scenario a). However, spatially resolved star-formation histories and gas metallicity gradients, like the ones to be provided by MEGADES, are a robust measure of the burst fraction in these proposed transitioning galaxies.

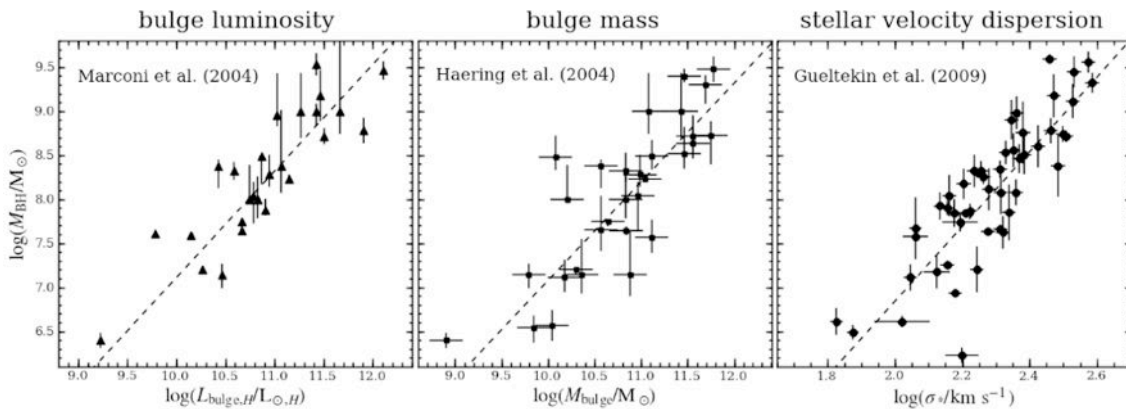


Figure 3.18: Three different results in the literature probe the link between the central BH mass and different Bulge properties (Luminosity, Mass and velocity dispersion), indicating the connection between the evolution of these two different properties of galaxies.

Although a link between nuclear activity, merging events and the morphological/type transformation of galaxies was proposed long time ago (Sanders et al. 1998), it is still not clear how the AGN activity fits in the overall picture. It is known that AGN hosts have, on average, younger stellar populations than early-type inactive galaxies of equal stellar mass (Kauffmann et al. 2003; Jahnke et al. 2004; Sánchez et al. 2004), suggesting that the growth of SMBHs by accretion and of galactic bulges by star formation are somehow synchronized (Heckman et al. 2004). Yet we still know little about the actual spatial distribution of the young stellar populations in AGN host galaxies (but see Sarzi et al. 2009). The comparison of SDSS and GALEX images of AGN, surprisingly, show that the stellar UV excess in AGN host galaxies typically occurs in the outer parts of the galaxy and not in the central regions (Kauffmann et al. 2007), contrary to what is naively expected. The kinematics structure of apparently (morphologically) quiescent galaxies, and the fraction of AGNs in different morphological and spectroscopic types of galaxies will allow us to quantify the relative importance of the standard merging-AGN scenario and the different disk-stable ones. In particular when focused on the comparison of the spatially resolved spectroscopic properties of the proposed transition objects, either green-valley members and/or red/barred spirals.



3.1.1.8 *Massive stars in Local Group galaxies*

As we have discussed above, massive stars might have a profound impact on the surrounding interstellar medium and, eventually, on the spectro-photometric and chemical evolution of galaxies. However, the massive stars deserve a detail analysis on their own. As part of the planned observations within MEGADES we will obtain deep optical spectroscopy of a large sample of massive blue stars in Local Group galaxies that will be used to analyze (1) the single-star chemical-abundance spatial distribution in these galaxies and (2) the kinematics of the youngest stellar population in disks and also (3) to address fundamental open questions on the evolution of massive stars themselves.

Massive stars are central engines to the evolution of the Cosmos. Their influence is thought to begin at very early times, when the first generation of stars, believed to be extremely massive, led to the epoch of reionization and brought to an end the so-called dark ages. Although we cannot directly detect these first stars, the search for their imprint has already begun (Nomoto et al. 2007). Massive stars can be traced back to very high redshifts thanks to their fate as Gamma Ray Bursts (GRBs, Woosley & Bloom 2006) and, at intermediate redshifts, due to their UV radiation that reaches us either directly from starbursts and star formation regions or indirectly from extended HII regions. They are important contributors to the dynamical evolution of their host galaxies through the input into the interstellar medium of large amounts of mechanical and radiative energy via stellar winds, eruptions and SN explosions (Leitherer 1998). These processes are also crucial to the chemical evolution of galaxies and the Universe since they expell matter processed in their interior into the interstellar medium (ISM). This processed matter is brought to the surface through poorly understood mixing processes (Herrero & Lennon 2004; Hunter et al. 2008). Even mass loss, the undisputed main process modifying the evolution of these stars, is again controversial (Puls et al. 2006). The structure of stellar winds is still poorly constrained with a number of outstanding problems; the amount and extension of wind clumping, the origin of non-thermal X-rays in winds, explanation for weak winds, and the mass loss rates in different evolutionary phases. Concerning the latter, catastrophic mass loss during LBV and WR phases may drive the subsequent evolution and even determine whether a SN explosion leaves a neutron star or black hole behind (Heger et al. 2003). Moreover, with the SN explosion ends the life of the massive star, but not its influence, as it can trigger the star formation in nearby regions, forming new stars (see for instance Walborn et al. 2002).

Being related to so many astrophysical problems on so many spatial and temporal scales, massive stars are excellent probes for understanding our own Galaxy, the Local Cosmos and the early times of the Universe. However, their use as cosmic tools is conditional on our ability to model and correctly interpret their spectra, the physical processes in their interior and atmospheres and their interaction with their environments. For example, we may use massive stars to study the physics, structure and evolution of galaxies at $z \sim 3$, but first we need to correctly predict their UV spectra within a very broad parameter space. In order to test our degree of knowledge about the different aspects of massive stars we must observe and analyze a large number of objects under different local conditions, as those offered by nearby galaxies, with our theoretical and numerical tools.



3.1.1.8.1 Advanced stages of massive star evolution

Because of their interaction with the interstellar medium, and because they power highly energetic processes of the Universe, the exact way in which massive stars evolve strongly affects our interpretation of a large number of observations, including part of our own MEGADES observations. However, recent results are challenging the current paradigm of massive star evolution and reveal clear gaps in our knowledge. The traditional picture described by the so-called Conti scenario (Conti 1984) has been subject to many variations (e.g., Massey 2003; Crowther 2007 among others). Most recent progress is related to the short-lived phases of massive stars between the end of the Main Sequence and the Wolf-Rayet phase, including the brightest B- and A- supergiants in their redward phases as well as their possible (but not confirmed) bluewards counterparts, the hypergiants of different spectral types, the cool red supergiants and the stars classified as Luminous Blue Variables. These phases are conveniently very bright, so we can study them in external galaxies with a variety of environmental conditions (metallicity, stellar density, SFH and SFR). The determination of their stellar parameters and the number of stars found in each stage are powerful constraints to evolutionary models.

The evolution of massive stars is complex, governed by numerous factors besides mass and metallicity. Blue massive stars, for instance, experience matter outflows or winds, driven by their ultraviolet radiation (see Kudritzki & Puls 2000 for a review). The mass lost during the main sequence of massive stars determines the duration of this and subsequent stages, and can even decide the fate of object and the leftover remnant (Maeder & Meynet 2000; Woosley et al. 2002). Stellar rotation, on the other hand, modifies the size and duration of the stellar convective core, a powerful mixing mechanism that may favour the formation of blue-loop stars. Some models predict blue loops during the evolution of massive stars (Maeder & Meynet, 2001; Heger & Langer, 2000), but the existence of objects in such stage has never been proved. A fraction of the blue supergiants surrounded by ring nebulae may be blue loop stars descendants of the red supergiant phase (Chita et al. 2008).

Blue loops may make the star overluminous, bringing it close to the Eddington limit and the region of Luminous Blue Variables (LBVs). The LBV phase is also far from being well understood. Apart from the three descriptive words that give them their name (they are luminous, they are blue, they are variable), LBVs are a heterogeneous group characterized by strong mass loss, which reveals itself in P-Cygni line profiles. Occasionally (and unpredictably), they suffer episodic outbursts, with brightness increase and eruptions. The impact of the LBV phase on the global evolution of massive stars and their interaction with the ISM is not known, but it is presumed to be large given their high mass loss rates. Although the winds of LBVs are driven by line radiation pressure (Vink & de Koter 2002) we find them even at very low metallicities. For example, we have found a LBV candidate (LBVc) in IC 1613 (Herrero et al. 2010) at $12+\log(O/H)=7.90\pm 0.08$ (Bresolin et al. 2007). There is also increasing suspicion that LBVs may explode as type II In SN (Gal-Yam et al. 2007; Kotak & Vink 2006; Smith et al. 2007), but the suggested mechanisms imply very different initial masses for the LBV progenitors. Abundance determinations in LBVs (see Najarro 2001) can provide us with



important clues about their previous evolutionary stages and masses.

B- and A- supergiants play the central role in our efforts to understand the evolution of massive stars. The surface chemical composition of B- and A-supergiants after the Main Sequence (MS), as well as effective temperatures, luminosities, masses and mass loss rates (see Markova & Puls 2008) are needed to understand the processes driving the evolution of massive stars. Surface abundances should vary according to the degree of mixing suffered during the MS phase and immediately after. Variations will follow the CNO pattern, and will depend on the initial stellar mass, rotation, metallicity and mass loss rate. This issue has been partly addressed by our group in the FLAMES Survey of Massive Stars (P.I., S.J. Smartt, see Evans et al. 2008). Hunter et al. (2008) have found an unexpected chemical composition pattern for some B supergiants, which may constitute a challenge for current theories of rotational mixing or represent an evolutionary path more complex than presently assumed. Together with the stellar location in the Hertzsprung-Russell diagram (HRD), surface abundances provide us with the clues needed to determine the evolutionary paths followed by massive stars. If blue loops exist, they should be revealed by the presence of B-, A- and F- supergiants that should be particularly luminous for their masses and display a peculiar pattern of chemical composition.

The spectral collection we expect to get with MEGARA will constitute a large and homogeneous database of bright massive stars that will allow us to address the following questions: (i) Are the abundances and luminosities of extreme B- and A- supergiants consistent with evolutionary model predictions? (ii) How many LBVs do we find? Does their luminosity depend on metallicity? (iii) Do blue-loop stars exist? Are the abundances of LBVs and extreme blue supergiants consistent only with blueward evolution?



3.1.2 Objectives

The ultimate goal of MEGADES is to determine the role played by secular processes on the evolution of disks (see Section 3.1.1). In this regard, we have identified (1) a list of specific objectives that are directly related with our current view of the evolution of galaxy disks as a whole and (2) others that are related with phenomena that, albeit having a strong impact on the evolution of individual disks, play a yet unknown role on the evolution of the overall population of disks.

Among the former we include as objectives of MEGADES:

- 1) To confirm whether or not gas in-fall (including its dissipation and collapse), as the driver of the inside-out formation of disks, is the main mechanism responsible for the evolution of disks. This should include the comparison of the spectroscopic properties of disks in 2D with the predictions of spectro-photometric models developed in the context of the inside-out scenario for the formation and evolution of galaxy disks. In order to achieve this goal the following tasks should be carried out:
 - a) Analysis of the spectra of individual stars at different galactocentric distances in Local Group galaxies in order to derive the spatial distribution of stellar ages and chemical abundances. This analysis will include a comparison with the predictions of the inside-out scenario.
 - b) Analysis of the integrated (unresolved) absorption spectrum at different galactocentric distances of nearby galaxies (Local Volume⁵). This analysis should include the measurement and comparison with the models of both full-spectra and age/metallicity/ α -enhancement-sensitive spectroscopic indices.
 - c) Analysis of the ionized-gas abundances of HII regions throughout the disks of both Local Group and Local Volume galaxies. This will include the determination of abundances of as many elements as possible and the comparison between abundance estimates based on recombination and collisionally-excited lines (using both temperature-sensitive line ratios and strong-line methods). Chemo-dynamical effects will be also studied in order to ensure a precise chemical-abundance determination.
- 2) To establish the existence and significance of departures from the predictions of the inside-out scenario. The analysis of the spectra of disks in 2D should allow us to identify such departures. These are expected to be particularly noticeable in both the inner regions and the very outer edges of the disks. This objective will require to carry out the tasks described above (1.a, 1.b and 1.c) plus the following kinematical analysis of the disks:

⁵ Although in the literature the term Local Volume commonly refers to a region of 10 Mpc in radius centered in our Milky Way, we will refer by this term to a volume with a radius of 40 Mpc, which is the limiting distance considered in MEGADES for the study of spatially-resolved spectroscopic properties of disks (MEGADES S4G sample limiting distance).



- a) To analyze the kinematics of individual stars in Local Group galaxies at different galactocentric distances. Both young (massive blue stars; MBs) and old (AGB and RGB stars) should be studied and the velocity dispersions of both populations compared as a function of the position in the galaxy.
- b) To identify and analyze kinematical features in the inner regions of disks that could be testimony of the existence of distinct structures such as inner disks or bars and that could then be used to infer to what extent these could be responsible for any deviations in the spectro-photometric and chemical properties derived (points 1.a, 1.b and 1.c) compared to the predictions of the inside-out scenario (see e.g. Gómez et al. 2012).
- 3) To determine what are the mechanisms responsible for such departures. These might include stellar migration, satellite bombardment and minor merging, nuclear activity, intense star formation (starbursts). This objective basically means putting the analysis described above in the context of both idealized (e.g. Roskar et al. 2008) and full cosmological simulations of the formation of disks (e.g. Sánchez-Blázquez et al. 2009). In some specific cases the results of this analysis should be also compared with the predictions of customized numerical simulations for the formation of inner disks, bars, etc. (e.g. Eliche-Moral 2011).

We also aim at studying the physical properties and possible impact on the evolution of galaxies as a whole (not yet fully determined neither quantified) of the following processes:

- 4) M82-like Super Galactic Winds. The study of these SGWs includes:
 - a) To analyze the kinematics of the gas in the starburst using the velocity and line shape derived from the H α emission line.
 - b) To identify the "Super Stellar Clusters" ensembles responsible for the observed filamentary structures seen in the SGWs. This requires a combined analysis with HST/ACS imaging data.
 - c) To study the kinematics and physical conditions of the ionized gas around the SSCs.
 - d) To determine precise ages for the SSCs from the analysis of their optical spectra. The analysis of the properties of the SSCs and the surrounding ISM should allow us to constrain some of the ingredients of the dynamical modeling of the wind, such as the heating parameter.
 - e) To study the kinematics and physical properties of the ionized gas present in the filaments. A comparison with the predictions of our models is also critical in this regard.
- 5) Neutral Super Galactic Winds. This study should include:
 - a) To determine the frequency of Galactic Winds in apparently quiescent galaxies.



- b) To establish in which of these cases (if any) the wind velocity is high enough for some material to escape from the galaxy potential.
 - c) To determine in which of the remaining cases of Galactic Winds identified (and to what level) a redistribution of gas, dust and metals is expected.
- 6) Massive-star feedback in the Local Group. In order to analyze the interplay between massive stars and the surrounding ISM we will also carry out a detailed analysis of the properties of a sample of massive stars in the Local Group and the winds driven by them.
- 7) Nuclear activity (AGN). The ultimate goal in this case would be to determine which of the different mechanisms proposed dominate the evolutionary connections between galaxies in the blue cloud and in the red sequence and what is the role of green-valley galaxies in this evolution. In order to reach this goal the following specific objectives should be pursued:
- a) To study the physical properties of the ionized gas associated to the active nucleus in both type I and type II AGN in the MEGADES sample.
 - b) To study the stellar populations (both in the bulge and the disk) of the host galaxies.
 - c) To study the gas and stellar kinematics in their nuclear regions.
- 8) Finally, given the relevance of massive stars on some of the phenomena described above and motivated by our still poor understanding of the evolution of these objects, the observations to be carried out as part of MEGADES will also address fundamental issues on the evolution of the most massive stars in the Local Group. The objectives of this study will include:
- a) To analyze the spectra of a large number of massive stars so to obtain their physical parameters and surface abundances: He, CNO, and α -elements for the early types (B, hot LBVs), CNO and Fe from the later types (A, cool LBVs).
 - b) The analysis of these physical properties, spectral types and abundances, together with their location in the HRD, will lead to a wider picture of the impact of metallicity on massive star evolution. This should be achieved by exploring an unprecedented range in metal abundances.
 - c) To characterize the winds of O stars and B-supergiants, by inferring mass loss rates from quantitative analysis of the targets' spectra.
 - c) To analyze the spatial distributions of these properties in order to constrain the chemical evolution of the parent galaxies. The comparison with the ionized-gas abundances, derived by different methods, is a topic where MEGARA will also break new ground.



3.1.3 Methodology

As commented in Section 3.1.1, fully understanding the mechanisms that govern the evolution of galaxy disks must rely on a precise determination of the chemical and star formation histories out to their optical edges and also on a proper quantification of the actual stellar migration along with the contribution from other mechanisms (both internal and external) to the evolution of disks. These objectives, described in more detail in Section 3.1.2, require of the use of mid-to-high-resolution spectroscopy and large collecting area, both in terms of telescope mirror and contiguous spatial coverage. As we will show in Section 3.1.5 of this document these requirements can only be achieved by using an instrument like MEGARA at GTC.

The strategy to be followed within the MEGADES survey is twofold. We will first analyze (1) the Local-Group disk galaxy M33 where individual massive-blue and RGB stars will be resolved. This analysis will be used to quantify the inside-out formation of stars with unprecedented accuracy and the possible effects (departures from this simple picture) associated to other phenomena, such as stellar migration, satellite accretion or bombardment, etc. We will achieve this through the detailed analysis of stellar kinematics (velocity ellipsoid), spectral-indices fitting, and chemical abundance measurements. Then, we will analyze (2) a magnitude-, diameter- and volume-limited sample of nearby disks (distance <40 Mpc; drawn from the S4G sample; Sheth et al. 2010) in order to determine their light-weighted (i) star formation and (ii) chemical histories and (iii) velocity ellipsoids. This latter sample will be selected to cover a wide range of physical parameters, such luminosity, color, or environment, not available in the Local Group. The combination of the two approaches will give us, for the first time, a complete picture of the evolution of galaxy disks.

Finally, and with the objective of analyzing the potential impact of relatively rare phenomena (rare both in the Local Group and in diameter/volume-limited samples of more distant galaxies), on the spectro-photometric and chemical evolution of disks, such as starburst activity, we will include the detailed study of the starburst galaxy M82 and of a sample of actively star forming nearby ULIRGs ($0.04 < z < 0.08$; Murphy et al. 1996). The properties of massive stars as the drivers of these phenomena and an important source of chemical enrichment in galaxies will deserve special attention. In this regard and in order to extend the analysis planned on the massive-blue stars of M33 we will carry out a similar single-star analysis on the metal-poor late-type galaxy IC1613.

In this section we describe in detail the methodology followed to address the scientific objectives of MEGADES and we also demonstrate how the characteristics of MEGARA will allow us to achieve them.

3.1.3.1 *Determining the role of secular processes: beyond inside-out formation*

3.1.3.1.1 Stellar kinematics

Out of all the secular internal processes involved on shaping the properties of present-day disks, the understanding of the role of stellar migration is currently the major stopover in fully understanding galaxy disk evolution (see e.g. Roskar et al. 2008 and references therein). Fortunately, stellar migration has a profound impact on the kinematical properties and effective

star formation histories of galaxies (and thus, on their colors, absorption features, and chemical abundances) that can be quantified observationally. In Figure 3.19 we show the σ_z profiles in the fully cosmological disk simulation of Sánchez-Blázquez et al. (2009). Different lines represent the σ_z profiles of the young stars ($<10^7$ yr), the RGB star population, and the light-weighted values in the near-infrared Calcium Triplet, which is equivalent to the σ_z one would measure from an unresolved stellar population in the CaT lines. The differences between these values are due to kinematical heating, the main mechanism for stellar migration in massive disks (see right panel of Figure 3.19).

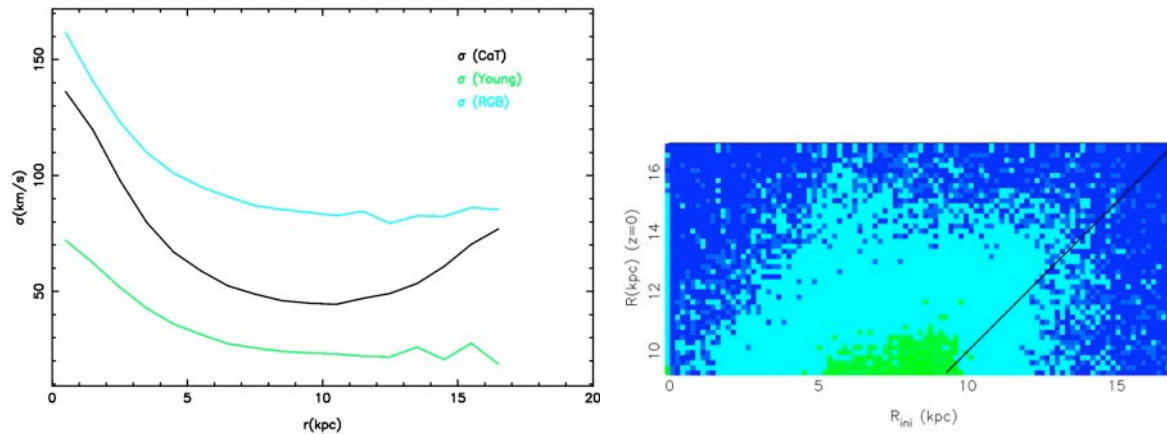


Figure 3.19: Left: Radial profiles in σ_z for young stars (green solid line), RGB stars (cyan solid line), and integrated light in the CaT (black solid lines). These profiles correspond to the disk simulated by Sánchez-Blázquez et al. (2009). Right: Distribution of the present-day galactocentric distance of stars as a function of their formation radius for this same model.

Migration in this disk can yield to a difference in σ_z that can reach ~ 60 km/s between young and RGB stars and ~ 25 km/s between young stars and the unresolved CaT. In the case where σ_z should be measured from individual stars the required precision in the individual star velocities is ~ 10 km/s. For the measurement of σ_z in the CaT region of unresolved stellar populations the precision in velocity dispersion should be better than ~ 40 km/s (FWHM ~ 100 km/s). Both requirements can be achieved using MEGARA as shown in Section 3.1.5.1.1.

In Figure 3.20 we show the predictions for another disk that have been recently simulated by Sánchez-Blázquez et al. (2012). In contrast with the simulation presented in Sánchez-Blázquez et al. (2009), this disk have a much lower mass ($\sim 2 \times 10^{10} M_\odot$), which results in significantly less *heating*. In these disks, the main mechanism responsible for stellar migration is *churning*. The large dispersion in final radii for those stars born at $\sim 3-4$ kpc are likely the result of the effects of transient spiral arms near co-rotation. As expected, now the difference between the σ_z measured in individual young and old stars and between old stars and that measured from unresolved stellar light is very small, significantly smaller than in more massive disks that are dominated by *heating*. Note that the σ_z values for RGB and young blue stars here are still easily measurable using $R=6,000$ and $R=11,000$ spectroscopy, respectively.

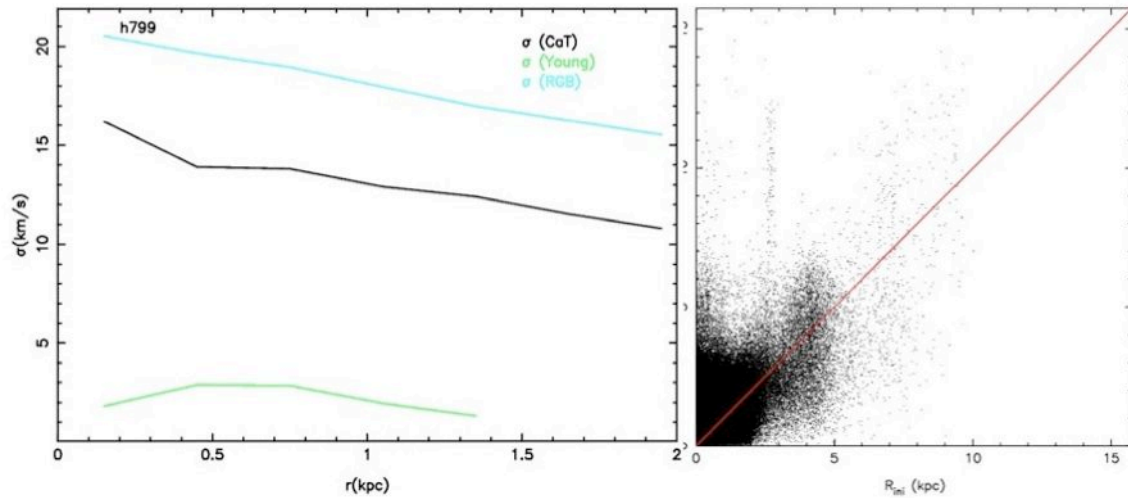


Figure 3.20: Left: The same as Figure 3.19 for a significantly less massive disk (Sánchez-Blázquez et al. 2012). Right: Distribution of the present-day galactocentric distance of stars as a function of their formation radius for this same model.

The measurement of σ_z in a number of relatively face-on disks from individual (young massive and RGB) stars and integrated light (when RGB stars cannot be resolved individually, either because distance or crowding) will provide fundamental information on the magnitude of the expected stellar migration in these systems and whether *heating* or *churning* drive such migration.

Moreover, should have the disk been exposed to the bombardment from relatively massive subhalos (that could have also lead to a significant contribution of stars accreted from these satellites in the outer disks) we would also expect to have signatures of those events, either in the morphology (Kazantzidis et al. 2008; see Figure 3.21), e.g. the Monoceros Ring in our own Milky Way, or in the stellar kinematics (Kazantzidis et al. 2009; see Figure 3.22). In particular, as shown in Figure 3.22, the bombardment of disks yields a clear increase in σ_z in the outer parts of disks, which could be measured if the spectral resolution (in σ) is better than 10% the galaxy circular velocity, which even in the case of relatively low-mass disks (with $v_{\text{circ}} \sim 100 \text{ km s}^{-1}$) can be easily achieved with MEGARA.

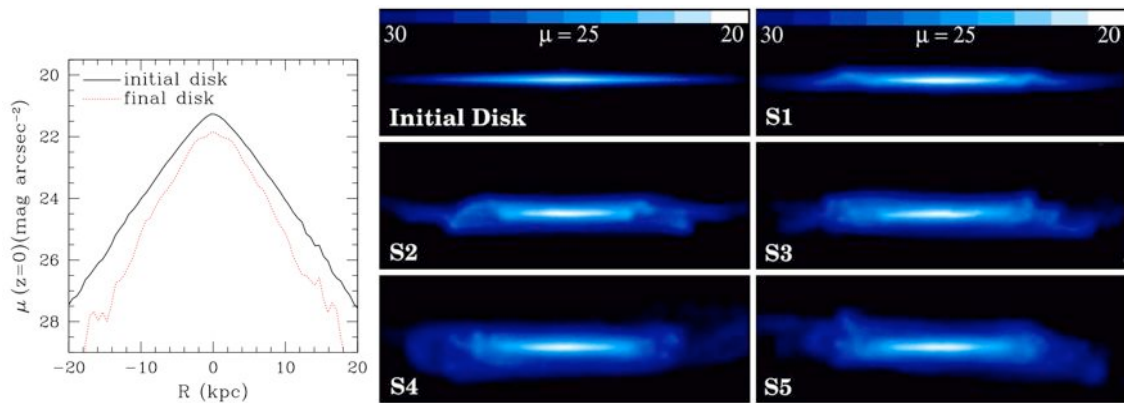


Figure 3.21: Evidence for disk flaring in the simulated disk after several consecutive passages of a satellite (Kazantzidis et al. 2008). Left: Edge-on surface brightness profiles of the stellar disk as a function of projected radius. The final disk (dotted line) exhibits a steepening in surface brightness distribution beyond $R \sim 3.5 R_d$ compared to the initial disk (solid line). Right: Each of these boxes correspond to the same 3D simulations at different consecutive passages. The boxes are all 18 kpc x 60 kpc in size.

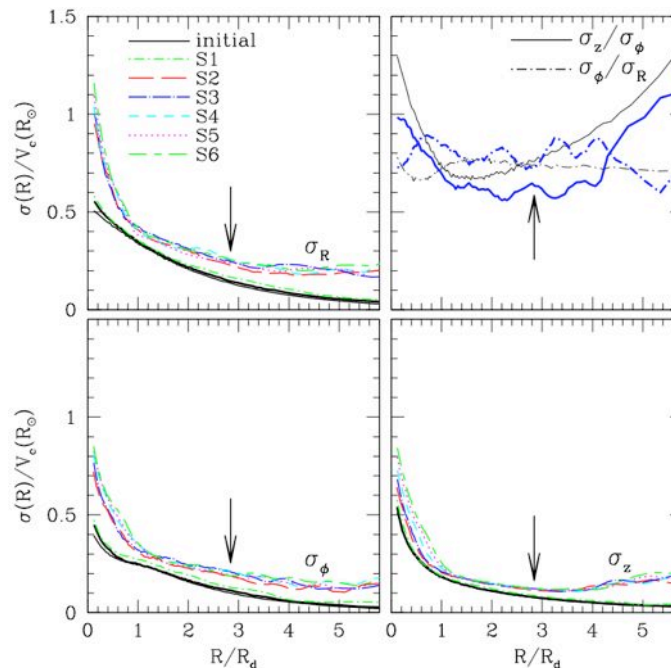


Figure 3.22: Velocity dispersion profiles of the disk simulated by Kazantzidis et al. (2009) as a function of projected radius in units of the radial scale length of the initial disk. Color lines represent the profiles after each consecutive satellite passage. Note the raise in σ_z in the outer parts of the disk. In the upper right panel the velocity dispersion ratios σ_z/σ_ϕ (solid lines) and σ_ϕ/σ_R (dot-dashed lines) are shown for the initial (thin lines) and final (thick lines) disk. Bombardment heats the thin galactic disk considerably in all three directions and causes its velocity ellipsoid to become more anisotropic.



While this increase in the different components of the velocity ellipsoid (mainly in σ_z) in the outer parts of the disks with relatively massive orbiting satellites is primarily due to the heating of the stars already in the disks, stars from the satellites themselves can also be accreted, leading to a change in the properties of the outer disks that also compete with the effects of migration and *in-situ* star formation. As previously discussed, according to Casertano et al. (1990) these stars would also inherit the distinct kinematics of the galaxy halo and well-differentiated chemical abundances and abundance ratios. In this latter regard, the N-body simulations of Cooper et al. (2010) show that the stars accreted from orbiting satellites are expected to yield a flat or negative metallicity gradient, opposite to the effect expected from stellar migration.

Ideally, we should analyze stellar kinematics as a function of those galaxy parameters that drive disk evolution (and the potential role of migration and satellite accretion on it): galaxy luminosity, disk-mass fraction, specific angular momentum, and environment. Parameters that will be all obtained from the proposed MEGARA observations. Note, however, that the number of objects where velocity dispersions from individual stars can be measured is limited (there are only 2 bona-fide spiral disks in the Local Group and 8 spirals disks within 4 Mpc accessible from La Palma, Lee et al. 2009). Therefore, only a limited region of the parameter space can be explored inside the volume where single stars are resolved from the ground. In more distant objects only the σ_z of the unresolved stellar population can be measured. For those objects not completely face-on we will extract σ_z via decomposition of the line-of-sight (LOS) velocity dispersion and we will use it in combination with the σ_z/σ_R ratio to provide an alternative measure of the disk heating (e.g. Westfall et al. 2007 and references therein) and of the possible role of satellite accretion events. For these more distant systems we will also combine this analysis with that of their SFHs. Both the kinematical information and the effective SFH will be used (1) to constrain the potential impact of migration and satellite accretion and (2) to determine the disk growth as a function of each of the galaxy parameters listed above (see Section 3.1.1.3).

3.1.3.1.2 Spectral indices

As a first step to determine the effective SFH of disk galaxies we ought to go beyond the analysis of highly degenerated color profiles (Taylor et al. 2005; Muñoz-Mateos et al. 2007). The study of the spatial distribution of the underlying absorption spectra is a fundamental step in that direction. The use of low-resolution spectra has been demonstrated to be insufficient for breaking the age-metallicity-SFH degeneracy; resolutions $R > 3000$ (at very least; ideally $R = 5000-7000$) should be procured (Vazdekis 1999). Note that this range in spectral resolution is comparable to that of the *X-shooter Spectral Library* (XSL; Cheng et al. 2011), a next generation spectral library. Our MEGARA observations will take full advantage of this spectral library in the study of stellar populations as the low LOS velocity dispersion of face-on spiral disks reduces line blending to the minimum possible in relatively massive external galaxies.

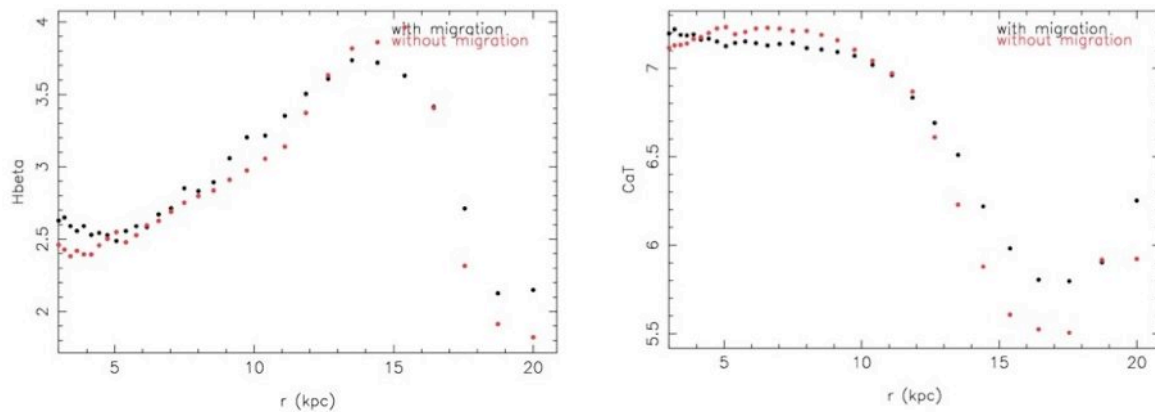


Figure 3.23: Left: Radial profile of the $H\beta$ index for the disk simulated by Sánchez-Blázquez et al. (2009) with and without stellar migration. $H\beta$ does not include the contribution from nebular line emission. Right: The same for the CaT.

Not only we have to improve the analysis of the stellar populations across the disks of galaxies we also need to reach the outer limits of the disks, where the effects of stellar migration and satellite accretion are most notorious. In this regard, Figure 3.23 shows the radial profiles in the $H\beta$ and CaT spectral indices predicted by the simulated disk of Sánchez-Blázquez et al. (2009). Note the sharp change in the indices beyond the break in star formation, which in the case of this massive, dynamically hot disk it is mainly due to the evolution of the position of the break with redshift.

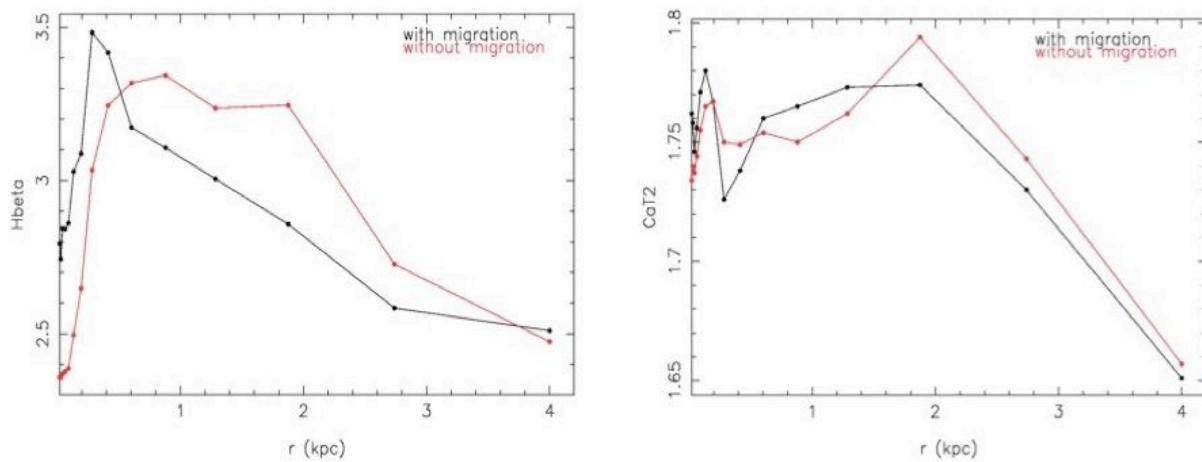


Figure 3.24: The same as Figure 3.23 for the low-mass disk simulated by Sánchez-Blázquez et al. (2010). Points are connected with solid lines for the sake of clarity.

These plots also show that the differences between the indices predicted with and without stellar migration are also maximal beyond the star formation break. In general, stellar migration leads to somewhat flatter or even positive spectral indices gradients in the outer parts of disks (see Yoachim et al. 2010). Similar predictions for the dynamically cooler (and less massive) disk of Sánchez-Blázquez et al. (2010) are shown in Figure 3.24.



The figures above indicate that the spectral indices are very sensitive to differences in the SFH of the unresolved stellar population within and outside the star formation break. However, determining whether stellar migration or evolution of the position of the break with redshift are responsible for the change in spectral properties beyond the break is difficult in this case and should be combined with a kinematical and chemical abundances analysis. Note that an idealized model (such as the one from Roskar et al. 2008), with negligible star formation beyond the break, would also predict a drastic change in the spectral indices at its position. In that case the change would be exclusively due to stellar migration.

Spectral-indices and metal-abundance measurements from unresolved stellar populations are particularly relevant in those regions or galaxies where the chemical composition of individual stars could not be determined because of either crowding or distance (see Section 3.1.3.1). This is the case of our diameter-limited ($2.5' < D_{25} < 4'$) sample of objects within 40-Mpc distance that are selected from a relatively large volume so to include galaxies that would span a wide range of galaxy properties (luminosity, color, environment).

In order to analyze this sample, in particular, the variation of the disk growth rate and role of stellar migration and satellite accretion with those properties we will fit their spectral-indices and chemical abundances radial profiles with the predictions of chemo-spectrophotometric models for the evolution of galaxy disks (also known as *backward* models; Mollá et al. 1999, 2002, 2006; Boissier & Prantzos 1999). These models, as in the case of the idealized N-body simulations of Roskar et al. (2008), grow from inside-out by construction. Therefore, the results from our model fitting of the profiles would first evidence galaxy-to-galaxy variations in the inside-out growth (see Section 3.1.1.3) while departures from the models would be evidence for the impact of mechanisms different from gas infall, including stellar migration and satellite accretion or minor merging. As commented elsewhere this is possible only because we are going beyond the analysis of broad-band photometric data by making use of spectral-indices, chemical-abundances, and abundance-ratios radial profiles.

In Figure 3.25 we show the spectral-indices predictions of the *backward* models by Mollá et al. (2006) for different galaxy halo masses and efficiencies of star formation (note that in the models of Boissier et al. 2001 the secondary parameter is the specific angular momentum, λ , which is intimately related to the star formation efficiency). The combination of age, metallicity, and α /Fe-sensitive indices will provide the necessary information to analyze both the *in-situ* star formation history and the impact of a significant amount of migration/satellite accretion on possible departures from these models, should those mechanisms play a major role.

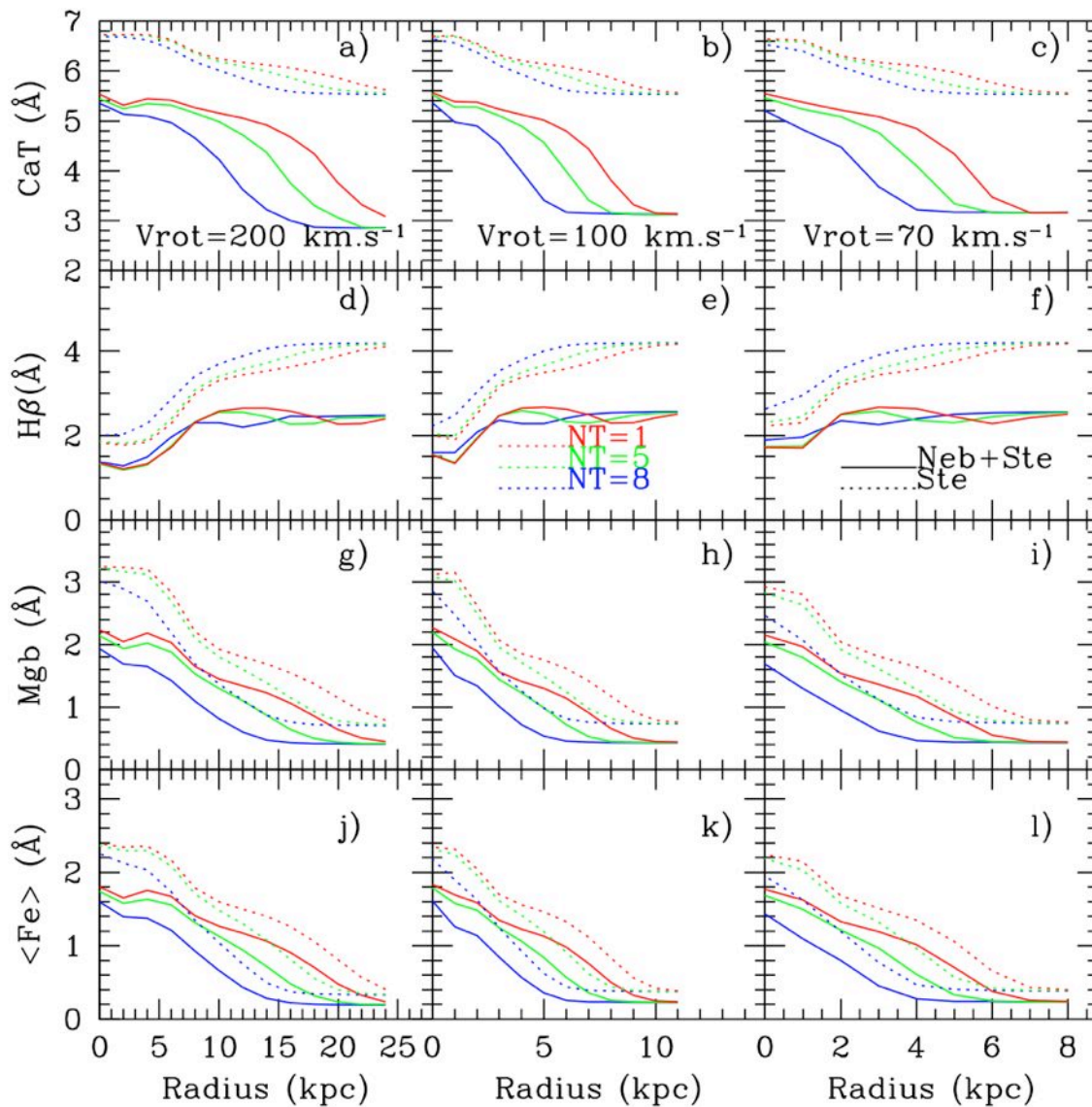


Figure 3.25: Predictions of the Mollá et al. (2006) chemo-spectrophotometric models for the spectral indices of disks with decreasing masses (or circular velocities) from left to right. The predictions for different star formation efficiencies are also shown (from high SFE in red to low SFE in blue). The spectral indices shown correspond to, from top to bottom, CaT, H β , Mgb, and the average of two iron indices (Fe5270 y Fe5335). Dotted lines represent the predictions for the stellar component only, while the solid lines include the contribution of the emission lines and nebular continuum to the windows used to define the spectral indices.

3.1.3.1.3 Chemical abundances

Another fundamental clue in the study of the evolution of disk galaxies is the analysis of chemical abundance patterns. Early studies of the chemical abundances of disks demonstrated that these show negative metallicity gradients which, when computed normalized to the disk scale length, show a very small scatter around a Universal value of $\sim -0.15 \text{ dex/scale-length}$

(e.g. Garnett 1998). This early results were in perfect agreement with the predictions of the inside-out scenario. However, recent studies on some nearby disks have demonstrated that many of these objects show a flattening and even a turn-over in their abundance gradients, which have been interpreted as an effect of stellar migration (Vlajic et al. 2009; Bresolin et al. 2009).

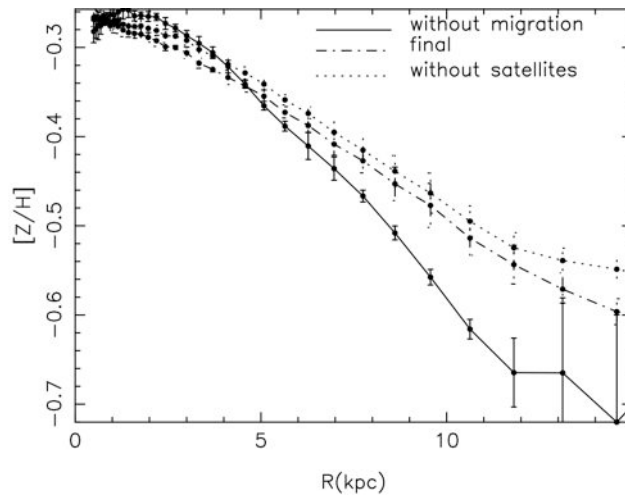


Figure 3.26: Metal abundance gradient of the simulated disk of Sánchez-Blázquez et al. (2009) (dot-dashed line) and without migration (solid line) or satellites (dotted line).

According to the Sánchez-Blázquez et al. simulations, while the effect of migration on the spectral indices is barely measurable ($\Delta < 0.2\text{\AA}$ in the indices), the metal abundances show a clear flattening, especially in those cases where the contribution of accreted satellites (rich in metal-poor stars) is negligible (see Figure 3.26). Not only the abundance of individual elements but also the change in the abundance ratios (typically N/O in the case of the ionized-gas abundances, or the Mg/Fe from the analysis of the absorption spectrum) is key to determine what really populates the outskirts of disks (stars migrated from the inner disk, stars formed *in-situ*, or satellite accretion) (Mollá et al. 2006; Bresolin et al. 2010; see also Section 3.1.3.1.3). In this regard, the stars accreted from satellites should have an effect on the metallicity gradients opposite to that of stellar migration (see Figure 3.26 and the results from Cooper et al. 2010).

In the case of the more distant diameter-limited sample of galaxies proposed as part of MEGADES, we would compare the abundance profiles with the predictions of a complete suite of chemo-spectrophotometric models (Mollá et al. 2006). As already discussed, the departures from these models will be used to estimate the impact of secular mechanisms besides gas in-fall, e.g. stellar migration, satellite accretion, minor merging. In Figure 3.27 we show the predictions of these models for different chemical elements (O, N, Fe), along with the Mg/Fe abundance ratio. More details on how metal abundances will be determined and on the information contained on the analysis of the bi-dimensional distribution on metals on galaxy disks is given later in this document.



3.1.3.2 Mapping the spatial distribution of metals in galaxy disks

3.1.3.2.1 Chemical abundances and abundance ratios

As discussed above, the analysis of chemical abundance patterns is a fundamental clue in the study of the evolution of disks. The first chemical-abundance studies were based in the analysis of spectra of HII regions, which have large masses of gas ionized by young, massive stars, and provide a useful way to derive the chemical abundances of the interstellar medium in galaxies. HII regions show spectra with prominent emission lines of different elements, which can be easily measured up to large distances. The study of HII regions allowed early derivations of the chemical composition and radial gradients in galaxy disks (see Shaver et al. 1983, McCall 1982, Vila-Costas & Edmunds 1992, Belley & Roy 1992, Díaz 1992, Zaritsky et al. 1994; Figure 3.12). These works demonstrated that disks show negative metallicity radial gradients which, when computed normalized to the disk scale length, show a very small scatter around a Universal value of ~ -0.15 dex/scale-length (e.g. Garnett 1998).

These radial gradients in turn can be related to the macroscopic characteristics of galaxies (e.g. Smith 1975; Vila-Costas and Edmunds 1992; Zaritsky et al 1994; Pilyugin Vilchez and Contini 2004) since the chemical evolution of galaxies is intimately related to the star formation histories of galaxies and other fundamental parameters like galaxy mass, luminosity or Hubble type. Thus, this early results were in perfect agreement with the predictions of the inside-out scenario models (Lacey & Fall 1985, Matteucci & Francois 1989, Ferrini et al. 1994, Mollá et al. 1996, 1999, Boissier & Prantzos 1999). Following most of these models, the star formation rate and the infall of gas rate vary from the inner regions of disk to the outer ones, being stronger in the central zones of disks than in the external ones. This characteristic is essential to reproduce the radial gradient of abundances. In Fig.3.1.1.2.2 we show the predictions of radial distributions by models from Mollá & Díaz (2005) for different elements (O, N and Fe) along with the [Mg/Fe] abundance ratio. This complete suite of models is calculated for a wide rotation velocity values and for a set of star formation and molecular clouds efficiencies. We show three different spiral galaxy masses and three different efficiencies (low, medium and high shown by blue, green and red lines, respectively).

Models which successfully predict the abundance gradient help us understand (1) the local processes discussed above plus the distribution of matter across the disk which fuels them and (2) the metallicity and rate of infall of the halo material which formed the disk at different radii. See Henry & Worthey (1999) for a review on the galactic abundance gradients in disk galaxies and ellipticals.

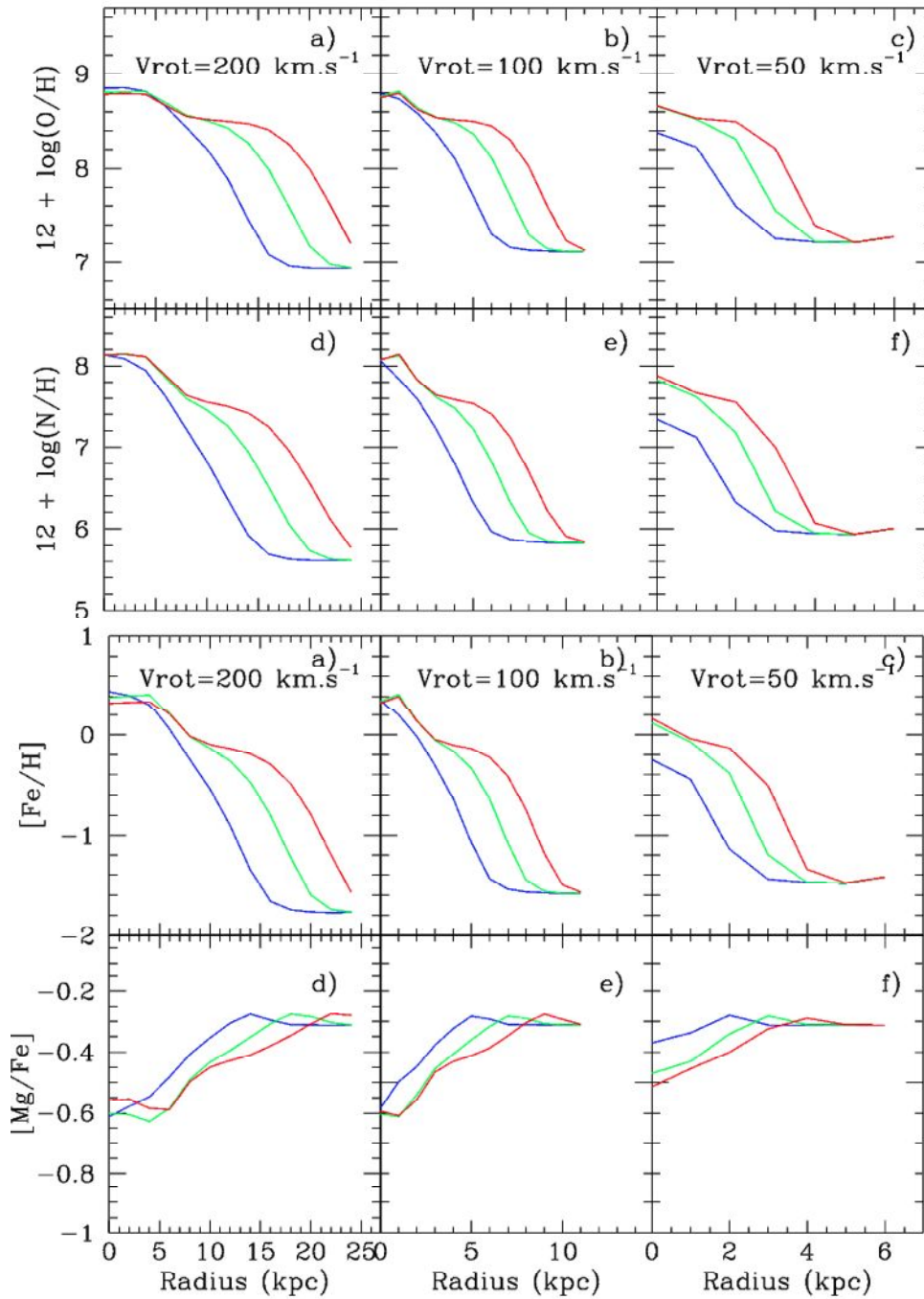


Figure 3.27: Predictions of the Mollá et al. (2006) chemo-spectrophotometric models for the abundances of disks with decreasing masses (or circular velocities) from left to right. The predictions for different star formation efficiencies are also shown (from high SFE in red to low SFE in blue).



3.1.3.2.2 Radial abundance gradients

The study of the radial abundance gradients has shown to be an essential tool to find behaviors different than the standard one (a standard that we presently identify with the inside-out scenario for the evolution of disks). Thus, it was early shown that the presence of the stellar bars in the center of galaxies had an important effect over the elemental abundances distribution on the whole disk: the O/H abundance radial gradient in barred galaxies is considerably shallower in barred galaxies than in normal spiral galaxies and this flattening is correlated to the strength of the bar (Belley & Roy 1992, Martin & Roy 1994, Roy & Walsh 1997, but see recent work by Ellison et al. 2011; Sanchez-Blazquez et al. 2011; Zahid & Bresolin 2011; Rosales-Ortega et al. 2011). This has been attributed to homogenization of the abundances by large-scale gas flows proceeding from the instabilities due to the non-axisymmetrical gravitational potential produced by the bar. Simulations by Friedli et al. (1994) demonstrated that the gas accretion into the center of galaxies leads to a local increase in the star formation, resulting in an increase in the chemical abundance, while large-scale gas motions lead to a mixing outside the corotation radius. This mixing homogenizes the outer part of the galaxy resulting in a break at the corotation radius in the radial abundance gradient. This break may be, therefore, an indication of a recently formed bar. In some cases, bars can also host star formation, for example when large amounts of gas are driven inwards by the effect of a nascent bar. In such cases, this might result in a temporary steepening of the abundance gradient in the central regions instead (see Marino et al. 2012 and references therein).

On the other hand, recent studies on some nearby disks have demonstrated that many of these disk objects show a flattening and even a turn-over in the outer parts of their abundance gradients. For instance, the analysis of the outer disks of M33, NGC 300, or M83 among others indicate a flattening or even a reversal in the metal abundance gradient (either of the stars or the ionized gas) that cannot be explained by a simple inside-out growth model (Mendes de Oliveira et al. 2004; Barker et al. 2007; Vlajic et al. 2009; Bresolin et al. 2009; Marino et al. 2012). The same results were obtained by Pedicelli et al. (2009; see also Vílchez and Esteban 1996) while others, as Henry et al. (2010) find, however, that the radial gradient in our Galaxy steepens at large galactocentric radius. In fact, both results challenge the standard the inside-out scenario that predicts a roughly constant (and rather universal) negative gradient throughout the entire galaxy disk.

The flattening of gradients in the outside regions of disks may be interpreted as an effect of stellar migration (Vlajic et al. 2009; Bresolin et al. 2009; Yoachim et al. 2010) but, other explanations are also possible as the infall of non-primordial gas or the existence of radial flows by a stellar bar (see Section 3.1.1.5).

According to the Sánchez-Blázquez et al. (2009, 2012) simulations the metal abundances show a clear flattening when the stellar migration is included in the models, especially in those cases where the contribution of accreted satellites (rich in metal-poor stars) is negligible (see Figure 3.26). Not only the abundance of individual elements but also the change in the abundance ratios (typically N/O in the case of the ionized-gas abundances, or the Mg/Fe from the analysis of the absorption spectrum) is key to determine what really populates the outskirts of disks: stars migrated from the inner disk, stars formed *in-situ*, or satellite accretion (Mollá et al. 2006;



Bresolin et al. 2010; see also Section 3.1.1.5). Again, the stars accreted from satellites should have an effect on the metallicity gradients opposite to that of stellar migration (see Figure 3.26 and the results from Cooper et al. 2010) in addition to the kinematical effects associated to satellite bombardment that have been discussed elsewhere.

3.1.3.2.3 Metals distribution in galaxies traced in 2D

New instrumental developments such as MEGARA at GTC will allow us to carry out a new observational strategy aimed at deriving true 2D chemical abundance distributions of galaxies. This challenge is still pending given the lack of optimized instrumentation. The MEGARA IFU placed at the Folded-Cassegrain focus of the 10.4m GTC will provide the necessary combination of reasonably wide coverage and large collecting area, thus making this instrument unique within the 10m-class telescopes league.

Powerful constraints on the star formation histories and on the chemical evolution of galaxies can be derived making use of this robust determination of the chemical abundances in two dimensions. Observables like the shape of the metallicity gradient (e.g. slope, flatness), the existence of non-axially symmetric abundance distribution or local perturbations can give us information about the action of gas flows, the influence of bars, environment, among others (see e.g. Vorobyov 2006; Bresolin et al. 2009; Montuori et al. 2010). In turns, this chemical information can be linked to the gas kinematics and color maps of the galaxies as well as it will provide precious clues on the effects of the environment of galaxies on their photo-chemical evolution (Montuori et al. 2010; Rupke et al. 2010; Gavilán, Mollá and Díaz 2009; Iglesias-Páramo et al 2011).

From the theoretical point of view, the shape of the gradient can be a key ingredient for models of galaxy formation. First, although light, the inside-out scenario of galaxy formation already predicts some degree of flattening in the metallicity gradients at large galactocentric distances. The disk is built up via gas infall with a time scale of formation increasing with galactocentric distance (Matteucci and Francois 1989; Boissier and Prantzos 1999; Chiappini et al. 2003; Molla and Diaz 2005). Chemodynamical models also predict a plateau of the abundance gradient at large galactocentric distance and likewise in the central region (Samland et al 1997; Hensler and Recchi 2010). Finally, the theory of viscous evolution of a star-forming disk (e.g. Lin and Pringle 1987; Ferguson and Clarke 2001) predicts an angular momentum redistribution and gas flows, which in turns could lead to a somewhat flatter abundance gradient of the ISM in the outer parts of spirals (e.g. Sommer-Larsen and Yoshii 1990; Thon and Meusinger 1998). Not to mention the rather severe effects associated to stellar migration, bars, minor merging, etc. These effects are important to bear in mind given that the derivation of the slope of the gradient, as well as, the maximum and minimum metallicity, are valuable observational clues in order to test different theoretical predictions.



3.1.3.2.4 Long-standing questions on the determination of chemical abundances

Chemo-dynamical effects

Chemodynamics intends to provide a global dynamical description of the interplay between the major physical components of galaxies: in a gravitational potential essentially dominated by dark matter, stars structure the multi-phase interstellar medium (ISM) through radiation, winds and supernovae explosions, and enrich it in heavy elements. The ISM self-regulates and the star formation rate (SFR) in galaxies is ultimately controlled by feedback processes. But in addition to small scale processes, chemodynamics also may refer to large scale processes like the non homogeneous distribution of stars and metal abundances in galaxy disks and bulges, the star formation triggered by the flows of gas towards the nuclei of interacting galaxies during the early phases of merging or the galaxy wide shocks resulting from galactic collisions among others.

To this respect, chemodynamical models of formation and evolution of galaxies are becoming increasingly present for the study of the physical mechanisms that occur within galaxies; in particular, they provide quantitative predictions for the observable consequences of these mechanisms. Perhaps the main conclusion raised from these studies is that observations over a wide range of wavelengths must be linked in order to gather the information required to answer the key questions related to this topic.

Large surveys in the local Universe allow probing galaxies panchromatically from X-rays (XMM, CHANDRA) through UV (GALEX) to IR (Spitzer, AKARI, WISE). In addition, the recent availability of Integral Field Units in many optical telescopes allows bidimensional spectroscopic studies with full coverage of regions where recent star formation is taking place and the physical processes involving the stellar populations and the ISM can be studied in detail from both the spatial and the spectral field of views.

A point in common between all these processes is the far from simple kinematical structure of the ISM, as it is observed in optical spectra: multiple components or simply lines broader than normal thermally excited lines have been reported for galactic winds and/or shocks in mergers induced by tidal forces (Monreal-Ibero et al. 2010a; Rosales-Ortega et al. 2011) or in galaxy collisions (SQ, Iglesias-Páramo et al. 2011). In this last case, the different kinematical components are associated to gas phases with a different metal content. Also, kinematical decoupling between lines of different excitation of the same component has been reported for HII regions in starburst galaxies (e.g. NGC 5253, Monreal-Ibero et al. 2010b; Mrk 996, James et al. 2009).

The detailed study of the physical mechanisms involved in the interaction of the ISM with the ionizing stellar populations in star forming regions, or the physical properties of the emission line regions in interacting galaxies, require not only bidimensional spatial information but also high spectral resolution in order to resolve each kinematical component, mapping the actual velocity field. Thus, the chemodynamical approach includes the complete study of the physical properties and the chemical composition of each kinematical component of the emission lines. This is a challenging technique for galaxy research using conventional spectrographs; MEGARA delivers the spatial coverage and spectral resolution necessary to carry this out.



Abundance Discrepancy Factor in nebulae: recombination vs. collisionally-excited lines

Determining chemical abundances is not an easy task. Abundance measurements can be affected by multiple systematic uncertainties that yield non-negligible offsets when abundances obtained from different methods are compared. These methods include stellar abundances from B- and A-supergiants (e.g. Urbaneja et al. 2005a, 2005b) or RGB stars (from the CaT at resolutions down to $R \sim 5000$; e.g. Armandroff & da Costa 1991), or ionized-gas abundances from HII regions (e.g. Vilchez et al. 1988; Magrini et al. 2007) or PNe (e.g. Leisy & Dennefeld 2006; Bresolin et al 2010), either from recombination lines (ORLs; Liu et al. 2006; Tsamis et al. 2008) or collisionally-excited forbidden lines (CELs; which can then be based on T_e measurements or strong-line methods; see Kennicutt et al. 2003; Pérez-Montero & Díaz 2005; Nagao et al. 2006; Yin et al. 2007; Liang et al. 2007; Shi et al. 2007; Kewley & Ellison 2008). Some of these differences are intrinsic, such as the depletion of metals in the gas phase, dredge-up processes, or the presence of a cool gas phase component not traced by CELs.

The field is at a crossroads as no consensus has been reached on the long-standing *abundance discrepancy* problem (e.g. Peimbert et al. 1993; Tsamis et al. 2003; Esteban et al. 2009): for several Galactic and extragalactic HII regions (in the Magellanic Clouds and in Local Group galaxies) the abundances of the aforementioned elements, relative to hydrogen, derived from analyses of their faint optical recombination lines (ORLs) are systematically larger than those obtained from the bright collisionally excited lines (CELs) of the same elements. The discrepancies for oxygen in HII regions are typically a factor of $\sim 0.2-0.3$ dex (Mesa-Delgado et al 2010): this is most worrying as the abundance of oxygen is the most common way of measuring the metallicity both in star-forming regions or distant galaxies (Pagel & Edmunds 1981).

At the moment there is no consensus whether the elevated measurements from ORLs are robust indicators of the mean metallicity of an HII region (e.g. Peimbert et al. 2007) or whether the ORLs may be biased towards a discrete, minor component of a nebula consisting of relatively hydrogen-deficient, clumped gas (e.g. Tsamis & Pequignot 2005). This is unfortunate since as long as the problem remains unsolved the field of galactic chemical evolution remains also in limbo. The strongest ORLs of oxygen and carbon are found in the optical range between $4000 - 5000 \text{ \AA}$ and are due to OII $3s-3p$ and CII $4f-3d$ transitions at 4650 and 4267 \AA , respectively. The lines are intrinsically faint with intensities of the order of less than one per cent of $H\beta$ but offer the advantage that the ratio of their emissivities to HI lines is a weak function of the plasma temperature and density (Storey 1994; Tsamis et al. 2008). The derived abundances should thus be less prone to errors resulting from uncertainties in the measurement of these quantities. This is in contrast to abundances derived from ratios of CELs to HI lines (e.g. $[O III] \lambda 5007 \text{ \AA} / H\beta$, $[C III] \lambda 1908 \text{ \AA} / H\beta$) which have an exponential sensitivity to the electron temperature, and also depend on the plasma density when CELs of low critical densities are used (Rubin 1989).

The abundance results gathered from massive A, B supergiants in galaxy disks (NGC 300, Bresolin et al. 2010; M33, Monteverde et al. 2000, Urbaneja et al. 2005; see also U et al. 2009 and references therein) show an overall agreement between stellar and nebular abundances, though within a large scatter. Thus, it seems necessary to compare the chemical abundances of



B stars with the nearby H II regions, since these abundances should be similar once all the potential sources of error have been taken into account (e.g. Simon-Díaz and Stasinska 2010), for example (1) the fraction of O atoms embedded in dust grains, (2) possible modifications of O/H in the stars due to mixing, (3) other aspects related with the abundance determination. Kewley & Ellison (2008) have reviewed 10 different strong-line abundance calibrations in use to derive the O/H ratio from H II regions. Differences between photoionization model-based and empirical calibrations as high as a factor of 5 have been found! It is clear that this issue is an important problem and has to be improved. The direct method based on the measurement of the [O III] 4363/5007 ratio in HII regions yields values up to 2 times lower than those derived from adjusting [O II]3727 and [O III]5007 with photoionization models (without adjusting [O III] 4363); and yields factors 2 to 3 times lower than those derived from recombination lines; see the discussion by Peimbert & Peimbert (2011).

The O/H overall budget of the Universe

A very important problem in modern astrophysics related to the chemical evolution of galaxies and of the Universe as a whole is the one of the O/H overall budget of the Universe. According to some authors there is a deficiency in the O/H budget of the observable universe. One of the ingredients to study the O/H budget and the chemical evolution of galaxies is provided by the O/H value derived from HII regions.

An O/H ratio higher by a factor of two implies that the galaxies have formed twice as many stars in the past, if all the parameters that enter into this computation are assumed to be the same. To address this problem what is needed is to reduce the errors of the abundance determination by about a factor of two or three in order to be able to pose strong constraints in the chemical evolution of galaxies and of the Universe as a whole.

It would be desirable to observe a set of HII regions and PNe of Type II to approach all these problems; it would also be important to determine stellar abundances from B supergiants in these galaxies.

The obvious objects where it is possible to get data of reasonable quality are given in the observational strategy section. Although some data pertaining to these issues have already been obtained, we think that higher quality data can be secured with MEGARA. The higher spatial resolution provided by MEGARA will permit to study the variation of physical parameters across the face of extended HII regions. MEGARA will allow us to obtain data with a higher signal-to-noise ratio than previously achieved, and with higher spectral resolution than most other data available. Moreover, the data can be analyzed with higher detail and with more sophisticated models than those used in the past.



3.1.3.3 *Determining the role of minor mergers*

The predictions of N-body simulations and the high frequency of these events both suggest that minor mergers might play a leading role in the formation of inner disks and rings in early-type galaxies (S0-Sa). However, the role of minor mergers in the generation of these dynamically-cold inner substructures is still unknown and supporting observational data is still lacking.

In this regard, it is only recently that the specific properties of the stellar populations in *each* structural and kinematical sub-component of galaxies are starting to be analyzed separately (e.g. the SAURON survey). In this sense, the present study aims to be pioneer in establishing the properties of the stellar populations of inner disks in relation with the other galaxy components, and their possible minor-merger origin.

As an illustration of the potential of this technique, in Figure 3.28 we compare the typical morphology of several inner components detected in real spiral galaxies with similar cases formed in N-body experiments of minor mergers onto spiral galaxies (Eliche-Moral et al. 2006, 2011, 2012). The similarity of the structures is striking. But besides their impact on the structural properties of disks, minor mergers also produce characteristic features in the dynamics and stellar populations of the inner components formed (Tutukov & Fedorova, 2006; Eliche-Moral et al. 2006, 2011, 2012; Gómez et al. 2012). Thus, according to some of these numerical simulations, it should be possible to distinguish between a minor-merger origin and an internally-driven secular one through an exhaustive analysis of the kinematics and properties of the different galactic sub-components.

Aiming at disentangling between these two possible origins for these inner components, we propose to obtain 2D spectroscopy of the inner disks and their surroundings for a sample of nearby S0-Sa galaxies with detected inner components from the S4G survey (Laurikainen et al. 2010, Sheth et al. 2010). Based on the results of the precedent NIRS0S survey, roughly half of our sample should exhibit clear interaction relics (such as tidal tails or shells), whereas the other half must have no detectable merger signs (which will constitute our control sample).

The main goal is to characterize the inner components a sample of nearby S0-S0/a galaxies with inner disks in terms of their stellar populations and kinematics, as well as their relation to those of the main disk and the underlying bulge, including galaxies with and without merger traces. This requires to map the flux spatial distribution of the most relevant emission and absorption lines in the optical range to so derive the kinematical and structural properties of the gas and stellar populations in the different sub-components.

The resulting distributions in age and metallicity of stars at the different sub-components of these galaxies, as well as their velocity maps, will be compared to those obtained from N-body simulation models of minor mergers onto S0 galaxies including gas and star formation (Eliche-Moral et al. 2012, in preparation) and from internal secular evolution models (Debattista et al. 2005) to derive conclusions concerning the possible minor-merger or pure bar-driven origin of the inner disks and rings in this S0-Sa sample.

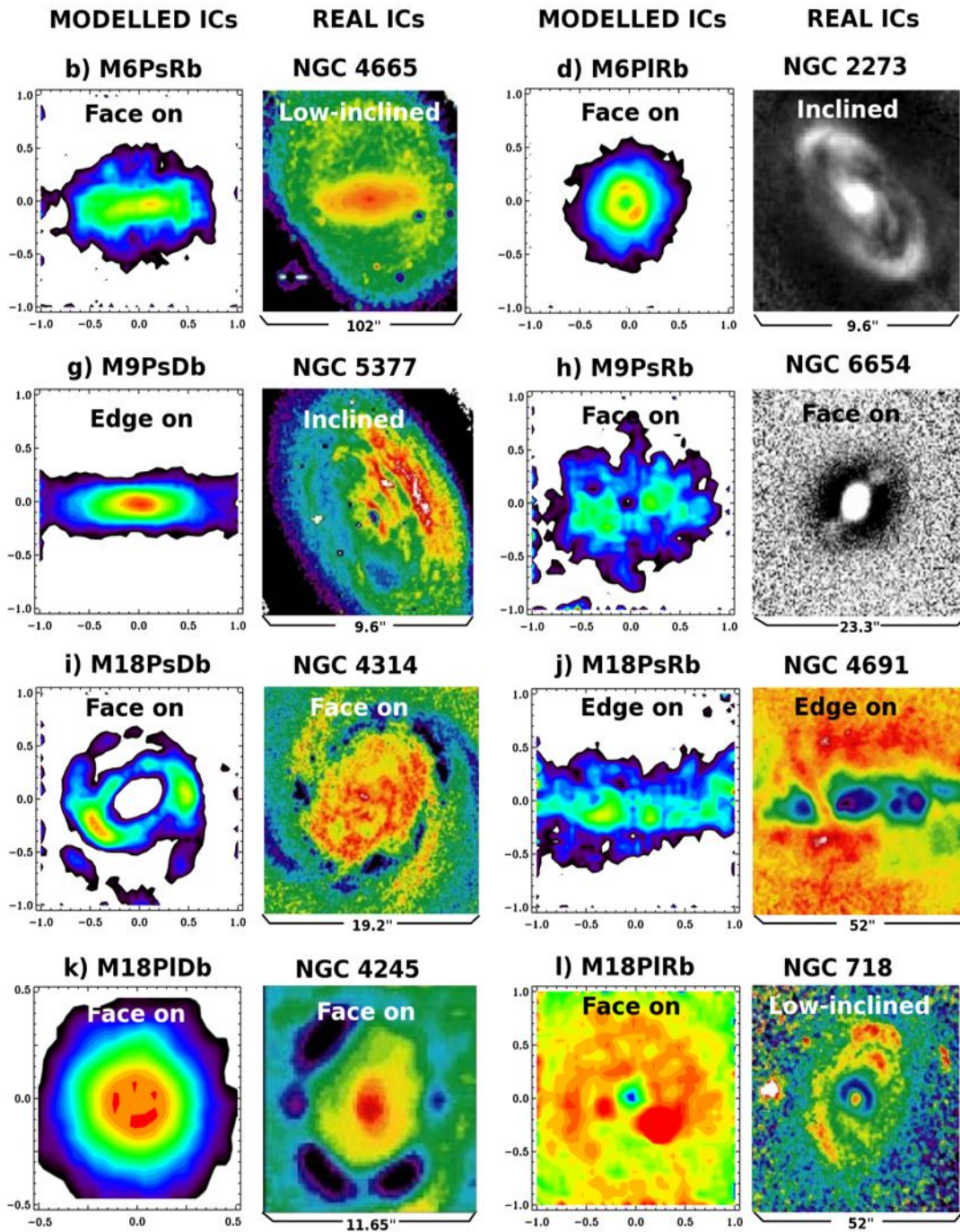


Figure 3.28: Comparison of some inner rings and disks formed in the minor merger simulations by Eliche-Moral et al. (2011) to some structures with similar morphologies detected in some early-type galaxies (1st and 3rd and 2nd and 4th columns, respectively). Colored maps of real galaxies correspond to $B - R$ or $V - I$ color maps of the galaxies by Erwin & Sparke (2003), while the grey-scale maps represent unsharp masks in V , R or H bands by the same authors. North is up and East is left in real images, except in NGC 4665, which is rotated 90° clockwise.



3.1.3.4 Determining the role of starburst activity

3.1.3.4.1 M82-like Super Galactic Winds

Here we describe the methodology that we will follow to study the nearby galaxy M82 as the ideal laboratory to understand dense Super Galactic Winds (SGWs) and their possible role on the spectro-photometric and chemical evolution of galaxies.

The stellar winds of the SSCs discovered in starburst galaxies as M82 are found to either produce a bubble at their places of origin or to interact with the winds from neighboring SSCs to give rise to a filament. The final aim of this study is to determine the detailed physical link between SSCs and the filamentary structure seen in M82. To achieve this, we need first to fully characterize the properties of the SSC culprit of the SGW, and secondly to understand the ionized structure of the filaments.

According to our models, the evolutionary stage of compact sources (age of the SSCs) determines what fraction of the mechanical luminosity of the young cluster is to be delivered to the associated wind. The heating parameter (η) is then a factor to be estimated for SSCs within the core of M82. With this in mind we will make use of the SSCs catalog from Melo et al. (2005) where our group has already identified a region with higher overabundance of young SSCs in M82. Given the level of crowding in this region the use of a IFU with a good spatial resolution and sampling, such as that of both the IFU LCB and SCB bundles, is a must in this case. Both the age of the SSCs (from LR spectra) and the ionized-gas kinematics at the position of the SSCs should be determined in order to understand the feedback mechanism in place at the position of the SSCs and the potential interaction between individual SSCs to give rise to the SGW in M82.

The properties of the SGW itself, mainly the kinematics associated to its filamentary structure, will be analyzed all along the M82 biconical wind using the MEGARA MOS component with the highest resolution possible. The comparison of the kinematics of these filaments with the predictions of our models plus the constraints provided by the analysis of the SSCs is the most powerful tool in hand to understand the transition *from* a wind dominated by local effects (associated to individual SSCs) *to* a well-defined large-scale SGW.

3.1.3.4.2 Neutral Galactic Winds

Winds in low-activity galaxies

Most studies on galactic winds are strongly biased towards strong starbursts and luminous active galaxies, but very little is known of this phenomenon in quiescent, low-activity galaxies. Nevertheless, the case of the wind in NGC 4321 and the discovery of low-luminosity nuclear activity in nearby galaxies (undetected by standard optical diagnostics) prove that quiescent galaxies may also host strong winds. Should NGC 4321 be representative of the abundant family of low-activity galaxies, the amount of dust and metals in the intergalactic medium could



be severely underestimated.

Even if the velocities in the wind are not high enough to allow it to escape the galaxy potential, a less powerful wind can play a very relevant role in redistributing dust and metals within the galaxy itself. Therefore, the relevant question is: how representative is the wind in NGC 4321 of similar phenomena in other “normal”, relatively inactive galaxies? This question can only be answered by observing a significant sample of low- to moderate-activity galaxies with the techniques used for NGC 4321.

We intend to use MEGARA at GTC to study the existence, frequency and strength of winds in a sample of nearby galaxies, including objects with little or no detected nuclear activity for which this phenomenon remains mostly unexplored, and how they compare to active galaxies.

The spectral coverage and resolution provided by MEGARA will allow us to study the presence of winds in the nuclear region of a sample of nearby galaxies (not biased either towards or against star-formation/AGN activity) through the detection in the spectra of blueshifted component in Na I D interstellar absorption line, as well as through the existence of multiple kinematical components in the emission lines. The spatial coverage and the spectral resolution of MEGARA will provide unprecedented information on the wind geometry and kinematics. The detection of the absorbing material throughout the field of view will allow us to map the distribution and kinematics of the cold absorbers. In addition, we will be able to discriminate kinematically the ionized component of the outflowing material and to produce maps for the distribution and kinematics of this warmer phase of the wind. A single observation provides therefore complementary and simultaneous views of the wind for different gas phases on the same object, which is essential for a better understanding of this complex phenomenon.

Winds in ULIRGs

In addition to the study of neutral winds in a sample of galaxies not biased in terms of star formation or nuclear activity we intend to use MEGARA at GTC for studying the physics of the winds in nearby ULIRGs ($0.04 < z < 0.08$). Previous studies of winds in these objects with long-slit spectra have detected widespread (up to 15 kpc) massive (up to $10^8 L_{\odot}$) strong winds, and have pointed to a complex underlying structure and kinematics. In particular, strong velocity gradients suggest that extended star formation and not only the nuclear starburst, are responsible for the energy input of the wind (cf. Martin 2006). It is worth mentioning that the density of ULIRGs in the Local Universe is so low ($2.5 \times 10^{-7} \text{ Mpc}^{-3}$; Sanders et al. 2003) that in order to have a statistically significant sample of these objects a volume significantly larger than that used for the rest of the MEGADES science (i.e. the Local Group or the 40-Mpc-radius S4G volume) should be explored.

The spectral coverage and resolution provided by MEGARA will allow us to study the complex kinematics and distribution of the different phases in galactic winds by covering simultaneously emission and absorption features. Both, 2D coverage and kinematical information for several spectral lines are needed to properly understand the multi-phase structure of the winds.



We will study the presence of winds in ULIRGs through the detection in the spectra of blueshifted component in Na I D interstellar absorption line as well as through the existence of multiple kinematical components in the emission lines. The spatial coverage (with the IFU LCB) and spectral resolution of MEGARA will provide unprecedented information on the wind geometry and kinematics. On one hand, the detection of the absorbing material throughout the field of view will allow us to map the distribution and kinematics of the cold absorbers. On the other hand, we will be able to discriminate kinematically the ionized component of the outflowing material and to produce maps for the distribution and kinematics of this warmer phase of the wind. This approach provides a unique simultaneous global view of these two phases of a galactic wind.

Integral-field spectroscopy data from MEGARA will help us to better understand the important role of galactic winds in ULIRGs on galaxy evolution and cosmology. These observations will allow to estimate the total mass of gas in the wind, and the fraction of the gas that is able to escape the gravitational potential of the galaxy and pollute the IGM with dust and/or metals. Both estimates are critical to be able to understand the global picture of galaxy evolution.

3.1.3.4.3 Direct observation of massive-star feedback

As part of MEGADES we will observe a number of massive stars in the disk of M33 and in IC 1613 associated to ionized-gas regions. As one of the objectives of these observations we will characterize the winds of O stars and B-supergiants, by yielding mass loss rates for the targets from quantitative spectroscopic analysis. The wind parameters will then be the key to understand the interplay of massive stars and gas, and to determine the origin of the carved ionized structures. These results will also extend the current observational metallicity–mass loss relation in the poorly studied metal-poor end. Additionally, we will be able to test the predictions of the theory of radiation driven winds at very low metallicities and confirm (or otherwise discard) its apparent break down found at the SMC for luminosities $\log L/L_{\odot} \sim 5.6$ (Bouret et al. 2003; Martins et al. 2004), the so-called weak wind problem.

3.1.3.5 *Determining the role of nuclear activity*

The study of a large sample of galaxies of different types (including AGNs), as proposed in the MEGADES survey, would allow us to make a comparative analysis of the gradients in the stellar and gas properties for active and inactive galaxies. On one hand, the central IFU LCB observations will provide us with a direct insight of the central *few* kpc regions (e.g. Stoklasova et al. 2009), which will allow us to determine the frequency of kinematics evidence of past mergers (e.g. central counter-rotating disks and or kinematic decoupled gas/stars, see Section 3.1.1.4). Evidence of gas feeding and/or feedback from the nuclei can be easily identified by this technique (e.g. the central outflow in M51). The spectral resolution, FOV and spatial sampling of the IFU LCB would provide unique information on these dynamical features. On the other hand, the external MEGARA MOS observations will provide us with the large-scale dynamical information, for which a complete coverage is not needed.

The different scenarios proposed for the transition between the blue-cloud and the red-sequence



predict different gradients in the light-weighted age and metallicity of the stellar populations and their metallicities and in the gas properties (ionization, chemical abundance). Therefore, the comparative study of these properties between active and inactive galaxies would provide us with (i) statistical differences among both samples (i.e. which properties are “peculiar” for AGN hosts and which ones are not), and (ii) a way of discriminating between the different proposed hypothesis. The central IFU LCB observations, with detailed spatially-resolved information of the central kpc regions (fundamental to understand the evolution of galaxies, as demonstrated by the results of the SAURON survey), and the MOS, with a sparse but wide coverage of the outer regions, will both provide fundamental information in order to measure these radial variation in the spectroscopic properties of galaxies.

To achieve the proposed science goals it is required to analyze the spatially-resolved properties of the stellar populations and gas content for both the different transition galaxies, the AGN hosts, the proposed progenitors, and a large set of comparison galaxies. We will apply the analysis procedures that we have developed during the last years to decouple the stellar and ionized gas components and to analyze each of them so to derive their physical conditions (e.g. García-Lorenzo et al. 2005; Sánchez et al. 2005)

The stellar populations will be studied using different (complementary) approaches:

1. Fitting the underlying continuum using synthetic models that reproduce both the continuum shape and absorption features. This is possible thanks to the wide spectral range and good spectral resolution of (i) the observations proposed within MEGADES, (ii) state-of-the-art spectral libraries such as MILES (Sánchez-Blazquez et al. 2006; and soon XSL; Cheng et al. 2011), and advanced multi-SSP fitting procedures like Starlight (González Delgado et al. 2005) or FIT3D (Sánchez et al. 2012). In order to study the spectra of these unresolved stellar populations it is essential to perform an accurate subtraction of the emission of the ionized gas. This will be done in an iterative way using tools that have been developed by Sánchez et al. (2006, 2007a) and by others in the last few years (e.g. Cid Fernandes et al. 2005, 2007, 2009; Koleva et al. 2009; MacArthur et al. 2009).
2. The analysis of different absorption features, including typical age indicators (like the hydrogen Balmer lines) and metallicity indicators (like Mgb and multiple Fe absorption lines; e.g. Trager et al. 2000).
3. An analysis of full multi-wavelength spectral energy distributions (SEDs) will be carried out by combining the spectra provided by MEGARA with measurements from the UV to the near- and mid-infrared. We will make use of data from Spitzer (available by sample construction), GALEX, SDSS, ground-based H α (available for the majority of the targets) and WISE data (at 24 μ m at least).

The requirements in terms of observing time will be identical to those used to derive the spatial distribution of the stellar populations and chemical abundances in disks described in Section 3.1.5.1.2. This is a perfect example of how two different science goals can be accomplished using the same dataset. In other cases additional observations will be needed in order to fully understand the physical mechanisms in place, for example, regarding the study of the evolution of Galactic Winds or the formation of merger-driven inner disks.

3.1.3.6 Studying the evolution of massive stars in external galaxies

Some of most important open questions on the issue of massive star evolution (and in other topics) remain unanswered mainly because both our Galaxy and other well-studied Local Group galaxies (M31, M33) cover a very limited range in physical properties, mass, luminosity, color, metallicity, nuclear activity. In this regard, metallicity is an important agent of the evolution of massive stars (perhaps only surpassed by the stellar mass) directly, through the equations of stellar structure, and indirectly, through its modulation of the wind mass loss rate ($dM/dt \propto Z^m$, with $m = 0.83 \pm 0.16$; Mokiem et al. 2007). Even though Local Group spirals, including M33, exhibit a metallicity gradient, the covered Z range is rather limited, especially in the metal-poor end. Dwarf irregular galaxies in the Local Group are the ideal reservoirs of massive stars at low metallicity. The two "Massive Stars FLAMES Surveys" (Evans et al. 2005, 2010) have devoted a large amount of VLT time to characterize massive stars in the Magellanic Clouds. While the resulting vast dataset has produced new important insight into stellar evolution (for instance, the role played by stellar rotation in surface abundance enrichment, Hunter et al. 2008, or the characterization of mass loss rate with metallicity, Mokiem et al. 2007), it is still limited to a narrow metallicity range. To extend the range of metallicities to values below the SMC we ought to observe other nearby irregulars (e.g. IC 1613; see Figure 3.29).

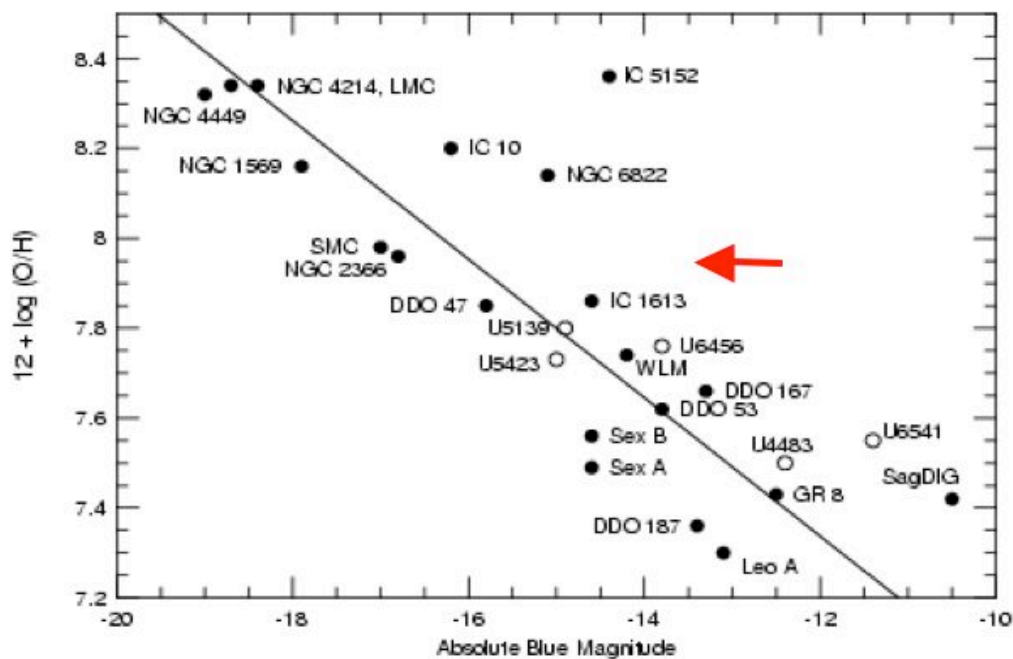


Figure 3.29: Metal abundance of Local Group irregular galaxies as a function of magnitude, from Skillman et al. (1989). While still bright and close enough for efficient spectroscopy of its massive population, the metal content of IC 1613 is significantly lower than the SMC's.

The proposed MEGARA observations in the Local Group will cover a metallicity range from $1.3Z_{\odot}$ (in the central parts of M33) to $0.04Z_{\odot}$ (IC 1613). We estimate that the number of bright ($V \leq 19.5$) blue massive stars enclosed in the MEGARA MOS FOV ($3.5 \times 3.5 \text{ arcmin}^2$) in M33



and IC 1613 is close to 100 in the dense areas and about 50 in the less populated regions. Consequently, we will have a large database of high resolution, high quality spectra of blue massive stars out of which we expect to find a variety of evolutionary stages. Our explicit objective is to analyze quantitatively the spectra to obtain the physical parameters and surface abundances of the stars: He, CNO, and α -elements for the early types (B, hot LBVs), CNO and Fe from the later types (A, cool LBVs). For the analysis, we will use advanced stellar atmosphere codes FASTWIND (Puls et al. 2005) and CMFGEN (Hillier & Miller 1998) that properly account for the physics in the atmospheres of massive stars. Their physical properties, spectral types and abundances, together with their location in the HRD, will lead to a wider picture of the impact of metallicity on massive star evolution.

From the total collected sample, we will have A- and B-supergiants distributed across the surface of M33 and IC 1613. The analysis of their spectra will produce chemical abundances for a number of elements (see Section 3.1.1.8). The spatial distribution of their chemical abundances would put additional constraints on the chemical evolution of the parent galaxies.

We will also extend the study of individual stars outside the Local Group as far as possible. The observations proposed as part of other projects proposed by the MEGARA Science Team will be used for this purpose (e.g. the Early Science observations on M81). Besides probes of the chemical composition, massive stars can also be used as distance candles based on spectroscopically derived properties (Kudritzki 2010; Kudritzki et al. 1995).



3.1.4 Sample

3.1.4.1 *Local Group disk galaxies*

As discussed in previous sections, the analysis of the velocity dispersions of individual young and old stars along with chemical abundances measurements from those same stars provides key information to determine the role of different secular mechanisms in order to drive the spectrophotometric and chemical evolution of galaxies and should allow us, for example, to disentangle the relative contribution of *in-situ* star formation, stellar migration, and satellite accretion (among other processes) on the stellar population content of disks.

The only bona-fide spiral disks in the Local Group are those of M31 and M33 (both visible from La Palma). The disk of M31 is inclined 77° with respect to the line of sight. This makes difficult (and uncertain) the determination of the σ_z component of the velocity ellipsoid. In addition to that, M31 is particularly dusty, which further complicates any stellar population or chemical abundances study by means of attenuating the light from individual stars and by worsening the well-known age-extinction-metallicity degeneracies.

Therefore, we decided to study the significantly less inclined disk of M33 ($i=56^\circ$; Corbelli & Schneider 1997). With regard to the determination of the velocity ellipsoid, the inclination of M33 is ideal as, on one hand, a minimum inclination of 40° is needed in order to ensure that rotational motion and other in-plane velocities are observable in the LOS velocities and, on the other hand, disks with inclinations $>70^\circ$ should not be attempted in order to avoid extreme projection effects along the LOS and to ensure that the minor axis kinematics are properly spatially resolved (see e.g. Noordermeer et al. 2008). Besides, Koch et al. (2008) intensively studied the RGB population of the disk of M31 (>3500 stars) in CaT spectroscopy using Keck already (see also Gilbert et al. 2009).

3.1.4.1.1 The Local Group spiral galaxy M33

M33 is a SA(s)cd spiral galaxy placed at 840 kpc from our own Milky Way (Freeman et al. 2001). It hosts up to ten amorphous spiral arms (e.g. Humphreys and Sandage 1980) and a rather small and faint bulge. The spiral structure is better traced by the UV emission (Marcum et al. 2001; Gil de Paz et al. 2007) than by $H\alpha$ (Massey et al. 1996). The $H\alpha$ morphology is dominated by a number of giant extragalactic HII regions, including the massive NGC 604 (see Figure 3.30). M33 is a relatively low mass system, with a total stellar mass of $4 \times 10^9 M_\odot$ and a total dynamical mass of $5 \times 10^{10} M_\odot$ (the rotation curve reaches only a maximum velocity of 120 km s^{-1} in the disk region; see e.g. Simon et al. 2006). With an inclination of 56 degrees (Zaritsky et al. 1989) the disk of M33 is perfectly suited for measuring its velocity ellipsoid.

One important issue regarding the adequation of M33 for the study of secular (internal and external) effects on the evolution of disks is whether the possible past interaction between M33 and M31 might have altered the recent spectro-photometric, chemical and kinematical evolution of the former. During the past few years, several works have argued that M33 and M31 may have interacted during cosmologically-recent epochs, and that such an interaction may have affected the properties of the M33 disk. The HI structure analyzed by Braun & Thilker (2004)



also suggests the presence of a HI structure apparently linking M33 and M31. The simulations by Bekki (2008) explain this as a tidal feature result of an interaction 4 – 8 Gyr ago. Other models (Putman et al. 2009) focused on the possible orbital trajectories of M31 and M33 infer that the interaction could have taken place $\sim 1\text{--}3$ Gyr ago with a tidal radius in the case of M33 of 15 kpc (similar results have been obtained by McConnachie et al. 2009).

Despite these results, both the works of Muñoz-Mateos et al. (2007) and Li et al. (2004) indicate that the spectral energy distribution of the disk of M33 is broadly compatible with an inside-out formation except for a reversal in the mean age gradient (compared to the inside-out predictions) beyond a 8 kpc (Williams et al. 2009), in agreement with the expectations from some level of stellar migration taking place in its disk. Finally, Davidge & Puzia (2011) have demonstrated that the recent SFR in the inner disk (within 8 kpc) has been rather constant which suggests that M33 has evolved in isolation for at least the past ~ 0.5 Gyr.

Finally, it is worth noting that even the most isolated galaxies in the Local Universe are believed to have experienced galaxy-galaxy interactions comparable to that believed to have occurred between M31 and M33 roughly 3 Gyr ago, with a pericentric radius of ~ 40 kpc (McConnachie et al. 2009; see Font et al. 2001 for the distribution of pericentric radii between dark-matter halos). Indeed, even one of the most isolated galaxies in the Local Volume, M83, is believed to have interacted with nearby NGC 5253 in the last Gyr or so (van den Bergh 1980; Kobulnicky & Skillman 1995). The present-day projected distance between these two systems is only 150 kpc.

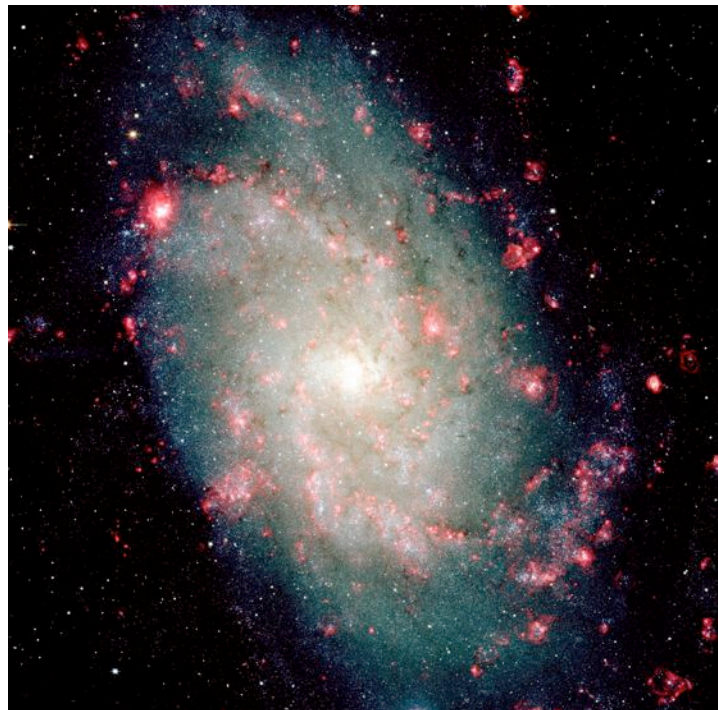


Figure 3.30: False-color image of M33 obtained as part of the Local Group imaging survey by Massey et al. (2006). This picture is made up of two continuum broad-band images (green and blue channels) and one H α narrow-band image (red channel). North is up, East is to the left. The luminous, high-surface-brightness HII region NGC 604 is seen at the northeast corner of the image.

3.1.4.1.2 The Local Group galaxy IC 1613

In order to extend the study of the massive star population in the Local Group in metallicity beyond that of M33 we look for a star-forming system with the lowest metallicity measured that would also be as close as possible to the Milky Way. The magellanic irregular galaxy IC 1613 is an ideal target in this regard as it has a metal abundance significantly smaller than that of the SMC (0.04 to 0.2 Z_{\odot} , Talent et al. 1980; Peimbert et al. 1988; Tautvaišienė et al. 2007). Indeed, from the analysis of the blue massive star population of IC1613 we can study (1) the physical properties of the individual OB stars themselves and (2) the interplay of their winds with the ISM both in an unprecedented low metallicity regime.

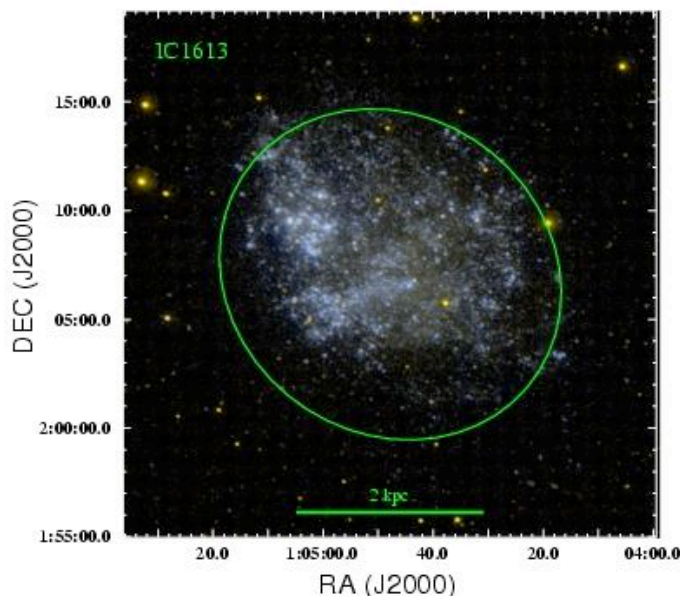


Figure 3.31: GALEX false-color image of Local Group galaxy IC 1613 (Gil de Paz et al. 2007) obtained as a combination of GALEX FUV (blue), NUV (red) and a linear combination of FUV and NUV (green).

The stellar body of the IC 1613 stellar component extends about 16.5 arcmin from its centre (Bernard et al. 2007), but the young population is mainly concentrated in the central 9×9 arcmin² shown (see Figure 3.31). The largest, most massive OB associations are found in the NE lobe of the galaxy (Garcia et al. 2010a; Borissova et al. 2004) where giant HII shells are also seen (Meaburn et al. 1988; Valdez-Gutiérrez et al. 2001; Lozinskaya et al. 2003); Figure 3.31.

Given its close distance, IC 1613 has been the subject of numerous studies in the last 50 years, having a determination of its Cepheids distance already by Baade (1963). The recent estimate by Dolphin et al. (2001) yields a distance of 714.5 kpc. Other early works on IC 1613 include Sandage (1971), van den Bergh (1975), van den Bergh (1977); de Vaucouleurs (1978), Mc Alary et al. (1984), Freedman (1988), Madore & Freedman (1991), Carlson & Sandage (1990). Despite the intense observational work carried out on IC 1613 whether this galaxy actually host a rotationally supported disk is still not settled, with some authors referring to the same regions as "the IC1613 halo" (Dolphin et al. 2001) or "the IC1613 disk" (Tikhonov & Galazutdinova 2002). For the purposes of the scientific exploitation of MEGARA we will initially focus on IC 1613 for the analysis of the population of massive-blue stars and their interaction with the ISM alone. Whether or not the spectroscopic and kinematic analysis of its RGB stars is worth pursuing regarding the topic of the evolution of disks is yet to be determined.



3.1.4.2 *Nearby galaxies (beyond the Local Group)*

As we have discussed above, the Local Group offers rather limited choices for the study of the evolution of spiral disks. With regard to bona-fide disks in the northern hemisphere (or elsewhere), only M33 offers the right inclination for a proper spectro-photometric, chemical and (especially) kinematical analysis. However, basically any of the mechanisms proposed to play a role on the evolution of disks depend strongly on galaxy morphology, mass and environment. Therefore, a large number of galaxy disks must be analyzed should the results to be obtained from MEGADES be applicable to the entire population of disks. By going a bit beyond the Local Group, to a distance of 4 Mpc, we could increase the sample of northern spiral disks to 8 systems, namely M31, M33, NGC 2403, M81, M82, NGC 3077, NGC 2976 and Maffei 2 (Lee et al. 2009). This would partially alleviate the lack of more massive disks (M81 and NGC 2403 are rather massive systems) but to the expenses of not being able to resolve individual RGB stars anymore and with the need of still covering very large areas on the sky.

3.1.4.2.1 S4G survey

Due to these limitations we decided instead to look for a complete sample of disks in a significantly larger volume and select galaxies whose optical size (D_{25}) would fit the MEGARA MOS field of view ($\sim 3.5 \times 3.5$ arcmin²). Note that the use of a diameter-limited sample has been shown to be a very efficient way of selecting galaxies for IFU surveys (e.g. CALIFA; Sánchez et al. 2012). Besides, it turns out that by applying such selection criteria we end up with a sample that is suitable not only for the study of the spectro-photometry and kinematics of disks but also for the rest of the nearby-galaxies science being carried out within the MEGARA Science Team in what now constitutes the MEGADES survey.

The best choice in this regard is the Spitzer Survey of Stellar Structure in Galaxies (S4G hereafter; Sheth et al. 2010). S4G is an Exploration Science Legacy Program of 632 hours of observing time, which was approved for the Spitzer post-cryogenic mission, also known as the Warm Spitzer mission, and that is now complete. S4G Principal Investigator (PI) is Dr. Kartik Sheth (NRAO). The S4G is a volume-, magnitude-, and diameter-limited ($d < 40$ Mpc, $|b| > 30^\circ$, $m_{B,corr} < 15.5$ mag and $D_{25} > 1''$) survey of 2331 galaxies using the Infrared Array Camera (IRAC) at 3.6 and 4.5 microns. Each galaxy was observed for 240 seconds and mapped to an extension of at least 1.5 times D_{25} . This large, relatively unbiased and extremely deep sample of all morphological types provides an unprecedented data set for the study of the distribution of mass and stellar structures in the Local Universe.

The IR photometric data provided by S4G gives already important information for the study of the evolution of galaxy disks. Among other things, it allows to carry out a detailed morphological analysis (including morphological decomposition) of the stellar mass as IRAC 1 and 2 bands are any of them an excellent measure of the stellar content in galaxies (Meidt et al. 2012). Besides, this analysis can be done in a region of the spectrum where the effects of dust attenuation and reddening are rather small.



3.1.4.2.2 The MEGADES-S4G sample

The fact that S4G is limited to galaxies that can be as small as 1 arcmin leads to the presence of numerous dwarf systems in the sample. In addition to that, the S4G also includes a large number of elliptical galaxies, which are clearly non-rotationally supported in most cases. Finally, even within the disk galaxies in S4G many objects show inclinations ($i > 70^\circ$) which make them not usable for deriving the velocity ellipsoid neither the metal abundance gradient.

With these limitations in mind (and the fact that a sample of 2331 galaxies is not practical in terms of telescope time) we imposed further selection criteria to the S4G sample in order to derive, which we will call hereafter, the MEGADES-S4G sample. These additional criteria are a limit in diameter ($2.5' < D_{25} < 4'$), in inclination ($i < 70^\circ$)⁶, plus a limit in declination [$\text{Dec}(J2000) > -20^\circ$]. Therefore, if we combine the original selection criteria from S4G plus these new selection criteria the range of parameters explored would be:

- Distance < 40 Mpc
- Galactic latitude $|b| > 30^\circ$
- Declination $\text{Dec}(J2000) > -20^\circ$
- Apparent magnitude $m_{B,\text{corr}} < 15.5$ mag.
- Apparent diameter $2.5' < D_{25} < 4'$
- Inclination $i < 70^\circ$

This sample would be perfectly suited for most scientific applications within MEGADES. However, in order to ensure that rotational motion and other in-plane velocities are observable in the LOS velocities a subsample where the velocity ellipsoids could be measured must be also defined. For these galaxies we also impose that the inclination is larger than 40° (Noordermeer et al. 2008).

In Figures 3.32 and 3.33 below we show the distributions in radial velocity and apparent magnitude of both the full S4G sample (in black) and the MEGADES-S4G subsample (limited only to $i < 70^\circ$; in red). The blue line in Figure 3.32 represents the redshift distribution expected for a pure volume-limited sample. The selection of targets within a range in diameter clearly results in a bias towards relatively bright targets ($11 \text{ mag} < m_{B,\text{corr}} < 14 \text{ mag}$). This, as we will show below, allows excluding most dwarf systems from the sample.

⁶ Note that the inclination has been computed from the axial ratio, $q=b/a$, after adopting an intrinsic axial ratio $q_0=0.2$, according to the relation given by Hubble (1926).

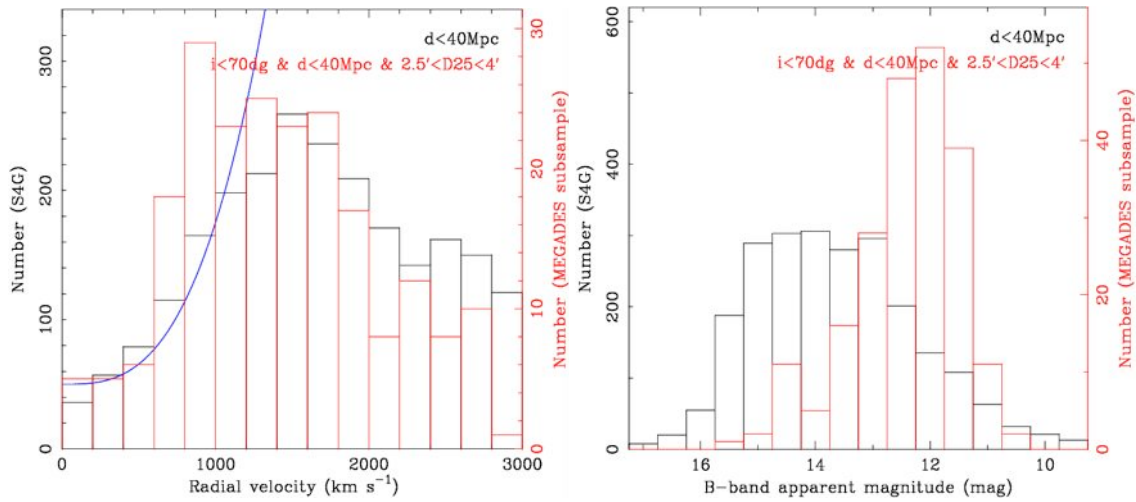


Figure 3.32: Left: Frequency histogram in heliocentric radial velocity of the S4G full sample ($d < 40$ Mpc; black solid line histogram) and the S4G subsample selected for MEGADES (red solid line histogram). The distribution expected for a complete volume-limited sample is also shown (blue solid line). Right: The same for the B-band absolute magnitude. Note that the MEGADES-S4G subsample includes only objects with D25 diameter between 2.5–4 arcmin and objects with inclinations below 70° . Our diameter selection biases the sample towards excluding dwarf systems.

Below we show the distributions in the case of the RC3 morphological type and the B-band absolute magnitude (Figure 3.33). The paucity of objects with B-band absolute magnitude below -18 mag illustrates the successful rejection of dwarfs from our sample.

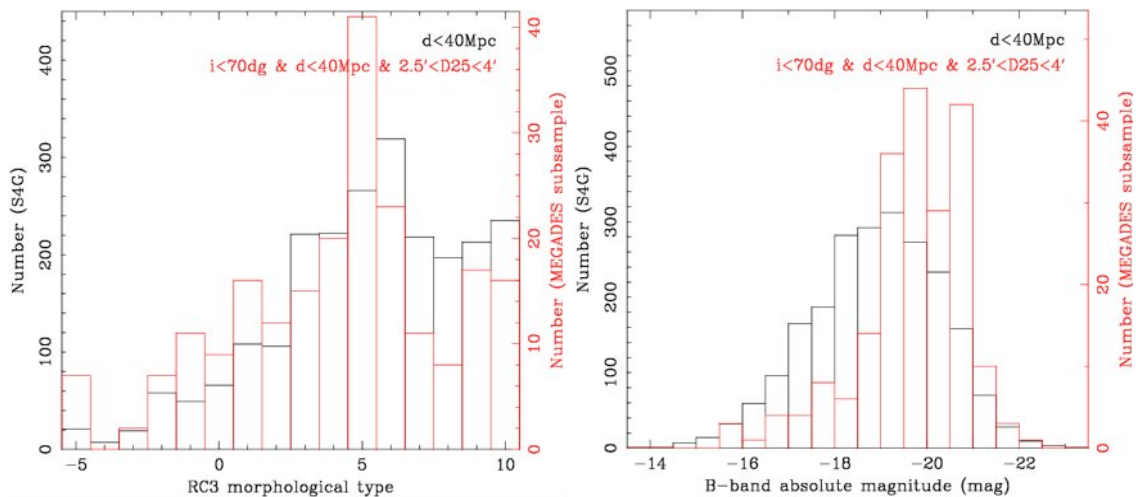


Figure 3.33: Left: Frequency histogram in RC3 morphological type of the S4G full sample ($d < 40$ Mpc; black solid line histogram) and the S4G subsample selected for MEGADES (red solid line histogram). Right: The same for the B-band absolute magnitude. Note that the MEGADES subsample includes only objects with D25 diameter between 2.5–4 arcmin and objects with inclinations below 70° . Our diameter selection biases the sample towards excluding dwarf systems.



In Table 3.1 below we list the entire MEGADES-S4G sample and include their central coordinates (J2000), morphological type (RC3 numerical type), diameter (D25), axial ratio (b/a), position angle, apparent magnitude (B_T), absolute magnitude (M_B), recession velocity and the availability of UV (GALEX), ground-based $H\alpha$ and SDSS-DR7 corollary data.



MEGARA Preliminary Design. Science Case

TEC/MEG/024 2.A - 1/02/12



Galaxy	RA (J2000) (degrees)	Dec (J2000) (degrees)	Morp. Type	D25 (arcmin)	b/a	PA (degrees)	B _T (mag)	MB (mag)	V _{rad} (km s ⁻¹)	Other data
UGC00099	2.669850	13.709440	8.8	2.51	1.00	-99.0	14.65	-17.7	1740	UV
NGC0157	8.694150	-8.396300	4.0	3.72	0.51	28.1	11.07	-21.4	1671	UV
ESO541-004	14.741700	-18.742640	4.2	2.95	0.46	25.4	13.30	-19.5	2000	UV
NGC0337	14.958750	-7.577940	6.7	2.95	0.65	-99.0	12.01	-20.6	1650	Ha UV
NGC0337A	15.390750	-7.587710	7.9	2.63	0.66	8.0	12.90	-18.6	1075	UV
NGC0428	18.232050	0.981560	8.6	2.82	0.74	113.2	11.95	-19.4	1154	Ha UV SDSS
NGC0450	18.876750	-0.860970	5.9	2.95	0.66	75.1	12.73	-19.7	1761	Ha UV SDSS
NGC0470	19.936800	3.409940	3.1	2.88	0.56	155.6	12.54	-20.6	2372	Ha UV
NGC0474	20.027850	3.415250	-2.0 (E)	2.63	0.91	-99.0	12.38	-20.4	2372	UV
UGC00891	20.329500	12.411670	8.8	2.75	0.48	47.0	14.68	-15.9	643	Ha
NGC0514	21.016200	12.917330	5.2	3.47	0.71	105.0	12.30	-20.9	2471	UV
NGC0584	22.836450	-6.868060	-4.6 (E)	3.80	0.66	104.5	11.33	-20.9	1796	Ha UV
NGC0600	23.272050	-7.311400	6.9	2.63	0.98	-99.0	13.02	-19.2	1842	UV
UGC01133	23.761800	4.381300	9.9	3.47	0.51	-99.0	14.33	-18.6	1964	UV
UGC01176	25.041300	15.904600	9.9	3.89	0.79	-99.0	14.40	-15.9	632	Ha UV
PGC006667	27.292950	-10.061240	6.7	2.75	0.79	129.6	14.09	-18.4	1992	SDSS
NGC0681	27.295200	-10.426620	1.9	2.51	0.72	67.5	12.77	-19.4	1757	SDSS
NGC0691	27.673800	21.759890	4.0	2.69	0.69	91.6	12.28	-21.3	2663	Ha UV
UGC01551	30.906150	24.075500	6.1	2.63	0.56	107.5	13.89	-20.0	2671	UV
PGC007900	31.130850	-6.198900	8.9	3.09	0.41	91.5	14.59	-17.6	1363	UV
NGC0864	33.864750	6.001990	5.1	3.72	0.69	24.0	11.62	-20.6	1561	Ha UV SDSS
NGC0895	35.400900	-5.520560	5.9	3.31	0.68	111.8	12.30	-20.6	2288	Ha UV
NGC0918	36.461250	18.496400	5.2	3.09	0.56	159.3	13.07	-20.6	1509	Ha
NGC1022	39.636300	-6.677390	1.1	2.57	0.58	67.6	12.11	-19.7	1453	Ha UV SDSS
NGC1042	40.099950	-8.433720	6.0	3.89	0.55	6.3	11.64	-20.2	1370	Ha UV SDSS
NGC1052	40.269750	-8.255440	-4.7 (E)	2.95	0.71	109.0	11.44	-20.2	1472	UV SDSS
NGC1073	40.917750	1.375800	5.3	3.55	0.63	31.6	11.68	-19.9	1208	Ha UV
NGC1084	41.499600	-7.578570	4.9	3.31	0.66	35.5	11.19	-20.6	1409	UV SDSS
NGC1087	41.604900	-0.498680	5.2	2.95	0.60	12.0	11.52	-20.6	1520	Ha UV SDSS
NGC1090	41.641350	-0.247030	3.7	3.31	0.44	101.0	12.60	-21.0	2758	Ha UV SDSS
UGC02345	42.969600	-1.172100	8.7	2.82	1.00	-99.0	14.30	-17.6	1506	Ha UV SDSS
NGC1179	45.660150	-18.897730	5.9	3.63	0.68	43.1	12.67	-19.6	1777	Ha UV
NGC1357	53.321250	-13.664140	2.0	3.39	0.76	76.0	12.40	-20.1	2019	UV
NGC1637	70.367400	-2.857640	5.0	3.16	0.87	16.3	11.56	-18.4	715	Ha
NGC2541	123.667050	49.061580	6.0	3.02	0.51	169.9	12.25	-18.6	559	SDSS
NGC2552	124.834200	50.008800	8.9	2.95	0.54	53.7	12.69	-18.0	518	Ha UV SDSS
NGC2681	133.386000	51.313100	0.4	3.89	1.00	-99.0	11.15	-19.4	676	Ha UV SDSS
NGC2655	133.911900	78.223680	0.1	3.89	0.52	16.0	10.98	-21.2	1384	Ha UV
NGC2712	134.876850	44.914000	3.1	2.88	0.54	4.3	12.78	-20.0	1819	Ha SDSS
NGC2742	136.889700	60.479280	5.3	3.02	0.52	88.3	12.07	-20.3	1295	Ha UV SDSS
NGC2748	138.429300	76.475330	4.0	2.69	0.43	39.3	12.39	-20.5	1470	UV
NGC2782	138.521700	40.112930	1.1	3.24	0.74	-99.0	12.32	-20.9	2557	Ha UV SDSS
IC0529	139.636350	73.760020	5.2	3.24	0.48	141.8	12.60	-20.8	2259	UV
NGC2787	139.829850	69.203400	-1.1 (E)	3.24	0.56	113.5	11.60	-19.6	699	Ha UV
NGC2805	140.084850	64.102880	6.9	3.39	0.81	174.1	11.79	-20.8	1734	Ha UV SDSS
NGC2859	141.077250	34.513360	-1.2 (E)	3.16	0.87	85.0	11.87	-20.3	1687	UV SDSS
UGC05139	145.134750	71.182080	9.9	3.31	0.95	-99.0	13.37	-99.0	140	Ha UV
NGC2974	145.635300	-3.701770	-4.7 (E)	3.47	0.62	41.0	11.80	-20.6	1890	UV
NGC2964	145.726800	31.847030	4.1	2.95	0.74	97.0	12.04	-19.8	1317	UV SDSS
NGC2968	145.800000	31.928730	1.6	2.57	0.66	54.0	12.73	-19.5	1526	UV SDSS
NGC2985	147.592350	72.279080	2.3	3.63	0.81	175.5	11.21	-20.8	1323	Ha UV
NGC3041	148.279800	16.677670	5.4	3.09	0.65	92.7	12.30	-19.8	1412	SDSS
NGC3104	150.987900	40.755750	9.9	3.02	0.68	35.0	13.79	-16.8	603	Ha SDSS
NGC3227	155.877450	19.864940	1.4	3.98	0.47	156.5	11.55	-20.1	1147	Ha SDSS
UGC05612	156.027750	70.882200	7.9	2.63	0.63	154.0	12.77	-19.2	1010	UV
NGC3239	156.270150	17.163630	9.8	3.63	0.76	-99.0	11.67	-19.1	752	Ha UV SDSS
UGC05688	157.603500	70.050400	8.8	3.09	0.59	145.0	13.81	-19.2	1921	Ha UV
NGC3294	159.067650	37.324590	5.2	3.09	0.52	117.6	12.14	-20.4	1573	UV SDSS
IC0630	159.640650	-7.170420	-1.9 (E)	3.24	0.79	150.0	12.98	-19.7	2183	UV
NGC3319	159.789600	41.686780	5.9	3.63	0.49	34.7	11.77	-19.4	742	Ha UV SDSS
NGC3346	160.912050	14.871930	6.0	2.63	0.83	104.2	12.45	-19.2	1262	UV SDSS
NGC3389	162.116400	12.533130	5.3	2.63	0.45	102.9	12.51	-19.7	1303	UV SDSS
UGC05918	162.403350	65.531000	10.0	2.51	0.98	-99.0	15.14	-99.0	339	Ha UV SDSS
NGC3396	162.479250	32.990970	9.4	3.09	0.41	98.5	12.43	-20.4	1660	UV SDSS
NGC3423	162.809700	5.840070	6.0	3.55	0.85	1.7	11.60	-19.5	1012	UV SDSS
NGC3414	162.817650	27.974940	-2.0 (E)	2.69	0.51	9.3	12.06	-19.8	1414	UV SDSS
NGC3433	163.015950	10.148220	5.2	2.51	0.95	-99.0	13.09	-20.1	2719	UV SDSS
NGC3430	163.047600	32.951230	5.1	3.98	0.56	32.3	12.19	-20.3	1584	UV SDSS
NGC3447	163.350000	16.772440	8.8	3.39	0.58	25.6	14.44	-17.2	1070	UV SDSS
NGC3489	165.077400	13.901250	-1.3 (E)	3.39	0.59	70.0	11.06	-19.2	708	UV SDSS
NGC3507	165.855750	18.135330	3.1	2.88	0.85	-99.0	12.09	-19.1	979	Ha UV SDSS
NGC3556	167.879100	55.674010	6.0	3.98	0.42	79.0	10.70	-20.7	697	Ha UV SDSS
NGC3596	168.775950	14.787110	5.1	3.55	0.95	-99.0	11.79	-19.6	1192	SDSS
NGC3608	169.245600	18.148530	-4.8 (E)	2.95	0.83	80.0	11.57	-19.7	1108	UV SDSS
NGC3619	169.838700	57.578360	-0.8 (E)	3.89	0.79	-99.0	12.53	-19.6	1540	UV SDSS
NGC3626	170.015850	18.356780	-0.7 (E)	2.95	0.66	156.3	11.80	-20.1	1476	UV SDSS
NGC3631	170.265300	53.171030	5.2	3.72	0.83	118.0	10.71	-21.0	1163	Ha UV SDSS
NGC3672	171.260250	-9.795390	5.0	2.88	0.58	6.5	12.07	-20.6	1866	UV SDSS
NGC3686	171.933150	17.224060	4.1	3.02	0.76	22.7	12.00	-19.6	1157	UV SDSS
NGC3729	173.455950	53.124780	1.3	2.88	0.72	15.0	11.72	-19.7	1012	UV SDSS
NGC3755	174.139050	36.410280	5.2	2.88	0.40	123.4	13.69	-19.1	1568	UV SDSS
NGC3780	174.843300	56.270760	5.2	2.69	0.83	68.2	12.12	-21.0	2390	UV SDSS
NGC3810	175.244850	11.471110	5.2	3.31	0.68	31.6	11.27	-20.1	994	Ha UV SDSS
NGC3887	176.769000	-16.854640	3.9	3.63	0.79	9.5	11.41	-20.0	1208	UV
NGC3892	177.004050	-10.962000	-1.0 (E)	3.02	0.87	98.2	12.69	-19.4	1746	UV
NGC3893	177.159900	48.709500	5.1	2.69	0.52	161.5	10.82	-20.9	970	Ha UV SDSS



MEGARA Preliminary Design. Science Case

TEC/MEG/024 2.A - 1/02/12



Galaxy	RA (J2000) (degrees)	Dec (J2000) (degrees)	Morp. Type	D25 (arcmin)	b/a	PA (degrees)	B _T (mag)	MB (mag)	V _{rad} (km s ⁻¹)	Other data
UGC06817	177.719850	38.880710	9.9	3.98	0.40	65.0	13.43	-99.0	243	Ha SDSS
NGC3930	177.940950	38.015010	5.1	2.69	0.74	29.5	13.18	-18.1	918	Ha SDSS
NGC3938	178.205100	44.121400	5.1	3.55	0.98	-99.0	10.92	-20.0	809	Ha UV SDSS
NGC3941	178.230600	36.986360	-2.0 (E)	3.63	0.66	10.0	11.27	-19.8	914	UV SDSS
NGC3981	179.026950	-19.895000	4.1	3.31	0.63	14.3	12.14	-20.2	1708	UV
UGC06917	179.119800	50.428340	8.8	2.51	0.59	130.0	13.15	-18.4	913	Ha UV SDSS
NGC3998	179.484000	55.453560	-2.1 (E)	2.75	0.81	138.3	11.41	-20.0	1040	SDSS
NGC4027	179.875500	-19.265180	7.8	3.55	0.79	162.7	11.58	-20.6	1671	
NGC4030	180.097650	-1.100050	4.0	3.80	0.71	8.6	11.23	-20.8	1462	Ha UV SDSS
NGC4045	180.676650	1.976740	1.3	2.57	0.62	89.3	12.73	-19.9	1982	Ha UV SDSS
NGC4050	180.724200	-16.373290	2.2	3.39	0.63	89.0	13.04	-19.4	1761	UV
NGC4064	181.046550	18.443440	1.3	3.24	0.41	151.7	12.25	-19.1	936	Ha UV SDSS
NGC4102	181.598850	52.710920	3.0	2.95	0.58	38.0	12.09	-19.3	844	Ha UV SDSS
NGC4116	181.902900	2.691900	7.4	2.57	0.58	155.5	12.49	-19.5	1310	Ha UV SDSS
NGC4123	182.046300	2.878260	5.0	3.16	0.72	123.7	11.93	-19.8	1328	Ha UV SDSS
NGC4138	182.374050	43.685310	-0.8 (E)	2.95	0.56	150.0	12.29	-18.7	877	UV SDSS
NGC4151	182.636100	39.405750	2.1	2.88	0.78	50.0	11.36	-20.1	999	Ha UV SDSS
NGC4203	183.770550	33.198300	-2.7 (E)	3.39	0.42	8.7	11.72	-19.6	1091	UV SDSS
NGC4212	183.914100	13.901470	4.9	2.82	0.60	73.2	11.78	-20.4	-85	Ha UV SDSS
NGC4224	184.140600	7.462110	1.0	2.88	0.40	56.3	12.89	-20.5	2598	Ha UV SDSS
NGC4242	184.375800	45.619370	7.9	3.80	0.71	20.8	11.59	-18.9	516	Ha UV SDSS
NGC4245	184.403100	29.607990	0.1	2.57	0.63	145.8	12.34	-18.7	886	Ha UV SDSS
NGC4260	184.842750	6.098710	1.0	2.51	0.46	59.1	12.69	-20.0	1958	Ha UV SDSS
NGC4267	184.939050	12.799300	-2.5 (E)	2.51	0.69	161.0	11.84	-19.3	972	UV SDSS
NGC4274	184.960350	29.614190	1.6	3.63	0.47	101.7	11.33	-20.1	927	UV SDSS
NGC4278	185.028900	29.281500	-4.8 (E)	2.88	0.98	-99.0	11.04	-19.4	621	UV SDSS
NGC4298	185.386650	14.606070	5.2	3.24	0.55	135.7	12.04	-19.8	1138	Ha UV SDSS
NGC4314	185.634000	29.894880	1.0	3.72	0.95	-99.0	11.42	-19.8	983	Ha UV SDSS
NGC4324	185.774250	5.249680	-0.7 (E)	2.88	0.41	55.0	12.50	-19.6	1662	Ha UV SDSS
NGC4371	186.230850	11.704280	-1.3 (E)	3.80	0.47	96.5	11.82	-19.1	914	UV SDSS
NGC4380	186.342150	10.016830	2.3	3.31	0.54	159.7	12.63	-18.7	970	Ha UV SDSS
NGC4393	186.463800	27.560810	6.7	3.02	0.93	-99.0	13.73	-17.0	755	Ha SDSS
NGC4394	186.481800	18.213920	2.9	3.47	0.95	-99.0	11.59	-19.4	915	Ha UV SDSS
UGC07534	186.533100	58.321800	9.9	2.51	0.79	-99.0	13.43	-17.5	723	SDSS
UGC07559	186.770100	37.144190	9.9	3.72	0.65	-99.0	14.16	-99.0	217	Ha UV SDSS
UGC07557	186.797400	7.262650	8.6	2.82	0.89	-99.0	13.48	-17.5	935	Ha UV SDSS
NGC4424	186.798750	9.420310	1.2	3.02	0.51	95.3	12.38	-99.0	437	Ha UV SDSS
UGC07577	186.923100	43.494240	9.8	3.80	0.65	130.0	12.88	-99.0	196	Ha UV SDSS
IC3392	187.180350	14.999450	2.5	2.69	0.43	39.8	13.07	-19.6	1681	Ha UV SDSS
UGC07608	187.186800	43.224760	9.9	3.47	0.89	-99.0	13.67	-16.7	536	UV SDSS
NGC4457	187.245900	3.570580	0.4	2.82	0.85	78.5	11.71	-19.1	888	Ha UV SDSS
NGC4487	187.768650	-8.053890	5.9	3.47	0.55	74.2	11.83	-19.6	1037	Ha UV
NGC4496A	187.914300	3.939500	7.5	3.39	0.83	70.0	12.12	-20.2	1730	UV SDSS
NGC4498	187.914450	16.852010	6.4	2.82	0.54	130.7	12.77	-19.7	1505	Ha UV SDSS
NGC4503	188.025750	11.176420	-1.8 (E)	3.47	0.46	11.3	12.09	-19.7	1359	Ha UV SDSS
NGC4504	188.027200	-7.563420	6.0	3.16	0.62	163.0	12.17	-19.1	998	UV
NGC4534	188.522550	35.518460	7.6	2.75	0.59	122.8	12.98	-18.2	802	UV SDSS
NGC4531	188.566200	13.075450	-0.4 (E)	3.02	0.65	155.4	12.47	-18.7	195	Ha UV SDSS
NGC4539	188.644800	18.202620	0.7	2.75	0.40	95.2	12.86	-19.1	1287	UV SDSS
NGC4546	188.872950	-3.793220	-2.7 (E)	3.24	0.56	89.7	11.35	-19.7	1050	UV
NGC4567	189.136200	11.257950	4.0	2.75	0.79	90.0	12.10	-20.9	2277	Ha UV SDSS
NGC4571	189.234900	14.217300	6.3	3.55	0.93	-99.0	11.97	-99.0	336	Ha UV SDSS
NGC4596	189.983850	10.175600	-0.9 (E)	3.89	0.83	135.0	11.44	-20.9	1870	UV SDSS
NGC4597	190.052550	-5.799170	8.6	3.55	0.40	-99.0	12.87	-18.8	1040	UV SDSS
NGC4618	190.386600	41.150910	8.6	3.55	0.65	40.2	11.31	-19.3	546	Ha UV SDSS
IC3687	190.563150	38.503200	9.9	3.31	0.69	-99.0	13.73	-99.0	355	UV SDSS
NGC4639	190.718400	13.256610	3.5	2.88	0.66	130.5	12.19	-19.1	984	Ha UV SDSS
NGC4647	190.885500	11.582480	5.2	2.75	0.85	148.5	12.09	-19.8	1396	Ha UV SDSS
NGC4651	190.927650	16.393390	5.2	3.80	0.66	76.8	11.38	-19.6	799	Ha UV SDSS
PGC043020	191.422200	-6.072530	8.9	2.51	0.71	19.5	13.02	-19.0	1476	UV SDSS
NGC4682	191.814450	-10.063440	5.8	2.57	0.46	84.3	13.12	-20.2	2335	UV SDSS
NGC4689	191.939700	13.762670	4.7	3.80	0.76	166.4	11.58	-20.7	1619	Ha SDSS
NGC4688	191.943600	4.336060	6.0	3.72	0.91	-99.0	13.51	-17.6	984	Ha UV SDSS
NGC4691	192.056700	-3.332730	0.4	3.02	0.81	15.3	11.68	-19.6	1119	Ha UV SDSS
NGC4698	192.095550	8.487470	1.4	3.80	0.41	170.0	11.55	-19.9	1008	Ha UV SDSS
NGC4781	193.597050	-10.536070	7.0	3.63	0.40	118.3	11.39	-20.8	1262	UV
UGC08041	193.802700	0.116610	6.9	3.16	0.60	169.2	13.38	-18.6	1324	Ha UV SDSS
NGC4897	195.220650	-13.449780	3.9	2.63	0.79	153.3	13.24	-19.9	2566	UV
NGC4902	195.248850	-14.513670	3.1	2.69	0.91	78.0	11.80	-21.4	2635	UV
NGC4941	196.054200	-5.551680	2.4	3.31	0.81	23.0	11.90	-19.4	1113	UV
PGC045195	196.129950	-3.572440	7.6	3.63	0.83	63.2	14.59	-17.2	1361	UV SDSS
UGC08201	196.603350	67.706800	9.9	3.31	0.51	-99.0	12.91	-99.0	34	Ha UV SDSS
NGC4981	197.203350	-6.778230	4.0	2.69	0.72	159.2	12.07	-20.2	1677	UV
NGC4984	197.238300	-15.516280	-0.8 (E)	3.31	0.74	45.0	12.20	-19.2	1206	UV
PGC045652	197.445450	-10.325470	6.7	3.55	0.95	-99.0	14.50	-16.9	1214	UV
NGC5012	197.904450	22.915440	5.2	2.63	0.55	9.8	12.79	-20.7	2612	UV SDSS
NGC5018	198.254250	-19.518560	-4.6 (E)	3.47	0.62	99.9	11.68	-21.8	2850	UV
UGC08320	198.615900	45.919900	9.9	3.39	0.39	150.0	12.74	-99.0	194	Ha UV SDSS
NGC5112	200.485200	38.734590	5.8	3.02	0.62	129.2	12.63	-18.9	968	Ha SDSS
UGC08614	204.359250	7.645100	9.8	3.39	0.52	-99.0	13.20	-18.5	1053	UV SDSS
NGC5254	204.907950	-11.493860	5.1	3.31	0.43	126.8	12.67	-20.9	2318	UV
NGC5300	207.066900	3.950900	5.2	2.82	0.65	146.2	12.90	-18.8	1173	UV SDSS
NGC5313	207.435000	39.984650	3.1	2.75	0.59	42.7	12.69	-20.7	2537	UV SDSS
NGC5334	208.226700	-1.114460	5.1	3.39	0.72	18.2	12.88	-19.1	1382	Ha UV SDSS
NGC5350	208.340100	40.363940	3.6	2.69	0.62	34.0	12.28	-20.9	2323	UV SDSS
NGC5376	208.816950	59.506620	2.3	2.57	0.62	64.8	12.89	-20.1	2016	UV SDSS



Galaxy	RA (J2000) (degrees)	Dec (J2000) (degrees)	Morp. Type	D25 (arcmin)	b/a	PA (degrees)	B _T (mag)	MB (mag)	V _{rad} (km s ⁻¹)	Other data
UGC08839	208.853250	17.794880	9.9	2.75	0.71	-99.0	15.48	-15.9	958	Ha UV SDSS
NGC5371	208.916400	40.461640	4.0	3.98	0.62	5.9	11.28	-22.1	2556	Ha UV SDSS
NGC5448	210.708450	49.172650	1.4	3.63	0.51	105.8	12.12	-20.8	2022	UV SDSS
NGC5426	210.853650	-6.070500	5.0	3.09	0.40	0.5	12.71	-21.0	2620	UV
NGC5427	210.858300	-6.030560	5.0	3.63	0.91	-99.0	11.96	-21.2	2729	Ha UV
NGC5576	215.265300	3.271030	-4.8 (E)	2.82	0.66	89.7	11.78	-20.1	1482	UV SDSS
NGC5584	215.599050	-0.387610	5.9	3.16	0.74	157.5	12.50	-19.8	1638	UV SDSS
NGC5660	217.457550	49.622610	5.2	2.51	0.91	75.0	12.38	-20.6	2325	UV SDSS
NGC5678	218.023350	57.921400	3.3	3.16	0.52	1.4	12.02	-20.9	1907	UV SDSS
NGC5669	218.183100	9.891710	5.9	2.57	0.58	56.7	12.73	-19.5	1370	UV SDSS
NGC5676	218.195250	49.457850	4.7	3.55	0.45	45.2	11.87	-21.5	2102	UV SDSS
NGC5719	220.234800	-0.317940	2.4	3.09	0.42	97.8	13.26	-19.5	1732	UV SDSS
NGC5728	220.599300	-17.252570	1.2	3.16	0.59	14.5	12.23	-21.5	2786	Ha UV
NGC5740	221.101800	1.679740	3.0	2.69	0.50	168.3	12.60	-19.9	1570	UV SDSS
NGC5750	221.546400	-0.222970	0.4	2.69	0.51	70.6	12.52	-19.9	1687	UV SDSS
NGC5792	224.594400	-1.090890	3.0	3.55	0.39	88.5	12.12	-21.0	1924	UV SDSS
NGC5806	225.001650	1.891270	3.1	3.02	0.54	172.5	12.35	-19.8	1354	Ha UV SDSS
NGC5850	226.782000	1.544580	3.1	3.31	0.71	114.4	11.89	-21.5	2559	Ha UV SDSS
NGC5861	227.317050	-11.321810	5.0	2.75	0.40	149.2	12.34	-20.9	1854	UV
NGC5866B	228.030000	55.784990	7.8	2.69	0.71	19.2	15.18	-16.2	842	Ha UV SDSS
NGC5892	228.450900	-15.463670	7.0	3.09	0.78	-99.0	13.27	-19.9	2285	UV
NGC5885	228.767250	-10.085820	5.0	3.09	0.85	57.7	12.34	-20.6	2000	UV
NGC5921	230.485050	5.070600	4.0	3.02	0.68	140.0	11.68	-20.6	1480	Ha UV SDSS
NGC5963	233.365800	56.559680	4.3	3.16	0.79	63.1	13.03	-17.8	655	Ha UV SDSS
NGC5964	234.401250	5.973670	6.9	3.39	0.76	147.7	13.42	-18.8	1447	Ha UV SDSS
NGC5970	234.624900	12.186200	5.0	2.75	0.69	87.8	12.00	-20.9	1957	SDSS
NGC5985	234.904500	59.331940	3.1	3.98	0.50	15.3	11.95	-21.6	2519	UV SDSS
NGC6070	242.496000	0.709610	6.0	3.47	0.52	64.0	12.42	-21.1	2008	UV SDSS
UGC10310	244.075950	47.045650	9.2	2.57	0.79	165.0	13.68	-17.3	716	Ha SDSS
NGC6207	250.765950	36.832730	4.9	3.55	0.47	17.5	11.86	-19.9	852	Ha UV SDSS
NGC6255	253.696650	36.501700	6.0	3.09	0.45	85.0	13.38	-18.4	918	Ha UV SDSS
NGC6340	257.604000	72.304330	0.4	2.57	0.95	-99.0	12.00	-19.9	1202	Ha UV SDSS
NGC7218	332.548500	-16.661740	5.6	2.57	0.42	-99.0	12.40	-20.2	1661	UV
NGC7479	346.236150	12.322860	4.3	3.63	0.74	26.6	11.73	-21.7	2381	Ha UV
UGC12709	354.349650	0.391660	8.7	2.75	0.63	153.2	14.39	-19.1	2682	UV SDSS
NGC7723	354.737400	-12.960640	3.1	3.24	0.71	41.5	11.93	-20.5	1862	UV
NGC7727	354.974400	-12.292310	1.1	3.63	0.76	-99.0	11.57	-20.8	1870	Ha UV
UGC12732	355.166550	26.236090	8.7	2.75	0.91	-99.0	14.28	-16.6	746	Ha UV
NGC7741	355.977150	26.075750	6.0	3.63	0.66	163.0	11.82	-19.3	750	Ha UV

Table 3.1: Summary of the properties of the MEGADES-S4G sample.

In summary, the MEGADES-S4G sample includes a total of 215 galaxies (29 ellipticals) with 150 of them having SDSS-DR7 optical data publicly available. Regarding galaxies that show inclinations larger than 40° and can therefore be used to determine their velocity ellipsoids (those with white background in Table 3.1) the total number of galaxies in the sample is 158 (19 ellipticals).

SDSS-DR7 false-color optical images are shown in Figure 3.34 below. Note the good spatial resolution from these ground-based observations (comparable to that to be obtained with MEGARA) along with the variety in galaxy morphology. We consider this sample to constitute an excellent set of targets for the scientific goals of MEGADES. In this regard, it is also worth noting that 13% of the 150 MEGADES-S4G galaxies in the SDSS spectroscopic database were classified (based on the SDSS nuclear spectra) as either BROADLINE or AGN.

The size of the postage stamps included in this figure is ~3.5 x 3.5 arcmin² in all cases. All images are oriented North up and East to the left.

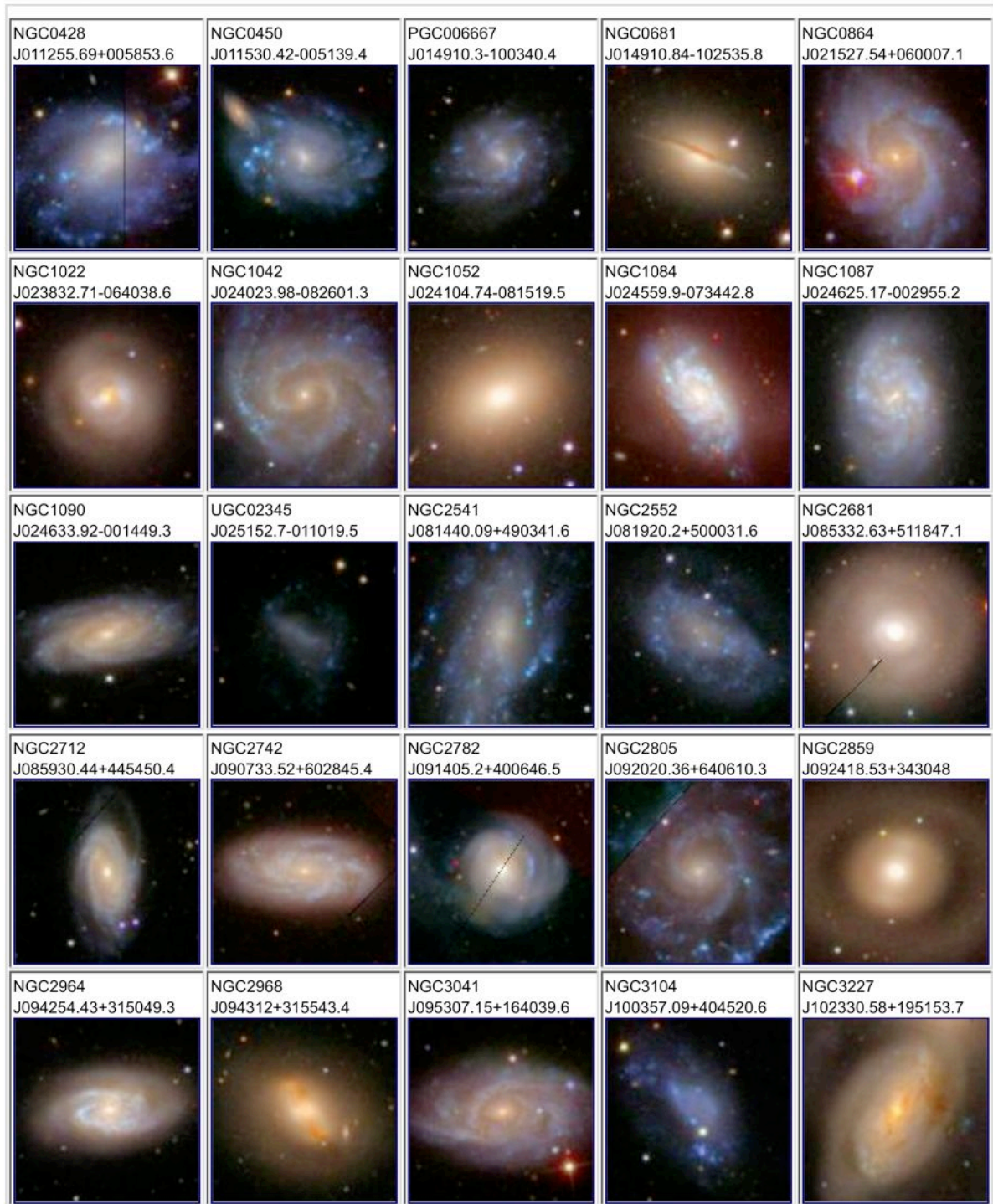


Figure 3.34: Sloan Digital Sky Survey (SDSS) false-color images of the sample of galaxies extracted from the S4G survey to be analyzed as part of MEGADES ($d < 40$ Mpc; $2.5' < D_{25} < 4'$; $i < 70^\circ$). All postage stamps are $\sim 3.5 \times 3.5$ arcmin² in size (i.e. the size of the MEGARA MOS FOV). North is up, East is to the left. Galaxies are sorted by Right Ascension.

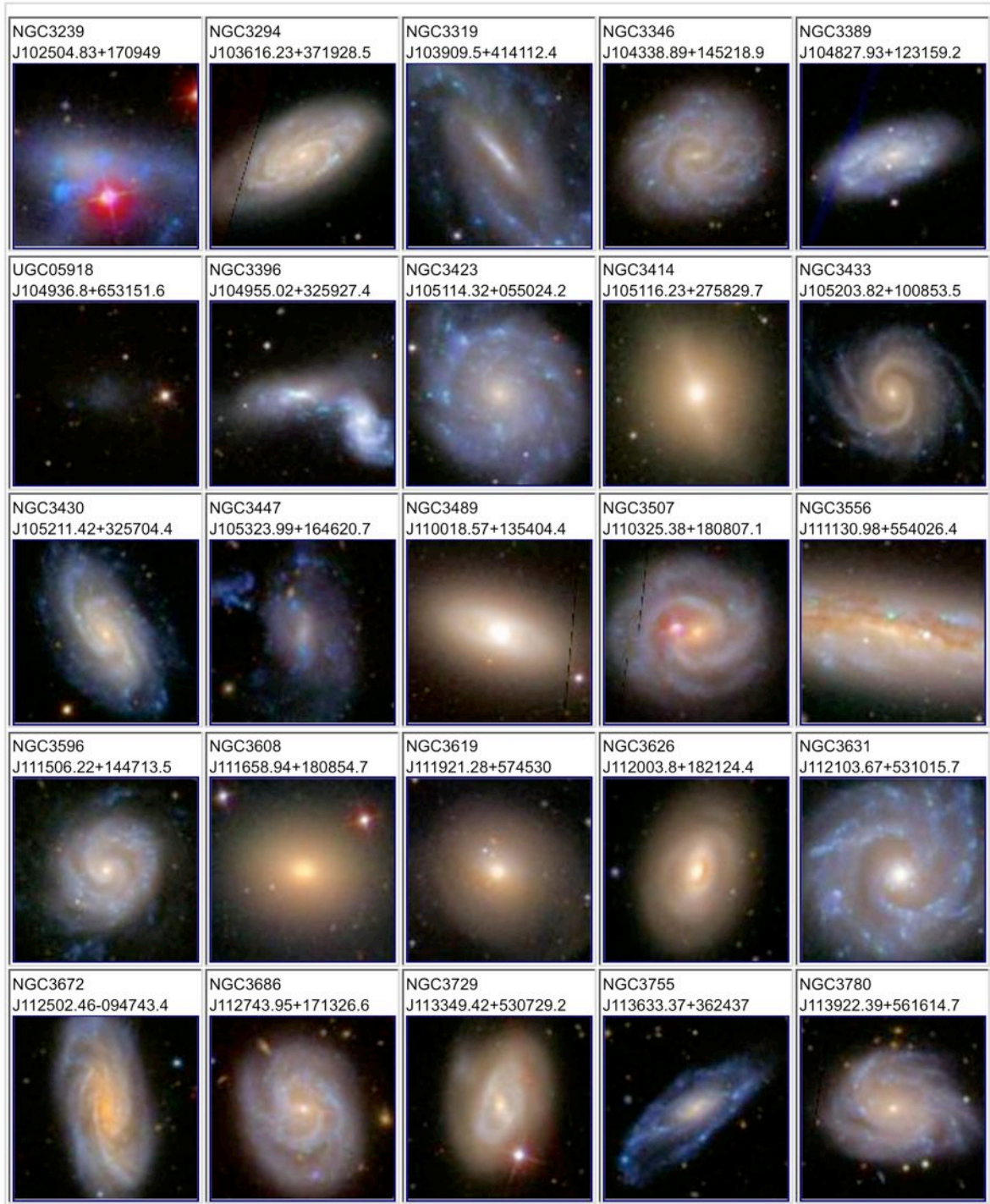


Figure 3.34 (cont.): Sloan Digital Sky Survey (SDSS) false-color images of the sample of galaxies extracted from the S4G survey to be analyzed as part of MEGADES ($d < 40$ Mpc; $2.5' < D_{25} < 4'$; $i < 70^\circ$). All postage stamps are $\sim 3.5 \times 3.5$ arcmin² in size (i.e. the size of the MEGARA MOS FOV). North is up, East is to the left. Galaxies are sorted by Right Ascension.

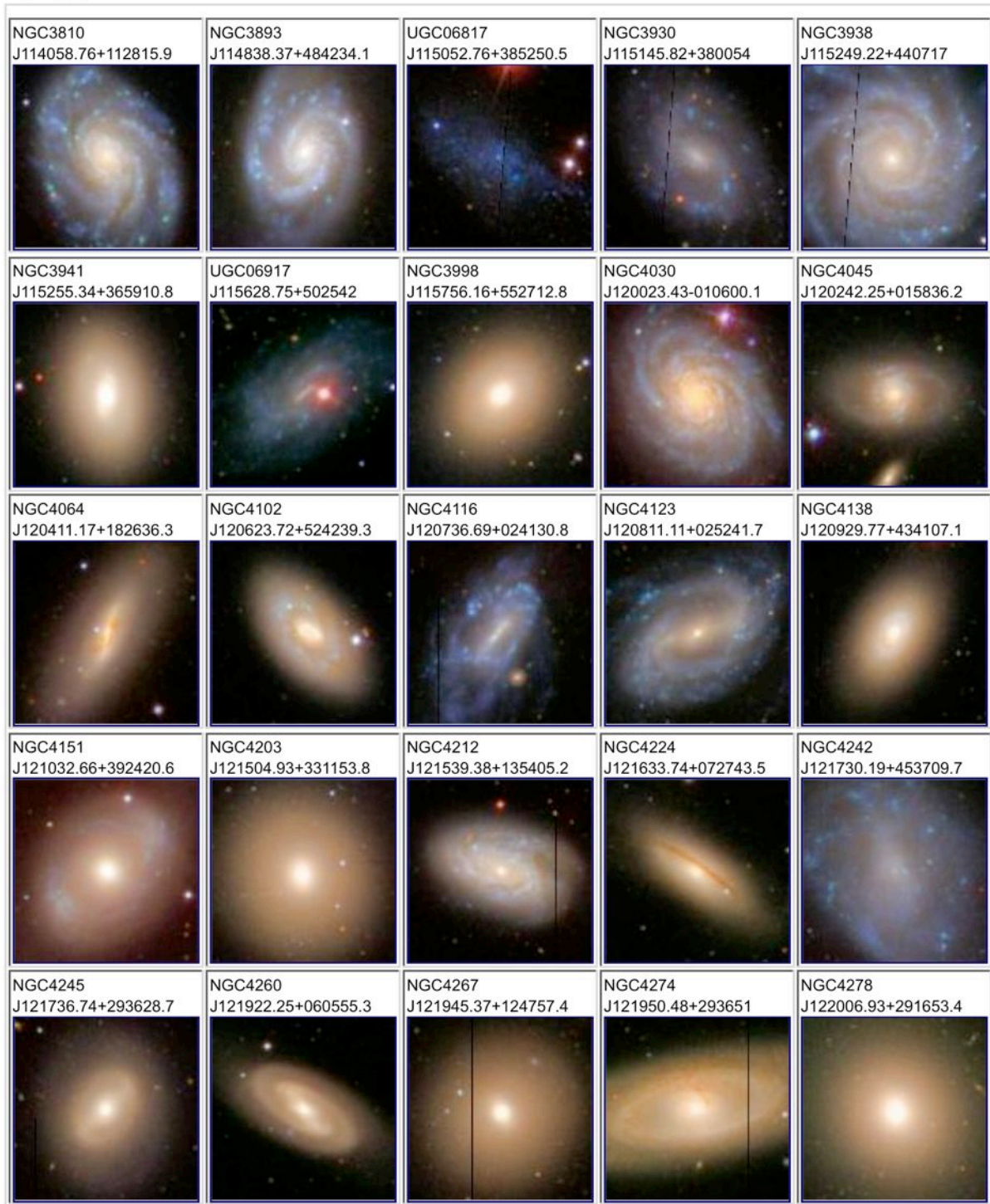


Figure 3.34 (cont.): Sloan Digital Sky Survey (SDSS) false-color images of the sample of galaxies extracted from the S4G survey to be analyzed as part of MEGADES ($d < 40$ Mpc; $2.5' < D_{25} < 4'$; $i < 70^\circ$). All postage stamps are $\sim 3.5 \times 3.5$ arcmin² in size (i.e. the size of the MEGARA MOS FOV). North is up, East is to the left. Galaxies are sorted by Right Ascension.

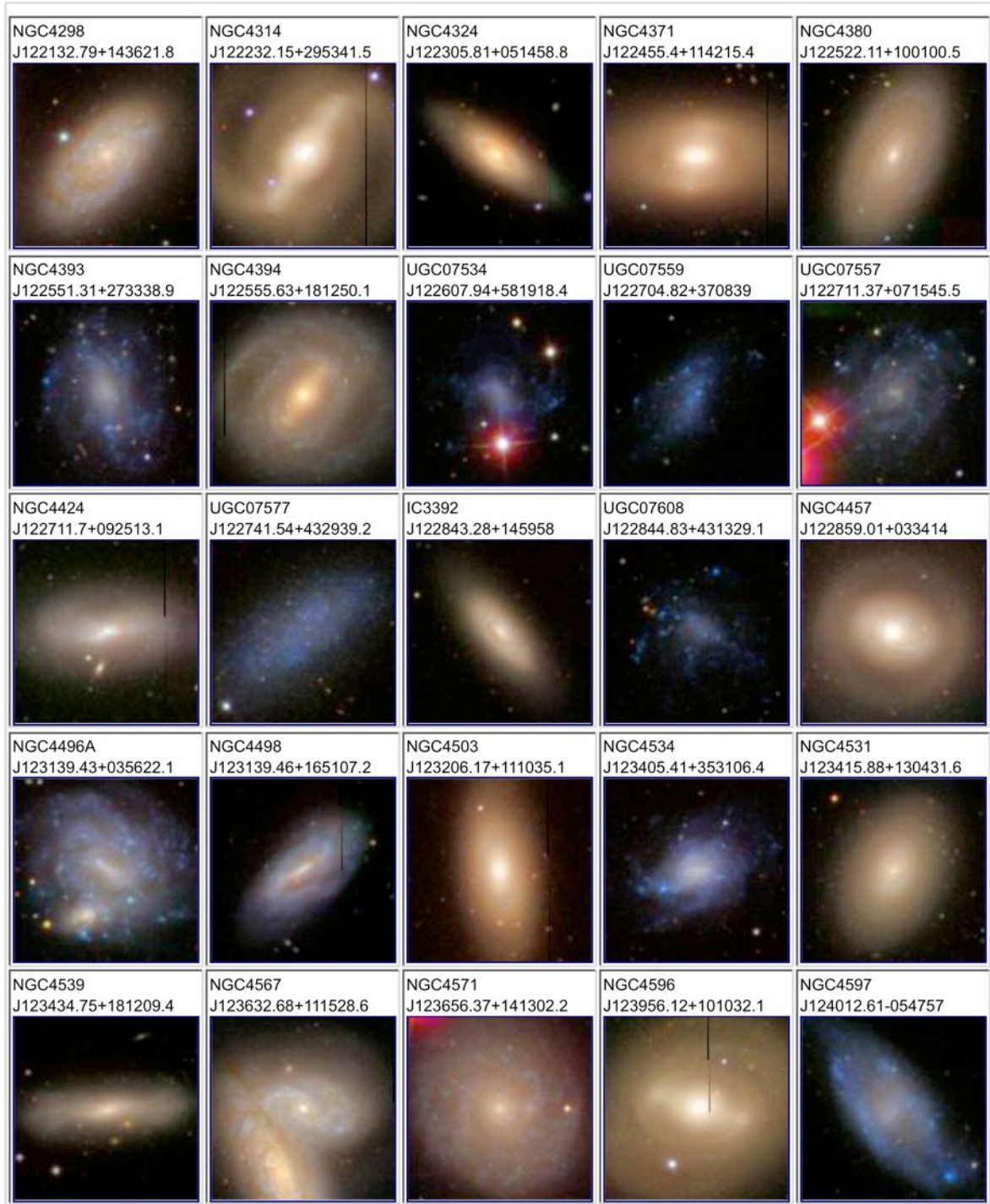


Figure 3.34 (cont.): Sloan Digital Sky Survey (SDSS) false-color images of the sample of galaxies extracted from the S4G survey to be analyzed as part of MEGADES ($d < 40$ Mpc; $2.5' < D < 4'$; $i < 70^\circ$). All postage stamps are $\sim 3.5 \times 3.5$ arcmin² in size (i.e. the size of the MEGARA MOS FOV). North is up, East is to the left. Galaxies are sorted by Right Ascension.

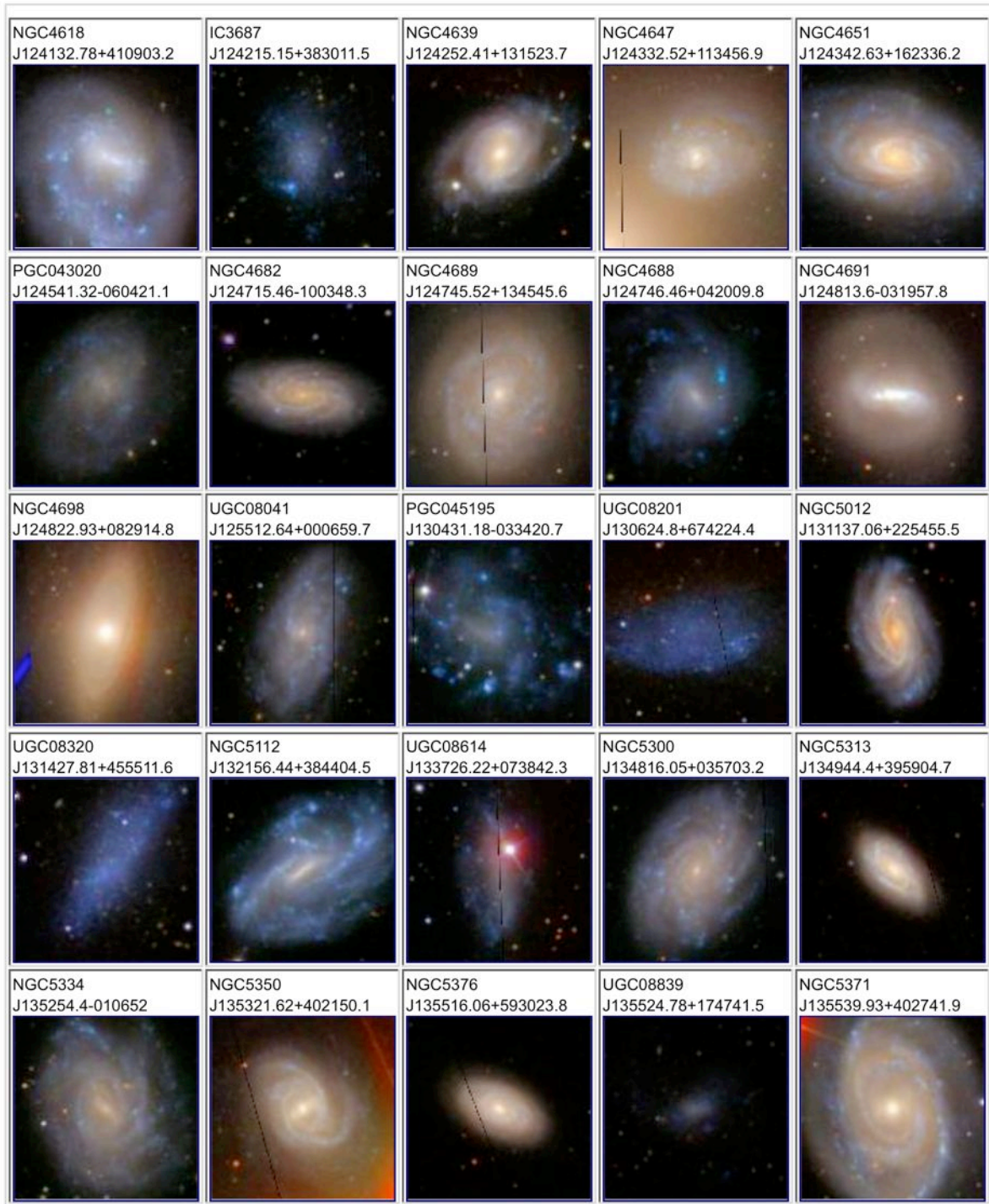


Figure 3.34 (cont.): Sloan Digital Sky Survey (SDSS) false-color images of the sample of galaxies extracted from the S4G survey to be analyzed as part of MEGADES ($d < 40$ Mpc; $2.5' < D_{25} < 4'$; $i < 70^\circ$). All postage stamps are $\sim 3.5 \times 3.5$ arcmin² in size (i.e. the size of the MEGARA MOS FOV). North is up, East is to the left. Galaxies are sorted by Right Ascension.

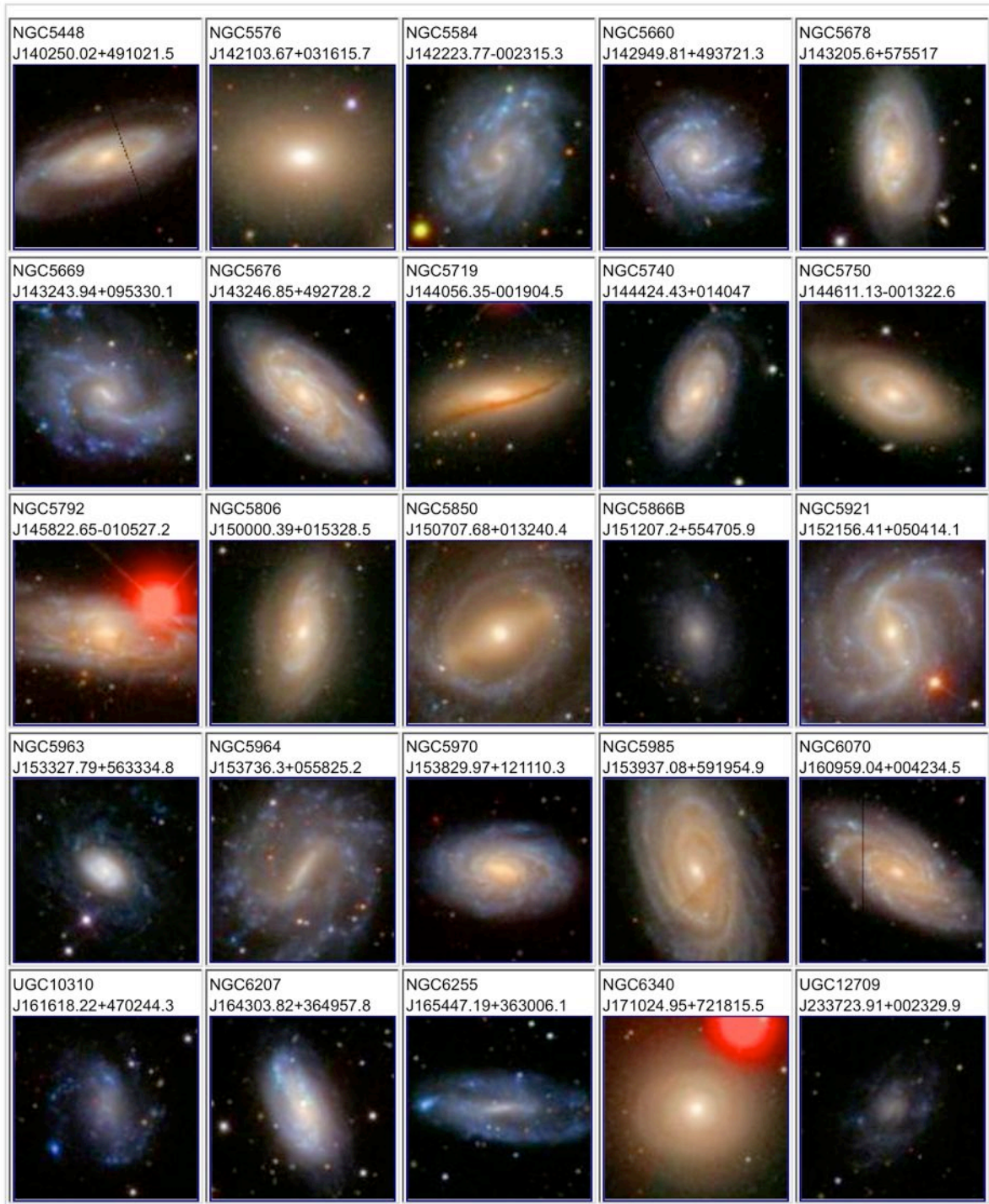


Figure 3.34 (cont.): Sloan Digital Sky Survey (SDSS) false-color images of the sample of galaxies extracted from the S4G survey to be analyzed as part of MEGADES ($d < 40$ Mpc; $2.5' < D_{25} < 4'$; $i < 70^\circ$). All postage stamps are $\sim 3.5 \times 3.5$ arcmin² in size (i.e. the size of the MEGARA MOS FOV). North is up, East is to the left. Galaxies are sorted by Right Ascension.



3.1.4.3 Additional MEGADES targets

3.1.4.3.1 M82

M82 is the companion galaxy to the nearby grand-design spiral M81. Its morphology is rather complex with a very high inclination and opaque dust lanes that dramatically alter its ultraviolet and optical appearance. In the central 500 pc M82 contains a massive starburst with a SFR as high as $10 M_{\odot} \text{ yr}^{-1}$ and a bolometric luminosity 100x that of the corresponding volume in the Milky Way (O'Connell et al. 1995). Associated to this central 500 pc a large concentration of Super Stellar Clusters have been identified (Melo et al. 2005). The collective effect of all these SSCs is believed to have led to the remarkable outflow of gas seen in $H\alpha$ and that extends beyond 4 kpc perpendicular to the plane of the galaxy. This outflow shows a hourglass morphology in $H\alpha$ and a emission-line splitting of $\sim 300 \text{ km s}^{-1}$ (Martin 1998).

The starburst galaxy M82 is placed at a distance of 3.63 Mpc (image scale $17.6 \text{ pc arcsec}^{-1}$; Freedman et al. 1994). Although originally classified as an irregular galaxy, the detailed analysis of near-infrared images by Mayya et al. (2005) revealed the presence of two trailing spiral arms whose morphology suggests a Sbc morphological type.

As the nearest starburst galaxy and thanks to its high inclination M82 is the ideal laboratory to study starburst-driven Super Galactic Winds in emission. Fortunately, M82 is also favorably located in sky for being observed with GTC as part of MEGADES.

3.1.4.3.2 ULIRGs

Given the paucity of these objects in the Local Universe, there are none ULIRGs within the MEGADES-S4G. In order to study the properties of neutral winds in this kind of objects a complementary sample has to be defined.

As part of this scientific objective we propose to observe the central region of a sample of ULIRGs with MEGARA to study the galactic winds by means of the analysis of the Na I D absorption features. Our targets have been chosen from the Northern Hemisphere 2-Jy ULIRG sample (64 galaxies) of Murphy et al. (1996). This sample was selected from the complete 2-Jy IRAS flux-limited sample of Strauss et al. (1990, 1992) as those galaxies having FIR luminosities greater than $5.0 \times 10^{11} L_{\odot}$, a 60 μm bump so $F_{\nu}^2(60 \mu\text{m}) > F_{\nu}(12 \mu\text{m})F_{\nu}(25 \mu\text{m})$, and a declination Dec (J2000) $> -35^{\circ}$.

The observed wavelength range for our study should contain the interstellar absorption line Na I D which will allow us to trace the structure and kinematics of the neutral cold phase of the gas, as well as emission lines from warm ionized gas ($H\alpha$, [NII] $\lambda\lambda 6583\text{\AA}$, [SII] $\lambda\lambda 6716, 6731\text{\AA}$ lines). In the case of the MEGARA spectral setup VPH-675-LR (6115-7334 \AA) a total of 20 ULIRGs from the Murphy et al. (1996) sample are located within the proper redshift range ($0.04 < z < 0.08$) to contain all the above mentioned absorption and emission interstellar lines. Furthermore, the wavelength range selected contains a few stellar absorption lines (mostly Fe, Ca and TiO) that would allow us to derive an estimate of the contribution of stars to the Na I D absorption.



3.1.5 Observations

In this section we describe the observing needs for each of the science cases described in previous sections. In addition to fulfill the requirements of each of these scientific applications the observing strategy proposed should make optimal use of MEGARA in either its Basic or Advanced configurations. In Table 3.2 below we provide a summary of the observing targets and observing time devoted to each of them that we propose as part of MEGADES (see Table 4.1 in Section 4 for a similar description of the nearby extragalactic Targets of Interest to be carried as part of the MEGARA Early Science observations).

Observing Modes		IFU						MOS						
M33 Disk														
Pointings/fields	Setup	LR-U	LR-B	LR-V	LR-R	LR-I	Total*	MRU	UB	MRB	MRG	HR-R	LR-U	Total**
16 (<i>p1a/b-p8a/b</i>)	t(exp)	2h	1.5h	1.5h	1h	1h	129 h	1h	1h	1h	1h	1h	2h	129 h
NGC 604 (ToI)														
Pointings/fields	Setup	LR-U	LR-B	LR-V	LR-R	LR-I	Total	MRU	UB	MRB	MRG	HR-R	LR-U	Total**
3 (<i>p1-p3</i>)	t(exp)	2h	1.5h	1.5h	1h	1h	24 h	1h	1h	1h	1h	1h	2h	24 h
IC 1613														
Pointings/fields	Setup	MR-U	UB	MR-B	HR-R		Total	MRU	UB	MRB	HR-R			Total**
4 (<i>p1-p4</i>)	t(exp)	7h	5h	4h	4h		105 h	7h	5h	4h	4h			105 h
MEGADES-S4G														
Pointings/fields	Setup	LR-U (Cent)	MRUB (Cent)	MR-B (Cent)	LR-I (Cent)	HR-R (Cent)	Total /target	LR-U (HII)	MRUB (HII)	MRB (HII)	LR-V (HII)	LR-R (HII)	LR-I (HII)	Total per target
133 (<i>p1a-p133a</i>)	t(exp)	20m	30m	15m	15m	30m	2.1 h	20m	30m	15m	15m	15m	15m	2.1 h
Ellipticals	Setup	LR-U (Cent)	LR-B (Cent)	LR-V (Cent)	LR-R (Cent)	LR-I (Cent)	Total	LR-U (Grid)	LR-B (Grid)	LR-V (Grid)	LR-R (Grid)	LR-I (Grid)		Total**
17 (<i>p1-p17</i>)	t(exp)	20m	10m	10m	10m	30m	27 h	30m	30m	30m	30m	30m		27 h
Minor+major axes scanning	Setup	LR-U (axes)	LR-B (axes)	LR-V (axes)	LR-I (axes)	MR-B (axes)	Total /target	LR-U (Grid)	LR-B (Grid)	LR-V (Grid)	LR-I (Grid)	MRB (Grid)		Total per target
1(x95) ($\mu_r=24.5$)	t(exp)	120m	40m	30m	120m	40m	6.7 h	120m	40m	30m	120m	40m		6.7 h
2(x95) ($\mu_r=23.5$)	t(exp)	20m	5m	5m	25m	5m	2.4 h	20m	5m	5m	25m	5m		2.4 h
2(x95) ($\mu_r=22.0$)	t(exp)	5m	2m	2m	5m	2m	1 h	5m	2m	2m	5m	2m		1 h



Inner Disks	Setup	LR-U (map)	LR-B (map)	LR-V (map)	LR-R (map)		Total	LR-U (HII)	LR-B (HII)	LR-V (HII)	LR-R (HII)			Total**
6x20 (<i>p1b-p20g</i>)	t(exp)	0.2h	0.1h	0.1h	0.1h		60 h	0.2h	0.1h	0.1h	0.1h			60 h
Galactic Winds	Setup	LR-B (map)	LR-V (map)	LR-R (map)			Total	LR-B (Grid)	LR-V (Grid)	LR-R (Grid)				Total**
6x20 (<i>p1b-p20g</i>)	t(exp)	0.5h	0.5h	0.5h			144 h	0.5h	0.5h	0.5h				144 h
M82														
	Setup	LR-R	HR-R				Total	LR-R	HR-R					Total**
1 (<i>p1</i>)	t(exp)	1.5h	1.5h				3.5 h	1.5h	1.5h					3.5 h
ULIRGS														
	Setup	LR-R					Total	LR-R						Total**
20 (<i>p1-p20</i>)	t(exp)	2h					48 h	2h						48 h

(*Note: the total exposure times include the on-target time for all pointings/fields listed plus 15% overheads [30% in the case of IC 1613 and the observations of inner disks and 20% in the case of the SGWs and the ellipticals], which includes readout time, object acquisition and blank-sky observations if needed. **Note: The observations of field *a* & *b* for each pointing could be carried out on the same -or different- MOS targets if needed, although using different positioners as both fields are 14 arcsec apart; in order to exhaust simultaneous IFU observations in the case of MEGARA-Advanced).

Table 3.2: Summary of the observing times proposed for the different sub-programmes within MEGADES.

3.1.5.1 Local Group galaxy M33

3.1.5.1.1 Disk RGB-stars chemical abundances and kinematics

As discussed in Section 3.1.3, the main objective of the analysis of M33 within MEGADES is the analysis of the single-star chemical composition and kinematics of a sample of massive blue and RGB stars at different galactocentric distances.

With regard to the observations of the population of massive blue stars we refer the reader to Section 3.1.5.1.5, which is devoted to the analysis of this population both in M33 and in IC 1613. Here we will focus on the MEGARA observations proposed for the M33 red giants, both AGB and RGBs. Based on the study by Barker et al. (2007) using HST we can estimate the number counts (and expected magnitudes) of AGB and RGB stars in the disk of M33. The average value for the observed magnitude of the tip of the RGB in M33 is $I=20.85$ mag. We aim to reach 2.5 mag below the tip, which should provide enough stars for a proper measurement of the velocity dispersion of the RGB star population and would provide information on the bulk of the RGB. Based on the results from Barker et al. (2007) and Ferguson et al. (2007) we estimate ~ 50 , ~ 25 , ~ 5 stars (1000, 500, 100 stars) per MEGARA LCB IFU (MOS) field at 15, 25, 35 arcmin de-projected radius, respectively (see Figures 3.35). The range in surface densities per arcmin quoted make of the combined use of the MEGARA IFU and MOS (i.e. of MEGARA-Advanced) a very efficient way of carrying out this project. Within 25 arcmin the IFU would be a better option but outside that radius, the use of the MOS mode, which is optimized for the observations of fields with number densities of $\sim 7\text{-}8$ arcmin $^{-1}$, is more profitable. Regarding the galactocentric distances of interest, we should aim to reach at least ~ 7.5 kpc, as this is the position where the surface brightness of the M33 disk decreases rather abruptly and where the effects of stellar migration could be best identified.

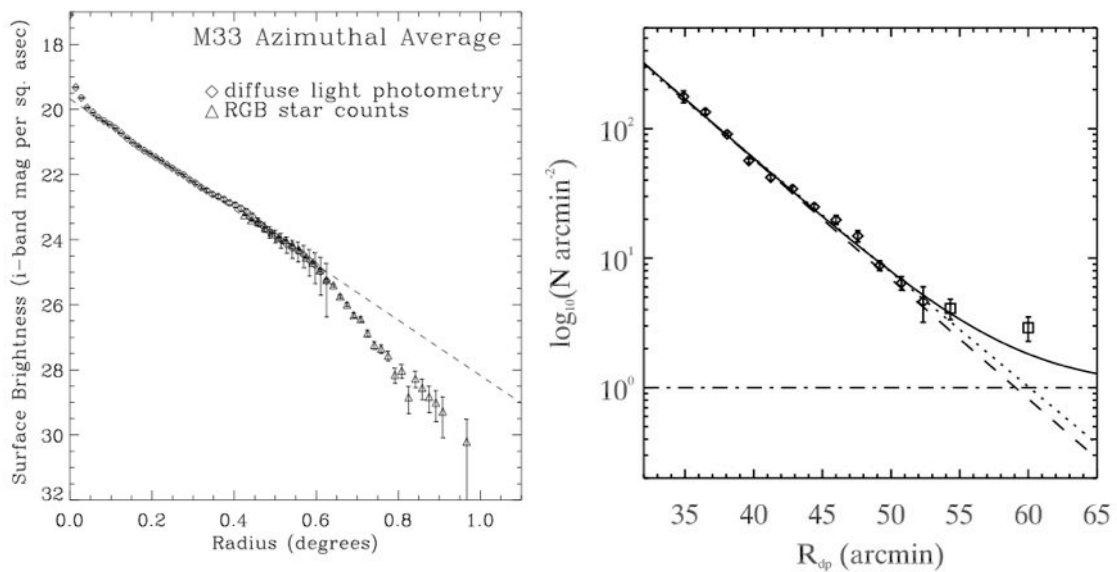


Figure 3.35: Left: M33 surface brightness photometry obtained from diffuse (unresolved light) and RGB star counts (Ferguson et al. 2007). Right: Surface density of RGB stars as a function of deprojected radius (Barker et al. 2007). These authors set a faint limit of $I=24$ mag to isolate RGB stars in the M33 CMD.

In Figure 3.36 we show the GALEX NUV image of M33 along with the proposed MEGARA MOS + LCB IFU observations to be carried out as part of the MEGADES survey along the major and minor axes in M33. Additional pointings might be included as part of the Early Science observations (e.g. Target of Interest NGC 604). All pointings (except that in cyan color) coincide in position, orientation and FOV with ACS-WFC observations with the HST.

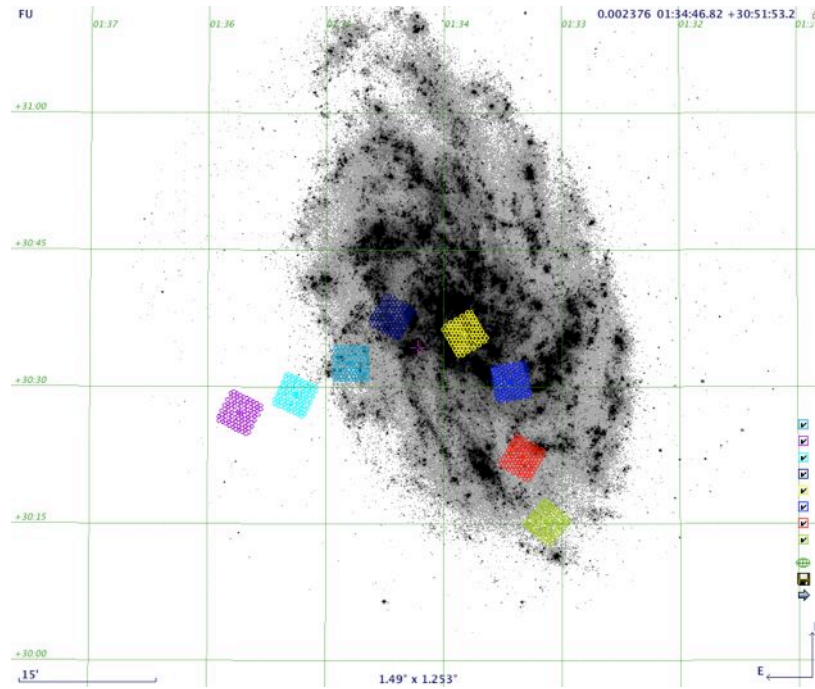


Figure 3.36: Layout of the proposed MEGARA MOS fields on the disk of M33. All except one pointing (in cyan) coincide in position, field-of-view (FOV) and orientation with observations obtained with ACS/HST in at least two bands, F606W and F814W. These will be used to identify potential spectroscopic blends.

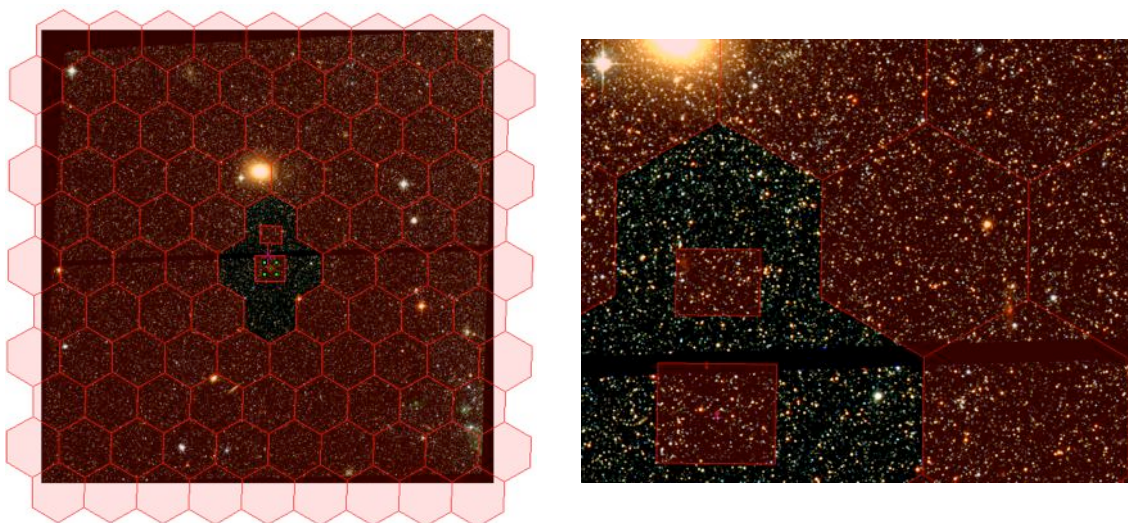


Figure 3.37: Left: False-color ACS/HST image of the outer disk of M33 (blue: F435W; green: F606W; red: F814W). We also overplot the MEGARA MOS+IFU-bundles footprint in red. Right: Detail of the central region of the same field. We recall the reader that the FOV of the IFU LCB is $14 \times 12 \text{ arcsec}^2$.

As an example of the appearance of the ACS/HST observations in the outer disk of M33 we show in Figure 3.37 the false-color ACS-WFC images (F435W, F606W and F814W) of one of the southwestern fields proposed for M33.

These ACS/HST observations have been also used to estimate the probability of having a blended star observed as part of our program. Figure 3.38 below shows a zoom of the ACS/HST observations of pointing 1 (south-westernmost pointings in Figure 3.36). On the left we show the image at the ACS-WFC observations at native resolution, while on the right the image have been degraded to a ground-based spatial resolution of ~ 0.8 arcsec (FWHM of the PSF). Note that for most cases the light from the source at ground-based resolution is dominated by one single HST source. For the massive blue stars we are mainly interested in observing the blue part of the spectrum while for the RGB stars we will focus on the CaT. This would further reduce the level of contamination of the spectra by blended (unresolved) sources.

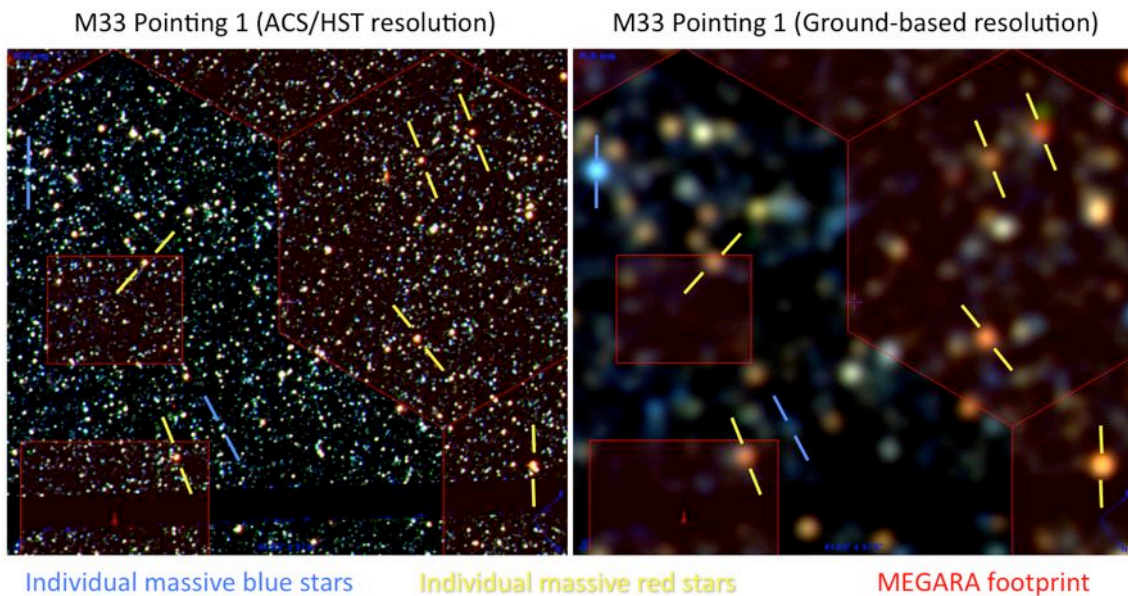


Figure 3.38: Left: False-color ACS-WFC image of the outer disk of M33 (blue: F435W; green: F606W; red: F814W). This region corresponds to the south-westernmost pointing in Figure 3.36 (which we will refer to as pointing 1). The positions of a number of massive blue (cyan tick-marks) and RGB stars (red tick-marks) in the disk of M33 are indicated.

In order to determine the level of crowding we also carried simulations of the single-star CMDs in the disk of M33 at different radii using the predictions of the IAC-STAR code for a continuous star formation history but different total surface brightness densities (Aparicio & Gallart 2004). These total surface brightness densities were obtained from the galaxy I-band surface brightness profiles and number counts obtained by Ferguson et al. (2007). In Figure 3.39 we show the results of these (noiseless) simulations in an area of 1 arcmin^2 at three different galactocentric distances (5, 7.5, 10 kpc, or 20, 30, 40 arcmin, respectively). Again, these galactocentric distances are most relevant for our science objectives as they located near the down-bending in the galaxy the surface brightness profile (see Figure 3.35), position

beyond which some authors propose the stellar population is dominated by stars migrated from the inner disk. Stars within different magnitude ranges in Figure 3.39 are shown with different colors: *blue*: stars brighter than the TRGB+4mag and V-I bluer than 0.5 mag (intermediate- and high-mass young stars); *red*: brighter than TRGB+4mag but V-I > 0.5 mag (AGB, RGB, RC); *green*: stars > 4mag fainter than the TRGB (low-mass MS and faint RGBs). This figure shows that this radial range is where the stellar density is best matched to the characteristics of MEGARA. We should be able to easily resolve individual RGB stars even at distances as close as 7.5 kpc to the galaxy center. The ACS observations shown in Figure 3.37 roughly correspond to a galactocentric distance of 6 kpc.

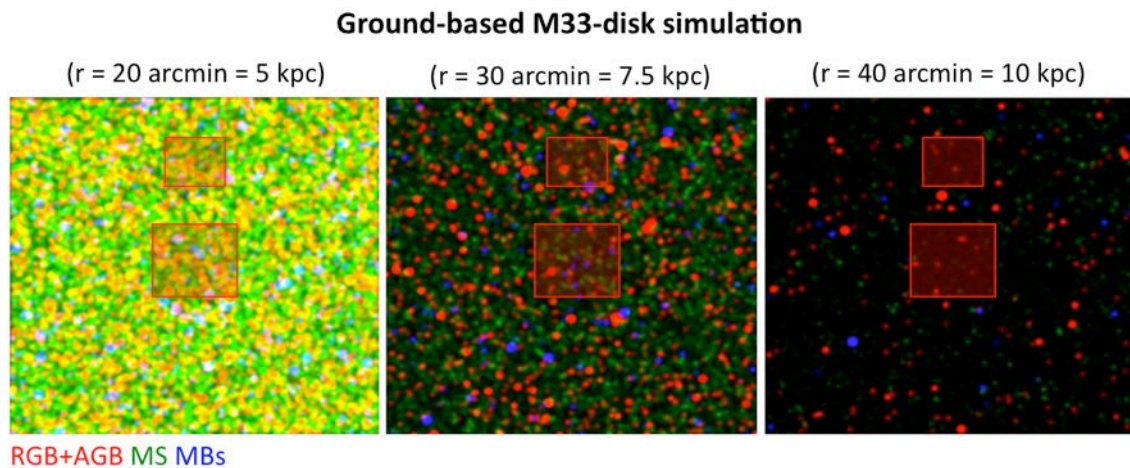


Figure 3.39: Simulations of the I-band images corresponding to the MEGARA IFU field of view at different galactocentric distances (left to right: 5 kpc, 7.5 kpc, 10 kpc) in the disk of M33 (see text for the meaning of the different colors used). A 0.8-arcsec FWHM PSF has been assumed for these simulations.

Using the MEGARA Exposure Time Calculator (ETC) we then determined the exposure time required to analyze the RGB star population down to $I \sim 23.3$ mag. According to our current best estimates of the efficiency of the entire system (including telescope, fibers, spectrograph, and detector) we should be able to detect a $I=23.3$ mag star with a $S/N > 10$ per angstrom in the CaT region (where both metal abundances and kinematics of the RGB stars should be determined) with a total exposure time of **3600 s** per pointing. In order to reach a total of 100-200 RGB stars at each galactocentric distance **two adjacent IFU fields per pointing** (plus the corresponding MOS setups) will be observed. These are represented as fields *a* & *b* for each pointing *p*1 through *p*8 in Table 3.2. This strategy leads to a total of **~20 h** of observing time for all pointings in the MEGARA-Advanced configuration (15% overheads are assumed). We estimate an additional 50-70% additional observing time should MEGARA-Basic the configuration to be used. Here we have adopted an average seeing of 0.8 arcsec, which is a conservative value in the case of the CaT region. Note that the resolution to be provided by the LR-I VPH ($R=6,000$ or $\sigma=21$ km/s) is good enough for measuring individual-star velocities with precisions better than ~ 10 km/s and also a spectral resolution down to which the calibration of metal-abundance calibration based on CaT has been proved to be valid using high-resolution data. Note that some of the observations proposed here could also be used to further (self)calibrate the relationship between stellar metallicity and the strength of the CaT lines.



3.1.5.1.2 Disk light-weighted star formation and chemical histories

In addition to the study of the kinematics and chemical composition of individual stars we will also analyze the light-weighted effective star formation and chemical histories of these regions, again, as a function of galactocentric distance. This is fundamental in order to determine the precision expected from the analysis of the MEGADES-S4G sample, where only unresolved light-weighted information will be available. This analysis will require combining the CaT observations described above with full coverage of the optical range using the other R=6,000 VPHs: LR-U, LR-B, LR-V, and LR-R. In this case and, in general, in all galaxies to be studied as part of MEGADES we aim to reach a surface brightness of $\mu_B=24.5-25$ mag/arcsec⁻² (i.e. the average surface brightness for the down-bending in the galaxies' surface brightness profiles; Pohlen & Trujillo 2006). Note that we will combine all spaxels at the same approximate surface brightness to be able to reach these levels when analyzing unresolved stellar populations. In the case of M33, given its proximity, we will assume that each entire MEGARA LCB IFU field would correspond to the same approximate surface brightness and the entire field will be combined for the stellar populations analysis. By combining the entire 14x12 arcsec² an average of ~3 hour per LR setup would be needed to reach a S/N>10 per angstrom (see Table 3.2). In order to observe with all four LR setups listed above we will need a total of 12 h to reach $\mu_r=24.5-25$ mag/arcsec⁻². Including the time devoted to CaT observations (see above) and 15% of overheads plus short blank-sky observations this leads to a total of **16 h per pointing**. The pointings to be observed will be those shown in Figure 3.36. As for the CaT observations the observing time will be split between two adjacent IFU fields; this should reduce potential stochastic effects in the bluest spectral setups associated to the outermost, lowest-SFR regions of the M33 disk. Thus, for the 8 pointings envisioned the total observing time required will be **129 hours**. Note that for all except the two outermost pointings 16 hours exposures will result in S/N>>10. However, the study of the properties of individual massive blue stars requires of such exposure times for all pointings (again, split between two adjacent fields 14 arcsec apart) when using MEGARA-Advanced. Should only MEGARA-Basic be available the length of the IFU LCB exposures would adapt to the (unresolved stellar population) surface brightness at each position.

3.1.5.1.3 Disk massive-blue-stars chemical abundances and kinematics

In addition to the acquisition of the LR spectra using the MEGARA IFU we will use the MOS mode (simultaneously, in the case of the MEGARA-Advanced configuration) to obtain mid-resolution [high-resolution] spectra in the blue [H α region] to study the kinematics and abundances [and interaction with the ISM] of the young massive stars using the MEGARA robotic positioners, whose population shows an intrinsically narrower velocity dispersion (Section 3.1.3.1.1). The much lower densities of these stars (see right panel of Figure 3.25) allow for an optimal use of the robotic positioners even when these are shared with the observations of ionized-gas regions (see Section 3.1.3.4.3). In this case we aim to reach stars as faint as V=19 mag, which corresponds to OB supergiants and early OB-dwarfs (Schmidt-Kahler 1982). These stars will be selected using pre-imaging data from HST and from the ground. The total exposure time devoted to the LR observations (16h on target per pointing; 8h per adjacent



IFU field) will be split between the four $R=11,000$ setups in the blue, namely MR-U, MR-UB, MR-B, and MR-G, and that at $R=19,000$ in the $H\alpha$ region (HR-R). Finally, we will also obtain LR-U MOS observations to extend the spectral coverage to include the $[OII]\lambda 3727\text{\AA}$ emission line (see below for a description of the observational requirements that lead to this need). In the very outer regions of the disk, where the surface density of massive-blue stars is rather low, we will place the remaining robotic positioners on RGB stars of M33 for full spectral analysis of a number of these targets.

The exposure time requirements for the study of the physical properties of the massive stars themselves (not necessarily in the context of the evolution of disks; as is the case of the velocity dispersion of this population) and their interaction with the surrounding ISM using the MOS configuration of MEGARA are described in Section 3.1.3.4.3. As we will show later, these latter requirements, although more stringent than those associated to the determination of the stars' radial velocities (a fundamental part of the study of the disk of M33), are less severe in terms of exposure time than those imposed by the simultaneous observations (in the case of MEGARA-Advanced) of the unresolved stellar light from the disk of M33 with the IFU LCB.

3.1.5.1.4 Ionized-gas metal abundance diagnostics

Our main objective in the study of the ionized-gas metal abundances in the disk of M33 is to ensure that we will be able to measure metal abundances from both temperature-sensitive forbidden emission-line ratios (i.e. CEL ratios) and from recombination lines (ORLs).

In the case of the former method, the weakest (but mandatory) line accessible at the distance of M33 is $[OIII]\lambda 4363\text{\AA}$, which in the disk of M33 is expected to have an intensity of $1/25$ - $1/50$ that of $H\beta$ ($f_{[OIII]\lambda 4363} \sim 4 \times 10^{-17}$ - 10^{-16} erg cm $^{-2}$ s $^{-1}$). This implies $S/N \sim 50$ per spaxel for average observing conditions in 1 hour in either the red side of the LR-U or the MR-UB setups. By default we assume that the LR-U VPH will be the one to be used as this allows simultaneously observing the $[OII]\lambda\lambda 3726, 3729\text{\AA}$ CEL doublet. However, in the central regions of M33, where the metal abundance is expected to be $\sim 1.3 Z_{\odot}$, $[OIII]\lambda 4363\text{\AA}$ is expected to be as faint as $1/500$ the intensity of $H\beta$. This leads to a S/N for this line of ~ 10 per spaxel. In any case, with regard to the analysis of T_e -based abundances from the diffuse ionized-gas emission in M33, the 1-hour-long exposures proposed for other studies in these fields are sufficient. In this case we are considering using MR-UB instead with a shorter exposure on the LR-U (for observing $[OII]\lambda\lambda 3726, 3729\text{\AA}$) as the $[OIII]\lambda 4363\text{\AA}$ is at the very edge of the range covered with LR-U.

Regarding the analysis of the metal abundances from ORLs, it should be noted that the strongest ORLs of oxygen and carbon are due to OII 3s--3p and CII 4f--3d transitions and are located at 4650\AA and 4267\AA , respectively. For the typical brightness of these features associated to the diffuse line emission in the disk of M33 ($\sim 10^{-17}$ erg cm $^{-2}$ s $^{-1}$; see Figure 3.53) the 1-hour exposures planned should allow reaching signal-to-noise ratios per spaxel of 20 and 25 respectively for the VPHs of interest MR-U and MR-B. Again, this exposure time is perfectly suited for the analysis of the ORL metal abundances in M33 and its comparison with those derived from collisionally-excited lines. It is worth noting that the exposure times derived for MEGARA compare favorably with those employed using other MOS instruments at Subaru, Keck or Gemini (see Bresolin 2011 and references therein).

3.1.5.1.5 Massive blue stars in the Local Group

The MEGARA design is partly driven by the need of studying blue massive stars in Local Group galaxies and, consequently, is well suited to carry out the proposed program. The MEGARA IFU can be located in the areas of higher concentration of blue massive star candidates, and used to disentangle crowded stellar knots (see the proposed studies on individual regions of M33 -ToI NGC 604- and on IC 1613). Adjacent fibers can be used for an accurate background subtraction. The robotic positioners can be devoted to the stars in surrounding less populated areas. Thanks to their 7-fiber minibundle design, the contamination from any local nebula could also be corrected in cases of very good seeing. However, the spectral resolution provided by MEGARA is also crucial for this kind of studies.

As part of the massive stars team project to study the Local Group galaxies, we have collected the spectra of about 40 O and B stars with VIMOS at the VLT in MOS mode. Besides being limited by the number of slits that could be allocated in the masks, we found that the low resolution of VIMOS ($R \sim 2,000$) makes the nebular contamination a serious problem. In the Balmer series, nebular and stellar contributions cannot be separated (see Figure 3.40), introducing errors in the derived values of stellar gravity. This would not be the case with MEGARA since this provides a much larger spectral and spatial resolution than VIMOS.

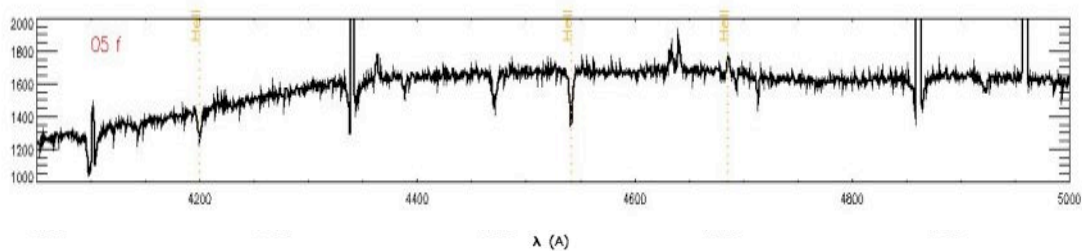


Figure 3.40: VLT-VIMOS spectra of an O5f star in IC 1613. The Balmer series is severely contaminated by nebular lines, even after a careful sky subtraction.

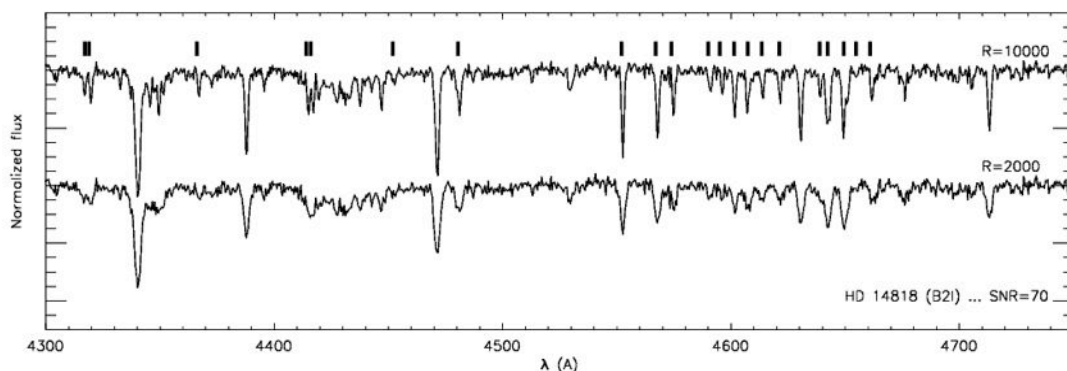


Figure 3.41: The spectra of a B2 supergiant as it would be observed with $R=2,000$ and $R=10,000$ and for a $S/N=70$. Vertical lines mark the spectral transitions used for abundance determination. The very weak lines blend or even disappear at low resolution.



A resolution of $R \sim 10,000$ is indeed crucial for determining accurate stellar abundances. We compare in Figure 3.41 the simulated spectra of a B-type supergiant observed with $R=10,000$ and $R=2,000$. The weaker spectral transitions used for abundance determination are lost in the lower resolution spectra, making it unsuitable for abundance determination. Detailed spectroscopic analyses of blue massive stars at $R \sim 6,000$ can produce stellar parameters. However, $R \sim 10,000$ resolution is determinant to derive accurate abundances and to study stars located in HII regions, as it allows us to separate nebular from stellar contributions in the Balmer (and sometimes HeII) lines. Similarly, in crowded areas, the chances to disentangle in velocity space the spectra of two nearby stars integrated in the same fiber increase with spectral resolution. The medium-resolution VPHs are therefore crucial for improving GTC's current capabilities for analyzing blue massive stars.

The proposed MEGARA observations in the Local Group will cover a metallicity range from $1.3Z_{\odot}$ (in the central parts of M33) to $0.04Z_{\odot}$ (IC 1613). They will produce a large database of high-resolution high-quality spectra of blue massive stars out of which we expect to find a variety of evolutionary stages. Their spectra will be analyzed quantitatively to obtain the physical parameters and surface abundances of the stars. Their physical properties, spectral types and abundances, together with their location in the HRD, will lead to a wider picture of the impact of metallicity on massive star evolution and winds. In HII-rich regions, the wind parameters will be key to understand the interplay of massive stars and gas, and to decide the origin of the carved ionized structures.

In particular, we will use MEGARA observations of IC 1613 to tackle three main issues: study the physics of the winds of O stars and B supergiants at low metallicity, study their impact on the surrounding interstellar medium, and study the evolutionary stages of massive stars in metal-poor environments as proxy for the early Universe. MEGARA is particularly well suited for these purposes: its IFU capabilities allow us to obtain simultaneous spectroscopy of stellar groups in the most crowded regions (and of the nebulosity around the stars, if any), and the MOS positioners can cover the surrounding less dense areas; overall, a large sample of stars can be observed in few pointings.

Most of the population of candidate blue massive stars in IC1613 can be covered in four MEGARA-Advanced setups, shown in Figure 3.42. The most interesting region is the NE lobe of the galaxy, which contains the largest, most massive OB associations of IC 1613 (García et al. 2010a), and the largest HII structures. Thanks to MEGARA MOS FOV of 3.5×3.5 arcmin² the area can be covered in one single shot. The IFU LCB would be used to obtain mid-resolution ($R \sim 11,000$) spectroscopy of the knots of stars at the intersection of two giant HII shells, as shown in Figure 3.42 (right). Since the spaxel separation is 0.685 arcsec and stars are about 1 arcsec away, the spectra collected by the IFU will allow us to separate the stars in the region.

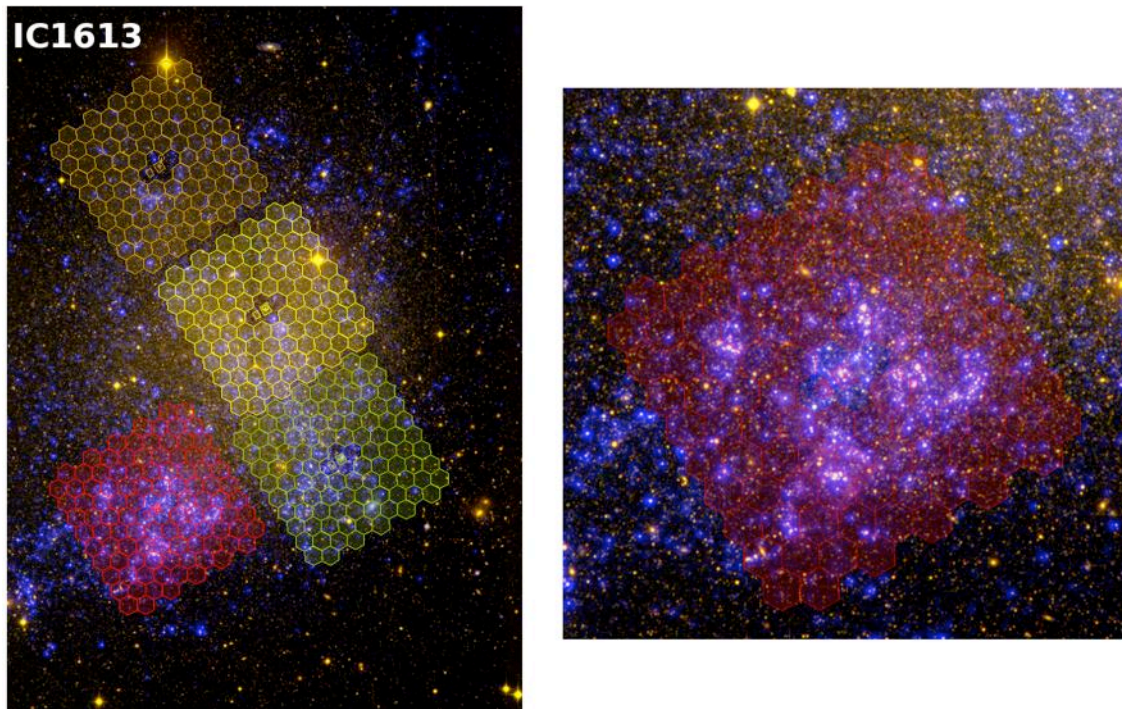


Figure 3.42: Left: IC 1613, RGB composition of INT-WFC images (R- and V-band, 0.33 arcsec/pixel) and GALEX FUV channel. The hexagon-combs mark the field of view covered by MEGARA's MOS in the four proposed pointings. Right: close-up of the NE lobe of the galaxy, home to large HII shells. The three MEGARA components are marked for reference. One single pointing in this region would allow us to observe a large number of massive stars and also study their interaction with the interstellar medium.

The MOS positioners would then register stars in the surrounding 3.5×3.5 arcmin² area, the results leading to new hints on the shaping agents of hydrogen in the region. If MEGARA-Advanced is available, these spectra will also be taken with mid-resolution VPHs at no additional observing time cost. However, if only MEGARA-Basic is available additional time will be needed to cover this region, critical to complete the census of blue massive stars in the area. We expect to find here additional interesting objects from the stellar evolution and feedback point of view that would have been overlooked because of their fainter V-magnitudes (we found in García et al. 2009 that extinction can be locally very high, and hide interesting evolutionary stages, as reported in Herrero et al. 2010). In this case, the spectra will be collected with the low resolution $R \sim 6,000$ VPHs. Targets will be taken from our own photometric catalogue (García et al. 2009), built from INT-WFC images. The accuracy of the astrometry of our target coordinates is apt for direct use on fiber-fed multi-object spectrographs such as the MEGARA MOS mode. Additional VLT-VIMOS or HST images will be used (when available) to check against blends (see Section 3.1.5.1.1 for some simulations in this regard in the case of the disk of M33). Candidate blue massive stars will be chosen from the reddening-free Q pseudo-color and V magnitudes, that has proved to be very successful for pre-selection of blue massive stars (García et al. 2009), and from the examination of the population of OB associations in IC 1613 from the catalogue of García et al. (2010a).



The observations will produce the first homogeneous sample of high-resolution spectra of blue massive stars in the NE lobe of IC1613, a breakthrough towards the chemo-dynamical enrichment history of the region.

The key point in order to carry out the science goals detailed in Section 3.1.2 is the quantitative spectroscopic analysis of massive stars in a variety of metallicity environments. The observations must cover the spectral range 4000-5000 Å, to include H β , H γ and H δ , HeI and HeII for O stars, and other crucial lines for the determination of effective temperatures of B supergiants (SiIII 4552, 4567, 4574, SiII 4128 and SiIV 4116 Å). The H α region is needed to estimate the mass loss rate experienced by the star and to characterize its wind.

Optimally, our observations will be carried out in the MR+HR mode with simultaneous use of the central large compact bundle and the MOS. We will devote **30 hours** to study the NE lobe of IC 1613. According to the MEGARA's ETC and Instrument Overview document, in this time we will secure S/N=70 spectra for V=19.5 stars, with full coverage of the 3890-5054Å range (MR-U, MR-UB and MR-B) with R~11,000 plus H α (HR-R) with R~19,000 (see Table 3.2). If only MEGARA-Basic was available, additional 17 hours would be needed to observe the bubble area with the MOS with the low resolution VPHs; while not suited for accurate abundance determination, the spectra will produce effective temperatures, gravities and wind parameters for the stars enabling evolutionary and feedback studies of the region. In Table 3.2 we summarize how this exposure time is split by spectral setup.

The exposure times quoted are rather conservative, as they were calculated from the addition of 1 hour long observing blocks (minus 30% overheads) and not very demanding atmospheric conditions: grey nights, airmass=1.3 and 0.8 arcsec seeing. Our expertise in extragalactic stellar spectroscopy advises that signal-to-noise ratio of 70 is the minimum needed for quantitative analysis (see for instance Castro et al. 2008). The limiting magnitude V=19.5 is required for studying the spectral stages of interest. The absolute magnitudes of A- and B- supergiants, and O stars range from M v =-8.5 to -4.5 (Schmidt-Kahler 1982). At the distance modulus and foreground extinction of IC 1613 (DM=24.27 mag, E(B-V)=0.02; Dolphin et al. 2001; Lee et al. 1994), this translates into a maximum magnitude V=19.8. Only the spectra of the faintest targets (O9 V) would be compromised: note, however, that useful results can still be obtained by rebinning their spectra to R~6,000.

We will spend **25 hours** in the three remaining fields in the same MR+HR configuration, preferably with simultaneous observations with the IFU LCB and the MOS. The signal-to-noise ratio achieved for V=19.5 stars will be under S/N=70 but since crowding and nebular contamination is not so severe in these regions spectral resolution is not as critical and we can again rebin the spectra of the faintest targets for enhanced S/N. Given the lower stellar density, observations will be taken with the MOS if only MEGARA-Basic would be available.

This yields a total observing time of **105 hours** (overhead included) to map the bulk of the massive-star population in IC 1613.



MEGARA-Advanced	V=18	V=19	V=19.5	V=20	V=20.5
R~11,000	Number of 1h-long Observing Blocks				
MR-U+MR-UB+MR-B+HR-R (3962-5119Å + H α)	5	15	30	55	109
MEGARA-Basic (additional obs. time)	V=18	V=19	V=19.5	V=20	V=20.5
R~6,000	Number of 1h-long Observing Blocks				
LR-U+LR-B+LR-R (3670-5216Å + H α)	4	8	17	27	61

Table 3.3: Number of total observing blocks needed to achieve $S/N=70$ for different VPH and magnitude combination, to cover the whole spectral range of interest. The S/N of individual OBs was calculated using exposure times of 2520s (1 hour long OBs minus 30% overheads), grey night, airmass=1.3 and 0.8 arcsec seeing.

In M33, we will use the fields proposed to study stellar migration in disks galaxies, using the MOS robotic positioners with the MR+HR configuration. In the 16 hours to be devoted to each field (see Section 3.1.5.1.2), we can secure the complete spectral range of interest (3900-5200Å + H α , i.e. MR-U, MR-UB, MR-B and HR-R, see above) with $S/N \geq 70$ down to V=19 stars (see Table 3.3). At the distance of M33 [DM=24.84, E(B-V)=0.04; U et al. 2009], this corresponds to $M_v = -6.0$, securing OBA supergiants and early-O dwarfs (Schmidt-Kahler 1982).



3.1.5.2 Nearby galaxies (beyond the Local Group): The MEGADES-S4G sample

Although the analysis of the disks' stellar kinematics, effective SFH, and chemical abundances each provides fundamental information, is the combined strength from all three sources what will allow us to disentangle the role of the different mechanisms proposed to drive the evolution of disks. However, as commented in Section 3.1.4.1, the number of spiral disks at the distances where the abundances and kinematics of individual stars can be measured is small, covering only a narrow range in the space of parameters. Below, we summarize the observations proposed as part of MEGADES for the study of a complete volume/magnitude/diameter-limited sample of nearby galaxies ($d < 40$ Mpc) whose spectroscopic properties (light-weighted kinematics, spectral indices, and chemical abundances) will allow us to determine the parameters that actually drive their evolution. For completeness this sample also incorporates a small number of elliptical galaxies that should allow extract conclusions on the evolution of galaxies as a whole (see the areas of expertise of our team in Section 2.1).

As the evolution of galaxies is a complex process that involves mechanisms acting at different spatial scales and in different regions (nuclear or starburst activity, bars, stellar migration, satellite accretion, minor mergers) and the FOV of the MEGARA IFU LCB by itself is not large enough to cover entire galaxies at a reasonable resolution from the ground the combined use of the MEGARA MOS and IFU will be required (this is particularly efficient in the case of the MEGARA-Advanced configuration although it would still be addressed with MEGARA-Basic alone).

3.1.5.2.1 Strategy

The observations of the MEGADES-S4G sample are designed to simultaneously provide information on the small and large spatial scales and at low and high spectral resolutions. This is the necessary combination to analyze the relative contribution to the evolution of disks of the different secular processes described throughout this document. In this regard, this analysis will make an optimal use of the MEGARA-Advanced configuration. The LCB IFU would be used (1) for the analysis of the galaxy stellar and ionized-gas kinematics along the major and minor axes and (2) all those physical processes taking place in the nuclear regions (nuclear activity and Galactic Winds) while, simultaneously, the Fiber MOS will be used for the study of (3) the global 2D velocity field (where the positioners would be placed at different galactocentric distances following a regular grid) and (4) the metallicity distribution (with positioners placed on top of individual HII regions). The LCB is preferred over the SCB for the larger FOV and better sky subtraction of the former.

The observational strategy from an operational point of view will be to first obtain a single pointing with the IFU LCB in the center of the galaxy (to identify or confirm potential Galactic Winds, AGN, inner disks) and the MOS in the HII regions previously identified in ground-based $H\alpha$ images (simultaneously in the case of MEGARA-Advanced). For those galaxies showing evidence of any of these features we will then map the galaxy central regions with the IFU (see Sections 3.1.5.2.4 through 3.1.5.2.6) and for disk galaxies with inclinations in the range $40^\circ < i < 70^\circ$ additional IFU observations along both the major and minor axes of the galaxy will be pursued (see Section 3.1.5.2.3).

In Figure 3.43 we show the footprint of both MEGARA modes (the IFU for all pointings along the major and minor axes and MOS only for the central pointing) on top one of the spiral galaxies in our MEGADES-S4G sample (NGC 5371).

As the galaxies in this sample span a range in diameters between $2.5' < D_{25} < 4'$, we will adopt an average number of 6 pointings per galaxy to map both the major and minor axes. As commented above, for disk galaxies with inclinations below 40° (where dynamical information is not usable for deriving the galaxies' velocity ellipsoid) or for ellipticals only one pointing will be obtained. Note that in this case there is no need of placing the positioners in a regular grid (as galaxy dynamics are not of interest anyway) and only HII regions will be targeted.

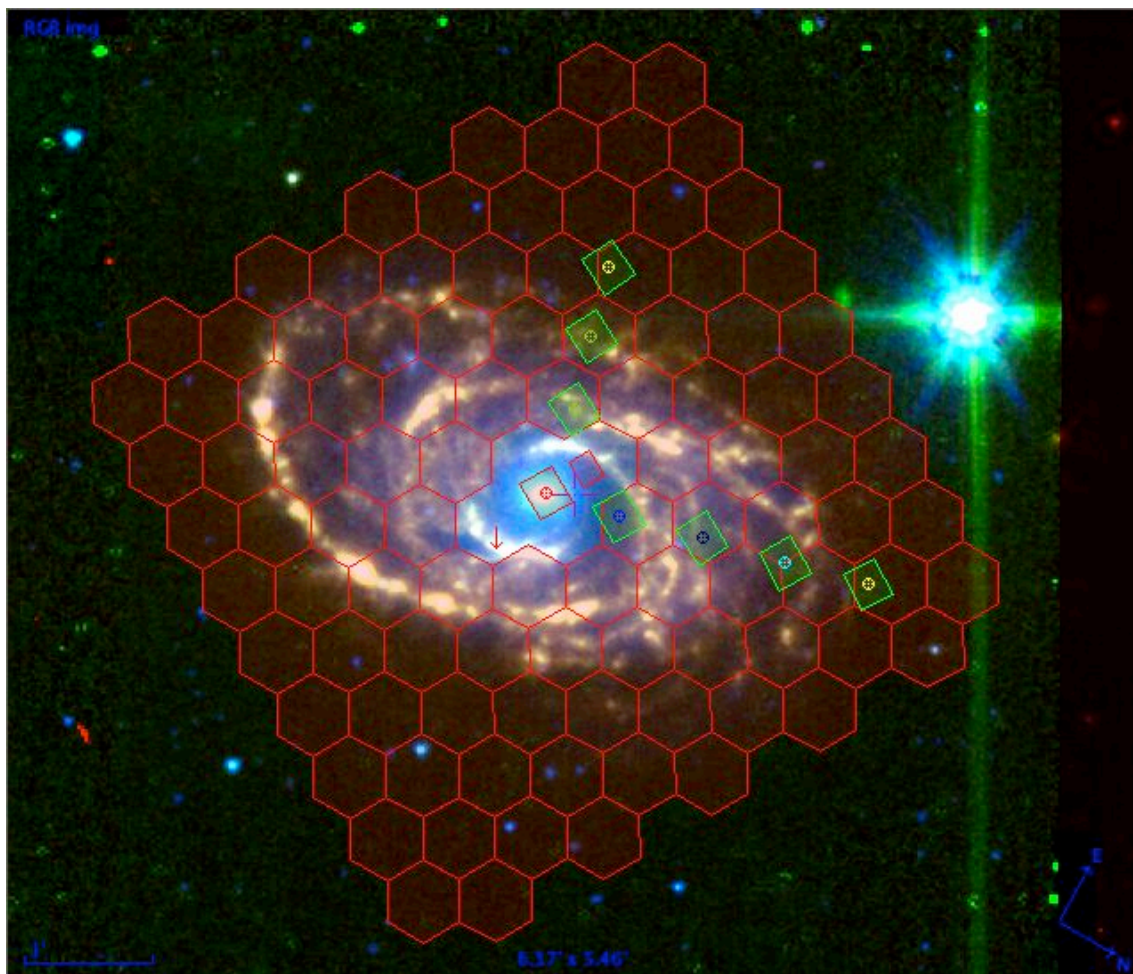


Figure 3.43: False-color IRAC image of MEGADES-S4G galaxy NGC 5371 with the footprint of the central MEGARA IFU+MOS pointing (in red) and the major and minor-axes IFU pointings (in green) over-plotted. The instrument position angle has been changed for an optimal use of the instrument. Note that the inclination angle of the target allows for a proper derivation of the galaxy velocity ellipsoid. In highly face-on systems only the central pointing will be obtained.

With this strategy in mind we estimate a total of 6×139 pointings (at different surface brightness levels; see next section) for galaxies where the velocity ellipsoid is measurable and 57 (19)

highly face-on spiral disks (elliptical galaxies) where only one pointing per galaxy will be obtained. Should we limit the sample to galaxies within the SDSS footprint exclusively we will need to observe 6x95 pointings, 38 face-on disks and 17 ellipticals. Our final time estimates are based on this latter sample (see Table 3.2).

In addition to these pointings, in the case of early-type disk galaxies whose photometric decomposition would reveal the presence of an inner disk (~20 S0-Sa galaxies based on the results of the NIRS0S sample; see Section 3.1.5.2.4) or galaxies where the central IFU observations show indications of the presence of a Galactic Wind (either in emission or neutral) a central map of 7 IFU LCB pointings will be obtained (see Figure 3.44). In this latter regard, it is difficult to anticipate the precise number of galaxies to show a Galactic Wind so we will assume another 20 galaxies (10 with wind in emission, 10 in interstellar absorption lines).

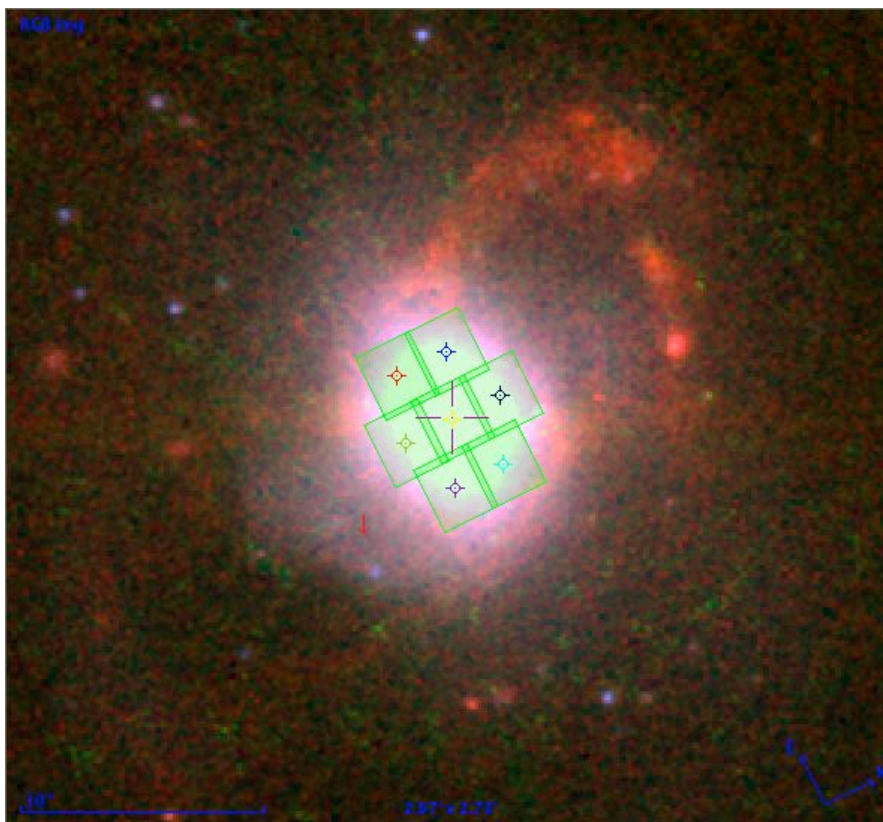


Figure 3.44: False-color IRAC image of the central region of MEGADES-S4G Sa galaxy NGC 7727 with the footprint of the 7-pointing mosaic to be used in galaxies where either a inner disk or the presence of a Galactic Wind are identified after then first (central) pointing is acquired and analyzed.

3.1.5.2.2 Analysis tools

While it would be ideal to have in hand a complete set of high-resolution of N-body simulations to compare with our data, these are time-consuming and only a few are available as of today (e.g. Sommer-Larsen et al. 2003; Brook et al. 2006, 2007; Kazantzidis et al. 2008, 2009; Sánchez-Blázquez et al. 2009, 2010; Martínez-Serrano et al. 2009).

As previously discussed, in the case of the study of a larger sample of nearby disks we will



analyze their spectroscopic properties by making use of the so-called *backward* models of galaxy evolution (Mollá et al. 1999, 2006; Boissier & Prantzos 1999; Matteucci & Franco 1989). Possible departures from the predictions of these models in terms of their spatially-resolved effective star formation histories and chemical abundances (including abundance ratios) will be interpreted in the context of effects associated to stellar migration or satellite bombardment (mostly in the outer regions), nuclear or starburst activity or minor merging (in the inner regions of disks). Note that the information content in the spectral indices and chemical abundance gradients is such that the study of these departures now becomes feasible (see Figure 3.25 and 3.27).

On the other hand, the measurement of light-weighted σ_z and σ_R profiles should tell us whether *heating* (and, thus, stellar migration) or satellite accretion are important. The contribution of *churning* to migration is more difficult to evaluate in this case and only the value of the disk-mass fraction, which can be measured from the light-weighted σ_z (Verheijen et al. 2004) could provide an estimate of the frequency and amplitude of transient spiral arms, and, therefore, of the potential *churning* (Sellwood & Binney 2002). Moreover, the lessons learnt from the star-by-star analysis of M33 could also provide clues to identify objects where stellar migration could mask the *in-situ* evolution of the star formation in disks.

Finally, kinematical information is also relevant in order to (1) diagnose a recent minor merger event as such events are believed to induce the formation of non-self-gravitating, spiral-like features which could be also seen in velocity space (Gómez et al. 2012) and (2) to identify Galactic Winds either in line emission or in interstellar absorption features.

3.1.5.2.3 Observing time: kinematics, stellar populations and metallicity of disks

Spectral setups

In order to study the velocity ellipsoid, chemical abundances, and stellar populations of the galaxies in the MEGADES-S4G sample we will need a suite of VPHs of different spectral resolutions. In particular, we will use both the R=6,000 LR-I VPH in the CaT region and the R=11,000 MR-B VPH in the blue for stellar kinematics (only in galaxies with inclination $40^\circ < i < 70^\circ$), the R=19,000 HR-R VPH in H α for the ionized-gas kinematics, including the detection and analysis of Galactic Winds and AGN (see Sections 3.1.3.4 and 3.1.3.5) and tests on the applicability of the asymmetric drift equation (see Noordermeer et al. 2008), and the R=6,000 LR-U, LR-B, LR-V setups for the study of unresolved stellar populations and chemical abundances (HR-R observations are also needed in this latter regard).

Central pointing: goal

As commented in Section 3.1.5.2.1 we will first observe all 133 disk galaxies within MEGADES-S4G (considering only those in the SDSS footprint) with the LCB centred on the galaxy nucleus and the robotic positioners placed on HII regions of its disk. The observations with the IFU have the objective of obtaining stellar and (ionized and neutral) gas kinematical information of around the nucleus. The robotic actuators will be used, on the other hand, to measure the ionized-gas chemical abundances in a number of individual HII regions and to obtain some information on the global 2D velocity field, both from the stars and the ionized gas.



As we show below it is actually the determination of the metallicity distribution what drives the total exposure time in this case.

Central pointing: MOS observing-time requirements

At the distance of some of our galaxies (especially those within 20 Mpc) we aim to obtain metal abundance measurements from temperature-sensitive collisionally-excited lines ratios, such as those based on the detection of the [OIII] λ 4363Å emission line. Of course, strong-line methods, such as those from Kewley & Dopita (2002) based on the photoionization models, could perfectly be carried out in any case.

In order to analyze the possibility of detecting [OIII] λ 4363Å in some of our galaxies we have explored the SDSS spectroscopic archive and found a number of our targets (e.g. NGC 0450, NGC 2541, NGC 3423 among others) where this spectral feature has been detected with fluxes of the order of $f_{[\text{OIII}]\lambda 4363} \sim 10^{-17} \text{ erg cm}^{-2} \text{ s}^{-1}$. Those line fluxes are reachable in the 30min-long exposures planned with signal-to-noise ratios per spaxel of $S/N \sim 18$ for the VPH of interest, MR-UB. Note that we prefer to use MR-UB (in combination with MR-B) rather than LR-B as the [OIII] λ 4363Å is well centered on the MR-UB setup and the MR-B also provides optimal information on the kinematics of the intrinsically low- σ blue stellar populations. We will complement this with LR-I observations for the study of the stellar velocity dispersion in the CaT region. Note that in this case we do not aim to reach a very high S/N (just a few adding up all positioners at a given galactocentric distance), as this will be the objective of the scan maps to be obtained along the galaxies' minor and major axes (see below). Exposure times of 15 minutes will be used both for MR-B and LR-I when using the MEGARA Fiber MOS. These exposure times are also sufficient to detect (at the same level as for the other emission-line features) the [SIII] λ 9069Å line with the LR-I setup (S23; Pérez-Montero & Díaz 2003).

Since most other emission lines are significantly brighter than [OIII] λ 4363Å the exposure times in the other setups that are needed to cover the entire wavelength range of interest, LR-U, LR-V and LR-R, are also short. Only in the case of the LR-U VPH the observing time reaches 20 minutes to compensate for the low sensitivity of the system below $\sim 3800\text{Å}$ (including the resolved [OII] $\lambda\lambda$ 3726, 3729Å doublet). Unfortunately, the possibility of detecting the faint ORLs at these distances is beyond the reach of current facilities anyway, even for very long integrations with MEGARA.

Adding up all observing time requirements listed above we come out with a total of **2.1 hours per target** (15% overheads included; see Table 3.2). For the 133 MEGADES-S4G galaxies (within the SDSS footprint) where metal abundances could be measured we would require ~ 280 hours. We anticipate that an additional selection for a subsample of targets might be needed.

Central pointing: IFU observing-time requirements

With regard to the IFU observations (simultaneous in the case of MEGARA-Advanced) the continuum surface brightness levels expected for this central pointing are bright enough so only short exposures (15min) are needed even for studying stellar kinematics in the MR-B and LR-I spectral setups (see below; see also Table 3.2). The same applies to the LR-U but, because the significantly lower sensitivity of the system at these wavelengths, in this case again we will



increase the observing time to 20 minutes per target.

As for the MOS observations described above, the study of the ionized-gas abundances from T_e -based methods requires of a total exposure time of 30 minutes with the MR-UB.

Finally, in the case of the observations in the $H\alpha$ region, the exposure time is driven by the necessity of studying the wings of the $H\alpha$ line and the possible presence of out-flowing material that these winds could trace. This implies a total exposure time on target with the HR-R of 30 minutes (see Section 3.1.5.2.5).

Such spectral configuration and exposure times allow taking full advantage of the versatility that MEGARA-Advanced provides but also ensures an optimal scientific exploitation should only one MEGARA spectrograph be available at GTC (MEGARA-Basic), although obviously with a penalty in terms of observing time. In particular, should only MEGARA-Basic be available this configuration would ensure that the IFU observations in the nuclear regions reach the central surface brightness of a Freeman disk ($\mu_{0,B}=21.65 \pm 0.3$ mag arcsec⁻²; Freeman 1970) with $S/N \geq 10$ per Angstrom and per arcsec² in any continuum band (an airmass of 1.3 and gray nights were assumed).

Central pointing: Ellipticals

In the case of the 17 elliptical galaxies in the sample we will prioritize spectral coverage and the whole set of 5 LR VPHs will be used (LR-U, LR-B, LR-V, LR-R, LR-I) with the same (conservative) limiting surface brightness. This would yield to exposure times of $\sim 1200/600/600/600/1800$ respectively for LR-U, LR-B, LR-V, LR-R, LR-I (see Table 3.2), i.e. 1.6 hours per galaxy (20% overheads included) or **27 hours** total.

Major and minor axes scans

As for M33, the aim of the analysis of the velocity ellipsoid and the stellar populations along the major and minor axes of MEGADES-S4G galaxies with inclinations $40^\circ < i < 70^\circ$ will be to reach a surface brightness in the outermost pointing of $\mu_r = 24.5-25$ mag/arcsec². At this surface brightness a change in properties associated with the threshold for star formation is typically found which also leads to the effects of stellar migration being most notorious. For the other intermediate pointings we will adopt an average of two pointings at $\mu_r = 23.5$ mag/arcsec² and two pointings at $\mu_r = 22$ mag/arcsec². The central pointing will be available for all galaxies as part of the observations described above.

In Table 3.2 we show the resulting exposure times (on target) for each pointing and at a given surface brightness for all the spectral setups of interest, namely LR-U, LR-B, LR-V (for the study of the stellar populations in the disks), LR-I and MR-B (for stellar kinematics). This yields a total observing time (15% overheads included) of **~ 10 hours per target** (~ 1 night). Note that in the case of the MEGARA-Advanced configuration all robotic positioners will be placed in a regular grid that will provide further information on the 2D distribution of these properties, which could reduce slightly our time needs. These time estimates are for a $S/N > 5$ (except for LR-I, which is $S/N > 3$) and are based on the results of the MEGARA Exposure Time Calculator assuming an airmass of 1.3 and dark nights.



Although the total number of galaxies with the right morphology (RC3 type >0) and inclination ($40^\circ < i < 70^\circ$) reaches 95 we will start this analysis by a subsample that should ensure a good sampling of the population of galaxy disks in terms of morphology, environment and luminosity.

3.1.5.2.4 Observing time: inner disks, stellar populations and dynamics

As part of the analysis of the inner disks present in the MEGADES-S4G sample and its possible minor-merger origin we plan to map the central region of each inner-disk host galaxy with the MEGARA LCB, using the following low-resolution VPHs (LR-U, LR-B, LR-V and LR-R) to cover a significant fraction of the optical spectrum. This will allow us to obtain chemical and dynamical diagnostics for the gaseous and stellar component at different spatial locations of these galaxies, using the 4000 Å break, H α , and several line indices based on absorption and emission lines from the [OII] λ 3727 Å to [SII] λ 6717,6731 Å. Gas kinematics and SFRs will be estimated using H α and [OII] λ 3727 Å fluxes (wherever emission is present). The derived H β line-emission maps will be corrected for underlying absorption using the EW(H β) using the best SP fitting model to the continuum and emission-free spectral absorption features. The other line maps will be corrected for dust attenuation using the H α /H β Balmer decrement, which is essential for getting realistic estimates of the age and metallicity of the stellar populations. Gas metallicity will be derived using different estimators when detectable, such as R23, N2, and O3N2 (Pilyugin 2001; Pettini & Pagel 2004; Tremonti et al. 2004). The data will be used for computing several optical absorption line indices, that will provide estimates on stellar velocity dispersions, rotation, ages, and metallicities (Faber et al. 1985; Gorgas et al. 1993; Worthey et al. 1994). Ages and metallicities of the stellar populations will be estimated from fits to the spectra with SSP models.

Considering the typical size of the region to be analyzed (~ 7 pointings of the LCB per galaxy; the central one plus 6 additional pointings; see Figure 3.44) and the typical R-band surface brightness of the central region of these galaxies ($\langle \mu_R \rangle \sim 18$ mag arcsec $^{-2}$), we would require ~ 3 hours of exposure time per galaxy to achieve a S/N > 10 in the continuum in the four VPHs listed above (accounting for an additional 30% time for overheads), under typical conditions (seeing with FWHM = 1", grey night). This makes a total of ~ 60 hours to obtain high S/N 2D spectroscopy data covering the most relevant emission line from the [OII] λ 3727 Å doublet to [SII] λ 6717,6731 Å for the ~ 20 galaxies expected to be found in the MEGADES-S4G sample.

The resulting distributions in age and metallicity of stars of the different sub-components of these galaxies, as well as their velocity maps, will be compared to those obtained from N-body simulations of minor mergers onto S0 galaxies including gas and star formation (Eliche-Moral et al. 2012, in preparation) and internal secular evolution models (Debattista et al. 2005, 2006) to derive conclusions concerning the possible minor-merger or pure bar-driven origin of the inner disks and rings in this S0-Sa sample.

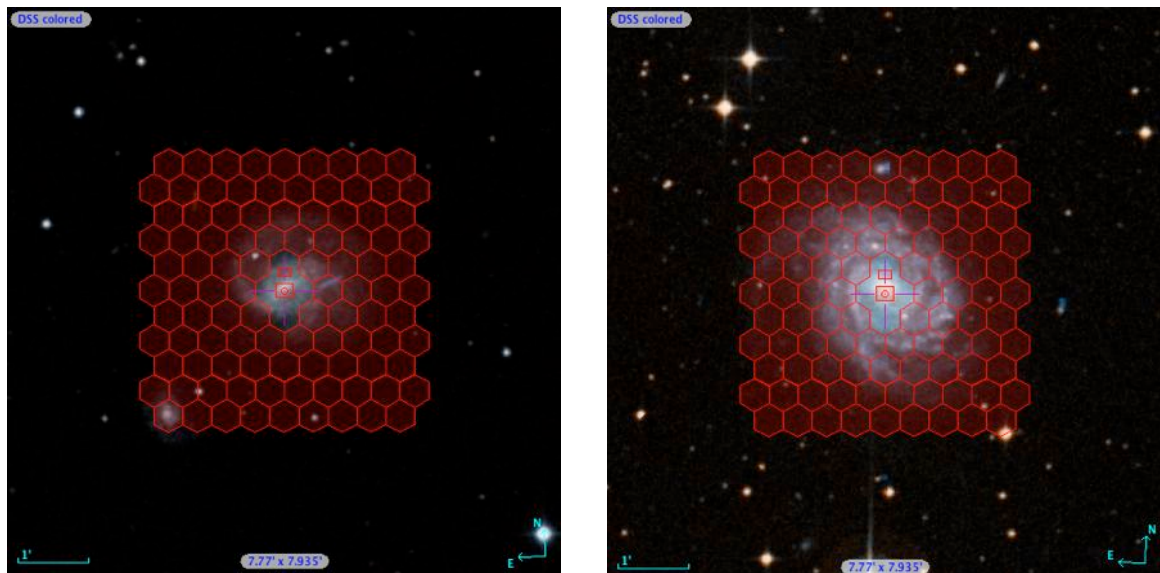
Previous 3D spectroscopic studies have analyzed central regions of nearby galaxies globally, but the specific properties of the stellar populations in each sub-component and their kinematics are starting to be analyzed (e.g. the SAURON survey). In this sense, the present study would be pioneering in establishing the properties of the stellar populations of inner disks in relation with

the other galaxy components, and their possible minor-merger or pure internal, secular origin.

3.1.5.2.5 Observing time: (neutral) galactic winds

As part of this study we have proposed to observe the central region of a sample of nearby spiral galaxies with MEGARA to study Galactic Winds by means of interstellar (Na I D) absorption and complementary line emission information (H α , [NII], [SII]). The strategy will be first identify the presence of these winds in galaxies belonging to the full MEGADES-S4G sample but located within the SDSS footprint (133 spiral galaxies with $i < 70^\circ$) and then for each Galactic Wind host galaxy to map the entire central region using a 7-pointing LCB mosaic (see Section 3.1.5.2.1 above). The dimensions of the galaxies in our sample ensure having a good spatial sampling and that some positioners of the Fiber MOS devoted to measure the sky background are actually sampling blank-sky regions. Most likely, the confirmed candidates will come from among the 38 disks in the MEGADES-S4G sample with inclinations $i < 40^\circ$, as this maximizes kinematical discrimination and allows better tracing the distribution of the outflowing absorbing material. Finally, we will also determine the frequency of galaxies hosting a Galactic Wind and the differences in the winds fed by nuclear activity or starbursts.

Figure 3.45: DSS images for NGC 4430 (left) and NGC 5085 (right) as example of a small and a large galaxy in our sample. The central region of the galaxy will be mapped with the IFU LCB. The FOV of the Fiber MOS is overplotted to show that we will be able to map blank-sky regions even in the case of the most extended targets in our sample.





The observed wavelength range for our study will contain (i) the stellar absorption triplet Mg I ($\lambda\lambda 5167, 5173, 5184\text{\AA}$) which, together with another, less prominent absorption lines, will allow us to subtract the stellar contribution from the observed spectra, in particular, its contribution to the Na I absorption, (ii) the interstellar absorption doublet Na I ($\lambda\lambda 5890, 5896\text{\AA}$) which will allow us to trace the structure and kinematics of the neutral cold phase of the gas, and (iii) emission lines from warm ionized gas ($H\alpha$, $[\text{NII}]\lambda 6583\text{\AA}$, $[\text{SII}]\lambda\lambda 6716, 6731\text{\AA}$ lines) which will allow us to trace the warm component of the wind. We will need three spectral setups to cover the whole wavelength range of interest: VPH-480-LR (LR-B), VPH-570-LR (LR-V) and VPH-675-LR (LR-R).

The velocity resolution of $\sim 50 \text{ km s}^{-1}$ (FWHM) provided by the LR configuration in MEGARA is better than that achieved by previous long-slit studies, and high enough for our purposes. According to the MEGARA Exposure Time Calculator, an average integration time of 1/2 h (for each target and spectral setup) is needed in order to achieve the necessary signal-to-noise ratio. We plan to split our observations in every spectral setup in 3 exposures of 600 seconds each to allow for cosmic ray removal. A total of **~ 120 hours on target** will be needed (~ 144 hours including overheads) in order to complete the sample.

As commented above, the proposed observations will provide valuable spatial information on the different phases of the wind. The key step in our analysis is the determination of the stellar contribution to the Na I D absorption doublet. For this step we compare the observed spectra (containing stellar absorption lines as MgI, Fe, Ca and TiO) with different templates (single stars and/or synthesized populations). The best fit is then subtracted from the observed spectra leaving exclusively the contribution of the interstellar (absorption and emission) lines. The presence of blueshifted Na I interstellar absorption doublet is an unambiguous signature of outflowing material. From a careful analysis of this doublet, the amount of cold gas in the wind and its kinematics can be calculated. For the emission lines, a decomposition of the line profiles will be performed in order to study the existence of several kinematical components. The kinematics and spatial distribution of the absorption and emission components will allow a better understanding of the physics of the wind. Furthermore, line-ratio maps will provide information on the energy sources and temperature/ionization conditions in the galactic wind.

3.1.5.2.6 Observing time: nuclear activity

The requirements in terms of observing for the study of the properties of the stellar populations, bidimensional chemical composition and kinematics of AGN hosts and their comparison with the properties of quiescent systems are identical to those stated above for the study of those properties in the context of the evolution of disks as a whole. Therefore, this specific goal will take full advantage of the MEGADES dataset as designed above.

This is a perfect example of how two different science goals can be accomplished using the same dataset. In other cases, such as the study of inner disks of Galactic Winds above, additional observations will be needed in order to fully understand the physical mechanisms involved. In the two cases mentioned basically these additional observations imply obtaining a 7-pointing IFU LCB map of the galaxy central regions.



3.1.5.3 Additional MEGADES targets

3.1.5.3.1 M82

Using the SSCs catalog from Melo et al. (2005) we have identified the central region of M82 with higher overabundance of young SSCs. We plan to center in this position the large compact bundle (in order to map the properties of the SSCs) and then we will position the robotic positioners of the Dispersed Bundle (MOS) over the filamentary structure around these central SSCs. We will use the two spectrographs (if available) with a different configuration in order to fully explore the powerful capabilities of MEGARA to fulfill our scientific goals.

For the LCB we will map the very central region of M82 using two different resolutions. First, we will use the low resolution VPH LR-R, which provides a spectral resolution of ~ 6000 , or equivalently, ~ 50 km/s. This will allow us to study the physical properties of the SSC and identify the real precursors of the SGWs. Then, we will use also the high resolution VPH HR-R to study the resolved H α line. This will allow us to understand the feedback mechanism at place in the position of the SSCs. The HR-R provides a spectral resolution of ~ 19000 , or equivalently 16 km s $^{-1}$.

For the dispersed bundle (MOS), we plan to use always the medium resolution VPH, HR-R which again provides a resolution of ~ 19000 , or equivalently ~ 18 km/s. Since in the case of the filamentary structure we are more interested in the analysis of the line shape (to study its kinematics) rather than the properties of the gas we will change the spatial configuration between the two pointing in order to map a large number of filamentary structures, but we will not change the spectral resolution.

Using the MEGARA Exposure Time Calculator with a typical seeing of 0.8 arcsec, airmass=1.2, and a grey night, we will be able to measure the diffuse ionized gas (with luminosities of the order of 10^{-17} erg s $^{-1}$ cm $^{-2}$) using the LR-R with an integration time of 1.5 hour at a S/N ~ 5 per \AA . In the case of the HR-R VPH the integration time required is the roughly the same since the luminosities of the SSCs is $\sim 10^{-15}$ erg s $^{-1}$ cm $^{-2}$. As a confirmation of the MEGARA ETC accuracy we found that similar exposure times were used by Westmoquette et al. (2009) to map the central region of M82 with GMOS@Gemini. Thus, this confirms that we will be able to fulfill our scientific objective with the proposed observing times.

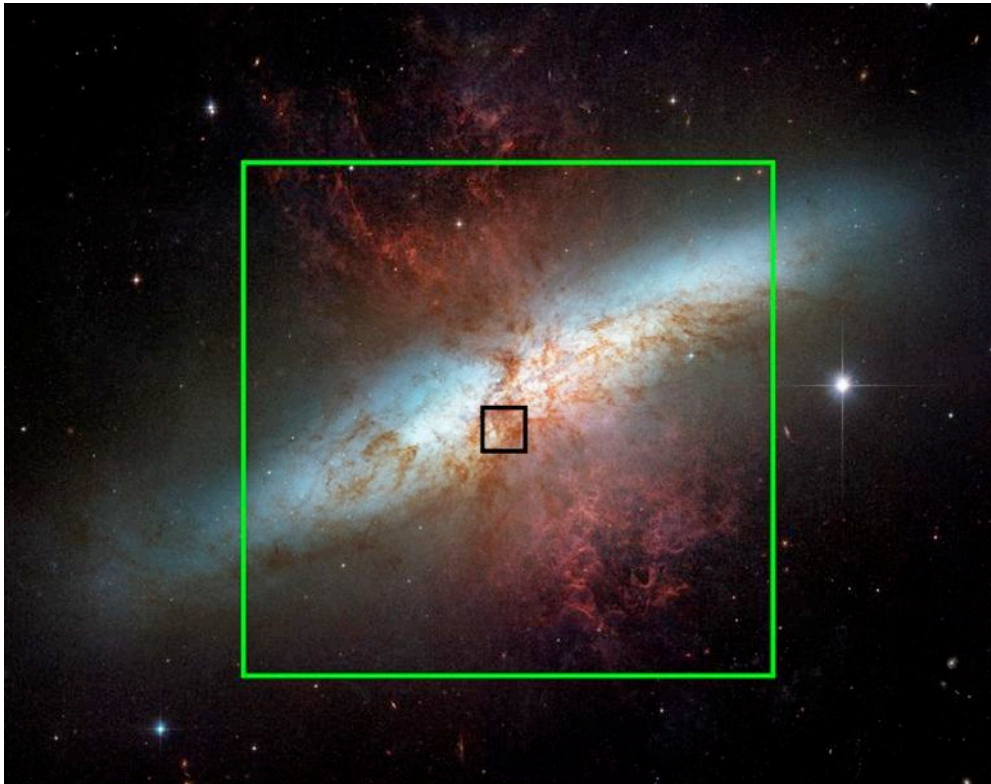


Figure 3.46: HST image of the starburst galaxy M82. The black square indicates roughly the dimensions of the MEGARA large compact bundle. The green square shows the dimensions of the dispersed bundle (MOS). A plethora of SSCs have been catalogued in the optical range by our team (Melo et al. 2005). Those located at the base of the filaments seen in the picture could be already observed using the MEGARA Large CompactBundle ($FOV=14 \times 12 \text{ arcsec}^2$).

Therefore, the final time estimated to fulfill our scientific objectives can be then broken down as follows: M82 (two pointings): $2 \times 1.5 \text{ hours} + 2 \times 0.16 \text{ hours} = 3.32 \text{ hours}$ (see Table 3.2).

3.1.5.3.2 ULIRGS

The wavelength range of choice for the study of the properties of Galactic Winds in ULIRGs should contain the interstellar absorption line Na I D, as this feature allow us to trace the structure and kinematics of the neutral cold phase of the gas, as well as emission lines from warm ionized gas ($H\alpha$, [NII] $\lambda 6583\text{\AA}$, [SII] $\lambda\lambda 6716, 6731\text{\AA}$ lines). We will use the VPH-675-LR (LR-R; $6115\text{-}7334\text{\AA}$), which contains the above-mentioned absorption and emission interstellar lines for ~ 20 ULIRGs from the Murphy et al. (1996) sample with redshifts in the range $0.04 < z < 0.08$. Furthermore, the wavelength range provided by this spectral setup contains a few stellar absorption lines (mostly Fe, Ca and TiO) that would allow an estimate of the contribution of stars to the Na I D absorption if needed.



The projected size of these galaxies rarely reaches 20 arcseconds, which matches perfectly to the dimensions of the MEGARA Large Compact Bundle (LCB) IFU (14×12 arcsec²) for the study of their central regions. The small projected sizes in our sample ensure a proper sky subtraction by using the positioners of the Fiber MOS placed at the edges of the MOS FOV and that are devoted to measure the sky background simultaneously with the LCB IFU observations (see Figure 1.1).

The spectral resolution of the LR-R setup is $R=6,250$, which give us a velocity resolution of ~ 50 km s⁻¹ (FWHM). This resolution is better than that achieved by previous long-slit studies on this topic and certainly high enough for our purposes. According to the MEGARA Exposure Time Calculator, an average integration time of 2h per galaxy is needed with the LR-R VPH in order to achieve the necessary signal-to-noise ratio. We plan to split our observation in 3 exposures of 2400 seconds each to allow for cosmic ray removal. A total of **~ 40 hours on target** will be needed (~ 48 hours including 20% overheads) in order to complete the sample.

The presence of blueshifted Na I D interstellar absorption line is an unambiguous signature of outflowing material. For the emission lines, a decomposition of the line profiles will be performed to study the existence of several kinematical components. The kinematics and spatial distribution of the absorption and emission components will be studied from the resulting maps, which would allow a better understanding of the physics of the wind. Furthermore, emission line ratio maps will provide information on the energy sources and temperature/ionization conditions in the Galactic Wind and in the regions of shocked gas.

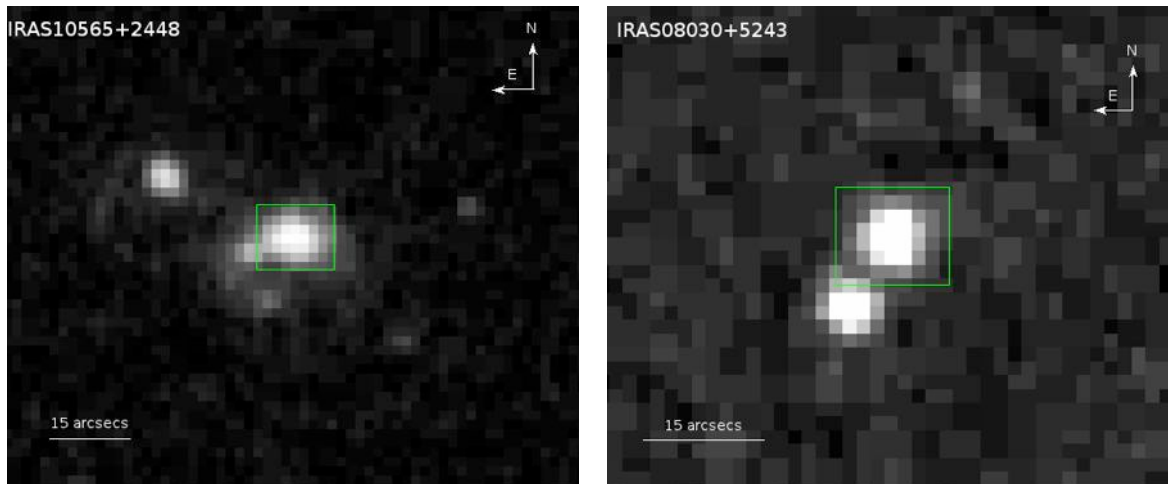


Figure 3.47: Palomar 48-inch Schmidt Telescope images for IRAS10565+2448 ($z=0.043$, left) and IRAS08030+5243 ($z=0.083$, right). The MEGARA LCB field of view ($14'' \times 12''$) is overplotted in green.



3.2 Galactic Planetary Nebulae

Intermediate mass stars ($\sim 1-8 M_{\odot}$) evolve from the Asymptotic Giant Branch (AGB) to the Planetary Nebula (PN) phase through a short-lived ($\sim 10^3 - 10^4$ yr) and intriguing evolutionary stage designated as the post-AGB or pre-Planetary Nebula (PPN) phase (see e.g. the review paper by van Winckel 2003). Spherical, slowly expanding ($V_{\text{exp}} \sim 15$ km/s) circumstellar envelopes (CSEs) result from the intense mass-loss process during the AGB. In the post-AGB phase, the mass-loss rate has decreased dramatically and the central star, which is making a high-speed journey to higher effective temperatures at roughly constant luminosity, is surrounded by a detached, expanding shell of gas and dust. The AGB-to-PN transition ends when the central star is hot enough to ionize most or all the circumstellar material. The complex phenomenology associated to these latest stages of the evolution, makes PPNs and PNs fascinating objects by themselves but also because they are the main contributors to the replenishment and chemical enrichment of the ISM, for example, they are an important source of fresh C, N and heavy elements formed by neutron-capture (s-) process.

In spite of dedicated observational and theoretical efforts by many researchers, the study of PPNs and PNs still confronts a growing list of paradoxes or dilemmas that have yet to find coherent solution. In this proposal, we focus on two of the main aspects of post-AGB evolution that remain badly understood: 1) the shaping of PPNs and PNs out of the round, slow AGB CSEs and 2) the temperature fluctuations and discrepancy of chemical abundances derived from optical recombination lines (ORLs) and collisional emission lines (CELs) in PNs.

3.2.1 Nebular shaping and acceleration beyond the AGB phase

3.2.1.1 *Scientific motivation and objectives*

PPNs and PNs display the most spectacular and varied morphologies, with elongated lobes expanding at high speeds (≥ 100 km/s) along one or more axes (see e.g. the review paper on PN shaping by Balick & Frank 2002 – Figure 3.48). The dazzling variety of morphologies of PPNs and PNs, which include not only axisymmetric (elliptical and bipolar) shells but also multipolar (multiaxial) structures, multiple co-axial shells, highly collimated point-symmetric features, etc and their expansive kinematics are difficult to explain without invoking the action of fast, collimated winds (jets) sculpting the spherical, slow AGB CSE (Sahai & Trauger 1998). Although there is no consensus yet, these outflows are believed to carve out an imprint within the AGB CSE producing and shaping the fast, bipolar lobes observed in most PPNs and PNs. The mechanism that powers and collimates post-AGB jets is a fundamental issue on stellar evolution that remains a mystery. Even basic aspects such as the nature (episodic or continuous?), typical mass-loss rates, momentum, lifetimes, etc., of post-AGB jets are poorly known. Moreover, the details of the interaction and the precise evolution from the slow, round AGB CSEs to the bewildering array of morphologies that characterize PPNs/PNs are not well understood. Detailed studies of PPNs and PNs are crucial to obtain information about the properties and dynamics of post-AGB winds and their exact role in the nebular shaping.

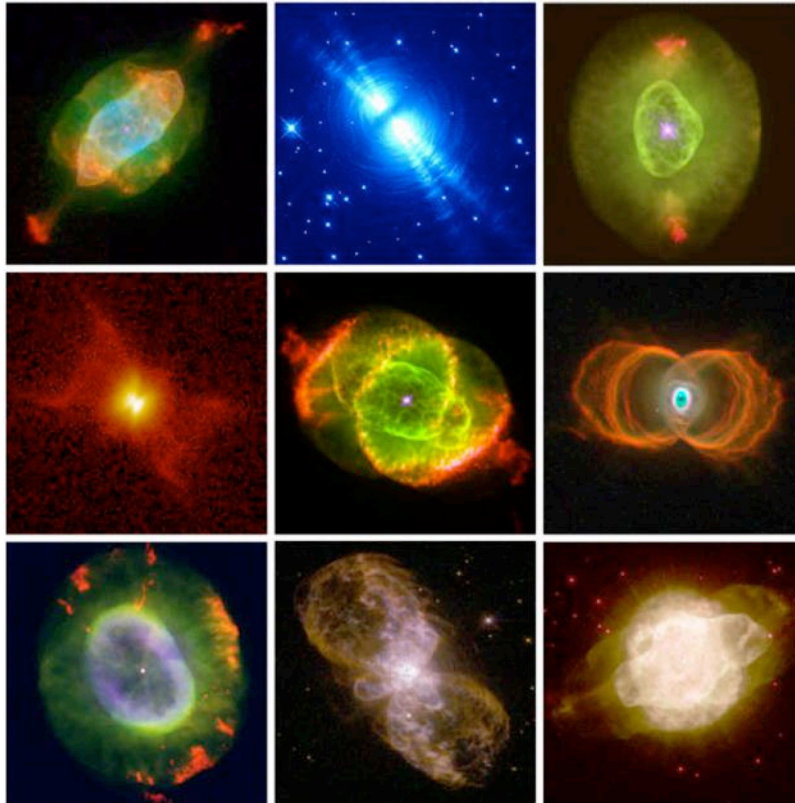


Figure 3.48: Compilation of false-color images of pPNs and PNs obtained with the Hubble Space Telescope (from Balick and Frank 2002) that illustrates the varied, puzzling morphologies of these objects. Fast, collimated outflows ejected in the late-AGB or early post-AGB phase are considered as the main shaping agent of these nebulae through their interaction with the slow, spherical envelope resulted from the heavy mass-loss process during the previous AGB phase.

Optical spectroscopic observations of PPNs and PNs have enabled considerable advances in our understanding of post-AGB evolution and, in particular, are very useful for probing the post-AGB winds and their interaction with the CSE formed in the previous AGB phase. Our current (very limited) knowledge of post-AGB evolution and, more particularly, of post-AGB winds is derived mainly in two ways. The first is indirect, that is, based on the effects of the post-AGB winds on the AGB CSEs. Many pPNs/PNs show extended lobes with, often, bow-shaped features at their tips that are visible through optical recombination and forbidden emission lines. Spectroscopic observations have been crucial for understanding the origin of these regions and building up the current picture of post-AGB evolution. From long-slit spectra we derive (i) the kinematics of the extended lobes, which are rapidly expanding with, usually, the velocity (V) linearly increasing with the distance to the central star (r); this linear dependence of V with r allow us to recover the 3D nebular structure (Figure 3.49); (ii) the nebular physical conditions (electron density and temperature) and the excitation mechanism from the analysis of diagnostic line ratios and their spatial variation across the nebula (Sánchez Contreras et al. 2000, 2002). Such studies indicate that the lobes of most PPNs are excited by the passage of fast shocks. From these results we infer the existence of fast, post-AGB winds that interact hydrodynamically with the AGB CSE leading to the formation of shocks and, ultimately, to the acceleration and shaping of the nebular material.

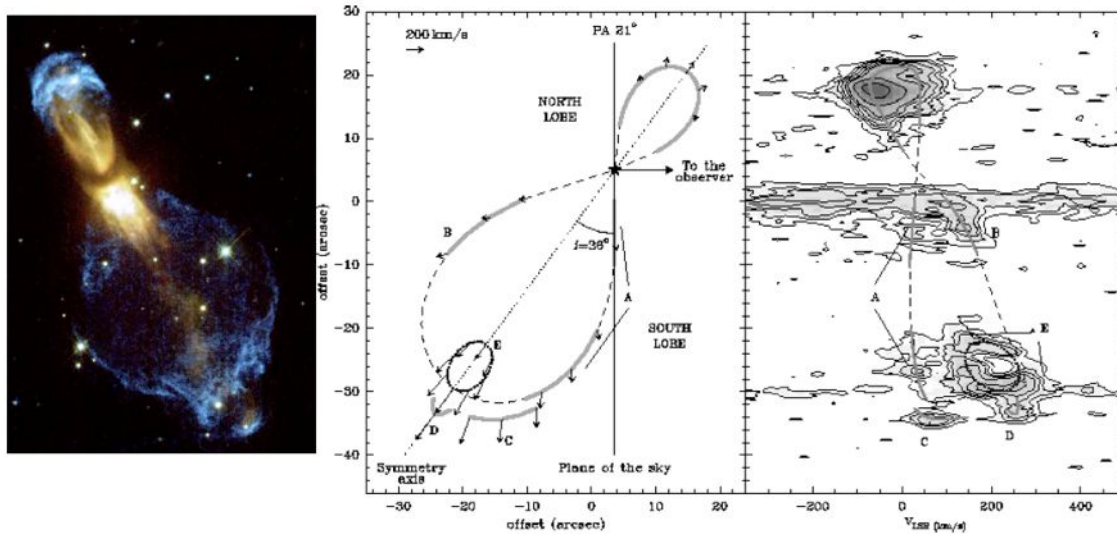


Figure 3.49: Left: HST+WFPC2 composite image of the PPN OH231.8+4.2 in the light of Ha (blue) and scattered continuum (yellow; from Bujarrabal et al. 2002). Right: Ha long-slit spectra along the axis of OH231.8+4.2 and schematic geometry of the nebula deduced from our spatio-kinematical model fitting (see Sánchez Contreras et al. 2000 for details). The Ha bubble-like lobes probe shock-excited gas moving away from the central star at velocities ($V \propto r$) up to ≈ 400 km/s. These lobes are believed to result from the quick interaction of post-AGB jets with the circumstellar envelope ejected during the AGB phase.

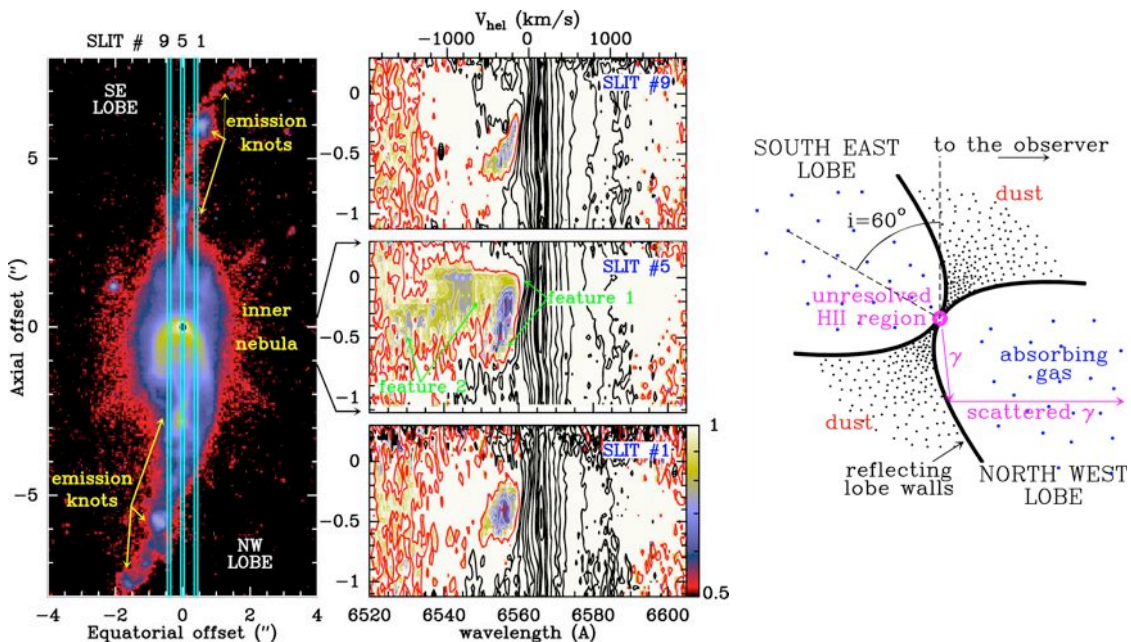


Figure 3.50: Left: HST/WFPC2 Ha+continuum image of the PPN He3-1475; three $0.1''$ -wide slits used for the HST/STIS observations are superimposed. Middle: STIS Ha spectra divided by the continuum for these slits in the $1''$ -inner nebula. In the central slit (#5), two blue-shifted absorption features are observed (white contours); feature 2 is not present in the outer slits. Right: Sketch of our model to explain the STIS data: the absorption features are produced by fast and ultra-fast "pristine" post-AGB winds inside the reflecting lobes (Sánchez Contreras & Sahai 2001). These observations allowed us to study directly the spatio-kinematical structure of the elusive post-AGB winds for the first time.

In some PPNs/PNs, fast, post-AGB winds are also revealed by P-Cygni profiles close to the central star. Recently, the spatio-kinematic structure of ‘pristine’ post-AGB winds, i.e. post-AGB winds not strongly altered in the interaction with the AGB envelope, has been resolved and directly studied for the first time in the PPN He 3-1475, through the analysis of P-Cygni absorption features in HST/STIS long-slit H α spectra (Figure 3.50). For the central slit, we observe two distinct absorption features which we interpret as resulting from neutral or partially-ionized fast- and ultra-fast outflows within the nebular lobes absorbing the H α and stellar photons scattered by the dust in the lobe walls (Figure 3.50, right). The ultra-fast ($\sim 2,300$ km s $^{-1}$) wind is highly collimated as deduced from the absence of feature 2 in the outer slits, and shows a large velocity gradient (the outermost parts are the fastest). These properties are best explained by magneto hydrodynamical wind collimation models (García-Segura 1999) and rule out, e.g., collimation via conical shocks (as originally proposed by Borkowski et al. 1997). This study demonstrates the effectiveness of optical spectroscopy in probing the elusive fast post-AGB winds and understanding their collimation mechanism.

Direct detection of post-AGB winds is limited to a few objects. In some cases there is recombination and forbidden line emission arising in a set of compact, shock-excited regions located along the nebular axis (e.g. like those seen in the PPN He3-1475, Figure 3.50; other examples are given in Figure 3.51). These ‘knots’, which usually move away from the star at high velocity, are thought to result from the propagation of backward shocks in the post-AGB wind itself, suggesting that post-AGB winds are collimated and directed along the nebular axis.

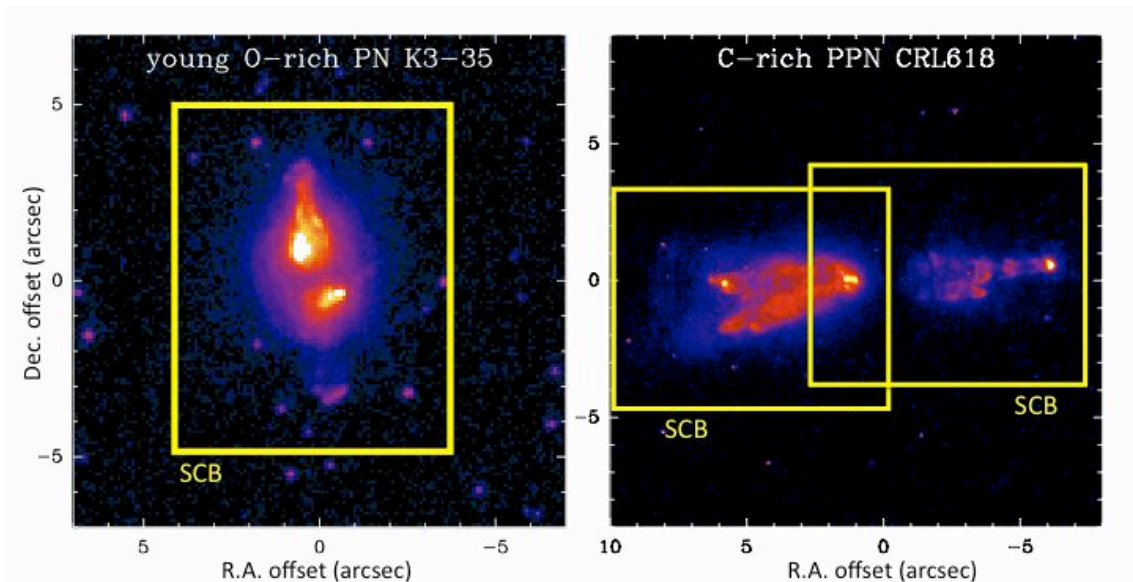


Figure 3.51: HST false-color images of two objects to be observed with MEGARA: the young PN K3-35 and the PPN CRL 618. The FOV of the SCB is superimposed on the images.

Recognizing the importance of optical spectroscopy in this field, we intend to use MEGARA at GTC for studying the physics of the high excitation gas in PPNs and PNs, including the shock-excited material in their extended lobes and the ‘pristine’ post-AGB winds (which are probed by



P-Cygni line profiles), as well as the connection between both components. GTC+MEGARA is the optimal telescope and instrument combination for this project since it will allow us to study very efficiently and in a reasonable amount of time a sizable sample of pPNs/PNs covering a range of properties, which is needed for a proper understanding of post-AGB evolution. The majority of pPNs and PNs have complex morphologies (e.g. multiple lobes with different orientations in the plane of the sky, point-symmetry, etc). Therefore, they will be most efficiently observed with an IFU, which will provide image data cubes within a given wavelength range (and thus velocity). Post-AGB objects are expected to show broad H α wings (FWZI~100-2000 km s⁻¹) and, in many cases, P-Cygni profiles that indicate currently active fast ejections. The spectral resolution provided by MEGARA is well adapted to resolve the emission and absorption features (the latter are significantly narrower than the line wings, FWHM~50-100 km/s) in these objects and, hence, to characterize the kinematics of fast ejections. Given the complex shapes of the line profiles of these objects, the use of an IFU, thanks to its better flux stability, is a better choice for this project than other 3D spectrometers, such as the Fabry-Perot systems. The spectral range covered by the planned different spectral setups of MEGARA (see below) will allow us to (i) study the nebular spatio-kinematic structure, (ii) observe important nebular lines, needed in order to diagnose the physical conditions in the gas and (iii) put constraints to the spectral type of the central star. Finally, GTC+MEGARA will offer the combination of a large telescope aperture coupled with a 0.480'' (0.685'') spaxel for the SCB (LCB) and a typical sub-arcsecond seeing at the site, which is necessary for observing most PPNs and PNs, which are optically faint and have angular sizes ranging from a few to tens of arcsecond.

3.2.1.2 Strategy: observations and analysis planned

We propose to use MEGARA to observe a sample of ~15 evolved stars and their surrounding nebulosities using the HR-R, LR-B, and LR-V VPHs. Our sample will include objects displaying diverse morphologies and spanning a range of evolutionary stages (early post-AGBs, PPNs, and young PNs) and chemistry (O- and C-rich). In most cases, we will use the SCB mode (FOV~10''x8'') of MEGARA for an improved spectral (R~8,000-25,000) and spatial resolution (spaxel~0.480''). Most PPNs and yPNs have indeed relatively small angular sizes and, therefore, they can be accommodated in the central SCB or can be fully mapped with a 2-point mosaic (Figure 3.51).

The HR-R setup will provide high-spectral resolution ($\Delta v_{\text{FWHM}} \sim 11 \text{ km/s}$) H α data cubes, which will enable studying the spatio-kinematical structure of the nebulae with unprecedented detail for the diverse structural components (shocked lobes, emission knots, arcs, etc) present in the sample objects. This setup also covers many other recombination and forbidden lines needed to diagnose the physical conditions of the gas and their variation across the nebulae such as the [SII] $\lambda\lambda 6717, 6731 \text{ \AA}$ doublet, which is an indicator of the electron density (n_e), the [NII] $\lambda\lambda 6540, 6584 \text{ \AA}$ transitions, which are excellent tracers of shock-excited regions and needed for an estimate of the electron temperature (T_e , by measuring their flux ratio relative to the [NII] $\lambda 5755 \text{ \AA}$ line, observed with the LR-V VPH). The LR-B setup will be mainly used for obtaining H γ and H β data-cubes, which will provide us with a 3D map of the circumstellar



extinction across the nebulae (from the Balmer line ratios). This setup also covers, amongst others, the $[\text{NII}]\lambda\lambda 5198, 5200\text{\AA}$ lines (another well known n_e diagnostic) and the $[\text{OIII}]\lambda 5007\text{\AA}$ transition, which is an indicator of the shock velocity in shock-excited regions. The LR-V VPH includes the already mentioned $[\text{NII}]\lambda 5755\text{\AA}$ line and also, for example, the He I 5876 \AA line, which is found to display a P-Cygni profile in many PPNs (e.g. in He3-1475, Sánchez Contreras et al. 2008) and the $[\text{OI}]\lambda 5577\text{\AA}$ line, also used as a diagnostic of the excitation mechanism. Finally, the spectral range covered by the different spectral setups selected will also allow us to put constraints to the spectral type of the central star.

In a second stage, we will also use MEGARA to study the extended, spherical or nearly spherical haloes that are found to surround the lobes of some PPNs and PNs (e.g. Sahai et al. 2007). These haloes are believed to be the remnants of the AGB CSEs that have not been reached by shocks generated by the interaction with post-AGB ejections. These haloes are not expected to have an intense emission line spectrum but rather to (1) reflect the photons arising from inner regions and/or (2) to produce absorption features by relatively cool gas or dust particles on bright background stars (see Maunon & Huggins 2010 and references therein for some examples of the use of this technique to probe CSEs around evolved stars). According to this, we will use the dispersed mode of MEGARA (FOV $\sim 3.5' \times 3.5'$) to probe these extended haloes along the line of sight, with the aim of recovering the mass-loss history of these targets back in the AGB phase, up to regions that were ejected several thousand of years ago. Our strategy will be to place a maximum of ~ 40 bundles on top of bright field stars around our targets and the same number of bundles near/off those stars; the rest of the bundles ($> \sim 10$) will be placed in emission-free regions in the field for sky background subtraction (a few mini-bundles will still be used for fine acquisition).

According to the MEGARA Exposure Time Calculator (ETC), average integration times ranging from 1.5 to 3 hours are needed to achieve a good/moderate signal-to-noise ratio at the line wings of Balmer lines and P-Cygni like absorption components (below the continuum) with the VPHs proposed. We aim to observe a sufficiently large number of post-AGB objects (~ 15) covering a reasonable range of properties: e.g. stellar spectral type, nebular age, morphology, and chemistry. A total of ~ 85 hours will be needed (**~ 100 hours** overheads included) in order to complete the sample. Objects will be selected from our multi-wavelength optical and spectroscopic surveys (Sahai et al. 2007, Sánchez Contreras et al. 2008) and the literature. The selection criteria for the objects in our sample are: (i) all sources show wide $\text{H}\alpha$ P-Cygni or asymmetrical profiles indicative of current post-AGB winds (Figure 3.52); (ii) for all sources there are large and small-scale nebular structures that signal bi- or multi-polar ejections; (iii) our sources are amongst the best-resolved PPNs from the ground; iv) extensive multiwavelength studies have been made: e.g. interferometric molecular emission mapping, optical/NIR imaging and/or spectroscopy (including HST data). Such studies guarantee a proper understanding of the complex processes governing post-AGB evolution.

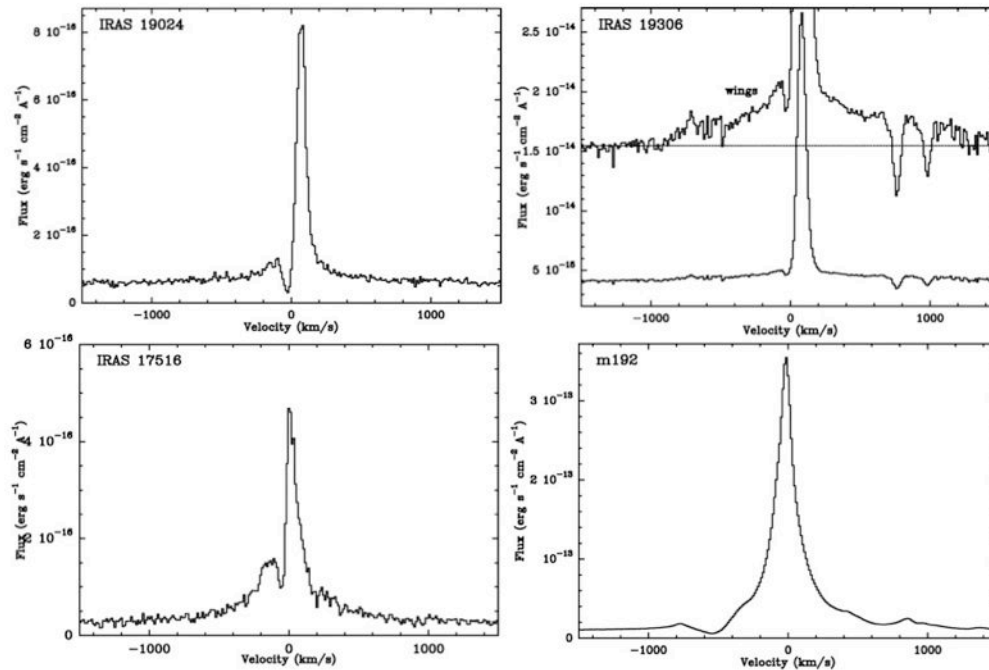


Figure 3.52: *H α* spectra for some of the pPN observed with KeckII+ESI (Sánchez Contreras et al. 2008). For IRAS 19306 we also plot the *H α* line with the Y-axis expanded (upper spectrum) to show the broad wings of this line. Note the blue-shifted absorption (P-Cygni like) component indicative of current post-AGB wind activity. The spectral resolution of these KeckII+ESI observations is $\Delta v_{FWHM} \sim 37 \text{ km s}^{-1}$ ($R \sim 8,100$).

Our team has extensive experience taking, reducing, analyzing, and interpreting optical long-slit spectra (including spatial-kinematical modeling). The MEGARA Science Team also includes world-wide experts on the processing and analysis of 2D spectroscopy data. The observations proposed will provide important information on the spatial kinematic structure and physical conditions of the extended, shocked lobes and the pristine post-AGB winds (probed by the blue-shifted absorption features) as well as the connection between both components in a sizable sample of pPNs and PNs, leading to a significant improvement in our understanding of post-AGB winds and their interaction with the AGB CEs. Despite morphological differences between post-AGB objects, there are most likely some unifying underlying physical mechanisms that result in the variety of shapes, e.g., episodic jets (which may either precess or be multi-axial). This proposal will help us to understand the basic nature of such mechanisms.

3.2.2 Chemical abundances in PNs and HII regions

3.2.2.1 *Scientific motivation and objectives*

The chemical abundances of some elements in the ionized gas of PNs (like oxygen at near solar metallicity, sulfur, or argon) reflect those prevailing in the ISM when the progenitor stars of these nebulae formed, up to several Gyr ago. For other elements, such as nitrogen, carbon, and helium, their concentrations are affected by processes that dredge up the products of stellar nucleosynthesis in the progenitor stars, and whose efficiencies depend on the mass of the



star (with $0.8 M_{\odot} < M < 8 M_{\odot}$) and its metallicity (see, e.g. Karakas 2010). All the material ejected by the star ends up mixing with the ISM and enriching it with several elements, which makes PNs useful tools for the study of galactic chemical evolution.

The techniques used to determine chemical abundances for PNs are very similar to those used for HII regions. Since HII regions reflect the composition of the present-day ISM, we can perform homogeneous analyses of both kinds of objects and obtain meaningful comparisons. A further advantage provided by HII regions is that their abundances can be measured even when their distances are large, although in that case just a few bright lines can be measured and the method used must be calibrated using nearby objects.

In fact, in order to derive the best estimates of chemical abundances in the ionized nebulae of any galaxy, nearby HII regions and PNs are fundamental, since they allow the measurement of many emission lines and their intensity variations within the objects. This wealth of data serves as a check on our understanding of the processes that take place in photoionized gas.

The best estimates of chemical abundances in nearby ionized nebulae require deep spectra with good wavelength coverage and spectral resolution, which are calibrated in flux and corrected for extinction. These deep spectra allow the measurement with good signal-to-noise of (1) the diagnostic lines needed to calculate electron densities and temperatures, and (2) emission lines for as many as possible ionization states of the element of interest. In case that only some of these ions are observed, we need ionization correction factors (generally based on photoionization models) to correct for the presence of the unobserved ions. Finally, we should not forget the atomic data needed to perform all the calculations, and the acquisition of good estimates for the uncertainties arising in each of the previous steps.

Deep spectra with good wavelength coverage and spectral resolution are more important than usually thought because they allow for the measurement of many diagnostic lines (needed to get good estimates of the physical conditions and their variations within the nebula), emission lines for more ions (like the iron lines that can be used to study depletions onto dust grains), and also because they permit the measurement of line intensities unaffected by contamination from nearby lines. This effect can be very important. For example, in HII regions of low degree of ionization, low-resolution spectra can result in derived electron temperatures $T_e([\text{O III}])$ higher by up to 1000 K (Rodríguez & Delgado-Inglada 2011a). Figure 3.53 illustrates these issues with part of the deep spectrum of the Orion Nebula obtained by Esteban et al. (2004) using UVES/VLT with a spectral resolution $R \sim 8,800$.

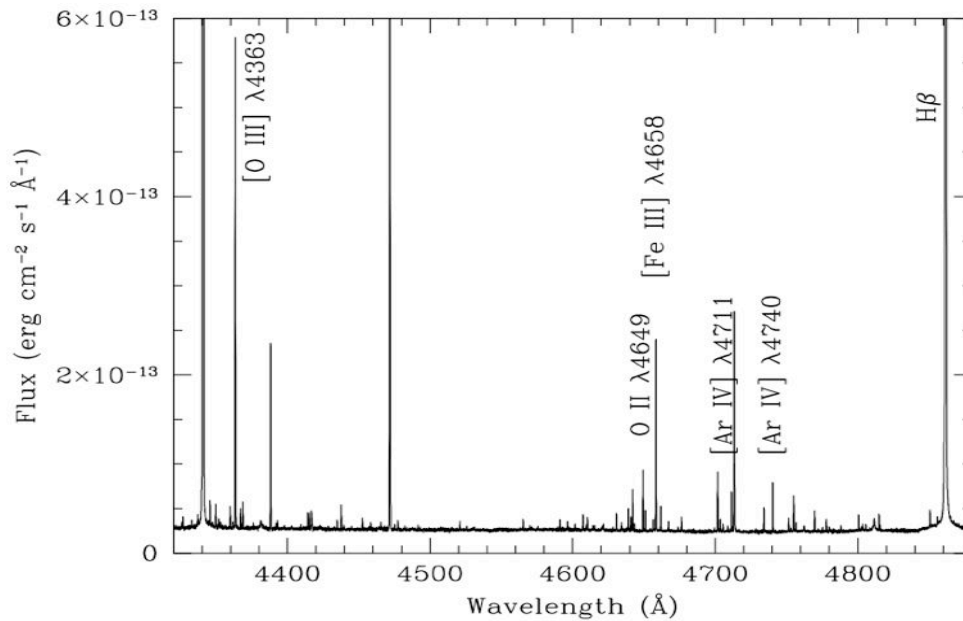


Figure 3.53: Part of the spectrum of the Orion Nebula observed by Esteban et al. (2004). Several lines are identified: $H\beta$, the weakest $[O\ III]$ line used to derive $Te([O\ III])$, the brightest $[Fe\ III]$ in this wavelength range, two $[Ar\ IV]$ lines that can be used to determine the electron density, and one bright $O\ II$ recombination line. Many of the weak lines observed with high spectral resolution appear blended in low-spectral resolution data, leading to incorrect abundance determinations.

Deep spectra with good spectral resolution of Galactic HII regions (Esteban et al. 2004; García-Rojas et al. 2004, 2005, 2006, 2007) and PNs (see, e.g., Liu et al. 2000, 2004; Tsamis et al. 2003) have also been used to measure the weak optical recombination lines (ORLs) of heavy elements. These studies have confirmed previous results for a handful of objects (Peimbert et al. 1993; Liu et al. 1995): there is a discrepancy between the abundances implied by collisionally excited lines (CELs) and recombination lines of some heavy elements. The discrepancy is most easily measured for $O\ II$ and $[O\ III]$ lines and produces values of $O^{++}(\text{RLs})/O^{++}(\text{CELs})$ that are around 2 for all HII regions and many PNs, but that go up to 70 for some PNs (Liu 2006 and references therein).

Three different explanations have been proposed to explain the discrepancy: temperature fluctuations within the nebulae (Peimbert 1967; see also Esteban et al. 2004; García-Rojas & Esteban 2007), the presence of metal-rich inclusions (Liu et al. 2000; Tsamis & Péquignot 2005; Stasińska et al. 2007; Henney & Stasińska 2010), and errors in the recombination coefficients, at least for the many objects where the discrepancy is around a factor of 2 (Rodríguez & García-Rojas 2010). All these explanations have problems. No mechanism has been found that can produce enough temperature fluctuations to reproduce the observed discrepancies, except for metal-rich inclusions, where the problem lies in explaining their origin and survival both in HII regions and PNs. The inclusions would have different origins in each kind of nebula: they have been proposed to be due to ejections from the central star or the destruction of planetary or cometary material in PNs (see Liu et al. 2000; Henney & Stasińska 2010), whereas in HII regions they could be due to still unmixed condensations from supernova



ejecta (Tsamis & Péquignot 2005; Stasińska et al. 2007). On the other hand, errors in the recombination coefficients may not be able to explain the largest discrepancies and should be invoked for other ions besides O^{++} . At stake here is not only our understanding of fundamental processes in the fields of stellar evolution and chemical enrichment, but also our ability to derive the abundances of ionized gas with uncertainties lower than a factor of 2 (or more).

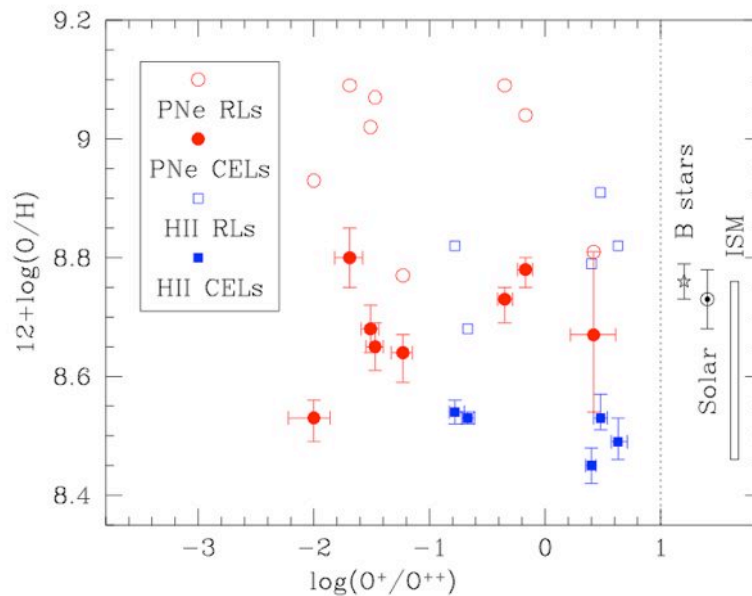


Figure 3.54: Oxygen abundances calculated by Rodríguez & Delgado-Inglada (2011a) using CELs and RLs for HII regions and PNs of the solar neighborhood. The results are compared with the abundances for the Sun (Asplund 2009), B stars (Przybilla et al. 2008), and the diffuse ISM (Jenkins 2009).

How do the derived abundances compare with those found for stars? Can we use this to decide on the more correct values? An attempt to explore this approach is presented in Rodríguez & Delgado-Inglada (2011a) with a comparative analysis of the oxygen abundances in 8 PNs and 5 HII regions of the solar neighborhood (at distances lower than 2 kpc, so as to avoid the effects of the Galactic abundance gradient). Only objects with high-quality spectra and good distance determinations were used, and their abundances were derived using both oxygen CELs and RLs. As shown in Figure 3.54, the H II regions were found to be underabundant in oxygen by 0.18 dex, independently of the method used (CELs or RLs). This is contrary to what one would expect from simple models of chemical evolution, but could be due to extensive stellar migration of the PNs progenitors from the inner Galaxy or to some kind of gas flow or infall. The results were compared with the oxygen abundances in the Sun (Asplund et al. 2009), B stars (Przybilla et al. 2008), and the diffuse ISM (Jenkins 2009). The abundances of all these objects could be reconciled with the nebular abundances implied by CELs if we take into account the almost flat age-metallicity relation implied by nearby F and G stars (e.g. Holmberg et al. 2009) and the similar shortfall of oxygen found in the diffuse ISM and in molecular clouds (Jenkins 2009; Whittet 2010). Whittet (2010) explains this shortfall invoking oxygen depletion in organic refractory dust grains, which could also be found in HII regions but are not expected in PNs.



This interpretation depends on the assumption that the method used to derive the oxygen abundances with CELs is not introducing a different bias in HII regions and PNs. The bias could be introduced by the assumed temperature structure, the temperature implied by the [N II] line ratio, $\text{Te}([\text{N II}])$, is used to derive O^+/H^+ , $\text{Te}([\text{O III}])$ is used for O^{++}/H^+ . The values derived for $\text{Te}([\text{N II}])/\text{Te}([\text{O III}])$ are especially critical for the H II regions, and though they can be reproduced by photoionization models (Rodríguez & García-Rojas 2010), there is disagreement on their validity (e.g. Tsamis et al. 2011). Temperature maps of several nebulae based on different diagnostics could be used to investigate further this issue (besides the [N II] and [O III] line intensity ratios, there are temperature-sensitive ratios of other lines, like [S III] and [O II]).

The explanation of the oxygen underabundance in HII regions as being due to depletion in refractory dust grains also rests on the assumption that the abundances for the Sun, B stars, and the diffuse ISM are not affected by important systematic errors. Note that if we manage to understand what is going on in ionized nebulae and thus get good estimates of their abundances, they would provide clues on the biases that can affect the abundance determinations in stars and the ISM.

One way to check the above interpretation for oxygen would be to compare the abundances of other elements, such as sulfur, argon, neon, or chlorine, in HII regions and PNs. However, these elements require the use of ionization correction factors to correct for the contribution of unobserved ions to the total abundances. Since the stars ionizing H II regions and PNs have different spectral energy distributions, these correction factors, which are based on the relative abundances of observed ions of other elements, are likely to introduce different biases in the two kinds of objects. This can be explored using photoionization models to predict spectra that in turn can be analyzed like those of real objects. Rodríguez & Delgado-Inglada (2011b) illustrated this effect for sulfur, showing that even for low-ionization PNs, the ionization correction factor generally used introduces systematic differences of up to 0.4 dex between H II regions and PNs that have the same S/H abundance ratio.

Rodríguez & Delgado-Inglada (2011b) also showed results for chlorine for the 5 HII regions and 6 out of the 8 PNs of the solar neighborhood studied by Rodríguez & Delgado-Inglada (2011a) for which the abundances could be derived with no correction for unobserved ions (see Figure 3.55). Similar values of Cl/H were obtained for all the objects, supporting the explanation given for the oxygen results, but the analysis was less homogeneous than in the case for oxygen, mainly because [Cl II] $\lambda 9124\text{\AA}$ and [Cl IV] $\lambda 8046\text{\AA}$ were outside of the observed wavelength ranges in most of the PNs. A more detailed study that includes more objects and uses the same lines for all of them would be valuable.

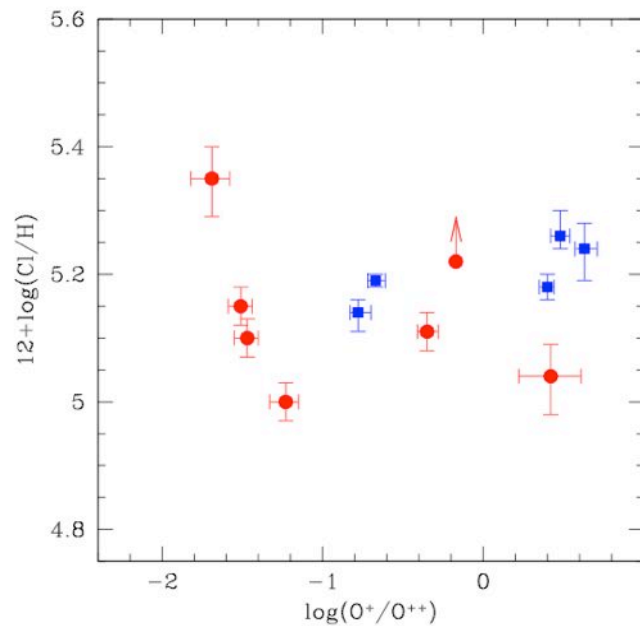


Figure 3.55: Chlorine abundances calculated by Rodríguez & Delgado-Inglada (2011b) for the same objects shown in Figure 3.54. Blue squares represent HII regions, red circles are for PNs. Two of the PNs only have lower limits (one appears in the figure, the other has an upper limit below the lowest abundance value shown in the y-axis).

The better understanding of the temperature structure within the nebulae that we obtain (from temperature maps plus photoionization modeling) the better abundance determinations for all the observed ions, since it would allow us to obtain better estimates of the electron temperatures that characterize the emission regions of each ion.

As for the abundance discrepancy between RLs and CELs, another way to explore its causes would be to create maps of the values of the discrepancy at different positions for several objects (see e.g. Tsamis et al. 2008). These maps could then be used to look for patterns and correlations, or to study the effects introduced by protoplanetary discs and Herbig-Haro objects (e.g., Mesa-Delgado et al. 2008; Tsamis et al. 2011).

We want to study the factors that affect abundance determinations in ionized gas through a detailed analysis of a sample of nearby bright HII regions and PNs. MEGARA can produce for these objects exceptional spectra in many senses: spatial information, spectral resolution, wavelength coverage, and total fluxes (if the nebula is mapped, which can be easily accomplished for some PNs). Total fluxes are generally needed when we want to use our spectra along with spectra at other wavelength regimes, like the UV or the infrared. Previous attempts to do this for Galactic PNs have relied on scans of the objects, a much less reliable procedure than the one we can use with MEGARA. Hence, we have selected a sample of PNs that can be covered with one to four positions of the LCB. On the other hand, MEGARA can obtain maps of bright areas of nearby HII regions, such as M8, M17, and M42 (the Orion Nebula), that will be extremely useful to address many of the issues described above. A comparison of the results with those obtained for extragalactic HII regions will also be valuable.



The presence of shocks in the HII regions and PNe can be established by looking for variations in the $[\text{OIII}]\lambda 4363\text{\AA}/\lambda 5007\text{\AA}$ (or $\lambda 4363\text{\AA}/\lambda 4959\text{\AA}$) ratio as a function of position. The expected ratio for photoionized nebulae is considerably smaller than the ratio expected in the presence of shocks (e. g. Peimbert et al. 1991, Mesa-Delgado et al. 2009, and references therein). The data on PNe and HII regions derived from MEGARA will permit to test the influence of shocks on the $\lambda 4363\text{\AA}/\lambda 5007\text{\AA}$ ratio and consequently its effect on the derived electron temperatures, the abundance determinations and the abundance discrepancy factor (ADF) problem. Another ratio that will permit to establish the presence of local density structure in HII regions is the ratio of $[\text{FeIII}]\lambda\lambda 4986+4987\text{\AA}$ to $\lambda 4658\text{\AA}$ (Keenan et al. 2001; Peimbert & Peimbert 2010). This ratio is more sensitive to density than the $[\text{SII}]\lambda 6717\text{\AA}/\lambda 6731\text{\AA}$ and $[\text{OII}]\lambda 3726\text{\AA}/\lambda 3829\text{\AA}$ ratios, particularly at densities lower than 300 cm^{-3} .

3.2.2.2 Strategy: observations and analysis planned

We will use the LCB to cover the full spectral range with the 5 LR VPHs in a balanced sample of both low- and high-abundance discrepancy factor (ADF) nebulae. Most of the sample PNs will be selected to have diameters below $14''$ (e.g., IC 418, IC 2149, IC 2165, M1-46, NGC 6572, NGC 6578, NGC 6884, and PC19) or below $28''$ (e.g., NGC 6210 and NGC 6543). Some of them (IC 418, NGC 6210, NGC 6543, NGC 6572, and NGC 6884) belong to the solar neighborhood sample analyzed in Rodríguez & Delgado-Inglada (2011a, 2011b) and shown in Figures 3.54 and 3.55. In order to better define the abundance distribution of PNs in the solar neighborhood, we have also selected two nearby extended PNs, NGC 7293 and NGC 6853. These two nebulae would only be observed at one position. Exposure times of 900-1200 s with each LR VPH would allow the measurement of many weak lines of interest in all the objects with enough signal-to-noise ratio. The full sample of PNs would require around **36 hours** (including overheads of 20%). Note also that the PN NGC 7027 will be observed as a ToI.

The HII regions M8, M17, and M42, also belong to the solar neighborhood sample discussed above. The Orion Nebula requires lower exposure times than the other objects: we estimate exposures of 300 s with each LR VPH. An area of $\sim 1' \times 1'$ could be mapped in 8 hours (including overheads; see Figure 3.56). M8 and M17 could be done with exposures of 600 s; 4 hours (including overheads) could be used to map areas of $30'' \times 30''$ in each nebula. The total exposure time for PNs and H II regions would be **50 hours**.

For the HII regions, we will observe the brightest regions in order to obtain, with relatively short exposure times, spectral maps of the weakest lines of interest. These maps can be used to study spatial variations of the physical conditions or the abundance discrepancy factors across each nebulae, as well as the relation of these variations with the presence of structural features such as Herbig-Haro objects or proplyds.

MEGARA has the potential to fast-scan several northern nebulae and to survey their proplyd populations thus enlarging the number of objects known beyond Orion (M42). These would appear as fuzzy compact nebulosities in HI and [OIII] emission lines in the vicinity of OB-type stars. Following robust background subtraction of the host HII region emission (one of the strengths of MEGARA), their physical conditions including metallicity can be determined separately from the ambient gas (e.g. Tsamis et al. 2011). Suitable targets would be selected



from e.g. the IPHAS H α survey of the northern Galactic plane (Drew et al 2005). This would allow us to quantify the effects of photoevaporation on circumstellar disks in a variety of external radiation fields and for a range of Galactocentric radii.

The wealth of data obtained in this program will allow us to perform many different analyses. We will start by measuring all detected lines in each spatial element after the wavelength and flux calibration. The data, once corrected for extinction, can be used to calculate electron densities, electron temperatures, and ionic abundances from all available diagnostics, both with CELs and RLs. Total abundances will be derived, with particular emphasis in some elements such as oxygen and chlorine. The analysis will also be performed for the integrated spectra and compared to the spatially resolved results. We will obtain maps of the intensities of some lines of interest, like for example the O II recombination lines. We will study the variations of each quantity within each object and from object to object, and the results will be compared to those predicted by suitable photoionization models constructed with Cloudy (Ferland et al. 1998). More details on the basic procedures can be found in the works cited above.

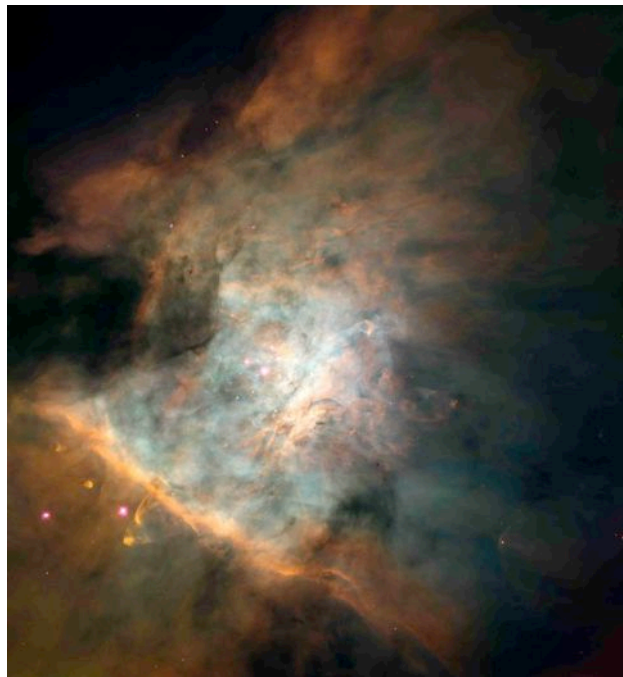


Figure 3.56: Central part of the Orion Nebula as observed with the Hubble Space Telescope (O'Dell & Wong 1996). The image size is about 5'x5'. We will observe an area of 1'x1' centered on the bright region West of the Trapezium, the central cluster of ionizing stars.



3.3 MEDUSA: MEGARA Distant-Universe Spectroscopic Analysis

3.3.1 Scientific motivation and objectives

How do galaxies form and evolve? This question has been rated as one of the four most fundamental topics in Astronomy (Astronet Science Vision 2007) and one of the top-priority science objectives to be pursued in the next decade (Astro2010 Decadal Survey). Consequently, the search for the origin of galaxies will be the area where the most significant advances and breakthroughs can be expected in the coming 10-20 years.

In order to advance in our understanding of the evolution of the Universe, we need to characterize in detail the properties of the galaxies at different redshifts. This implies obtaining better (more robust and certain) estimates of fundamental parameters such as the age of the stellar populations, the SFR, the effects of dust attenuation or the metallicity, the amount of gas, the dynamics, etc. This job is of remarkable relevance at $z > 1$, where current models of galaxy formation suffer their more demanding challenges, as observations seem to favor a somewhat anti-hierarchical galaxy formation scenario (known as downsizing; see, e.g., Heavens et al. 2004, Juneau et al. 2005, Pérez-González et al. 2005, 2008a), in (at least at first sight) contradiction with the current paradigm of galaxy formation. Indeed, this paradigm establishes that gas cooling and star formation are closely linked to the evolution of dark matter halos that coalesce in a hierarchical way to form bigger structures as we move along the Hubble time.

In addition, we need to relate those quantities to other key parameters in hierarchical models, such as the environment or the dynamics of the forming galaxies. Indeed, the detailed study of the large-scale structure in the Universe at different epochs is key for understanding the evolution of galaxies, also imposing strong constraints on cosmological parameters (e.g., Eke et al. 1998).

In this context, some topics are of extreme importance to advance in our understanding of galaxy formation:

- i. A detailed characterization of the mass assembly of galaxies, starting from the smallest systems, which are the building blocks of larger galaxies, and from these to of even larger ones. This study must be done using samples of galaxies selected in different ways to consider the whole zoo of galaxies detected at intermediate and high-redshift, and to relate some populations with others to establish possible evolution scenarios for the galaxies that we observe in the local Universe.
- ii. The analysis of the star formation in those systems that are still forming stars vigorously to understand the physics of the star formation and its dependence with other parameters such as the mass of the galaxy, the environment, etc.
- iii. The study of how these galaxies interact with others and how the environment affects their evolution, and how the different structures in the Universe (clusters, superclusters, filaments) evolve with time.

The MEGARA Science Team has identified several specific projects addressing the previous points and that would benefit from the existence of a high-resolution Integral Field Unit



spectrograph on a 10.4m telescope such as the GTC. Some of these projects could only be carried out with such an instrument.

These projects and the entire MEDUSA survey were introduced briefly in Section 2.3.3 and we now describe them in detail. All of them exploit the distinct characteristics of MEGARA, which will be able to obtain spectroscopic data with intermediate and high resolution, counting with spatial resolution, covering relatively large fields and with exceptional sensitivity. In addition, there are multiple interests within the MEGARA Science Team regarding the study of intermediate- and high-redshift galaxies: Intermediate-redshift Blue Compact Dwarf (BCD), clump-cluster, peas and starburst galaxies and high-redshift proto-clusters. In order to address all these topics with maximum efficiency a MOS with the capability of observing a relatively large number of objects within a small patch of the sky (density $\geq 1 \text{ arcmin}^{-2}$) is required. The high number densities of sources accessible with the MEGARA MOS will allow pursuing many of these goals as part of a common observing program. Only with a multiplexing capability such as that of MEGARA we can face all these different problems in an efficient way.

These are the main scientific projects in the study of galaxies at cosmological distances that would benefit from observations with the MEGARA instrument. We have ordered them as a function of the typical redshift at which the main targets would lie. For each case, we have highlighted the need for MEGARA to fully carry out the project.

3.3.2 Strategy of the MEDUSA Cosmological surveys

The projects within MEDUSA require observations of a variety of objects, from relatively close-by dwarfs to the very first galaxies at the highest redshifts. They nicely cover the entire spectrum of scientific questions that must be answered to understand galaxy formation and evolution.

A significant advantage of MEGARA over other spectrographs is its high multiplexing. This gives us (and the astronomical community) the opportunity to combine the different projects targeting different samples within our comprehensive cosmological survey. In the following, we sketch a possible optimal observation strategy conceived to provide data for all the scientific projects described previously.

Table 3.4 summarizes the relevant properties to be taken into account for the observational strategy of MEDUSA. These properties include the typical surface density of the targets, the spectral region to cover with MEGARA, the spectral resolution, the observing mode (IFU or/and robotic positioners), the typical exposure times and total observing time needed to complete each project. This table demonstrates that even in the unreal case where all different samples were orthogonal, the total surface density of the whole sample of interesting targets would be comparable to the multiplexing capabilities of MEGARA. We could simultaneously observe with roughly 90 positioners in $3.5 \times 3.5 \text{ arcmin}^2$, or 8 sources/ arcmin^2 , and with ~ 150 different fibers for the IFU (assuming one useful object per arcsec^2).



Project	Density (arcmin ⁻²)	Wavelength range	Resolution	Observing mode	t(exp) (hours/pointing)	Total time on source (hours)
Dwarfs at intermediate-z	0.1-2.5	VRI	LR	MOS	2	60
Green peas at intermediate-z	$>6 \times 10^{-4}$	UBRI	LR	IFU	2	60
Starbursts at intermediate-z	0.3	RI	LR, MR	IFU	1-2	60
Over-densities at $z > 1$	~ 5	BVRI	LR	IFU+MOS	2x16	120
Grav. lenses at $z \gg 1$	~ 3 (lenses for IFU) +5 (for positioners)	BVRI	LR	IFU+MOS	2x16	120

Table 3.4: Observing properties of the projects within the Cosmological survey with MEGARA (MEDUSA). These properties include the typical surface density of the targets for each project, the spectral region to cover with MEGARA, the spectral resolution, the observing mode (IFU or/and MOS), the typical exposure times, and total observing time needed to complete each project.

The best strategy to optimally carry out all projects within MEDUSA would be to concentrate in one or a few of the best cosmological fields in the sky. The best suited for the observations with GTC, and having enough ancillary data to be able to select robustly all the targets of interest, would be, for example, COSMOS, EGS, GOODS-N and UDS. Given the total target density, the high multiplexing of MEGARA, the need for LR observations in most cases, and the similar exposure times needed to reach our scientific goals, all projects except the last one could be done simultaneously by targeting the same field and combining the different samples.

In the case of the study of gravitationally lensed sources, we should point to clusters observed by HST, *Spitzer* and *Herschel* (e.g., the ones in the *Herschel Lensing Survey*; Egami et al. 2010), which would give us the candidates for very high- z star-forming galaxies. In these cluster fields, all the other projects could obtain useful data, i.e., green peas, starbursts and dwarf galaxies do exist in the cluster fields. Moreover, some of these sources could be lensed, so simultaneous observations for all projects in combination with the “lens survey” could be used to study fainter and/or higher redshift sources of the type of interest, and even gain in the spatial resolution, given the distortion introduced by the gravitational lens in some sources.



3.3.3 The nature and evolution of Green Pea galaxies

Green Pea galaxies (GPs) are dwarf systems characterized by their compact morphologies joined to very high star formation rates, what make their optical spectra to be dominated by very bright conspicuous emission lines above a very weak underlying stellar continuum. In particular, the high excitation of the gas in these systems leads to $[\text{OIII}]\lambda 5007\text{\AA}$ equivalent widths above 100\AA , so their r-band emission in the redshift range $0.11 < z < 0.35$ stands out, giving them their characteristic green color.

According to the study made by Cardamone et al. (2009) of a sample of about 80 GPs selected from the SDSS, their high UV luminosity combined with a relatively low inner extinction make them to resemble other dwarf star-forming objects in younger Universe. The analysis of their metal content carried out by Amorín, Pérez-Montero & Vílchez (2010) leads to the conclusion that GPs are genuine metal-poor starbursts, with an average metallicity around one fifth of the solar value, in agreement with the measurements made for other star forming dwarf systems, such as Lyman Break Analogs (e.g. Overzier et al. 2009).

The Integral Field Unit of MEGARA, provides an ideal tool to study GPs with enough spatial and spectral resolution to shed some light on the various puzzling issues still opened about the origin, triggering of the episode of star formation, or chemical evolution of these objects. Their compact aspect (no more than 2 arcsecs for those GPs for which there is available optical HST imaging) fits to the IFU LCB. Recent work by Amorín et al. (2011, submitted) has revealed that the sensitivity of GTC becomes crucial to make thorough analysis of the underlying stellar population of these objects and to give precise constraints to the derivation of their stellar masses. The found values, in the range $7.5 < \log(M^*) < 10$ put these objects much more below than expected in the mass-metallicity relation of other star-forming galaxies. On the other hand, the analysis of the gas phase nitrogen abundances reveals very large nitrogen-to-oxygen ratios, indicative of a possible early production of secondary nitrogen, typical of evolved systems. Therefore, the venue of new data provided by MEGARA/GTC with enough spatial resolution will also be crucial to constrain the spatial extents of possible chemical inhomogeneities in these objects. The high spectral resolution of the instrument will also help to analyse possible kinematical components in the emission lines in a highly probable very perturbed interstellar medium due to the presence of the starbursts.

In order to study the properties of these objects covering their entire range of stellar masses no less than 30 objects are needed. An average exposure time of 30 minutes per object and spectral setup should be sufficient to measure the weakest spectral features of interest. This is based on the emission line fluxes obtained using GTC-OSIRIS among other facilities. Note that the object density quoted in Table 3.4 refers only to objects brighter than $R=20.5$ mag.

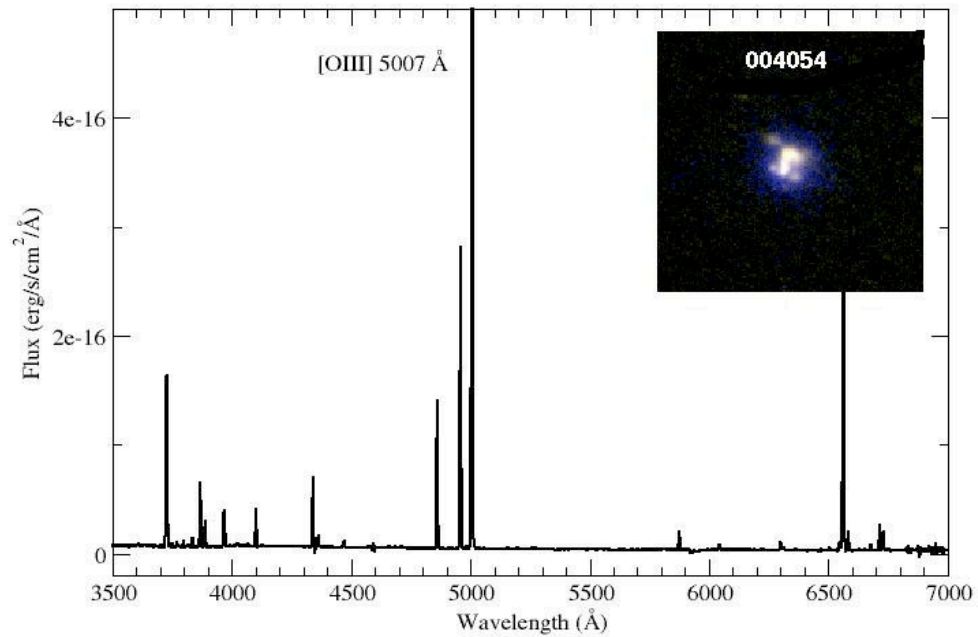


Figure 3.57: GTC-OSIRIS optical spectrum of the GP004054 (Amorín et al. 2011), with its prominent $[\text{OIII}]$ emission line. The inset shows a composite optical and UV $6'' \times 6''$ HST image of the same object (Overzier et al. 2009).



3.3.4 Star Formation Feedback in Massive systems at different redshifts

3.3.4.1 *Scientific motivation*

The effects of star-formation negative feedback have been invoked as an important issue in the Λ Cold Dark Matter paradigm of galaxy formation (Dekel & Silk 1986; Scannapieco et al. 2002). However, recent theoretical results based on hydrodynamic simulations of massive star formation regions (Tenorio-Tagle et al. 2005, 2007; Wunsch et al. 2008) have demonstrated how, in some cases, this feedback may be positive, implying that little or none of the returned matter is going to be ejected out of the system. These models have opened new scenarios of star formation. Large stellar densities may lead to strong radiative cooling causing the matter re-inserted by massive stars inside the inner zones of the cluster to remain gravitationally bound. Then, new stellar generations with different metallicities may form inside the star cluster volume (Tenorio-Tagle et al. 2005; Silich et al. 2007). As a result, star formation would be extremely efficient.

This theoretical framework was developed to the light of the discovery of Super Stellar Clusters (SSCs) in the core of nearby galaxies. These studies have shown that the interplay between the thermalization of the kinetic energy provided by massive stars, radiative cooling of the thermalized plasma, and the gravitational pull of the host galaxy lead to three different hydrodynamic regimes. These are: (1) quasi-adiabatic supergalactic winds; (2) bimodal flows, with mass accumulation in the central zones and gas expulsion from the outer zones of the assembling galaxy; and (3) the gravitationally bound regime, for which all of the gas returned by massive stars remains bound to the host galaxy and is likely to be reprocessed into further generations of stars. Which of the three possible solutions takes place depends on the mass of the star-forming region, its mechanical luminosity (or Star Formation Rate; SFR), and its size.

Recently, Tenorio-Tagle et al. (2010) have provided us with a new observable to detect the existence of these different regimes. They have shown that, contrary to what previously expected, broad nebular recombination lines may have nothing to do with the expansion of the nebula. The supersonic broad emission lines result only in clusters undergoing the bimodal hydrodynamic solution. The origin of the most intense broad lines is due to the large number of re-pressurizing shocks (RS), induced within the dense thermally unstable reinserted gas as this strives to maintain pressure balance with the much hotter gaseous counterpart. The less intense, although much broader Gaussian component detected only in some cases, is shown to be caused by the cluster wind; it becomes photoionized and less dense upon its own expansion. They show also that the maximum speed of the RSs and of the cluster wind are both functions of the temperature reached at the stagnation radius. This temperature depends only on the cluster heating efficiency (η , see Figure 3.58).

The cluster heating efficiency is a key parameter in defining the evolution of a massive and young stellar cluster. The energy released (L_{Mech}), is reduced by a factor η . Clusters with low heating efficiency are to be much less effective in producing both kinetic energy and mass via winds to the intergalactic medium (IGM). As a consequence, their star formation efficiency is expected to be enhanced.

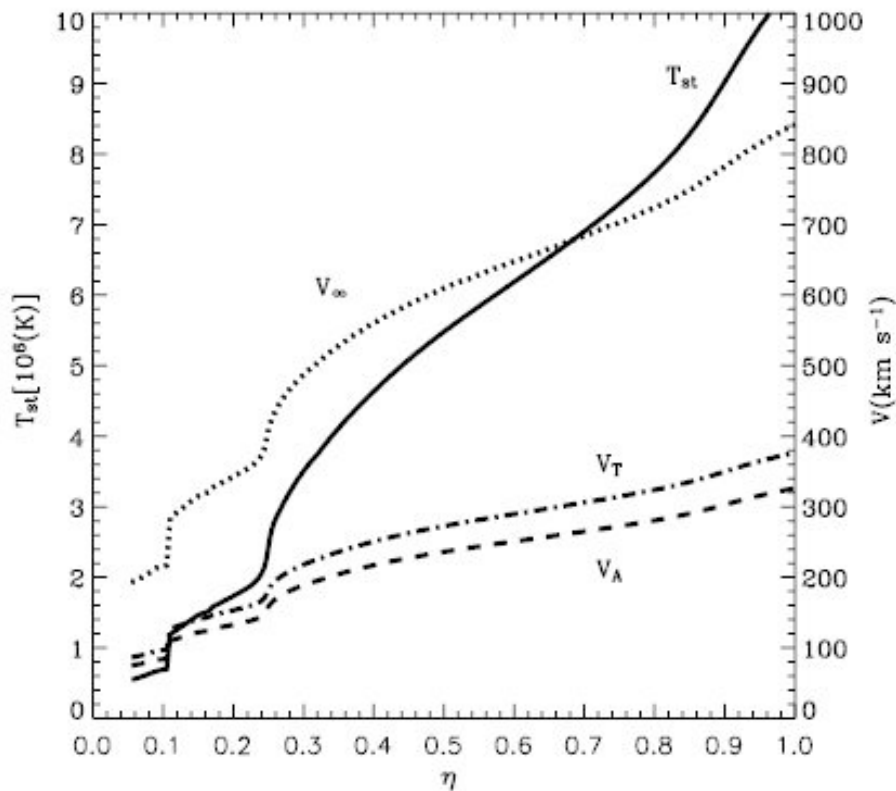


Figure 3.58: Velocity of the gas overtaken by the RS as a function of heating efficiency. The solid line marks the temperature at the stagnation radius (T_{st}), the dashed lines indicate the velocity of the gas overtaken by the RSs under the adiabatic (1) and isothermal (2) approximations, and the dotted line indicates the terminal speed of the cluster wind (V_{∞}), all of them plotted as a function of the heating efficiency, η .

3.3.4.2 Objectives

These new hydrodynamical models predict that massive assembling galaxies with large star formation rates are likely to evolve in a positive star formation feedback condition (Silich et al. 2010), either in the bimodal or in the gravitationally bound regime.

Large and massive clumps of star formation have been detected in more than half of the resolved $z > 1$ galaxies in the Hubble Ultra Deep Field (UDF; see Elmegreen et al. 2005). These star-forming entities are found in galaxies at all distances in the range $0.07 < z < 5$. They have sizes of about 2 kpc and masses often larger than $10^8 M_{\odot}$. They are so luminous that dominate the appearance of their host galaxies at optical wavelengths. Massive clumps like these are usually found in types not observed locally, including chain galaxies and their face-on counterparts, clump-cluster galaxies (see Elmegreen et al. 2005).

Photometric observations of these objects have been interpreted within the context of the models of galaxy evolution. They support a model in which star formation occurs primarily in highly turbulent disks by gravitational instabilities having a Jeans mass of $\sim 10^8 M_{\odot}$ and a length



of several kpc. Clump clusters are considered as examples of star-forming disks at their earliest stage, and maybe also initial seeds for spiral galaxies and, through mergers, spheroids as well (Elmegreen & Elmegreen 2005; 2006; Bournaud, Elmegreen, & Elmegreen 2007). These star-forming galaxies have so far been studied through broadband images from the HST. Paraphrasing Forster-Schreiber et al. (2006), "Much of our current knowledge about high-redshift galaxies rests on relatively crude broad-band photometric information, rarely on integrated spectra probing their restframe UV emission. As a result, very little is known about the dynamical and detailed physical properties of high-redshift galaxies". Details of the physical and dynamical properties of massive star-forming clumps can only be understood after analyzing the clump spectra. In order to model and understand the various feedback mechanisms (e.g., Tenorio-Tagle et al. 2007, 2010; Silich et al. 2010, and references therein), it is important to determine the kinematics and physical state of the gas in the clumps.

The spectroscopic observations provided by MEGARA will represent a necessary and definitive step forward in our knowledge of these objects and feedback processes. The basic questions we plan to answer are: Do the clumps show ionized-gas features? Do they show signs of negative feedback (e.g. shells, chimneys, winds)? Are they coeval star formation events or the result of continuous star formation? Are there cases of positive star-formation feedback? The 300 Myr upper-limit for the age of the clumps reported by Elmegreen & Elmegreen (2005) based on photometric studies justifies referring to them as ongoing massive starbursts. Whether or not emission-line features exist is crucial for their fate and evolution. Instantaneous star formation would lead to ionizing radiation for only a few tens of Myr, and the SN era is less than 50 Myr, whereas in the case of continuously decaying star formation these parameters would depend on the characteristic time scale of the star formation event. Clump ages and precise masses are needed in order to understand and parameterize the star-formation mechanism and in particular the star-formation feedback.

Using MEGARA we will be able to detect, resolve and characterize spectroscopically the targets and analyze their physical state. First we will confirm that they are massive young systems showing emission line features. Then, with a precise determination of their redshift we will derive their star-formation history and look for the presence of different velocity components that will enable us to determine their hydrodynamic state. The combination of the high spectral resolution of MEGARA together with the GTC collecting area will make possible to acquire the observations required to conclusively derive the feedback parameter.

3.3.4.3 *Sample and observing strategy*

Clump cluster sample selection

So far, most of the work carried out in order to understand the physical properties of these massive clumps of star formation have been done using only photometric data and using surveys available in the southern hemisphere. Therefore, the need for a large and well-defined sample of clump-cluster galaxies in the northern hemisphere is clear, as it is the need for accurate spectroscopic observations in order to analyze their physical properties.



In order to fill this gap we have produced a well-defined sample of massive clumps of star formation observable with GTC. The kpc-size star-forming clumps were extracted from the COSMOS database. COSMOS is an HST Treasury Project dedicated to survey a 2 square degree equatorial field with the Advanced Camera for Surveys (ACS). We started from a sample of 297.253 galaxies with accurately measured photometric redshifts and high-resolution images from the ACS-HST. In order to map the H α emission line in the wavelength range provided by MEGARA we restrict our sample to galaxies with redshifts $0.1 < z < 0.3$, resulting in 22.552 objects. Then, we applied the color criteria defined by Elmegreen et al. (2004) and Elmegreen & Elmegreen (2005) to identify massive star-formation galaxies. This was done after correcting the magnitudes by the effects of different filter transmission and K corrections. The final selection criteria (~ 2000 objects) were based on the absolute magnitude and the physical size of the objects. This catalog represents the first well-selected sample of massive and young objects in the north (Hinojosa-Goñi 2011, Ph.D. work, in progress; see Figure 3.59).

It is worth to notice that the typical projected size of these object spans a few arcseconds, typically they fall in the range between 1 to 6 arcsec matching perfectly into the dimensions of the MEGARA SCB, with a FOV of 10×8 arcsec². In addition, due to the number density calculated for these objects in COSMOS (~ 2 objects/MEGARA MOS FOV) the 92 positioners that can be located in the outer 3.5×3.5 arcmin² will allow us to highly increase the number of spectroscopically-confirmed clump-cluster galaxies without increasing the total exposure time. Even if no spatial information about these sources will be obtained, taking into account that no clump cluster galaxies have been spectroscopically observed up to now, this work will represent a cornerstone in the analysis of these objects.

Observing strategy

We plan to obtain spectroscopy for a subsample of ~ 100 candidate clump cluster galaxies using MEGARA at GTC.

We will first use the SCB equipped with the LR-R, or LR-I VPHs (depending on the estimated redshift of the object) in order to detect one or several of the most relevant emission lines expected to be present in these galaxies, e.g., [OII] $\lambda 3727\text{\AA}$, [OIII] $\lambda 5007\text{\AA}$, H α , [NII] $\lambda 6583\text{\AA}$, [SII] $\lambda\lambda 6716, 6731\text{\AA}$ with enough S/N, and perform a basic spectral analysis. The spectral resolution of these configurations is $R \sim 6,000$, which give us a velocity resolution of ~ 50 km s⁻¹ (FWHM). Using the MEGARA Exposure Time Calculator (ETC) we estimate that we should be able to reach the continuum flux of our objects with $S/N > 5$ with an exposure time ranging from 10 min to 1 hour depending on the target magnitude. We note that the size of the ACS footprint is comparable to the FOV covered by the MEGARA MOS (3.5×3.5 arcmin²). Using the MEGARA ETC assuming a seeing FWHM of $0.8''$, airmass=1.2, and a grey night, we will reach the continuum with $S/N > 5$ per \AA with integration times of 10 min, 30 min, and 1 hour for galaxies with $20 < i < 21$, $21 < i < 22$, and $22 < i < 23$, respectively.

In addition, for a small subsample (10 objects) of galaxies covering the parameter space (as measured by the LR observations described above), we aim at obtaining integral-field high-resolution spectroscopy. We will use the SCB to resolve spectroscopically (FWHM ~ 21 km/s)



and spatially (<1 kpc/resolution element) the line emission for the most massive clumps present in the galaxies of the sample. The resolved emission line profiles of the star-forming clumps in this galaxy will be analyzed looking for the presence of a single or a double component in the velocity space that will give us important insights on the hydrodynamical state of this object. In addition, by spatially resolving the different clumps using integral field spectroscopy we will obtain information on possible spatial differences where positive/negative feedback takes place. We will determine which feedback regime applies to each clump and find the net contribution of the clumps to the enrichment of the interstellar medium. We will use the MEGARA IFU SCB (10×8 arcsec²) with the MR-R, MR-I or MR-Z VPHs (depending on the galaxy redshift). This instrumental configuration gives us a spectral resolution of $R \sim 14,400$. Using the MEGARA ETC and assuming a seeing FWHM of $0.8''$, airmass=1.2, and the mean surface brightness of the object $\mu_i \sim 23$, we find $S/N \sim 10$ in the $H\alpha$ continuum with an integration time of ~ 2 hours.

Altogether, considering the number of object in each magnitude bin and including operational overhead, the total exposure time is given by

$$50 \text{ galaxies} \times 0.16 \text{ hours} + 50 \text{ overheads} \times 0.16 \text{ hours} = 16 \text{ hours}$$

$$30 \text{ galaxies} \times 0.5 \text{ hours} + 30 \text{ overheads} \times 0.16 \text{ hours} = 19.8 \text{ hours}$$

$$20 \text{ galaxies} \times 1 \text{ hours} + 20 \text{ overheads} \times 0.16 \text{ hours} = 23.2 \text{ hours}$$

$$10 \text{ galaxies} \times 2 \text{ hours} + 10 \text{ overheads} \times 0.16 \text{ hours} = 21.6 \text{ hours}$$

Which comes to a total of 80.6 hours needed to carry out the study of the star formation feedback proposed here.

3.3.4.4 *Serendipity project*

The objects proposed in this study are usually small and can be fully covered with the SCB. In order to benefit from the large field of view of the MEGARA MOS, and to optimize the observational program in the case of having MEGARA-Advanced at the telescope, we have explored the possibility of filling the whole MEGARA MOS FOV by completing the remaining area with other objects in the field. Since the sample was extracted from the COSMOS survey, which covers two squares degrees in the sky, we have access to a lot of information of other objects in the MEGARA FOV that will be studied for every particular case.

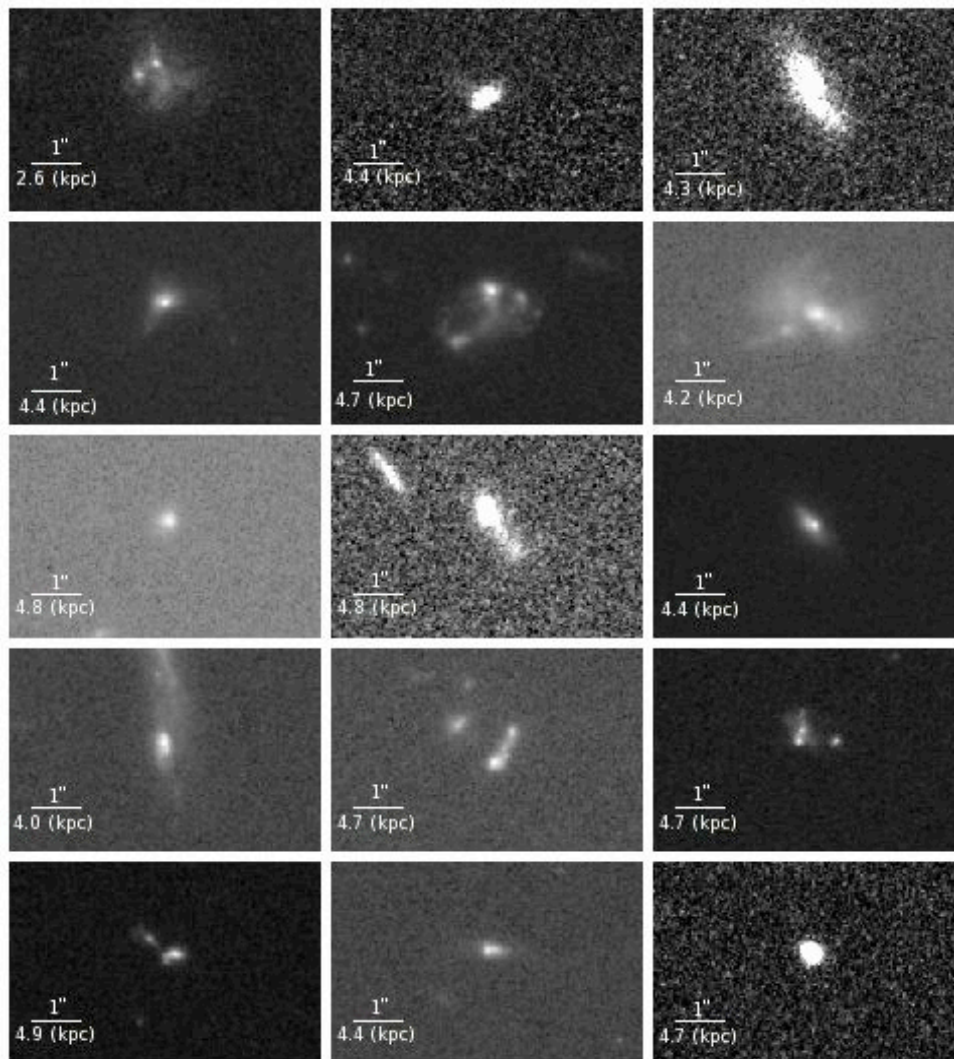


Figure 3.59: *F814W* images from the ACS-HST for a subsample of 15 massive kpc-size star-forming clumps candidates obtained from the COSMOS database. The bar indicates an angular size of 1'' and the physical size corresponding at the redshift of the corresponding galaxy. Note the compactness of most of these objects (images taken from R. Hinojosa Ph.D. work).



3.3.5 On the formation redshift of dwarf galaxies. Properties and star formation histories of low-mass galaxies.

3.3.5.1 Introduction: Scientific rationale

One of the most active fields in modern Astrophysics is the study of the formation and evolution of galaxies. To understand how and when the galaxies built up their stellar mass and they acquired their morphology are among the most important issues of extragalactic astrophysics and observational cosmology.

According to the state-of-the-art Λ CDM hierarchical models of galaxy formation, low mass dark matter halos assembled the earliest in the Universe. Most of these first halos merged to form more massive galaxies, but a fraction of them survived until the current epoch as proved by the existence of dwarf galaxies. While the history of low-mass dark matter halos is relatively well understood theoretically, the formation history of dwarf galaxies is still poorly reproduced by the models due to the distinct evolution of baryonic and dark matter in these halos. Indeed, low-mass dark matter halos are thought to be inefficient in either accreting or retaining gas and in cooling the remaining gas in order to form stars (Efstathiou 1992, Babul & Rees 1992; Haimann et al. 1997, Shaviv & Dekel 2003; Wyithe & Loeb 2006). The characteristic low luminosity of dwarfs has biased the study of these low mass objects to the Local Universe or clusters, where stellar populations are too evolved to estimate accurate ages and evolution is ruled mainly by interactions, respectively.

Blue Compact Dwarf galaxies (BCDs) are a well-studied galaxy population in the Local Universe that can be used as tracers of dwarf galaxies at intermediate redshift. BCDs were defined by Thuan & Martin (1981) as those systems with low intrinsic blue luminosity ($M_B \geq -18$, concordance cosmology), strong emission lines superposed on a blue continuum, and compact optical size (≤ 1 kpc in diameter; see Gil de Paz et al. 2003). These properties, associated to intense bursts of star formation, lead to significant observational advantages in this regard.

MEGARA working on GTC will allow the structural and kinematical analysis of numerous samples of dwarfs at intermediate redshifts, tracing their evolution along the age of the Universe. Apart from spectroscopic redshifts and measurements of emission lines such as $[\text{OII}]\lambda 3727\text{\AA}$ (a short for the $[\text{OII}]\lambda\lambda 3726, 3729\text{\AA}$ doublet), $\text{H}\beta$ and $[\text{OIII}]\lambda\lambda 4959, 5007\text{\AA}$, MEGARA spectroscopic data will provide average properties from full-spectrum fitting and spectral indexes (stacked per redshift bins) tightly related to the ages of stellar populations. This analysis will be crucial for our better understanding of the main processes involved in galaxy assembly and will provide valuable constraints to models of galaxy formation and evolution.

3.3.5.2 Proposed MEGARA observations

This project involves using MEGARA multiplexing and high spectral resolution to observe a complete, representative sample of low-mass star-forming galaxies (selected by stellar mass and SED) and BCDs (selected also by their colors and compact sizes) at different redshifts. The objects will be selected to have photometric redshifts in the range $0.5 < z < 1.3$. This epoch of

the Universe is critical in several ways: (1) it is when the cosmic Star Formation Rate (SFR) density started the decline; (2) it is when the overall galaxy population moved from highly active systems to the current Hubble sequence; and finally (3) it is when expansion accelerates. The Universe at lower redshifts ($z < 0.5$) was not considered because redshift evolution is not yet significant enough for our purposes and has already been covered by previous projects (see for example Barazza et al. 2006). Finally dwarfs are so faint that there are no objects in our deep broad band photometry and master catalog that meet the criteria for being a BCD at $z > 1.3$.

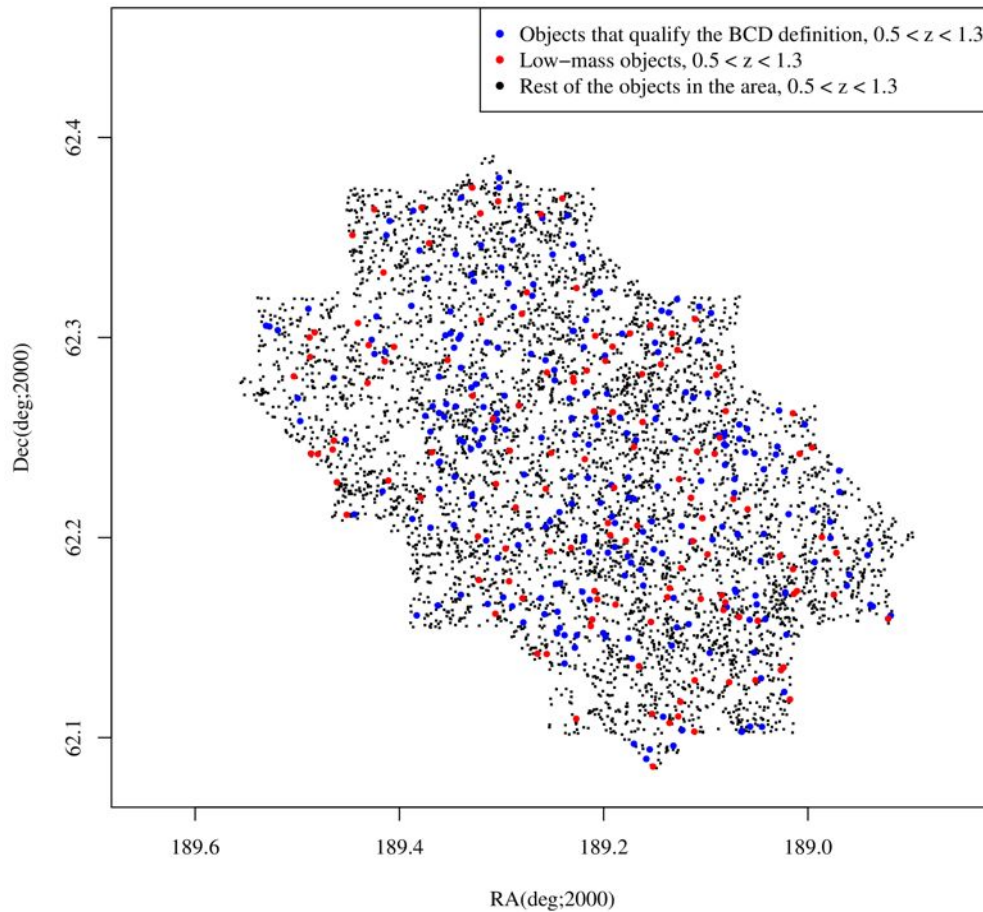


Figure 3.60: Galaxies in the range $0.5 < z < 1.3$ in the GOODS-North field. Black points are field galaxies. Blue and red circles are objects that meet the definition of BCD and of low-mass dwarfs, respectively.

The main goals are: (1) To exploit the MEGARA high spectral resolution and high multiplexing to measure emission line widths (at least for $[\text{OII}]\lambda 3727\text{\AA}$) for a complete and representative sample of low-mass galaxies at different redshifts to study the evolution of their kinematics. A sample of BCDs in the same redshift range will be observed simultaneously. Line widths will allow us to estimate velocity dispersions and dynamical masses and/or winds/turbulence of the systems. We want to know if there is any evolution in the physical mechanisms of this kind of objects as a function of redshift. This analysis will be complementary to those massive surveys as Alhambra or PAU (Benítez et al. 2009) using medium band filters to obtain Spectral Energy Distributions (SEDs) and redshifts for the overall population of galaxies up to $z \sim 1$. The study

will be also useful to compare with the evolution of the overall galaxy population as traced by the $[\text{OII}]\lambda 3727\text{\AA}$ emission (Zhu et al. 2009). (2) To estimate the age of the stellar populations using spectral indexes such as CNO3862 and H δ A (Sánchez-Blázquez et al. 2006), and thus, reduce the uncertainties in the formation redshift of dwarf galaxies and test models for the epoch of formation of low-mass galaxies. For those systems that appear close enough at the sky, differential velocities will allow us (3) to explore for dynamical bindings.

This kind of studies can be carried out only in cosmological fields covered by good (deep) ancillary data at different wavelengths. As a representative cosmological field we chose GOODS-North (see Figure 3.60) as it provides high spatial resolution HST images and has been covered by Spitzer and by the SHARDS ESO/GTC project (Pérez-González et al. 2012, in prep). To identify a sample of BCDs in GOODS-N, we select objects with rest-frame blue absolute magnitude $M_{B,0} > -18$, $(B-V)_0 < 0.6$ and $\mu_{\text{eff},B,0} < 23 \text{ mag arcsec}^{-2}$ at redshifts inside the range considered. We define the sample of dwarfs selecting objects with stellar masses under $10^8 M_{\odot}$. As reference database we use RAINBOW (Pérez-González et al. 2008a; Barro et al., 2010), which provides us with a homogeneous database of all objects detected in the field in all the HST, Spitzer and ground-based data previously obtained covering different wavelengths from the UV to the far infrared. In this way, before the MEGARA observations are secured, we already have Spectral Energy Distributions in hand and good estimates of the redshifts, sizes, colors, stellar masses and other physical parameters.

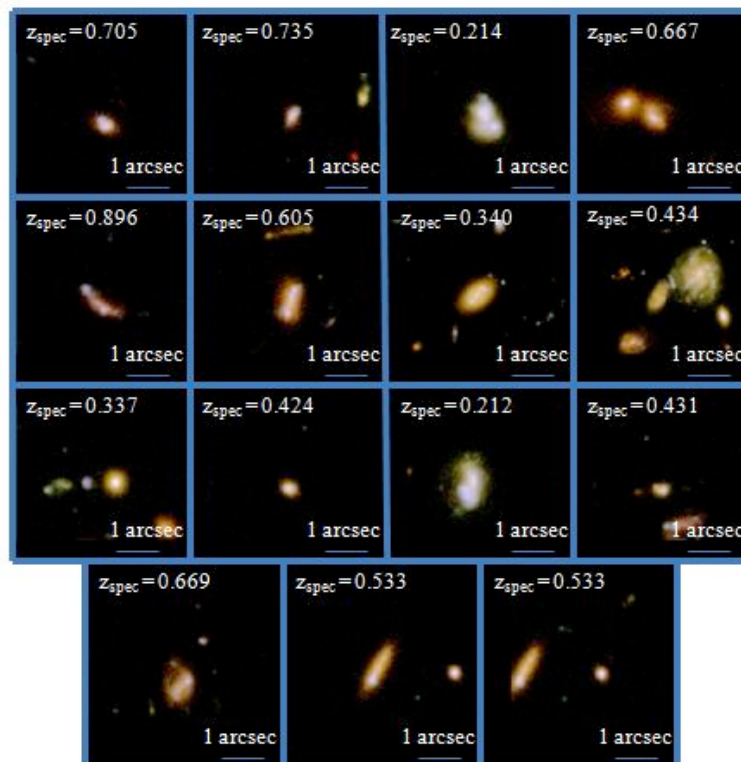


Figure 3.61: Color composite resulting from the HST images at different bands for a set of BCDs at low-to-intermediate redshifts. Low-redshift objects have been introduced for comparison purposes.

In Figure 3.61 we show a sample of BCDs located at intermediate redshifts (Gil de Paz et al 2012, ApJ in preparation; Rodríguez 2009).

3.3.5.3 Feasibility study and observational strategy

Our science case would extremely benefit from using MEGARA, as most of its characteristics match perfectly with our instrumental requirements. As master reference catalog, we used an ultra deep narrow-band image obtained with a 1% filter centered at 8200Å taken with Subaru telescope (Fujita et al. 2003; Capak et al. 2004). We find 247 galaxies that meet the BCD selection criteria and 128 low-mass objects in GOODS-N (Figure 3.62) in the selected redshift range. Hence, surface density of targets in the area is $\sim 1.2 \text{ arcmin}^{-2}$.

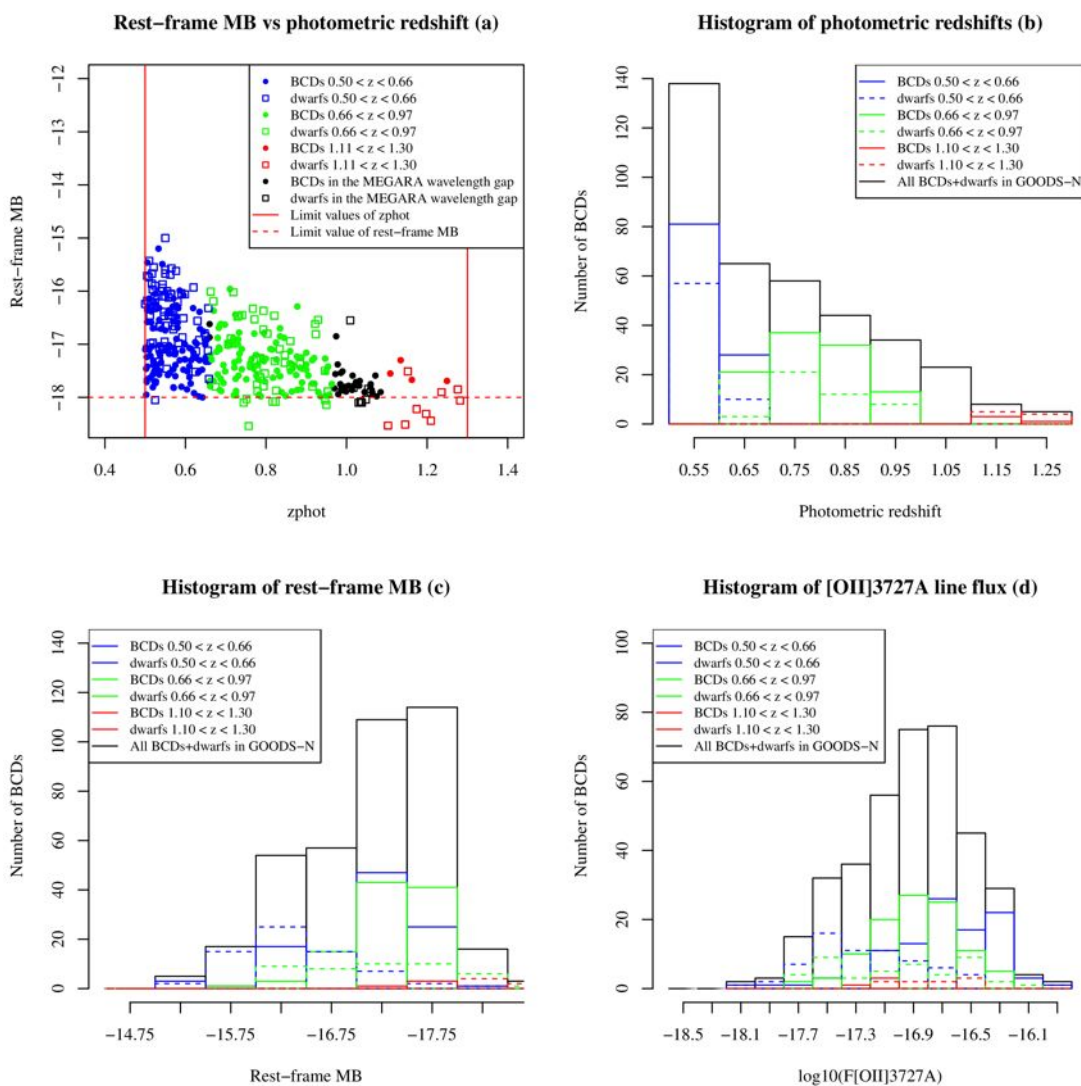


Figure 3.62: (a) Rest-frame M_B vs. photometric redshift, (b) histogram of photometric redshift, (c) histogram of rest-frame M_B and (d) histogram of integrated [OII] $\lambda\lambda 3726, 3729 \text{ \AA}$ doublet line flux for the targets selected in GOODS-N.



According to the position of the $[\text{OII}]\lambda 3727\text{\AA}$ line in the spectra different VPHs would be used for different redshifts. Here we focus on the low resolution VPHs, enough for our scientific objectives, and with the advantage of obtaining spectra with wider wavelength coverage. We are mainly interested in two of the spectral setups: LR-V and LR-R. LR-I would be used for the small fraction of targets at $z > 1$. The surface densities of targets in the redshift intervals defined by these VPHs are listed in Table 3.5. We will miss about 35 objects in the gap between LR-R and LR-I.

Set-up	R	$\Delta\lambda$ (\AA) $\Delta z_{[\text{OII}]\lambda 3727\text{\AA}}$	Number of BCDs+ dwarfs in the Δz range	Number of objects in the blue and faint sample in the Δz range	Total surface density (arcmin^{-2})	Number of objetcs in a MEGARA's pointing
LRV	6250	5164 - 6194 0.39 - 0.66	~ 176	~ 560	~ 2.3	~ 28
LRR	6249	6115 - 7334 0.64 - 0.97	~ 147	~ 388	~ 1.7	~ 20
LRI	6248	7836 - 9399 1.10 - 1.52	~ 13	~ 23	~ 0.1	~ 1

We estimate an integrated $[\text{OII}]\lambda 3727\text{\AA}$ line flux for each subset using the empirical expressions given by Gallagher (1989) and Kong et al. (2004). Results are shown in Figure 3.62.

We use $[\text{OII}]\lambda 3727\text{\AA}$ line flux values to estimate the exposure time needed to obtain S/N per spaxel ≥ 10 . The rest of the parameters used by the Exposure Time Calculator of MEGARA are dark nights with a seeing at the zenith of 0.5 arcsec and the assumption of these being point sources. We found that even the faintest sources could be observed with S/N per spaxel better than 10 at any redshift using time exposures of 1 hour (Table 3.7).

Considering the 92 robotic positioners available for each MEGARA pointing ($3.5' \times 3.5'$) and the surface densities obtained, the project could be finished in about 25 one-hour pointings for the lowest redshift interval, 24 one-hour pointings for the intermediate redshift interval and some few extra pointings for the highest interval. This amount of pointings corresponds to about 6 or 7 nights to observe the complete sample of ~ 336 objects covering the redshift range $0.5 < z < 1.3$. This efficiency could even be increased including a reference sample in the observations, such as objects matching BCDs rest-frame absolute B magnitude and blue color but not the surface brightness criterion. There is a population of about 800 galaxies matching these properties (BCDs excluded) in GOODS-N. This would increase the number of targets per pointing in 21, 15 and 1 objects for each one of the set-ups chosen, LR-V, LR-R and LR-I, respectively. Thus, the number of galaxies observed would reach a grand total of about 1100 in 6 nights. To better understand the overall galaxy population at the redshift ranges considered, we would use the rest of the robotic positioners to observe galaxies from the general field population (surface density of $\sim 5\text{-}6 \text{ arcmin}^{-2}$ per redshift bin).



Set-up	LR-V	LR-R	LR-I
FWHM (Å)	1,34	1,59	1,93
Continuum mag (I_{VEGA} band)	~ 25	~ 25	~ 25
Flux (erg/s/cm²)	S/N (1hr exp)	S/N (1hr exp)	S/N (1hr exp)
5,00E-18	27	28	28
2,00E-17	63	67	67
3,50E-17	86	92	92
5,00E-17	> 100	> 100	> 100
6,50E-17	> 100	> 100	> 100

3.3.6 Galaxy over-densities at high-redshift

3.3.6.1 *Scientific motivation*

According to the Λ Cold Dark Matter (Λ CDM) cosmological model (Springel et al. 2005), the cooling of the gas and the star formation are closely linked to the hierarchical evolution of dark matter halos that coalesce to form bigger structures as we move along the Hubble time. Consequently, the detailed study of the large-scale structure in the Universe at different epochs is key for understanding the evolution of galaxies, also imposing strong constraints on cosmological parameters (e.g. Eke et al. 1998).

Locally, the color distribution of galaxies is strongly bimodal (with a red and a blue peak), reflecting a relationship between color, morphology, and star formation activity (Strateva et al. 2001). Quiescent early-type galaxies populate the red sequence, while disk-like star-forming galaxies concentrate in the blue cloud. This bimodality remains mainly unchanged up to $z \approx 1$ (Brown et al. 2007). At higher redshifts, a rapid decrease in the density of red galaxies is observed, eventually disappearing by $z \sim 3$ (Cirasuolo et al. 2007, Labbé et al. 2007). The vanishing of the red sequence at $1 < z < 3$ is intimately connected to the process of stellar mass assembly in massive galaxies, which peaks, together with the cosmic SFR density, in the same epoch (Thomas et al. 2005; Pérez-González et al. 2005, 2008a; Arnouts et al. 2007; Figure 3.63), and quenched for some reason at $z > 1$ (e.g., AGN feedback: Croton et al. 2006, Daddi et al. 2007). These results constitute a strong evidence that a key epoch for the study of the formation of the red sequence is $z \gg 1$ (see also Fontana et al. 2004; Abraham et al. 2007).

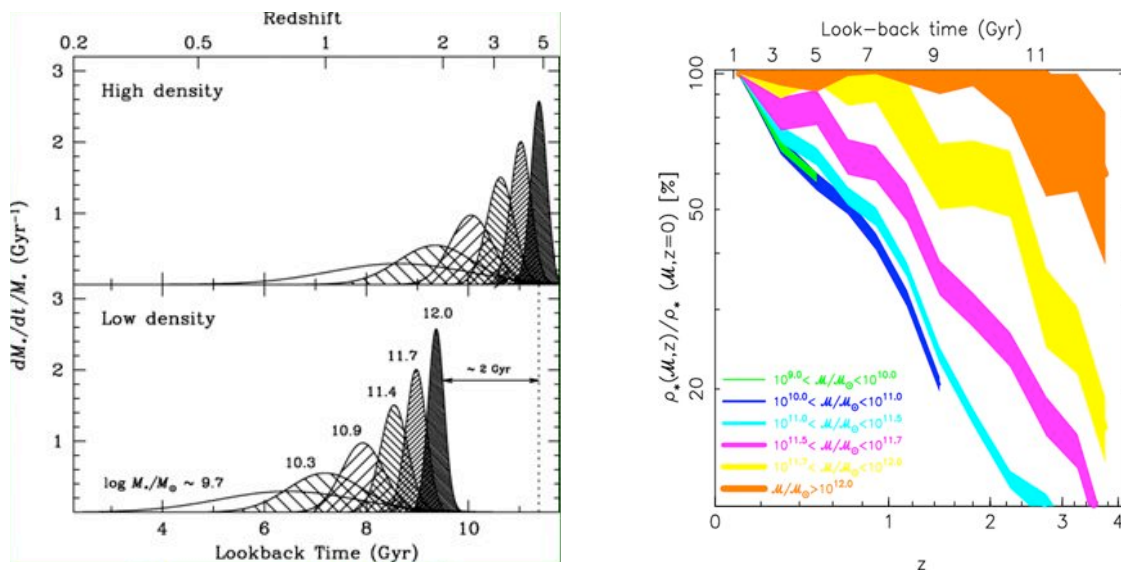


Figure 3.63: Figures extracted from Thomas et al. (2005, left) and Pérez-González et al. (2008, right), demonstrating the downsizing scenario for galaxy formation. In this scenario, the most massive galaxies would form in early epochs in the history of the Universe, in very rapid star formation events. The observations confirm that the local stellar mass density of galaxies with masses above $10^{12} M_{\odot}$ was reached at $z=2-3$. Less massive systems formed more slowly or/and in later epochs (left). Thomas et al. (2005) estimated that the formation of a galaxy is delayed about 2 Gyr in low-density environments in comparison with the formation of massive systems in high-density regions (right).

It is also known that the most common habitat of red quiescent galaxies in the nearby Universe is relatively dense regions (Dressler et al. 1980). Several recent works have focused on the environmental properties of galaxies at $z < 1$ (Cooper et al. 2007, Gerke et al. 2007, Elbaz et al. 2007), finding that red galaxies still prefer denser environments up to $z \sim 1$. However, by this redshift, there are more bright blue galaxies in over-densities than in the local Universe (Cooper et al. 2008). Interestingly, also at $z \geq 1$, (Ultra)Luminous Infrared Galaxies become much more common than in the present (e.g. Pérez-González et al. 2005), and they also live in over-dense environments (Marcillac et al. 2008).

Virtually all (3D) environmental studies published to date focus in the $z < 1$ period. The main reason is that photometric and spectroscopic surveys only reached adequate depth and area coverage to detect and analyze large enough samples of galaxies and over-densities at low- z . At higher redshifts, we could only reliably characterize the angular clustering of galaxies (e.g., Quadri et al. 2008), or detect massive clusters (with unresolved galaxies) emitting in X-ray's (e.g., Mullis et al. 2005). However, in order to understand galaxy evolution, it is necessary to study how (i.e., analyze the processes of mass accretion) the individual most massive galaxies seen today entered the red sequence, and that requires analyzing samples of galaxies at $z > 1$.

Within this topic, the study of the effect of the large-scale structure (LSS) on the assembly of galaxies is of special interest, given that massive galaxies tend to be clustered and the evolution in rich environments is accelerated and happened early in the Universe (e.g., Eisenhardt et al. 2008, Figure 3.64).

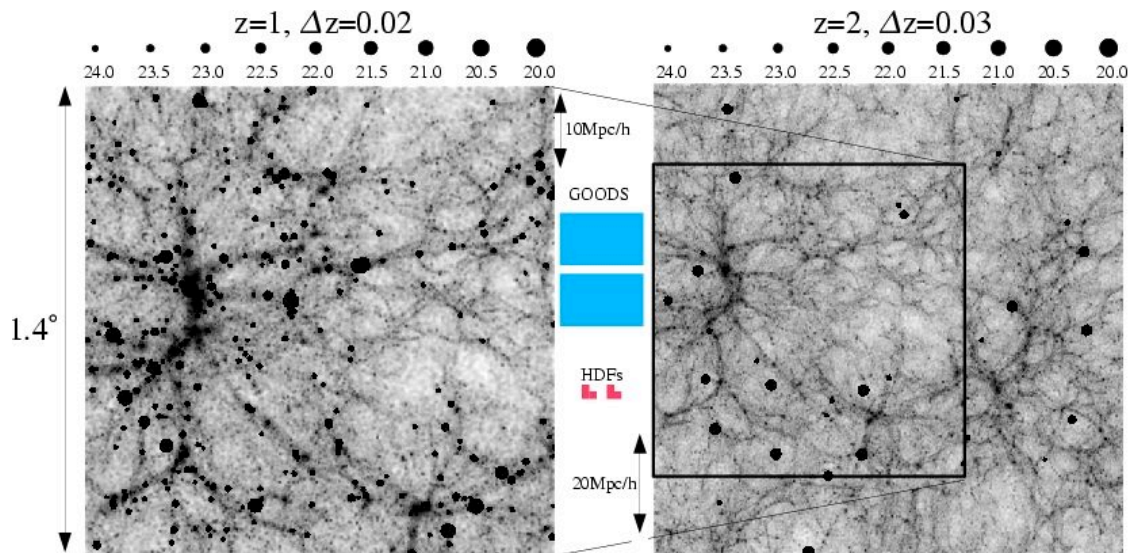


Figure 3.64: Distribution of dark matter (gray background) and galaxies (black dots, the size indicating the brightness of the galaxies) at $z=1$ and 2 from simulations of the Virgo Consortium. The Large Scale Structure is clearly visible with its clusters of galaxies, its filaments and voids. In between the two maps are the field sizes of the famous Hubble Deep Field North and South, as well as the two GOODS fields (figure extracted from the COSMOS Team webpage).



Only recently, wide field surveys (area $\geq 1 \text{ deg}^2$), such as the NDWFS (Jannuzi & Dey 1999), and also the deeper AEGIS (Davis et al. 2007), SXDS (Furusawa et al. 2008; surveying the same sky area as the UKIDSS UDS, Lawrence et al. 2007), and COSMOS (Scoville et al. 2007), have opened the possibility to study large scale structure above $z=1$ (see also Wilson et al. 2008). Indeed, large areas and ultra-deep multi-wavelength imaging are needed to detect galaxy over-densities (e.g., groups, clusters, super-clusters, walls, or filaments) at $z>1$, whose sizes are typically a few arcmin (4 arcmin corresponds to 4–6 Mpc at $1<z<2$), but their number density is $\leq 10 \text{ deg}^{-2}$ (Eisenhardt et al. 2008).

Although the detection of galaxy over-densities at high redshift is challenging because of the faintness of the sources, several recent works have shown the feasibility of identifying galaxy groups and cluster candidates using appropriately calibrated photometric redshifts and special 3D density finding algorithms (e.g. van Breukelen et al. 2006, Brodwin et al. 2006, Castellano et al. 2007, Salimbeni et al. 2009; Figures 3.65 and 3.66).

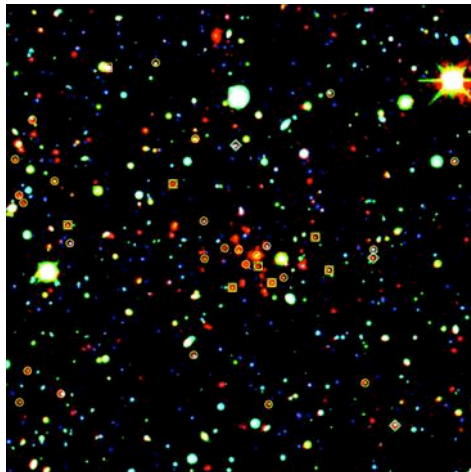


Figure 3.65: Cluster (or proto-cluster) candidate at $z\sim 1.3$ detected by Eisenhardt et al. (2008) in the NDWFS field using photometric redshifts. The image is an RGB composite using the Bw, I and IRAC 4.5 μm bands. Galaxies tentatively belonging to the over-density are marked with circles. Cluster members marked with squares have been confirmed spectroscopically. The image is 5' square, so the central part of the cluster could be covered with 1-4 MEGARA pointings and the rest of candidates for cluster member could be observed with the positioners.

Spectroscopy with GTC/MEGARA of different regions in extensively surveyed deep cosmological fields where photometric redshifts reveal galaxy over-densities at $z>>1$ (Figure 3.66) would have a high scientific impact on our understanding of the early formation of galaxies and the dependence on environment. MEGARA would allow us to probe the evolution of galaxies (with enough statistics and redshift resolution) in dense environments in the important redshift range between $z=1$ and $z\sim 6$ (5 Gyr time interval), when the red sequence formed. These spectroscopic data are essential to identify over-density members with confidence, and to study their properties.

The faintness of the cluster member candidates ($I<25$ AB mag) makes this project completely unfeasible for any other telescope but an 8-10m such as the GTC. The number of sources in the over-densities (50–150) is a perfect match for the multiplexing capabilities of MEGARA. The typical size of these (proto-) clusters is $\sim 1'$ across for the core and several arcmin for the outskirts. Therefore, MEGARA would allow studying in high detail the central part of the over-densities and targeting all the possible cluster members using the robotic positioners.

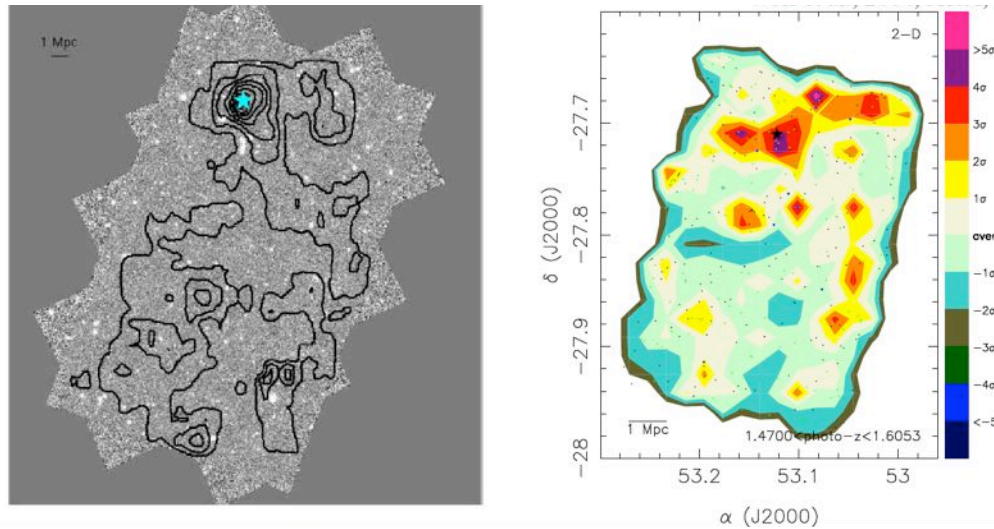


Figure 3.66: Left: Figure extracted from Castellano et al. (2007) showing the density isosurfaces at $z \sim 1.6$ superimposed on the ACS z-band image of the GOODS-South field. A cluster of galaxies is detected in the top left corner of the image, counting with spectroscopic confirmation for a bunch of galaxies. Right: Density map of the GOODS-S region built by our group (covering the Spitzer area, larger than the HST surveyed region) using the algorithms in Faure et al. (2004), Eisenhardt et al (2008), and Salimbeni et al. (2009). Magenta regions present surface densities more than 4σ above the average (shown in gray and light green) for the quoted redshift interval. We mark the higher density peak detected by Castellano et al. (2007) with cyan filled stars in both panels. We demonstrate that our algorithm is able to recover the position of this cluster.

The proposed observations will be used to build, for the first time, a complete census of star-forming and early-type galaxies in over-dense regions (probably clusters) down to $I \sim 25$ AB mag and masses $M \sim 10^9 M_{\odot}$, and to study the over-density dynamics and formation history. We will also be able to obtain more reliable estimations of the stellar mass and the stellar population age, which are significantly affected by photo-z errors (Kriek et al. 2008), and can be improved by introducing the intensity of the 4000 Å break or/and the Mg absorption index in the stellar population synthesis modeling (Kauffmann et al. 2003; Daddi et al. 2005; Cimatti et al. 2008). The stellar mass estimates will also be compared and validated with the dynamical masses inferred from the spectroscopy. In addition, we will carry out a complete and robust inventory of the stellar mass assembled in dense environments at $1 < z < 6$, probing the faint end of the luminosity function and the less massive galaxies with $M = 10^{9-10} M_{\odot}$.

3.3.6.2 Objective

Analyzing the environmental dependence of galaxy formation at high-redshift

We propose to obtain multi-object spectroscopy of several galaxy over-densities at redshifts between $z=1$ and $z=6$ in the deep cosmological fields such as GOODS-N, the Extended Groth Strip (EGS), COSMOS, or the *Spitzer* Ultra Deep Survey (SpUDS) field. Each region has 50-



150 cluster member candidates with $I < 25-26$ AB mag within a circular aperture of 4 arcmin.

Given that we are interested in studying large-scale structures, our program aims at obtaining very deep spectroscopic data in small fields (1-9 MEGARA pointings cover the typical size of high- z over-densities) of very specific regions in the sky, only pre-selectable in very large ultra-deep surveys such as the SXDS/UDS, EGS, or COSMOS.

The spectroscopic data obtained in this proposal will be used: (1) to obtain accurate spectroscopic redshifts with $\Delta(z) < 0.0005$ (< 2 Mpc comoving distance) and confirm the over-density members; (2) to build a reliable census of all the galaxies in the clusters down to $I \sim 25$ AB mag or masses $M \sim 10^9 M_{\odot}$; (3) to decrease the uncertainties in the estimates of the stellar mass using accurate spectroscopic redshifts and the addition of the 4000\AA break intensity (if detected) to the stellar mass determination (Kauffmann et al. 2003); (4) to estimate the age of the stellar populations in the quiescent galaxies using the 4000\AA break intensities and/or the Mg indices (Daddi et al. 2005); (5) to study the virial masses of the cluster members and compare them with the stellar mass estimations; (6) to analyze the cluster dynamics and investigate on how the baryonic mass is coupled with the cold dark matter nesting structure at high- z ; (7) to analyze the evolution of the galaxy population in rich environments (galaxy volume density, spatial extent, fraction of star-forming to quiescent systems) from $z \sim 1$ to $z \sim 6$ (~ 5 Gyr), the epoch where the SFR density of the Universe peaked and the red sequence of early-type galaxies is appearing; and (8) to analyze the SFRs and extinction properties of the galaxies belonging to these clusters. Note also that MEGARA will uniquely provide data for all galaxies in the region covered by the IFU (simultaneously in the case of MEGARA-Advanced), which might include low emission-line galaxies such as low redshift dwarfs, high redshift LBGs, or lensed galaxies behind the cluster whose detection might be difficult in the imaging data, but possible in the “blind deep spectroscopy” carried out simultaneously with MEGARA in parallel to our main project.

Our group has compiled an extensive public and proprietary dataset in fields such as GOODS-N, GOODS-S, COSMOS, EGS, Sp-UDS, including multi-wavelength data from the UV to the FIR (more noticeably *Spitzer* data): see a description of the RAINBOW database in the following URL <http://guaix.fis.ucm.es/~pgperez/Proyectos/databaseuse.en.html>. This database has been used to obtain high-quality estimations of parameters such as the photometric redshift, stellar mass, SFR, etc. (Pérez-González et al. 2005, 2008a, 2008b).

Using our database in the GOODS-N, EGS, COSMOS, and SpUDS fields, we have selected several over-densities at $z > 1$. Each over-density harbors 30–70 member candidates in the core ($3'$ or 1.5 Mpc box), as shown in Figure 3.66 (see also Figures 3.64 and 3.65, and Figure 9 in Brodwin et al. 2006 or Figure 2 in Salimbeni et al. 2009 for similar structures in other fields). Even more galaxies (90–100) may belong to the over-density at larger distances.

The main spectral features of interest for this study (depending on the redshift) are the $[\text{OII}]\lambda 3727\text{\AA}$ emission line, the 4000\AA break, the Mg absorption, the $\text{Ly}\alpha$ emission line, the Lyman break, or/and the $[\text{CIV}]$ emission, and other stellar and ISM lines. These features will provide the four key parameters needed for our scientific goals: redshifts, SFRs from $[\text{OII}]\lambda 3727\text{\AA}$ and $\text{Ly}\alpha$ fluxes, virial masses from emission-line velocity widths, and ages from

the D(4000) or/and Mg indices (Balogh et al. 1999, Daddi et al. 2005). For the galaxies at $z < 1.5$, the spectral range of interest is $7000\text{\AA} - 1\mu\text{m}$, given that the [OII] line is usually the brightest in this redshift range. At higher redshift, it is more efficient to observe in the blue ($3500 - 7000\text{\AA}$), where it is easier to detect emission or/and absorption lines since OH lines are not so bright as in the red, and the rest-frame UV spectrum of galaxies is full of them (see Steidel et al. 2004). However, MEGARA will also open the possibility of observing in the red, given that its high spectral resolution will uniquely attenuate the devastating effects of the OH sky lines.

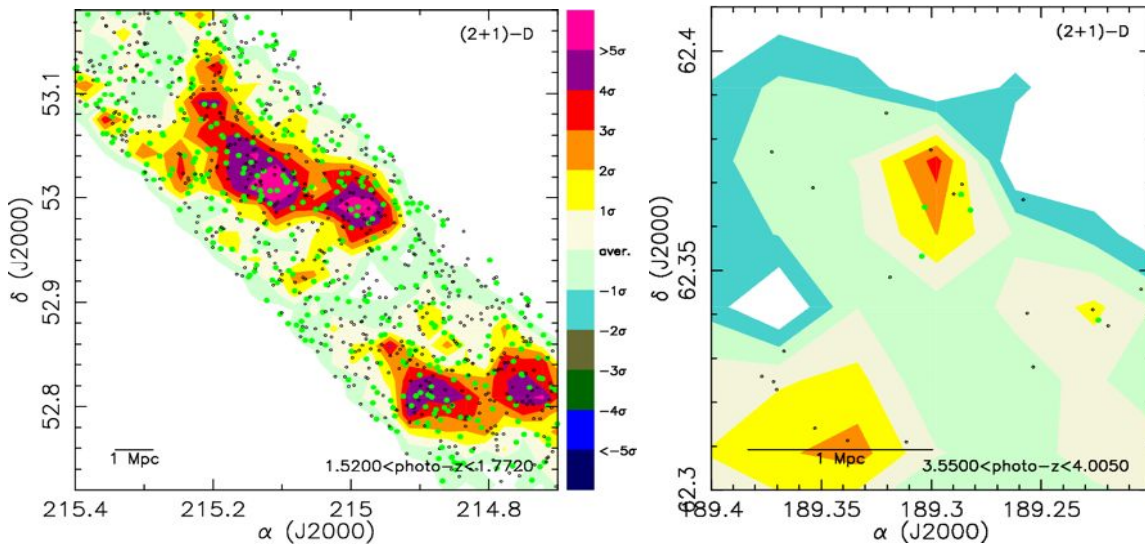


Figure 3.67: Left: Density map of the EGS IRAC Survey (covering $2^\circ \times 15'$) in the photo- z interval $1.52 < z < 1.77$ (a comoving distance slice of ~ 430 Mpc). The densities have been calculated with the methods described in Faure et al. (2004), Eisenhardt et al (2008), and Salimbeni et al. (2009), using a resolution corresponding to $\sim 1 \times 1$ Mpc 2 at $z \sim 1.6$. The red and magenta regions show the densest environments. Green dots depict the galaxies with $I < 25$ AB mag, and black dots show galaxies with $I > 25$ AB mag. None galaxies with already available optical spectroscopy from other surveys (e.g. DEEP) are found in the selected interval. This over-density is one of the most prominent at this redshift interval. The typical stellar mass of the sample is $10^{10.3} M_\odot$. MIPS detect about one third of the targets at $24 \mu\text{m}$, allowing the possibility to estimate IR-based SFRs (mainly for the low- z ones). Similar density maps have also been constructed for other redshift intervals at $z = 1 - 6$. Right: Over-density at $z \sim 4$ in the GOODS-N field, detected with the photometric redshifts in our database (color map) and consistent with the position of a spectroscopically confirmed cluster of galaxies at $z \sim 4.05$ (Daddi et al. 2009).

Typical [OII] fluxes of $z > 1$ galaxies are $f_{[\text{OII}]} \sim 10^{-18} - 10^{-19} \text{ erg s}^{-1} \text{ cm}^{-2}$ (Davies et al. 2009), and our sources are as faint as $R, I \sim 25 - 26$ AB mag. To measure accurate redshifts, fluxes, and velocity widths we need $S/N > 5$ in the emission line. MEGARA is just the right instrument to achieve these goals efficiently. Given the faintness and compactness of our targets, good seeing conditions ($< 0.9''$) and at least gray nights (if not dark) are needed to achieve the desired S/N with the integrations given below.



With MEGARA, we can obtain reliable ($S/N \sim 5$) detections of emission-lines with 2 hours integrations using the $R \sim 6,000$ VPHs and observing around 8000\AA for $z < 1.5$ clusters and in the blue for $z > 1.5$ over-densities. This integration is the typical used by spectroscopic surveys with VIMOS at VLT targeting $I=24-25$ AB mag galaxies, and it has been demonstrated to be also effective in detecting absorption features (e.g., Le Fevre et al. 2005; Vanzella et al. 2005, 2006; Lilly et al. 2007). We note that, in the red, although the emission-line (e.g. [OII]) fluxes may be also measured from data with low resolution, the OH forest would make these measurements highly uncertain and difficult, so the high resolution achieved with MEGARA is an important asset for our project. Furthermore, instruments working at lower resolutions would not provide velocity widths, which is an important property to study in high-density environments. Previous observations using DEIMOS at Keck (e.g., TKRS survey, Wirth et al. 2004) have shown that [OII] $\lambda 3727\text{\AA}$ emission line fluxes of galaxies with $R=25$ AB mag at $z > 1$ can be reliably measured also in ~ 2 hours using a spectral configuration $R=2,000$ around 9000\AA . Our higher spectral resolution has two main advantages: it optimizes detection of the [OII] $\lambda 3727\text{\AA}$ emission lines between the [OH] forest and allows measurements of the velocity widths down to $\Delta v = 50$ km/s. Thus, we would need 2 hours integration with MEGARA at GTC using $R=6,000$ around $8000-9000\text{\AA}$ for the over-densities at $z < 1.5$ and in the blue for $z > 1.5$ clusters. Assuming 16 MEGARA pointings to securely cover the whole core of each cluster, we would need **32 hours per cluster**. Using the robotic positioners we could target hundreds of sources in the vicinity of the over-densities. These sources could be members of the overdensity located in the outskirts and/or interesting objects in the background (maybe lensed galaxies at very high- z) or foreground of the proto-cluster. Allowing some positioners to target the same objects in several exposures, we could reach up to 32 hours of exposure time in several tens of very interesting sources around the cluster.

An allocation of about one third of the Guaranteed Time awarded to MEGARA would allow observing 5-6 clusters, which would already provide unique results in the study of high-redshift galaxy clusters. For example, observing one cluster at $1.0 < z < 1.3$, one at $1.3 < z < 1.7$, one at $1.7 < z < 3.5$, one at $3.5 < z < 5.5$, and another at $z > 5.5$ would allow us to study the formation of galaxies and its dependence on environment in a 5 Gyr time interval with 1 Gyr resolution. This would need about 150 hours of MEGARA time plus overheads.



3.3.7 Analyzing the faintest and/or most distant SFGs using gravitational lenses

3.3.7.1 *Scientific motivation*

The detailed characterization of the star-forming galaxies at $z > 1$ needs a robust analysis of the extinction properties of the star formation knots present in these sources. Moreover, obscured star formation is more and more important as we move to higher redshifts, where a good fraction of star-forming galaxies are strong emitters in the thermal IR (see, e.g., Chary & Elbaz 2001, Pérez-González et al. 2005). Therefore, a detailed analysis of the dust emission coming from high- z IR-bright sources is crucial to understand their nature and advance in our knowledge about the formation of galaxies.

The *Spitzer*/MIPS surveys showed that the cosmic SFR density is dominated by LIRGs at $z > 0.5$, and (U)LIRGs play a leading role in the formation of galaxies at $z \sim 2$ (e.g., Pérez-González et al. 2005, 2008a). Indeed, it is well established that the Universe had a period of high star formation activity between $z \sim 1$ and (at least) $z \sim 3$. The star formation rate (SFR) density of the Universe was approximately 10 times larger at $z = 1-2$ than at $z = 0$ (Hopkins 2004; Pérez-González et al. 2005; Hopkins & Beacom 2006; Figure 3.68). In addition, an important fraction (about 50%) of the total stellar mass density observed in galaxies today formed at $z > 1$ (Dickinson et al. 2003; Rudnick et al. 2003; Fontana et al. 2004, 2006; Glazebrook et al. 2004; Pérez-González et al. 2008). We now know that galaxies with dust-enshrouded star formation (ultra/luminous IR galaxies: U/LIRGs) have undergone strong evolution from $z \sim 1$ to $z = 0$ (Flores et al. 1999; Franceschini et al. 2001; Chary & Elbaz 2001). It has also been demonstrated that the cosmic SFR density was dominated by LIRGs at $z \sim 0.5$, and ULIRGs contribute non-negligibly at $z = 1-2$ (e.g., Pérez-González et al. 2005; Figure 3.68). Moreover, the IR luminosity density has evolved more rapidly than the far-UV luminosity density at $z < 1$ (Takeuchi et al. 2005), confirming the important role of IR bright star-forming galaxies in galaxy evolution. Beyond $z \sim 1.5$, sub-mm observations have also revealed a population of dusty star-forming galaxies that are hardly detected in the UV/optical (Smail et al. 1997; Chapman et al. 2003). These sources seem to be the progenitors of nearby massive elliptical galaxies.

Making further progress in our understanding of the formation of galaxies requires analyzing the processes behind the SFR peak at $z > 1$ and the formation of massive galaxies at $z = 1-3$. In this context, it is especially relevant to carry out a detailed study of LIRGs up to the highest redshifts possible, since this population of galaxies dominates the SFR density of the Universe at $z > 0.5$ and massive galaxies at $z \sim 2$ must have formed the bulk of their stellar content at $z > 4$. One of the main questions we have to answer is whether galaxies were forming stars more rapidly at high- z because they had larger fuel reservoirs (molecular gas), whether they were more efficient in turning that fuel into stars, or whether there was a combination of both processes. Consequently, we need to measure the gas contents and dynamics of $z \gg 1$ LIRGs, compare them with their SFRs, and analyze the efficiency of the star formation in representative samples of galaxies at different redshifts.

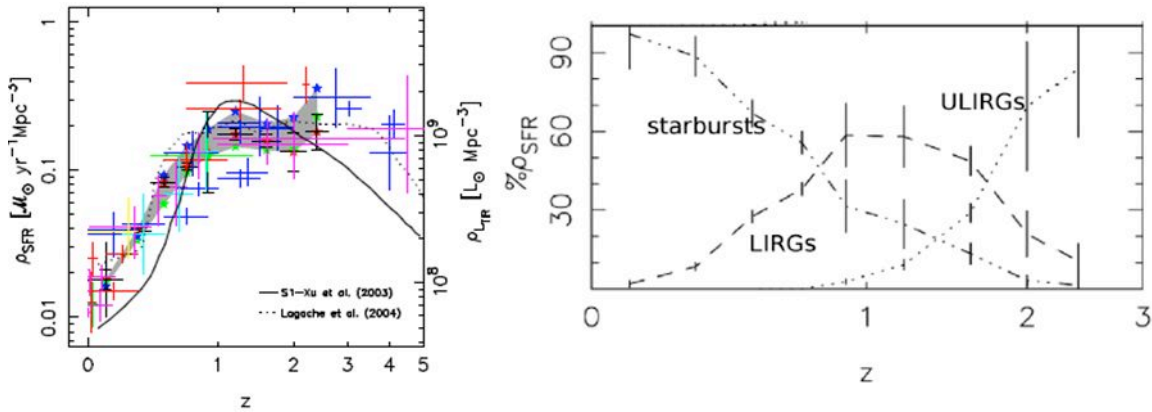


Figure 3.68: Left: Evolution of the cosmic SFR density obtained with different SFR tracers (Pérez-González et al. 2005), including an estimation based on Spitzer/MIPS observations (shaded region). Right: Contribution of galaxy populations of different SFR values to the total SFR density of the Universe as a function of redshift (Pérez-González et al. 2005). The IR luminosity and SFR densities increased by a factor of 10 between $z=0$ and $z=1$, where LIRGs accounted for more than 50% of the total density, and approximately 50% of the stars seen today were formed (see Pérez-González et al. 2008). This demonstrates that the detailed study of LIRGs at $z>1$ is especially relevant for understanding the formation of galaxies.

In order to obtain more precise information about IR-bright galaxies at high- z , we need to analyze their emission in the rest-frame MIR/FIR (sub-mm and mm wavelengths). This kind of study is now possible, thanks to the launch of the *Herschel* Space Telescope, which can observe in the wavelength region from 70 to 500 μm . One of the Key Programmes carried out by *Herschel* was conceived to observe the faintest IR-emitters at the highest redshifts. Its name is the *Herschel Lensing Survey* (HLS hereafter). This program was approved in 2010 and the data is currently being analyzed (see, e.g., Egami et al. 2010, Pérez-González et al. 2010, and several other papers in the 2010 *Herschel* A&A special issue).

The HLS tried to dig into the confusion noise typical of FIR images and improve the detection limit of *Herschel* to reach the faintest fluxes and the most distant objects. To penetrate through the confusion limit and reach the highest redshifts and the faintest galaxies, gravitational lensing by massive galaxy clusters offers a very powerful and yet cheap solution (e.g., Blain 1997). Magnification factors of 2–4x are quite common in the cluster core regions, and when a background source is strongly lensed (i.e., multiply imaged), magnification factors of 10x–20x are often seen. Note that a magnification factor of x10 corresponds to a factor of x100 in observing time when the sensitivity is background-limited. Therefore, a fairly short-integration image of a cluster core region would often reveal sources that are well below the detection limit of an ultra-deep blank-field image, giving the HLS a unique perspective of galaxy evolution.

Figure 3.69 shows one of the most spectacular lensed ultra-luminous infrared galaxies (ULIRGs; $10^{12} < L(\text{IR}) < 10^{13} L_{\odot}$) found so far, a triply lensed ULIRG at $z=2.5$ (Kneib et al. 2004). The magnification factor of the central image is 22. Because of the strong magnification, this source was detected by SCUBA at 450 and 850 μm as well as by PdBI in CO (Kneib et al. 2005). The figure also displays the Spitzer 4.5 and 24 μm images of the same cluster (Egami et

al. 2006), showing that this lensed ULIRG is quite easy to recognize at 24 μm because of the small contamination by the foreground cluster member galaxies. With the much-improved sensitivity of *Herschel*, the quality of the far-IR/sub-mm images of this cluster approaches that of the *Spitzer* 24 μm image.

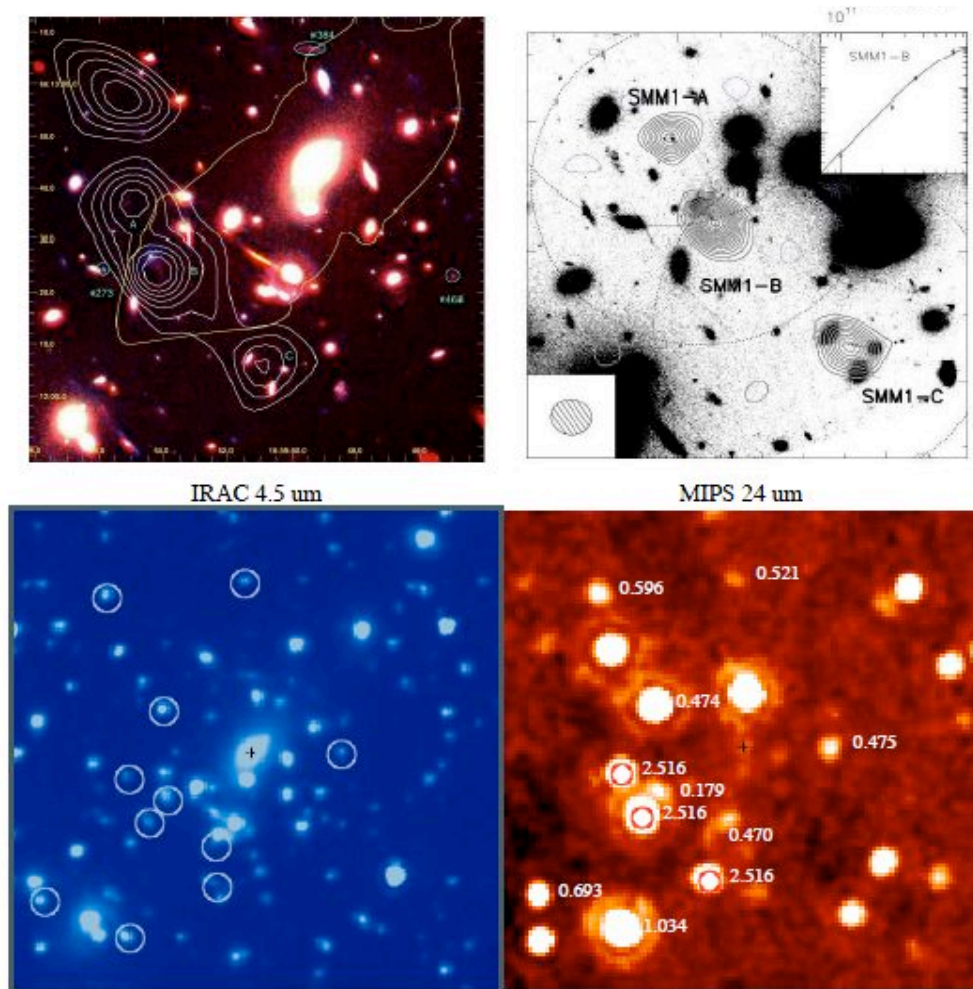


Figure 3.69: The massive lensing cluster Abell 2218 and its triply lensed ULIRG at $z=2.5$. Upper left: *HST* optical image with the 850 μm SCUBA map contours showing the triply lensed image (the lower three peaks, Kneib et al. 2004); Upper right: IRAM/PdBI CO map (Kneib et al. 2005); Lower left: *Spitzer*/IRAC 4.5 μm image. The white circles denote sources with spectroscopic redshifts; Lower right: *Spitzer*/MIPS 24 μm image. The numbers denote spectroscopic redshifts while the three red circles mark the positions of the triple images. The *Spitzer* images are 2.3' on a side (Egami et al. 2006).



3.3.7.2 Objective

Optical characterization of lensed and intrinsically faint galaxies at very high-redshift, the earliest progenitors of massive galaxies

Understanding the star-forming activities at $z > 3$ is particularly important because there are indications that most massive galaxies have formed most of their stars (and therefore assembled most of their masses) in this high-redshift range (Fontana et al. 2006, Pérez-González et al. 2008). The HLS has detected a statistically significant number of sub-mm sources well below the nominal confusion limits of PACS and SPIRE, so this program uniquely probe the faint and very high redshift regime (typical magnifications can exceed a factor of 10x), being especially suited for the characterization of the earliest progenitors of the massive galaxies which are already in place at $z=1-2$.

Given the very faint nature of the lensed sources we detect in the HLS, and being most of them arcs, no optical spectroscopy can be carried out with slits in the usual way, since the position of the sources is very uncertain. Indeed, typical uncertainty in the *Herschel* and *Spitzer* images is almost $1''$, and a fair fraction of the arcs are completely invisible in the deepest HST/ACS optical images. So only by using an IFU such as that of MEGARA, and counting with its superb sensitivity, the high coverage factor, and the field of view of the LCB, we can blindly target the regions in the cluster field with the highest magnifications and/or where IR emitters have been found and obtain optical spectroscopy. These data will be used to study the faintest (dust-enshrouded) star-forming galaxies at very high redshift, obtaining important parameters such as the redshift, SFR, dynamics, metallicity, spectral diagnostics, etc.

Our targets for this project to be carried out with MEGARA would be the low- and intermediate- z clusters that count with HST data (providing well characterized mass models), and with *Spitzer* and *Herschel* observations (revealing the galaxies with the highest star formation, the earliest progenitors of massive galaxies). GTM and/or ALMA will soon target these sources. The typical cluster size is $1' \times 1'$ (the core) and up to $3' \times 3'$ including the outskirts, where lensing by individual galaxies is commonly seen (see Combes et al. 2012). MEGARA would have significant advantages over classical multi-object spectrographs (such as OSIRIS): high multiplexing (5-6 galaxies/arcmin²), the negative effect of the OH lines could be notoriously suppressed due to its high spectral resolution capabilities, and the MEGARA IFU would allow a blind survey which may reveal optically faint emission-line arcs (whose position is unknown), cluster members, etc.

We estimate an exposure time of 2 hours to reach $\text{SNR} \sim 4$ for fluxes as low as 5×10^{-19} erg/s/cm². Assuming 16 MEGARA pointings to securely cover the whole core of each cluster (or the region with the highest magnification, as best characterized by HST imaging, see Figure 3.70), we would need 32 hours per cluster. Using the positioners we could target hundreds of sources in the cluster or in its background and foreground. These sources could be members of the cluster located in the outskirts and/or interesting objects in the background (the lensed galaxies at very high- z for which a position can be known a priori). Allowing some positioners to target the same objects in several exposures, we could reach up to 32 hours of exposure time in several tens of very interesting sources around the cluster.

An allocation of about one third of the Guaranteed Time awarded to MEGARA would allow observing 6-7 clusters, which would give us information about half a dozen or even ten very-high sources ($z > 5$) whose magnification could exceed a 5x factor. This would need about 150 hours of MEGARA time plus overheads.

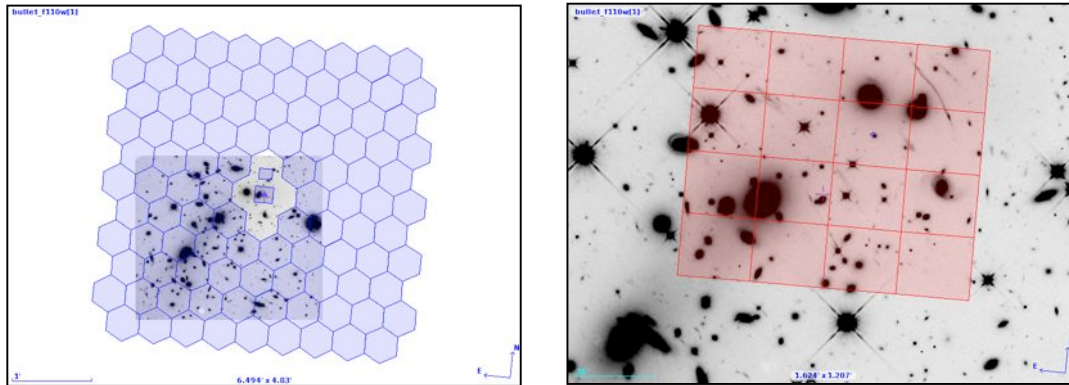


Figure 3.70: Layout of the observations proposed for MEGARA Guaranteed Time in order to study the formation of galaxies at the highest redshifts getting advantage of the gravitational telescopes (nearby clusters). We show the WFC3 NIR image of the Bullet cluster, where several arcs are visible, including an arc of one of the very few LIRGs detected by Spitzer and Herschel at $z > 3$ (see Pérez-González et al. 2010). For comparison, the highest redshift LIRG detected in the deepest Herschel observations in GOODS lies at $z \sim 1.5$ (see Figure 4 in Elbaz et al. 2011). On the left, we show the whole footprint of MEGARA, demonstrating the possibility of targeting with the robotic positioners interesting sources in the whole field of the cluster while concentrating in the arcs with the IFU. This would be just 1 of the 16 pointings to be carried out in this cluster. On the right, we show a zoom in the region with the highest magnification in the Bullet cluster, and how the 16 pointings with MEGARA's IFU proposed in this project would give us data about the arcs, a good fraction of them being only detectable in NIR ultra-deep images such as the ones showed here, but not in optical data (taken with WFC3).



3.4 Stellar astronomy with MEGARA

3.4.1 Chromospheric activity and age of solar analogs in open clusters

3.4.1.1 *Introduction*

Open clusters represent a most valuable laboratory for understanding the physics of stars. Having a common origin, member stars are usually considered coeval and initially chemically homogeneous. The age of the cluster can be therefore easily and quite precisely obtained (once the chemical abundances are known) by isochrone fitting.

On the contrary, age determination methods for field stars are usually affected by larger uncertainties (see, for instance, the excellent review on this topic by Soderblom 2010).

For this reason, stars in clusters are excellent targets to calibrate the connection between age and age-dependent stellar properties, correlations which can be eventually applied to field stars.

In this context, MEGARA, with its multi-object capability coupled to the huge collecting area of the GTC, represents a unique instrument for the study of the resolved stellar population of Galactic stellar clusters: it will efficiently gather high-quality spectra of fainter stars in the CMD diagrams of more distant objects. As we shall show below, observations of main sequence (MS) stars will be feasible on systems up to several kiloparsecs.

3.4.1.2 *Solar analogs*

The discovery of hundreds of extrasolar planets in the recent years has renewed the interest of the astrophysical community on solar-like stars, which for a long time were not considered attractive astronomical targets. Thus, in the last decade there has been a flourishing of studies, which also revealed some important relations between the presence of a planetary system and the properties of the host stars. One of the most relevant has been the work of Valenti & Fischer (2005), who found that extrasolar giant planets are more likely to form around metal-rich stars ($[Fe/H]>0$). More recently, Israelian et al. (2009) have found a negative correlation between the stellar lithium abundance and the existence of a planetary system, a correlation which is still under a vivid discussion.

A detailed characterization of MS stars (atmospheric parameters and age) is therefore fundamental in the understanding of planet formation and evolutionary status of the circumstellar disks of material which originate them.

In the case of intermediate- and late-type MS stars, chromospheric activity has been widely used as a clock⁷ since the magnetic activity in the upper atmospheric layers is correlated with the rotational period and this is expected to decay, as an effect of mass loss, during the lifetime of the stars.

⁷ Other methods include nucleocosmochronometry, asteroseismology, kinematic analysis, lithium depletion, etc.



One of the most used indicators of chromospheric activity is the emission of the Ca H and K lines at 3969Å and 3933Å, which is usually expressed as $R'_{HK} = L_{HK}/L_{bol}$, where L_{HK} is the luminosity within the emission lines and L_{bol} is the bolometric luminosity of the star. These transitions produce a strong photospheric absorption in solar-like stars but in an optically thin chromosphere, due to the temperature inversion, they generate emission lines (see Figure 3.71).

The strength of this (sometimes very tiny) emission at the very center of a strong absorption feature has been correlated with age, by means of observations of stars in clusters of known age.

The recent R'_{HK} -age calibration of Mamajek & Hillenbrand (2008), which is shown in Figure 3.72, has been obtained from a collection of literature data for just about 200 stars of 13 open clusters (plus a small number of field stars of Valenti & Fischer (2005), whose age has been obtained by isochrone placement). They claim to have reached a relative precision of ~60% for the age of solar analogs (in the age interval ~0.6-4.5 Gyr).

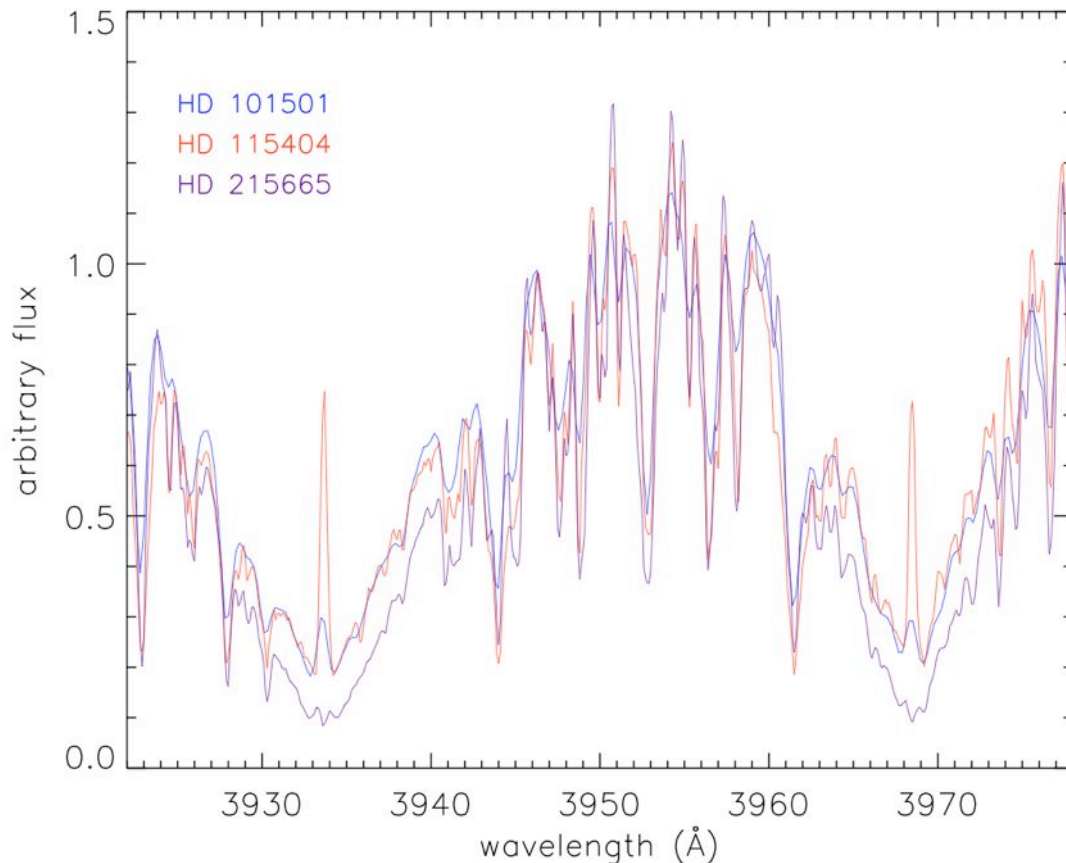


Figure 3.71: The Ca H and K lines for three stars presenting different level of chromospheric activity (data from Montes et al. 1997).

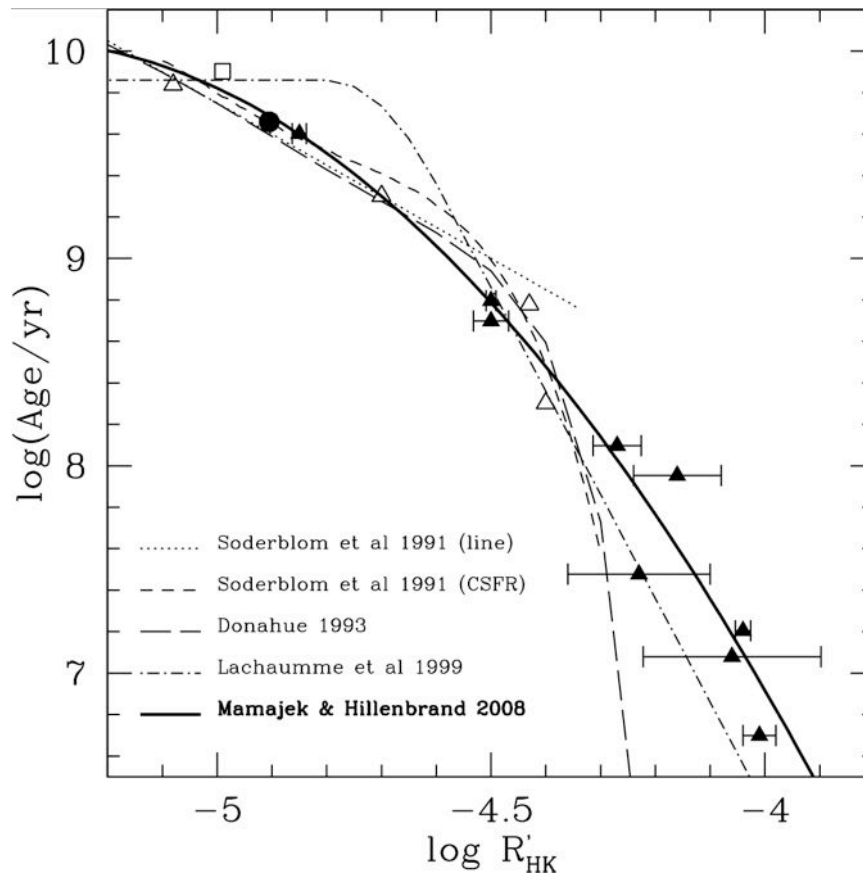


Figure 3.72: The chromospheric activity-age calibration from Mamajek & Hillenbrand (2008), compared with previous calibration from different authors. The triangles show the mean $\log(R'_{HK})$ values of star in cluster vs. cluster age; the square indicates the mean value for the sample of solar-type dwarfs from Valenti & Fischer (2005); the circle is the Sun.

3.4.1.3 Observing proposal

We propose to observe the Ca HK spectra of solar-type stars in a selected sample of 22 open clusters. These observations will considerably increase the number of cluster stars with a well measured R'_{HK} . This would allow to significantly decrease the uncertainty of the activity-age calibration, that we can then apply to field stars.

The sample of open clusters has been extracted from the WEBDA⁸ (Mermilliod J.-C. 2005), applying the following criteria:

- a) $B \leq 18.5$ for a G2V type star.

⁸ <http://www.univie.ac.at/webda/>



b) a total number of stars with (B-V) color typical of solar analogs (G0-G3 types) larger than 200

c) a declination Dec(J2000) $>$ -20°

The sample of open clusters to be targetted is described in Table 3.7, where we report the name of the cluster along with the coordinates, the density of solar analogs, the diameter, the age, and the distance. It is worth noticing that our sample includes 6 clusters with age $>$ 1 Gyr. This age interval is critical, since the Mamajek & Hillenbrand (2008) calibration is based only on one bona-fide cluster in this range, since these objects are usually located at large distances from the Sun. The observations of a large number of stars in these evolved systems will provide a comprehensive view, for the first time, of the saturation regime of stellar activity.

ID	Cluster	RA (J2000) (degrees)	Dec(J2000) (degrees)	# targets (arcmin ⁻²)	Diam. (arcmin)	log(t) (yr)	dist. (pc)
1	Stock 24	00 39 42	+61 57 00	108.5	5	8.08	2818
2	Berkeley 62	01 01 00	+63 57 00	80.2	5	7.18	1837
3	NGC 381	01 08 19	+61 35 00	102.5	6	8.51	1148
4	NGC 581	01 33 23	+60 39 00	295.3	5	7.34	2194
5	NGC 654	01 44 00	+61 53 06	86.5	5	7.15	2041
6	Berkeley 7	01 54 12	+62 22 00	57.5	4	6.60	2570
7	King 5	03 14 36	+52 43 00	68.7	5	9.00	1900
8	Berkeley 17	05 20 36	+30 36 00	115.4	7	10.08	2700
9	IC 2157	06 05 00	+24 00 00	103.9	5	7.80	2040
10	Saurer 1	07 18 18	+01 53 12	116.2	4	9.85	1970
11	Trumpler 32	18 17 30	-13 21 00	91.0	5	8.48	1720
12	NGC 6611	18 18 48	-13 48 24	75.9	6	6.88	1749
13	NGC 6631	18 27 11	-12 01 48	195.7	6	8.60	2600
14	Basel 1	18 48 12	-05 51 00	66.1	5	7.89	2178
15	NGC 6705	18 51 05	-06 16 12	63.7	13	8.30	1877
16	NGC 6819	19 41 18	+40 11 12	123.5	5	9.17	2360
17	NGC 6834	19 52 12	+29 24 30	72.2	5	7.88	2067
18	NGC 6996	20 56 30	+45 38 24	54.9	8	8.54	760
19	Berkeley 54	21 03 12	+40 28 00	198.5	4	9.60	2300
20	NGC 7235	22 12 25	+57 16 12	50.8	5	7.07	2823
21	King 11	23 47 48	+68 38 00	59.3	5	9.05	2892
22	NGC 7790	23 58 24	+61 12 30	133.3	5	7.75	2944

Table 3.7: The properties of the target open clusters.

As a first step, we plan to homogeneously derive the age of the clusters by using the latest Padova stellar tracks (Bressan et al. 2012, in preparation) to perform the isochrone fitting of the clusters' CMDs. The Padova group has recently revised their stellar evolution code, by including up-to-date physical ingredients (e.g., opacities, equation of state, nuclear reaction rates, chemistry, microscopic and turbulent diffusion, neutrino energy loss), and they have computed a new library of evolutionary tracks in a wide range of age and metallicity ($0.15 M_{\odot} < M < 120 M_{\odot}$ and $0.0001 < Z < 0.05$). An extremely important property of these tracks is that they adopted the

solar abundances from Ludwig et al. (2010), which have been obtained from 3D modelling of solar atmosphere and result in a total metallicity⁹ of $Z=0.0153$.

Since for MS stars is the chemical composition (and not age) what defines their location on the CMD, the use of a new set of isochrones, based on different reference solar abundances, will give rise to a modified chronology, which will affect the stellar activity vs. age calibration.

3.4.1.4 Observations

The MEGARA MOS mode will be used with the VPH410-MR MR-U grating: it covers the wavelength interval 3890-4309Å at a spectral resolution $R\sim 11,000$, which is very suitable for detailed observations of emission at the core of the Ca HK lines (Figure 3.73).

With observations of one hour of exposure time we should reach a $SNR>10$ for the Ca HK emission line even for the faintest stars of our sample and weak chromospheric activity. The observation of the full sample of 22 clusters should use therefore **25 hours total** (15% overheads included) of telescope time.

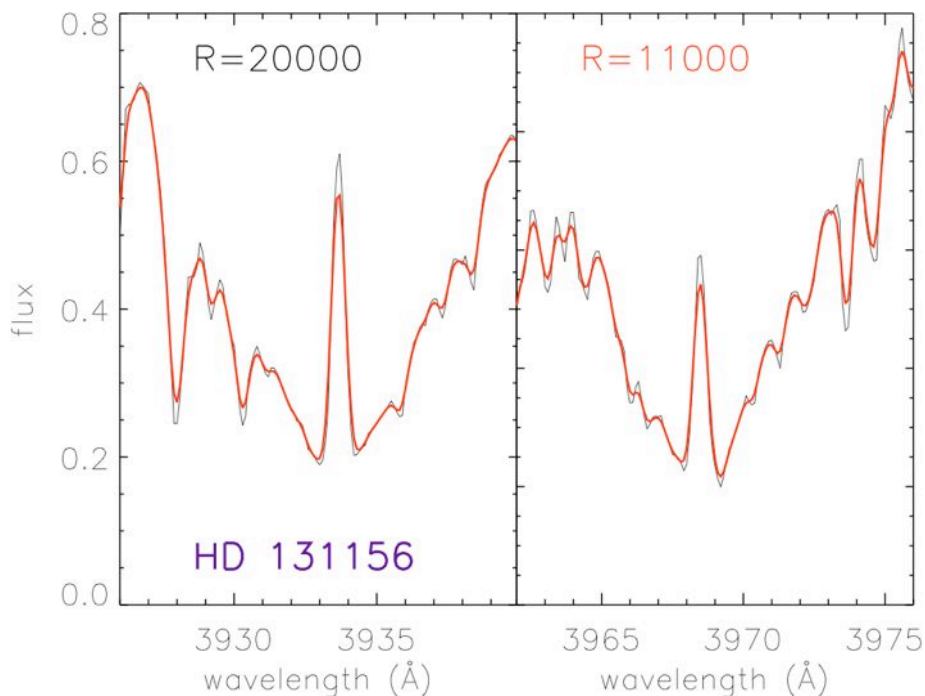


Figure 3.73: The Ca K and H spectrum of HD131156. The black lines indicates the original data from

⁹ The Ludwig et al. value $Z=0.0153$ is intermediate between the one proposed by Grevesse & Sauval (1998) ($Z=0.0171$) and the one obtained by Asplund et al. (2005) ($Z=0.0122$). However, the value of $Z=0.0171$ is not compatible with the most recent observations, while the Asplund solar metallicity is in conflict with helioseismological results.



Montes et al. (1997) at $R=20,000$, while the red curve shows the spectra degraded to the spectral resolution of MEGARA with the MR-U VPH.

3.4.1.5 *Stellar atmospheric parameters*

The spectra to be collected with the MEGARA MR-U spectral setup, in addition to the Ca HK chromospheric emission, will contain a wealth of information that can be exploited for determining the atmospheric parameters of all the observed stellar targets. The density of absorption lines in late-type stars is maximum in the blue interval and the $R\sim 11,000$ spectral resolving power, even if it is not enough to separate all individual lines, will certainly allow to define a set of line indices, that measure both the equivalent widths (or suitable Lick-like indices) and line flux ratios (e.g., Rose 1994; Liu et al. 2008), which have proved to be very sensitive to the main atmospheric parameters: effective temperature, surface gravity, and overall metallicity. The observed indices will be matched to those computed from a new library of suitable theoretical stellar spectra (Bertone et al. 2012, in preparation), which are being computed using the same solar partition (Ludwig et al. 2010) used to compute the new Padova evolutionary tracks.

Before this comparison, however, the theoretical indices will be calibrated against the observations, using a suitable sample of well known reference stars.

3.4.2 Low-mass star formation in ESO Gaia stellar clusters

3.4.2.1 *Introduction: Star Formation and the low-mass end*



Figure 3.74: The dark cloud Barnard 30, placed at ~ 400 parsecs. The image has been created from several observations obtained with the instruments IRAC and MIPS on board Spitzer. It allows us to see a new population of stars and brown dwarfs that have been formed recently. In many cases, they have circumstellar disks, which could originate planetary systems. Credit NASA/JPL - Caltech/D. Barrado y Navascués (CAB, INTA-CSIC).

Most our knowledge about stellar properties come, in fact, from observational data taken in the solar neighborhood and, in particular, from members of stellar associations of different ages located at distances closer than 0.5 kpc, such as Orion and Taurus –about 1 Myr, Upper Sco and Sigma Ori –about 5 Myr, or the Pleiades and the Hyades -125 and 600 Myr, respectively. Stellar associations offer the advantages of including a homogeneous population of coeval stars with the same metallicity. As an example, see the case of Lambda Orionis (Barrado y Navascués et al. 2004, 2007). Intercomparison of members of an association provides the dependence of different properties with mass, whereas intercomparison between different clusters provides the dependence with age and other, more subtle, parameters (metallicity, environment). However, due to the lack of collecting power, most of the associations beyond this small radius, insignificant from the perspective of the scale of the galaxy, have not been explored, except for the most massive members (O and B spectral types).

A large telescope such as GTC coupled with MEGARA, offers the possibility to investigate the properties of the cluster members farther away, which might be different to the solar vicinity. In particular, GTC is perfectly suited to investigate the Perseus Arm, located at about 2.5 kpc in the antigalactic center, and its very large number of star forming regions and open clusters with small to moderate angular sizes. At a distance modulus of 12 mag, a 10 Myr, $1 M_{\odot}$ star has $R=17.5$, non accessible for medium size telescopes with conventional spectrographs. MEGARA, with its FOV and large number of fibers, would be able to collect a large number of simultaneous medium- and high resolution spectra at high and moderate S/N, and track the properties of the members associations: from accretion rates and activity ($H\alpha$, CaII IRT or simply CaT) to rotation and age-dependant properties (lithium and other alkali lines), and, of



course, to conduct the first accurate spectroscopic cartography, using the resolution at $R=19,000$, of the metallicity in this arm.

Regarding the solar neighborhood, MEGARA will be able to provide a workhorse for star formation studies in rich and compact associations, and to investigate problems such as multiplicity, outflows and disk structure for young objects (stellar and substellar).

We propose a very ambitious project: the study of properties of very low mass stars (and brown dwarfs) belonging to young stellar associations, from a holistic perspective. First, within the Gould Belt (the Local Bubble, a structure few hundred parsec across), then, moving farther away, to the galactic anticenter and the Perseus Arm. The goal is to put star formation in a galactic perspective and to include the effects both of metallicity and environment. We will take full advantage of the data already provided by different surveys, including Spitzer and Gaia.

3.4.2.1.1 The Gaia mission

Gaia will dramatically improve our knowledge of the low-mass stellar formation process: first, it will detect a large number of members in nearby star forming regions and characterize them, and second, it will allow deriving fundamental properties, like the age, with very small uncertainties (at least for stars brighter than about $V=12$ mag), which is crucial to test pre-main sequence low-mass star evolutionary models.

Post-Gaia observations:

Gaia will provide accurate proper motion, parallaxes and G-mag for the sources. The Gaia spectroscopic data will allow a preliminary characterization through the Calcium triplet. However, higher resolution spectroscopic observations will be needed to derive more precise values of the radial velocity, temperature, $v \times \sin(i)$, surface gravity and other stellar parameters.

The limits of Gaia and the need for high-resolution spectroscopy:

- Accurate abundances will be derived only for stars brighter than $V=12$.
- Furthermore, the small intrinsic velocity dispersions within clusters and associations ($\sim 1-2 \text{ km s}^{-1}$) requires that radial velocities are measured with accuracies better than at least 1 km s^{-1} , in order to complement proper motions and the correct identification of members, and to study internal dynamics within clusters (see Figure 3.75)

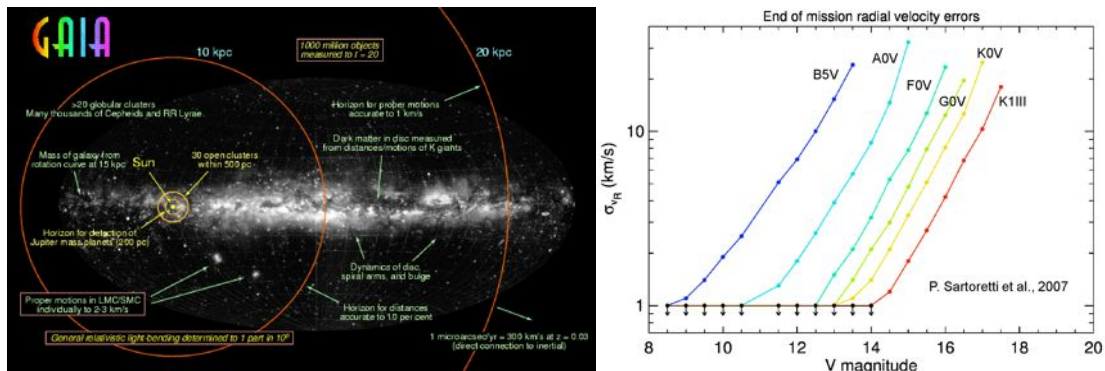


Figure 3.75: Left: How Gaia will see the Galaxy. Right: Accuracy of the radial velocities provided by Gaia as a function of the V magnitude and the spectral type.

- Gaia will yield radial velocities up to $V=17$, but faint low- and very low mass stars in young clusters as well as solar-type stars in intermediate-age and old clusters will have a rather poor radial velocity measurement even at relatively close distances. In particular, Gaia will not provide radial velocity for most of the substellar populations in young clusters.
- Gaia will provide low- and medium-spectral resolution data
- A real 6-D study (distances and positions, coupled with galactic velocities), requires precise radial velocity measurements.
- A fine analysis of many physical properties to be derived also demands spectral resolutions in the range $R=5,000-20,000$

3.4.2.1.2 The ESO-Gaia survey

The ESO-Gaia public spectroscopic survey, targeting hundred of thousand stars, systematically covering all major components of the Milky Way, from halo to star forming regions, will provide the first homogeneous overview of the distributions of kinematics and elemental abundances. This alone will revolutionize knowledge of Galactic and stellar evolution: when combined with Gaia astrometry the survey will quantify the formation history and evolution of young, mature and ancient Galactic populations. With well-defined samples, we will survey the bulge, thick and thin discs and halo components, and open star clusters of all ages and masses. The data will be obtained with the FLAMES spectrograph. The collected spectra will: quantify individual elemental abundances in each star; yield precise radial velocities for a 5-D kinematic phase-space; map kinematic gradients and abundance - phase-space structure throughout the Galaxy; follow the formation, evolution and dissolution of open clusters as they populate the disc, and provide a legacy dataset that adds enormous value to the Gaia mission and ongoing ESO imaging surveys. However, one obvious handicap will be the young, crowded stellar associations, since a significant number of cluster members will not be observed (due to the limited amount of fibers and the spatial distribution of possible targets within the large FOV of FLAMES). Moreover, Northern clusters will be left out of the survey.



3.4.2.2 Objectives

Gaia will provide a new window, a new era in stellar astrophysics, by providing essential astrophysical parameters in a comprehensive manner to the whole scientific community. From exoplanets to general relativity and quasar evolution, most field of Astrophysics (and some of Physics) will be changed. Both the European and the Spanish community are heavily involved in the Gaia exploitation. In particular, our team has been working with DPAC and developing specific projects to take full advantage of this opportunity.

Our main goal is to complement Gaia and ESO-Gaia data. Specifically, we will study the low-mass star formation in the Gould Belt (complete census, and stellar properties such as accretion, characterization of the lowest, planetary-mass objects), and extending the study to the Perseus Arm, in a completely different environment within the Galaxy.

3.4.2.3 Methodology

We plan to collect optical spectra covering the range between 6,000-9,000Å. This spectral range contains age indicators (e.g. lithium absorption line, Na and K gravity-sensitive lines), activity, accretion and outflow/jet indicators (e.g. H α line, Helium and Sulphur forbidden lines, Calcium triplet). The analysis of all these features will allow to classify the targets as bona-fide cluster members, and to estimate their age.

3.4.2.3.1 Chemical abundances

We will be able to carry out analysis of abundances using comparison with templates and spectral synthesis (such as MOOG, Sneden et al. 1973, 2009), specifically for the G and K stars, using the multiple iron lines located in this wavelength range. The treatment of highly obscured areas (and very young associations) will be come complicated, due to the effect of reddening and veiling (when a strong accretion is present). To minimize this effect, we will give more weight to the analysis in the redder part of the spectrum, where the continuum and the lines are less affected by these effects.

3.4.2.3.2 Ages

We will use different spectral features to derive the ages of young low-mass stars: the lithium absorption line (6708 Å) is expected to be intense in very young objects and will be compared with the lithium content of different clusters and associations. Some alkali lines (e.g. Sodium doublet: 8184Å and 8195Å) are gravity-sensitive, and therefore, well suited to estimate the age of the observed sample (see e.g. Bayo et al. 2011 for a full description of the methodology).

In addition, we will be able to use the Lithium Depletion Boundary technique (Stauffer et al. 1998, 1999; Barrado et al. 1999, 2004, 2012) in order to derive accurate, independent ages for clusters older than 10 Myr.



3.4.2.4 *Sample*

The sample of clusters and stellar associations to be observed will be selected based on the Gaia mission, ground-based surveys of the regions (e.g. CFHT/WIRCAM) and space missions archives (e.g. Spitzer, Akari).

The role of Gaia: Stellar associations as ideal Gaia targets

- 1800 (1400 confirmed) open clusters (Dias et al. 2002). We have selected target both in the Gould Belt and the Perseus Arm.
- From 1 Myr to 10 Gyr, and metallicities [Fe/H] from -0.5 dex to +0.4 dex.
- Gaia will allow us to drastically reduce the errors in distance to almost all known clusters. Gaia will indeed measure distances for *individual* stars in open clusters with a precision better than 1% for the nearby ones, within 1 kpc from the Sun, and better than 10% for almost the entire open-cluster family (only a few ones are farther than 10 kpc).
- An even higher precision will be reached for proper motions, leading to an accurate definition of membership.

Most stellar associations have angular sizes below a dozen arcminutes. They can be fitted in a multiobject spectrograph such as the MEGARA MOS mode.

The role of Spitzer: setting the stage for comprehensive protostellar taxonomy.

The Spitzer Space Observatory has done a superb job in stellar formation studies and a number of papers dealing with mid-IR spectroscopy have been published, mainly concentrated on Taurus members (see Calvet et al. 2005; Kessler-Silacci et al. 2006; Furlan et al. 2006, 2008). Some non-homogeneous analysis has been carried out on few Serpens and IC 1396A members (Reach et al. 2009; Boogert et al. 2008), among others. Moreover, a significant number of Class 0-II low-mass objects located in different, nearby star forming regions are accessible with new, sensitive ground-based instrumentation such as CanariCam. Spitzer has produced a very comprehensive photometric database covering the range 3.6-24 micron with IRAC and MIPS. However, Spitzer has the handicap of the lack of spatial resolution. In addition, several studies have extended the data up to sub-, milli-, and centimeter wavelengths (Dunham et al. 2008; Kauffmann et al. 2008; Froebrich 2005; Wu et al. 2007), helping to produce complete SEDs. This wealth of data is ready for fully scientific exploitation for complementary photometric and spectroscopic observations in the optical, near- and mid-IR, and to tackle the problem of low-mass evolution. The synergy between ground and space-based observations will allow us to carry out a detailed taxonomy of the sources covering a rather extensive space-parameter in luminosity, mass, temperature, SED shape, and possibly disk inclination.

The role of GTC

MEGARA and CanariCam will have a superb sensitivity. In addition, CanariCam will provide an exceptional spatial resolution, which will be able to detect faint companions at 0.2 arcsec (30AU at 140pc). Observations done at different wavelengths and taken with different techniques would provide a uniform database, a requirement for a correct classification of YSO.

Spectral features available such as H α , the Calcium Triplet, NaI8200 (stellar classification, accretion and age indicators) in the optical (MEGARA), and on the other hand PAH, ices and silicates from the disk in the mid-IR (CanariCam), plus the available Spitzer data, are essential to link stellar and disk evolution. In addition, it will provide a wide multiobject capability with high-spectral resolution, large enough to measure very accurate radial velocities and to study different properties, as detailed above.

1.1.1.4.1 Stellar Associations in the Gould Belt

Target selection and ancillary data: the targets will be selected from the analysis of data produced by with Spitzer data, complemented with the All Sky Survey carried out with the Japanese satellite Akari and Gaia. The Herschel Space telescope, successfully launched in May 2009, and Spica, after its launch beyond 2017, will be producing new results in this sense. Additional synergies will be obtained with the Mid-Infrared Instrument (MIRI) aboard of JWST (scheduled for launch in 2018) and with ALMA.

We will select three young clusters (<100 Myr), in order to mainly study star formation and evolution of stellar properties (such as NGC1333+IC348, NGC7160, IC4665).

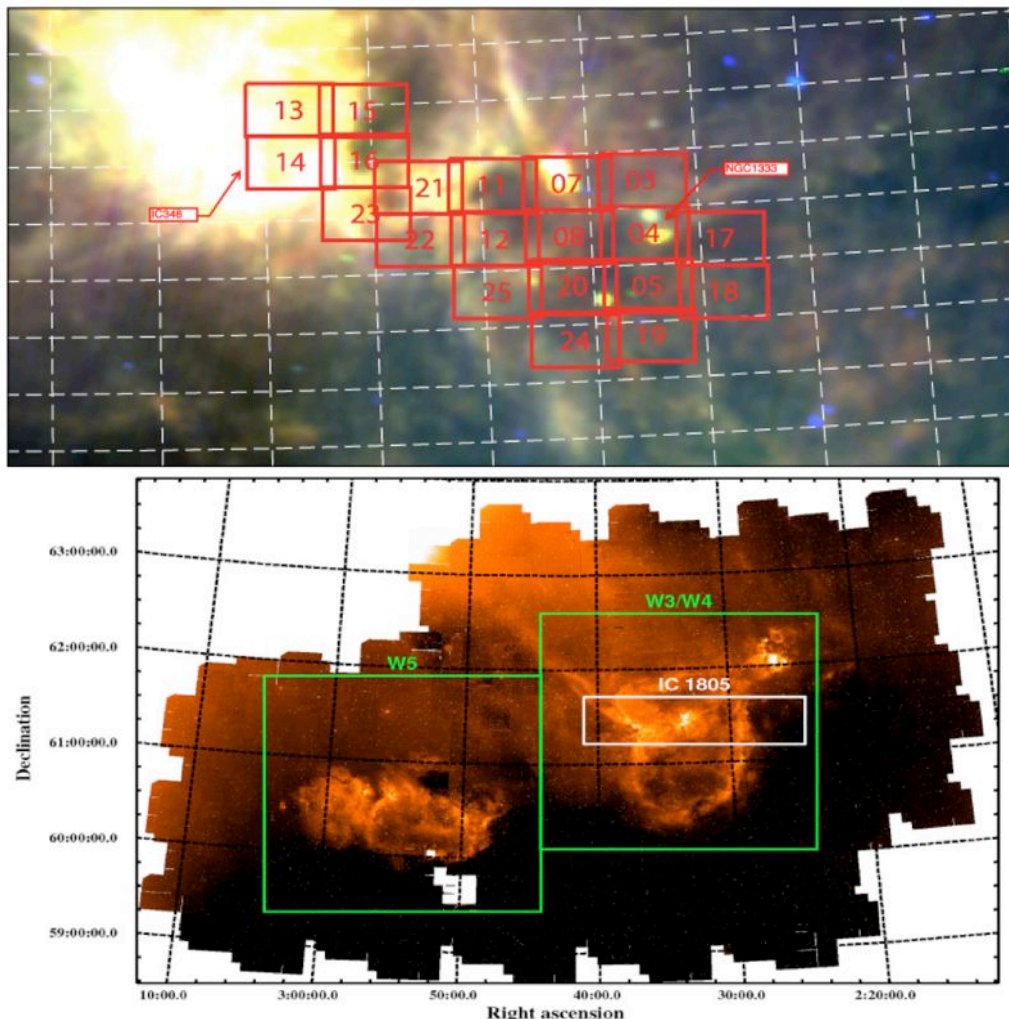


Figure 3.76: Our optical-nearIR surveys in IC348+NGC1333 and the star forming complex W3-W4-W5, all in the Gould Belt.



1.1.1.4.2 Perseus Arm

- The Perseus Arm is located in the antagalactic center.
- A prime target for GTC.
- Distance 1,500-5,000 pc, $\delta > -20^\circ$, 103 clusters, diameter 5-10 arcmin.
- Outer-disk clusters allow extending the range in metallicities and ages.

As in the case of the Gould Belt, we will select few stellar associations at different evolutionary stages. Among them, the complex formed by W3-W4 and W5 (Figure 3.76).

1.1.1.5 Observations

Required set-ups and observational Strategy

We will make use of the 92 positioners within the 3.5×3.5 arcmin² FOV of the MEGARA MOS.

- HR-R and HR-I VPHs at $R=19,000$ for $H\alpha$, Lithium at 6708\AA , forbidden lines (from outflows and jets), and the Calcium Infrared Triplet (accretion, activity, and to derive very accurate radial velocities). We aim to reach $S/N=20$ and 10 , respectively. We note that the continuum is not very important in this case, since we are interested in emission lines (except in the case of Lithium).
- LR-R and LR-I at $R=6200$ for $H\alpha$, Lithium, Sodium at 8200\AA , and in general metallicity. The goal is reaching $S/N=50$. In this case, the continuum is very important, since our aim is to study absorption lines (from alkali – $\text{LiI}6708$, $\text{NaI}8200$), iron or calcium lines.

The nearby associations (IC1333 at 250 pc, IC348 at 300 pc) in the Gould Belt would need about 25 pointings to cover about 20×20 arcminutes, each of them about 1 hour long. This leads a total of 75 h plus overheads (i.e. **~90 hours total**) and allow to characterize the substellar population down to 20 M_{Jup} , corresponding to $I=21$ mag for HR-R, or $I=18.1$ for LR-R, assuming 300 pc, 3 Myr and a moderate extinction for IC348. Similar results can be achieved for NGC1333, due to its younger age and closer distance (1 Myr, 250 pc), but higher internal reddening.

The Perseus Arm associations are much smaller in angular sizes, but are further away. Thus, each of them would need 3 hours in a 3×3 grid, giving a total 81 h plus overheads (i.e. **~97 hours total**) to reach the substellar regime $\sim 50 M_{\text{Jup}}$ ($I=22.1$ mag for HR-R, assuming an average distance of 2,500 pc).

The observational strategy is simple: the cluster candidate members will be classified in groups with different magnitude ranges. For each group, we will position the fibers on the objects and integrate in order to reach the S/N described above.

The confirmed candidates with most extreme properties and adequate brightness will be followed-up with high-resolution spectroscopy, in order to characterize accretion and its variability through $H\alpha$ observations, and derive accurate radial velocities.



4. MEGARA EARLY SCIENCE / TARGETS OF INTEREST

In this section we briefly describe some of the Early Science observations proposed to be obtained with MEGARA. These observations and the Targets of Interest (ToI) proposed should serve (1) to put to test all observing models in MEGARA, (2) to demonstrate the capabilities and versatility of MEGARA for carrying out various scientific projects and (3) to produce early scientific return and visibility for the instrument and GTC.

Observing Modes		IFU						MOS						
NGC 604														
Pointings/fields	Setup	LR-U	LR-B	LR-V	LR-R	LR-I	Total*	MR-U	UB	MR-B	MR-G	HR-R	LR-U	Total
3 (p1-p3)	t(exp)	2h	1.5h	1.5h	1h	1h	24 h	1h	1h	1h	1h	1h	2h	24 h
M81														
Pointings/fields	Setup	LR-U	LR-B	LR-V	LR-R	LR-I	Total*	MRU	UB	MRB	MRG	HR-R	LR-U	Total
3 (p1-p3)	t(exp)	2h	1.5h	1.5h	1h	1h	24 h	1h	1h	1h	1h	1h	2h	24 h
Stephan's Quintet														
Pointings/fields	Setup	HR-R												Total
3 (p1-p3)	t(exp)	2h												7 h
NGC 7027														
Pointings/fields	Setup	LR-U	LR-B	LR-V	LR-I	HR-R	Total*	LR-U	LR-B	LR-V	LR-R	LR-I		Total
1 (p1)	t(exp)	1h	0.5h	0.5h	0.5h	1.5h	5 h	1h	1h	1h	0.5h	0.5h		5 h
LRG 3-757 (Einstein ring)														
Pointings/fields	Setup	LR-V					Total*							
1 (p1)	t(exp)	6h					7 h							

*Total exposure times include 15% overheads due to readout time, acquisition & blank-sky observations.

Table 4.1: Summary of observing times to be devoted to the Targets of Interest (ToIs) as part of MEGARA's Early Science.

4.1 NGC 604

NGC604 is brightest HII region in the Local Group galaxy M33 and along with 30 Doradus are the two prototypical Giant HII Regions (GHR) in the Local Group. It is located at a distance of 840 kpc (Freedman et al. 2001). This along with a very low foreground MW extinction (González Delgado & Pérez 2000) make of NGC 604 an ideal target for Early Science observations with MEGARA. This region is powered by a massive young cluster with roughly 200 O and WR stars (Maíz-Apellániz 2001; Hunter et al. 1996; Drissen et al. 1993; see Figure 4.1) which is located inside a cavity in the gas distribution with kinematics that resemble those of an incomplete expanding bubble. Moreover, the brightest knots in this cluster have single-gaussian light profiles (Sabalisk et al. 1995; Maíz-Apellániz 2000, 2004), which suggest that NGC 604 is a young region where the overall dynamics are not yet dominated by the mechanical energy released by stellar winds and SNe (Tenorio-Tagle et al. 1996). In that regard NGC 604 is an excellent complement to the study of the more evolved SGW in M82.

With regard to the observing setup we will make use of the same VPHs and exposure times as for the diagnosis of the ionized-gas chemical abundances and massive-blue stars analysis described in Section 3.1.5.1 (see also Tables 3.2 and 4.1).

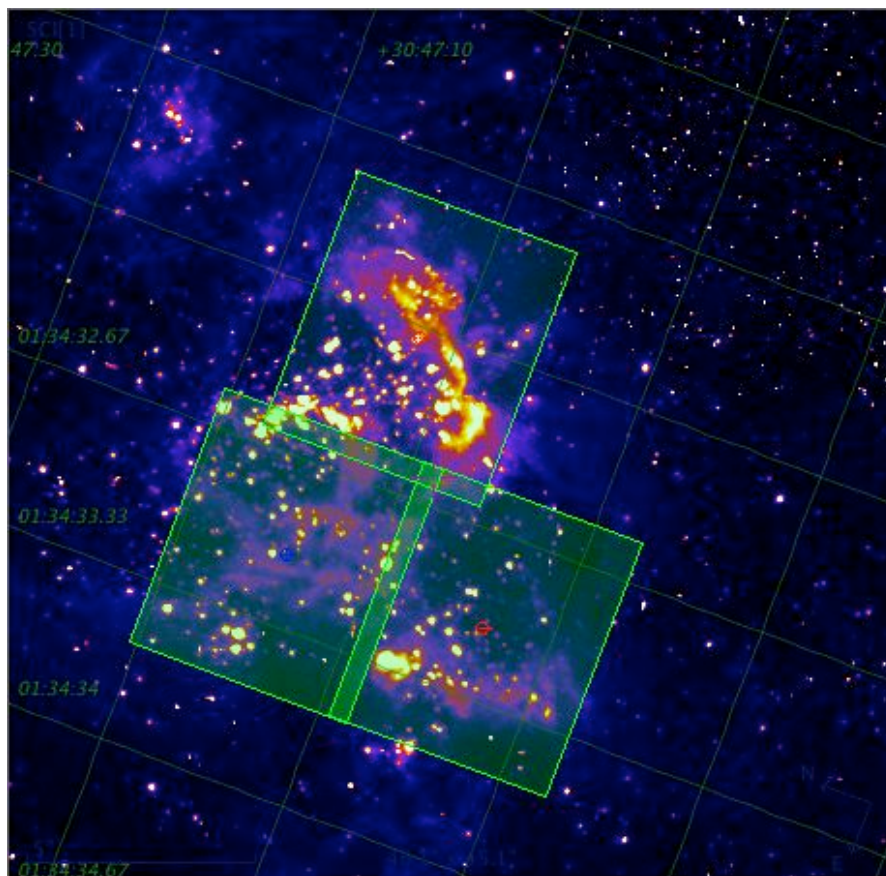


Figure 4.1: Layout of the IFU LCB map proposed for NGC 604 as part of the MEGARA Early Science observations. The FOV covered by the 3 LCB pointings is shown on top a HST-WFPC2 F555W image.



4.2 M81

The galaxy M81 is an early-type (Sab), grand-design spiral with a quite high gas and stellar content, which provides an excellent complement to the study of the stellar populations, chemical abundance and kinematics of disks planned for M33 as part of MEGADES.

Moreover, M81 contains a large number of both Compact Stellar Clusters (CSCs) and Globular Clusters (GCs) (Chandar et al. 2001; Santiago-Cortés et al. 2010), amounting a total of 263 CSCs brighter than $B=22$ mag in 29 HST/ACS field and 172 GCs (Santiago-Cortés et al. 2010). This allows, by means of a deep spectroscopic study of both samples (see e.g. Mayya et al. 2011), determining whether or not there is an evolutionary connection between both type of objects as previously claimed (de Grijs & Parmentier 2007).

Unfortunately, due to the much larger distance of M81 (3.7 Mpc) compared with that of M33 (the M81 distance modulus is roughly 3 mag fainter than that of M33), the study that we aim to carry out on M81 is necessarily less ambitious than that described for M33 throughout this document. It is because of this limitation that we will restrict this Early Science project on M81 to the study of its massive blue stars and population of CSCs and GCs (see below).

Regarding the study of massive blue stars, as for the case of M33, we will use ~ 8 hours (overheads included) per pointing split among the LR-U, MR-U, MR-UB, MR-G, HR-R spectral setups (see Table 4.1), or **24 hours** for the three pointings proposed (see Figure 4.2). Here we should be able to study only stars brighter than $M_v = -9$ mag ($V=19$ mag at the DM of M81). Note that the observations with the LR-U allow extending the wavelength range to the blue end of the optical spectrum, which is relevant for improving the spectral coverage and therefore the precision in the age dating of CSCs and GCs and for the diagnosis of the diffuse ionized-gas. Regions of ionized-gas emission are expected to be present both in the MOS observations proposed here or in parallel IFU observations, should MEGARA-Advanced be available.

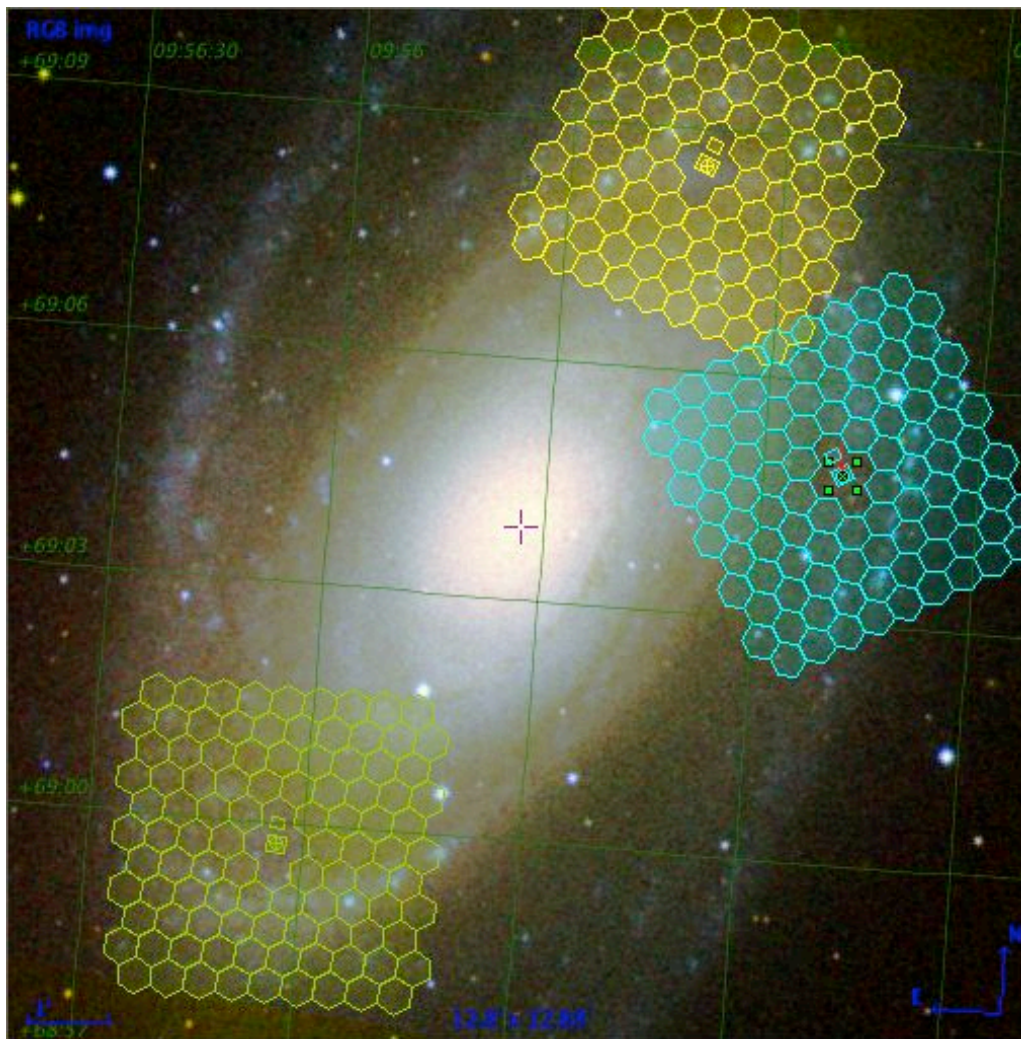


Figure 4.2: False-color DSS image of M81 with the proposed observations with the MEGARA MOS overplotted. HST using ACS-WFC observations has covered the entire face of M81.

4.3 Stephan's quintet: A galaxy-scale shock in a group of galaxies

Since the discovery of Stephan's Quintet (SQ) in 1877 it has become a paradigm in the field of galaxy interactions: tidal tails extending out of the main galaxies, diffuse material and strong starbursts show evidences of multiple past and ongoing collisions involving four of the ancient and present day group galaxies. But perhaps the feature that has most attracted the curiosity of the astronomers is the presence of a shock induced by the high velocity collision ($\sim 1,000 \text{ km s}^{-1}$) of an intruder galaxy with the intragroup medium. This shock has been surveyed at different wavelengths from radio continuum to X-rays. A recent optical spectroscopic study with IFU data (Iglesias-Páramo et al. 2012) shows that the shock involves at least two kinematically independent gaseous components, which appear severely blended along the ridge of the shock. The high resolution MEGARA capabilities with the HR-R setup will contribute to improve the analysis of the ionized components and thus to shed light on the intriguing evolutionary history of SQ. A total of 3 pointings with 2h-long total exposure per pointing will be secured.

4.4 NGC 7027: a multipolar PN in the making.

This is a widely studied young, dense PN with a dynamical age of ~ 600 yr. Due to its proximity (~ 900 pc), its high surface brightness and exceedingly rich spectrum at all wavelengths, NGC7027 has been one of the most intensively observed astronomical objects.

High angular-resolution optical images with HST show a bright, ellipsoidal ionized nebulosity of dimensions $\sim 14'' \times 9''$ (see Figure 4.3; Latter et al. 2000). The footprint of underlying bipolar ejections emanating from the nucleus along different axes is patent in these central regions. The bright central nebula, which is also partially composed of neutral gas and dust, is surrounded by a faint, round halo of dust and molecular gas that can be traced out to a radius of $\sim 40''$ in the optical images. Several bright, concentric ring-like features are observed in the halo, which is the AGB envelope remnant (Navarro et al. 2003). A dark line in the equatorial plane reveals a dense, dusty disk or torus obscuring the central star, with an effective temperature of $\sim 200,000$ K (Zhang et al. 2005) and an inferred progenitor mass of $4 M_{\odot}$.

The optical line emission spectrum of NGC 7027 shows a wealth of recombination and forbidden emission lines arising at the central photoionized and photodissociated nebulae. Spatial variations in temperature and density of the ionized gas as well as ionization and elemental abundance inhomogeneities have been investigated previously based on long-slit spectroscopy (e.g. Biegging et al. 2008). A more complete picture of the structural details in this dynamically evolving nebula awaits further high sensitivity observations with both spatial and spectral resolution, such as those proposed here with MEGARA. The objective and observing time to be devoted regarding the study of NGC 7027 are described in detailed in Section 3.2.

As a curiosity, NGC 7027 served as a target for CanariCam early commissioning observations.

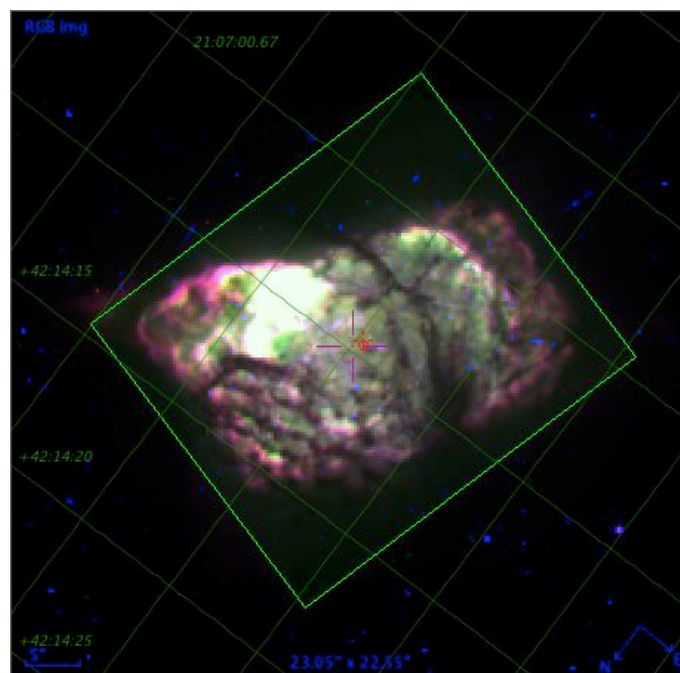


Figure 4.3: Layout of the IFU LCB pointing proposed for NGC 7027 as part of the MEGARA Early Science observations. The background RGB image is composed of HST/WFPC2 F658N, F631N, F502N.

4.5 Einstein ring LRG 3-757

As a prototype of strong lensing we will also study, as part of these MEGARA Early Science observations, the case of the galaxy-galaxy lens system produced by the red galaxy LRG 3-757 [RA(J2000)=11h48m33.33s; Dec(J2000)=+19°30'3.2"] that shapes a nearly complete blue Einstein ring with ~ 10 arcsec diameter known as the 'Cosmic Horseshoe' (J1148+1930; see Figure 4.4). Low-resolution spectroscopy by Belokurov et al. (2007) showed that the lens is a massive luminous red galaxy ($M \sim 6 \times 10^{12} M_{\odot}$) at $z = 0.444$ while the ring is a gravitationally lensed image of a star-forming galaxy at $z = 2.379$. The best estimate of the magnification factor suggests a value of 24 ± 2 (Dye et al. 2008).

This object has been previously studied in long-slit spectroscopy by Quider et al. (2008) using ESI at Keck-II for a total observing time of ~ 10 hours. The observations proposed here will serve (1) to determine the physical properties of the high-redshift lensed galaxy, (2) to improve the mass modeling of the host galaxy by means of combining 2D gravitational-lensing constraints and stellar kinematics of the lens galaxy (Trott et al. 2010) and (3) to show the advantage of IFU observations over traditional long-slit spectroscopy for studying these objects.

With these objectives in mind we aim to obtain a 6 hours-long spectrum in one single setup (LR-V) that will allow us (1) to study the stellar kinematics of the host galaxy in the CaII H+K region and (2) to improve the S/N of a part of the rest-frame UV spectrum of this object in least a factor of $\times 2$ compared to the Keck II observations by Quider et al. (2008). In this regard, our observations will allow us to study in unprecedented detail the interstellar absorption lines SiII $\lambda 1527\text{\AA}$ and CIV $\lambda\lambda 1548, 1551\text{\AA}$ in the galaxy at $z = 2.379$.

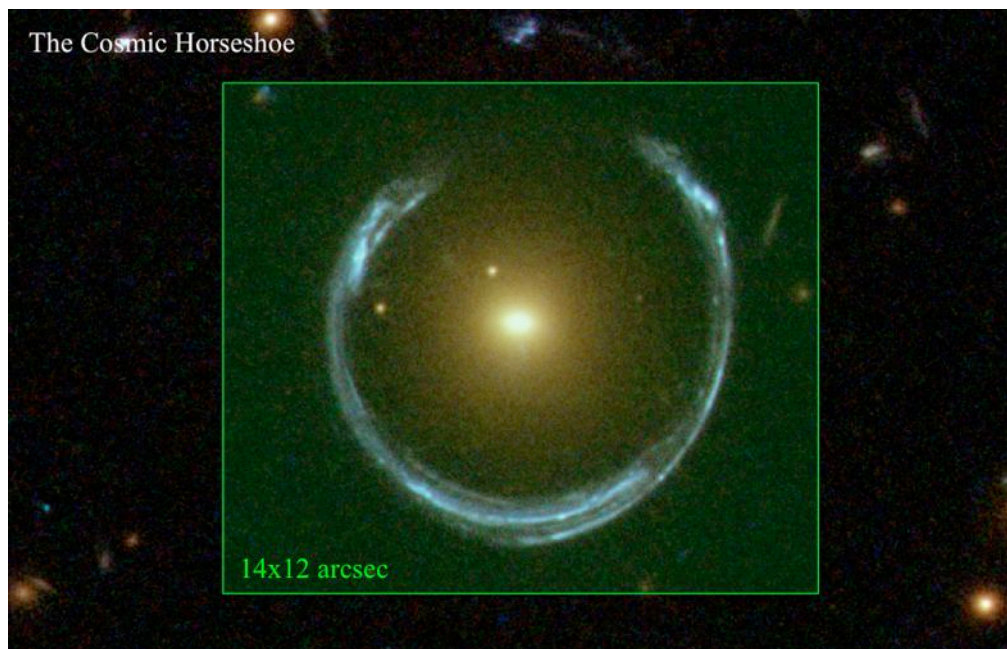


Figure 4.4: Layout of the IFU LCB pointing on top of The Cosmic Horseshoe centered on the lens galaxy LRG 3-757. Note the excellent match between the LCB and the apparent size of this nearly complete Einstein ring (background false-color image comes from recent HST/WFC3 observations).



5. BIBLIOGRAPHY

Abraham, R. G., et al. 2007, ApJ, 669, 184

Aller, L., 1942, ApJ, 95, 52

Amorín, R., Pérez-Montero, E., Vílchez, J.M., 2010, ApJ, 715L, 128

Aparicio, A., & Gallart, C., 2004, AJ, 128, 1465

Armandroff, T. E., & Da Costa, G. S., 1991, AJ, 101, 1329

Arnouts, S., et al. 2007, A&A, 476, 137

Asplund, M., et al. 2005, “Cosmic Abundances as Records of Stellar Evolution and Nucleosynthesis”, 336, 25

Asplund, M., et al. 2009, ARA&A, 47, 481

Baba, J., et al. 2009, ApJ, 706, 471

Babul, A., & Rees, M. J., 1992, MNRAS, 255, 346

Baaede, W., 1963, JRASC, 57, 232

Bakos, J., et al. 2008, ApJ, 683, 103

Balick, B., & Frank, A. 2002, ARA&A, 40, 439

Balogh, M., et al. 1999, ApJ, 527, 54

Balogh, M., et al. 2004, ApJ, 615, 101

Barker, M., et al. 2007, AJ, 133, 1125

Barrado y Navascués, D., et al. 1999, ApJ, 522, 53

Barrado y Navascués, D., et al. 2004, ApJ 610, 1064

Barrado y Navascués, D., et al. 2007, ApJ, 664, 481

Barrado y Navascués, D., et al. 2012, in preparation

Barro, G., et al. 2010, hsa5.conf, 259

Barro, G., et al. 2011a, ApJS, 193, 13

Bayo, A., et al. 2011, A&A, 536, 63

Belley, J., & Roy, J.R., 1992, ApJS, 78, 61

Bekki, K., 2008, MNRAS, 390, 24

Bekki, K., 2009, MNRAS, 399, 2221

Benítez, N., et al. 2009, ApJ, 692, L5

Bernard, E. J., et al. 2007, AJ, 134, 1124



- Biegging, J. H., Boley, P.A., Latter, W.B., & Tielens, A.G.G.M., 2008, ApJ, 676, 390
- Blain, A. W., 1997, MNRAS, 290, 553
- Boissier, S., et al. 2001, MNRAS, 321, 733
- Boissier, S., et al. 2003, MNRAS, 346, 1215
- Boissier, S., & Prantzos, N., 1999, MNRAS, 307, 857
- Boogert, A. C. A., et al. 2008, ApJ, 678, 985
- Borissova, J., et al. 2004, A&A, 413, 889
- Boselli, A., et al. 2006, ApJ, 651, 811
- Bouret, J. C., et al. 2003, ApJ, 595, 1182
- Bournaud, F., Elmegreen, B. G., & Elmegreen, D. M., 2007, ApJ, 670, 237
- Brandner, W., et al. 2000, AJ, 119, 292
- Braun, R., & Thilker, D. A., 2004, A&A, 417, 421
- Bresolin, F., et al. 2002, ApJ, 572, 838
- Bresolin, F., et al. 2005, A&A, 441, 981
- Bresolin, F., et al. 2007, ApJ, 671, 2028
- Bresolin, F., et al. 2007, ApJ, 678, 2021
- Bresolin, F., et al. 2009, ApJ, 695, 580
- Bresolin, F., et al. 2010, MNRAS, 404, 1679
- Bresolin, F., et al. 2011, ApJ, 730, 129
- Brodwin, M., et al. 2006, ApJ, 651, 791
- Brook, C., et al. 2006, ApJ, 639, 126
- Brook, C., et al. 2007, ApJ, 658, 60
- Brown, M., et al. 2007, ApJ, 654, 858
- Bujarrabal, V., Alcolea, J., Sánchez Contreras, C., & Sahai, R., 2002, A&A 389, 271
- Bundy, K., et al. 2010, ApJ, 719, 1969
- Carlson, G., & Sandage, A., 1990, ApJ, 352, 587
- Calvet, N., et al. 2005, ApJ, 630, 185
- Capak, P., Cowie, L. L, Hv, E., et al. 2004, AJ, 127, 180
- Cappellari, M., et al. 2007, MNRAS, 379, 418
- Casertano, S., et al. 1990, ApJ, 357, 435
- Castellano, M., et al. 2007, ApJ, 671, 149
- Castillo-Morales, A., et al. 2007, MNRAS, 380, 489



- Chandar, R., et al. 2001, AJ, 122, 1330
- Chapman, S. C., et al. 2003, ApJ, 599, 92
- Chary, R., & Elbaz, D., 2001, ApJ, 556, 562
- Cheng, Y., et al. 2011, arXiv:1112.3651v1
- Chita, S. M., et al. 2008, A&A, 488, L37
- Cid Fernandes, R., et al. 2005, MNRAS, 358, 363
- Cid Fernandes, R., et al. 2007, MNRAS, 375, 16
- Cid Fernandes, R., et al. 2009, ASPC, 408, 122
- Cimatti, A., et al. 2008, A&A, 482, 21
- Cirasuolo, M., et al. 2007, MNRAS, 380, 585
- Combes, F., et al. 1992, A&A, 259, 27
- Conti, P. S., 1984, IAUSymp. 105, p.253
- Cooper, M. C., et al. 2007, MNRAS, 376, 1445
- Cooper, M. C., et al. 2008, MNRAS, 383, 1058
- Cooper, A. P., et al. 2010, MNRAS, 406, 744
- Corbelli, E., & Schneider, S. E., 1997, ApJ, 479, 244
- Croton, D. J., et al. 2006, MNRAS, 365, 11
- Crowther, P. A., 2007, ARA&A, 45,177
- Daddi, E., et al. 2005, ApJ, 626, 680
- Daddi, E., et al. 2007, ApJ, 670, 173
- Daddi, E., et al. 2009, ApJ, 694, 1517
- Dahlem, M., et al. 1998, AJS, 118, 401
- Davidge, T. J., & Puzia, T. H., 2011, ApJ, 738, 144
- Davies, G. T., et al. 2009, MNRAS, 395, 76
- Davis, M., et al. 2007, ApJ, 660, 1
- De Avillez, M. A., et al. 2002, ApJ, 581, 1047
- De Grijs, R., & Parmentier, G., 2007, ChJAA, 7, 155
- Debattista, V. P., et al. 2005, ApJ, 628, 678
- Debattista, V. P., et al. 2006, ApJ, 645, 209
- Dekel, A., & Silk, J., 1986, ApJ, 303, 39
- De Vaucouleurs, G., et al. 1978, ApL, 19, 105



- Dias, W.S., et al. 2002, A&A, 389, 871
- Diaz, A. I., et al. 1991, MNRAS, 253, 245
- Diaz, A. I., et al. 1992, ASPC, 31, 181
- Dickinson, M., et al. 2003, ApJ, 587, 25
- Dodorico, S., et al. 1980, A&AS, 40, 67
- Dolphin, A., et al. 2001, ApJ, 550, 554
- Dressler, A. J., et al. 1980, ApJ, 236, 351
- Drissen, L., et al., 1993, AJ, 105, 1400
- Dunham, M. M., et al. 2008, ApJS, 179, 249
- Dye, S., et al. 2008, MNRAS, 388, 384
- Efstathiou, G., 1992, MNRAS, 256, 43
- Egami, E., et al. 2006, ASPC, 357, 242
- Egami, E., et al. 2010, A&A, 518, 12
- Eisenhardt, P. R., et al. 2008, ApJ, 684, 905
- Eke, V., et al. 1998, MNRAS, 298, 1145
- Elbaz, D., et al. 2007, A&A, 468, 33
- Eliche-Moral, M. C., et al. 2006, A&A, 457, 91
- Eliche-Moral, M. C., et al. 2011, A&A, 533A, 104
- Eliche-Moral, M. C., et al. 2012, A&A submitted.
- Ellison, S., et al. 2011, MNRAS, 418, 2043
- Elmegreen, B. G., et al 2004, ApJ, 604, 21
- Elmegreen, B. G., et al 2005, ApJ, 631, 85
- Elmegreen, B. G., & Elmegreen, D. M., 2005, ApJ, 627, 632
- Elmegreen, B. G., & Elmegreen, D. M., 2006, ApJ, 650, 644
- Elmegreen, D. M., & Elmegreen, B. G., 2006, ApJ, 651, 676
- Elmegreen, D. M., & Elmegreen, B. G., 20a07, ApJ, 658, 763
- Englmaier, P., & Shlosman, I., 2004, ApJ, 617, 115
- Erb, D. K., et al. 2006, ApJ, 644, 813
- Erwin, P., & Sparke, L., 2002, AJ, 124, 65



- Erwin, P., & Sparke, L., 2003, *ApJS*, 146, 299
- Esteban, C., et al. 2002, *ApJ*, 581, 241
- Esteban, C., et al. 2004, *MNRAS*, 355, 558
- Esteban, C., et al. 2009, *ApJ*, 700, 654
- Evans, C. J., et al. 2005, *A&A*, 437, 467
- Evans, C. J., et al. 2008, *The Messenger*, 131, 25
- Evans, C. J., et al. 2010, *IAU, Symposium*, 266, 35
- Faber, S., et al. 1985, *ApJS*, 57, 711
- Faure, C., et al. 2004, *A&A*, 428, 741
- Ferguson, A., et al. 2007, "Island Universes", *Ap&SS*
- Ferguson, A., & Clarke, C. J., 2001, *MNRAS*, 325, 781
- Ferland, G. J., et al. 1998, *PASP*, 110, 761
- Ferrini, F., et al. 1994, *ApJ*, 427, 745
- Flores, H., et al. 1999, *ApJ*, 517, 148
- Font, A., et al. 2001, *ApJ*, 563, 1
- Fontana, A., et al. 2004, *A&A*, 424, 23
- Forster-Schreiber, L., et al. 2006, *The Messenger*, 125, 11
- Franceschini, A., et al. 2001, *A&A*, 378, 1
- Freedman, W., 1988, *ApJ*, 326, 691
- Freedman, W., et al. 1994, *Nature*, 371, 757
- Freedman, W., et al. 2001, *ApJ*, 553, 47
- Freeman, K.C., et al. 2001, *ApJ*, 160, 81
- Friedli, D., et al. 1994, *ApJ*, 430, 105
- Froebrich, D., et al. 2005, *ApJS*, 156, 169
- Fujita S., et al. 2003, *ApJ* 586, L115
- Furlan, E., et al. 2006, *ApJS*, 165, 568
- Furusawa, H., et al. 2008, *ApJS*, 176, 1
- Gal-Yam, A., et al. 2007, *AJ*, 656, 372
- Gallagher, J. S., Hunter, D. A., & Bushouse, H., 1989, *AJ*, 97, 700
- García, M., et al. 2009, *A&A*, 502, 1015
- García, M., et al. 2010a, *A&A*, 523, 23



- García, M., et al. 2010b, *Cat*, 35021015
- García-Lorenzo, B., et al. 2005, *ApJ*, 621, 146
- García-Rojas, J., et al. 2004, *ApJS*, 153, 501
- García-Rojas, J., et al. 2005, *MNRAS*, 362, 301
- García-Rojas, J., et al. 2006, *MNRAS*, 368, 253
- García-Rojas, J., et al., *RMxAA*, 43, 3
- García-Segura, G., et al. 1999, *ApJ*, 517, 767
- Garnett, D. R., 1998, "Abundance Profiles: Diagnostic Tools for Galaxy History", *ASPC*, 147, 78
- Gavilan, M., et al. 2009, "Star-forming Dwarf Galaxies: Ariadne's Thread in the Cosmic Labyrinth" (astro-ph/0903.0932)
- Gerke, B., et al. 2007, *MNRAS*, 376, 1425
- Gilbert, K. M., et al. 2009, *ApJ*, 705, 1275
- Gil de Paz, A., et al. 2003, *ApJS*, 147, 29
- Gil de Paz, A., et al. 2005, *ApJ*, 619, 115
- Gil de Paz, A., et al. 2007, *ApJ*, 661, 115
- Gil de Paz, A., et al. 2012, *ApJ* in prep.
- Gil de Paz, A., & Madore, B.F., 2005, *ApJS*, 156, 345
- Gil de Paz, A., Madore, B.F., Pevunova, O., et al. 2003, *ApJ*, 147, 29
- Glazebrook, K., 2004, *Nature*, 430, 181
- Gómez, F., et al. 2012, *MNRAS*, 419, 2163
- Gonzalez, A
- González Delgado, M. R., et al. 2005, *MNRAS*, 357, 945
- González Delgado, M. R., & Pérez, E. et al. 2000, *MNRAS*, 317, 64
- Gorgas, J., et al. 1993, *ApJS*, 86, 153
- Gouliermis, D., et al. 2008, *ApJ*, 688, 1050
- Grevesse, N., & Sauval, A.J., 1998, *SSR*, 85, 161
- Haiman, Z., Loeb, A., 1997, *ApJ*, 483, 21
- Heavens, A., et al., 2004, *Nature*, 428, 625
- Heckman, T.M. et al. 1990, *ApJS*, 74, 833
- Heckman, T. M., et al. 2000, *AJS*, 129, 493



- Heger, A., & Langer, N., 2000, ApJ, 544, 1016
- Heger, A., et al. 2003, ApJ, 591, 288
- Henney, W. J., & Stasińska, G., 2010, ApJ, 711, 881
- Henry, R. B., et al. 2010, ApJ, 724, 748
- Henry, R. B., & Worthey, G., 1999, PASP, 111, 919
- Hensler, G., & Recchi, S., 2010, IAUS, 265, 325
- Herrero, A., et al. 2010, A&A, 513, 70
- Herrero, A. & Lennon, D. J., 2004, IAU Symp. 215, ASP, p. 209
- Hillier, D. J., & Miller, D. L., 1998, ApJ, 496, 407
- Holmberg, J., Nordström, B., & Andersen, J., 2009, A&A, 501, 941
- Hopkins, A. M., 2004, ApJ, 615, 209
- Hopkins, A. M., & Beacom, J.F., 2006, ApJ, 651, 142
- Hopkins, P. F., et al. 2008, ApJS, 175, 356
- Humphreys, R.M., & Sandage, A., 1980, ApJS, 44, 319
- Hunter, D. A., et al., 1996, ApJ, 468, 633
- Hunter, I., et al. 2008, A&A, 479, 541
- Hunter, I., et al. 2008, ApJ, 676, L29
- Iglesias-Páramo, J., et al. 2012, arXiv1201.4030I
- Jahnke, K., et al. 2004, ApJ, 614, 568
- James, B. L., et al., 2009, MNRAS, 398, 2
- Jannuzi, B. T., & Dey, A., 1999, ASPC, 191, 111
- Jenkins, E. B., 2009, ApJ, 700, 1299
- Jiménez-Vicente, J., et al. 2007, MNRAS, 382, L16
- Jones, T., et al. 2010, ApJ, 725, 176
- Juneau, S., et al. 2005, ApJ, 619, 135
- Karakas, A. I., 2010, MNRAS, 403, 1413
- Kauffmann, G., et al. 2003, MNRAS, 341, 33
- Kauffmann, G., et al. 2008, A&A, 487, 993
- Kazantzidis, S., et al. 2008, ApJ, 688, 254
- Kazantzidis, S., et al. 2009, ApJ, 700, 1896



- Keenan, F. P., et al. 2001, Proc. Natl. Acad. Sci., 98, 9476
- Kennicutt, R. C., Jr., 2003, ApJ, 591, 801
- Kennicutt, R. C., Jr., et al. 2003, PASP, 115, 928
- Kessler-Silacci, J., et al. 2006, ApJ, 639, 275
- Kewley, L. J., & Dopita, M. A., 2002, ApJS, 142, 35
- Kewley, L. J., & Ellison, S. L., 2008, ApJ, 681, 1183
- Kneib, J. P., et al. 2004, MNRAS, 349, 1211
- Kneib, J. P., et al. 2005, A&A, 434, 819
- Kobulnicky, H., & Skillman, E. D., 1995, ApJ, 454, 121
- Koch, A., et al. 2008, ApJ, 689, 958
- Koleva, M., et al. 2009, A&A, 501, 1269
- Kong, X., 2004, A&A, 425, 417
- Koposov, S., et al. 2009, ApJ, 696, 2179
- Kormendy, J., & Kennicutt, R. C. Jr, 2004, ARA&A, 42, 603
- Kotak, R., & Vink, J. S., 2006, A&A, 460, L5
- Kriek, M., et al. 2008, ApJ, 677, 219
- Kudritzki, R. P., et al. 1995, "Science with the VLT", 246
- Kudritzki, R. P., & Puls, J., 2000, ARA&A, 38, 613
- Kudritzki, R. P., 2010, AN, 331, 459
- Kwitter, K. B., & Aller, L. H., 1931, MNRAS, 195, 939
- Labbé, I., et al. 2007, ApJ, 665, 944
- Lacey, C. G., & Fall, S. M., 1985, ApJ, 290, 154
- Latter, W.B., et al. 2000, ApJ, 539, 783
- Laurikainen, E., et al. 2010, MNRAS, 405, 1089
- Le Fevre, O., et al. 2005, A&A, 439, 845
- Lee, J., et al. 2009, ApJ, 706, 599
- Lehnert, M.D., & Heckman, T.M., 1996, AJ, 462, 651
- Leisy, P., & Dennefeld, M., 2006, A&A, 456, 451
- Leitherer, C., 1998, VIII IAC Winter School of Astrophysics, CUP
- Li, J., et al. 2004, A&A, 420, 89
- Liang, Y. C., et al. 2007, A&A, 473, 411



- Lin, D. N. C., Pringle, J. E., 1987, ApJ, 320, 87
- Lilly, S. J., et al. 2007, ApJS, 172, 70
- Liu, X. W., et al. 2000, MNRAS, 312, 585
- Liu, X. W., et al. 2006, MNRAS, 368, 1959
- Liu, G.Q., Deng, L., Chávez, M., et al. 2008, MNRAS, 390, 665
- Liu, Y., Liu, X. W., Luo, S.-G., Barlow, M. J., 2004, MNRAS, 353, 1231
- Liu, X. W., Storey, P. J., Barlow, M. J., & Clegg, R. E. S., 1995, MNRAS, 272, 369
- Lotz, J. M., et al. 2011, ApJ, 742, 103
- Lozinskaya, T. A., et al. 2002, A&AT, 21, 223
- Lozinskaya, T. A., et al. 2003, AstL, 29, 77
- Lozinskaya, T. A., et al. 2003, RMxAC, 15, 284
- Lucas, P. W., et al. 2002, MNRAS, 326, 695
- Ludwig, H.-G., Caffau, E., Steffen, M., et al. 2010, IAU Symposium, 265, 201
- MacArthur, L. A., et al. 2009, MNRAS, 395, 28
- Madore, B. F., & Freedman, W. L., 1991, PASP, 103, 933
- Maeder, A., & Meynet, G., 2000, ARA&A, 38, 143
- Maeder, A., & Meynet, G., 2001, A&A, 373, 555-571
- Magrini, L., et al. 2007, A&A, 470, 843
- Maíz-Apellániz, J., et al. 2000, PASP, 112, 1138
- Maíz-Apellániz, J., 2001, AJ, 121, 2737
- Maíz-Apellániz, J., et al. 2004, AJ, 128, 1196
- Mamajek, E.E., & Hillenbrand, L.A., 2008, ApJ, 687, 1264
- Mannucci, F., et al. 2009, MNRAS, 398, 1915
- Marcillac, D., et al. 2008, ApJ, 675, 1156
- Marcum, P., et al. 2001, ApJS, 132, 129
- Marino, R. A., et al. 2012, ApJ submitted
- Markova, N., & Puls, J., 2008, A&A, 478, 823
- Marlowe, A. T., et al. 1995, ApJ, 438, 563
- Martig, M., et al. 2009, ApJ, 707, 250
- Martin, C. L., 1998, ApJ, 506, 222
- Martin, C. L., 2005, ApJ, 621, 227



- Martin, C. L., 2006, ApJ, 647, 222
- Martin, C. L., 2010, SPIE, 7735, 21
- Martin, P., & Roy, J. R., 1994, ApJ, 424, 599
- Martínez-Serrano, F. J., et al. 2009, ApJ, 705, 133
- Martins, F., et al. 2004, A&A, 420, 1087
- Massey, P., et al. 1996, ApJ, 469, 629
- Massey, P., 2003, ARA&A, 41, 15
- Masters, K. L., et al. 2010, MNRAS, 405, 783
- Matteucci, F., & Francois, P., 1989, MNRAS, 239, 885
- Mayya, Y. D., et al. 2005, ApJ, 628, 33
- Mayya, Y. D., et al. 2011, RMxAC, 40, 76
- McAlary, C. W., et al. 1984, ApJ, 276, 487
- McCall, M. L., 1982, PhDT, 35
- McCall, M. L., et al. 1985, ApJS, 57, 1
- McConnachie, A. W., et al. 2009, Nature, 461, 66
- McIntosh, D. H., et al. 2005, ApJ, 632, 191
- Meaburn, J., et al. 1988, MNRAS, 235, 479
- Melo, V. P., et al. 2005, ApJ, 619, 270
- Mendes de Oliveira, C., et al. 2004, ApJ, 605, 17
- Mermilliod, J.-C. 1995, Information and On-Line Data in Astronomy, 203, 127
- Mesa-Delgado, A., Esteban, C., & García-Rojas, J., 2008, ApJ, 675, 389
- Mesa-Delgado, A., et al. 2009, MNRAS, 394, 693
- Mesa-Delgado, A., Esteban, C., García-Rojas, J., et al. 2009, MNRAS, 395, 855
- Mesa-Delgado, A., et al. 2010, MNRAS, 405, 2651
- Moiseev, A. A., et al. 2004, A&A, 421, 433
- Mokiem, M. R., et al. 2007, A&A, 465, 1003
- Mokiem, M. R., et al. 2007, A&A, 473, 603
- Mollá, M., et al. 1996, ApJ, 466, 668
- Mollá, M., & Diaz, A. I., 2005, MNRAS, 358, 521
- Mollá, M., & Hardy, E. 2002, AJ, 123, 3055



- Mollá, M., et al. 1999, ApJ, 513, 695
- Mollá, M., et al. 2006, MNRAS, 372, 1069
- Monreal-Ibero, A., et al. 2010a, A&A, 517, 27
- Monreal-Ibero, A., et al. 2010b, A&A, 517, 28
- Montes, D., Martín, E.L., Fernández-Figueroa, M.J., Cornide, M., & de Castro, E.1997, A&AS, 123, 473
- Monteverde, M. I., et al. 2000, ApJ, 545, 813
- Montuori, M., et al. 2010, A&A, 518, 56
- Moustakas, J., et al. 2010, ApJS, 190, 233
- Mullis, C., et al. 2005, ApJ, 623, 85
- Muñoz-Mateos, J. C., et al. 2007, ApJ, 658, 1006
- Muñoz-Mateos, J. C., et al. 2009a, ApJ, 703, 1569
- Muñoz-Mateos, J. C., et al. 2009b, ApJ, 701, 1965
- Muñoz-Mateos, J. C., et al. 2011, ApJ, 731, 10
- Murphy, T.W., et al. 1996, AJ, 111, 1025
- Nagao, T., et al. 2006, A&A, 459, 85
- Najarro, F., 2001, ASPC, 233, 133
- Navarro, S.G., Corradi, R.L.M., & Mampaso, A., 2003, RMxAC, 18, 75
- Nomoto, K., et al. 2007, AIP Conf. Proc. 937, p. 412
- Noordermeer, E., et al. 2008, MNRAS, 388, 1381
- Norman, C., et al. 1996, ApJ, 462, 114
- O'Connell, R. W., et al. 1995, ApJ, 446, 1
- O'Dell, C. R., & Wong, K., 1996, AJ, 111, 846
- Overzier, R.A., et al. 2009, ApJ, 706, 203
- Pagel, B. E. J., et al. 1979, MNRAS, 189, 95
- Pagel, B. E. J., et al. 1980, MNRAS, 193, 219
- Pagel, B. E. J., & Edmunds, M. G., 1981, ARA&A, 19, 77
- Pedicelli, S., et al. 2009, A&A, 504, 81
- Peimbert, M., 1967, ApJ, 150, 825
- Peimbert, A., & Peimbert, M., 2010, ApJ, 724, 791
- Peimbert, M., & Peimbert, A., 2011, RmxAC, 39, 1



- Peimbert, M., et al. 1988, *ApL&C*, 26, 377
- Peimbert, M., et al. 1991, *PASP*, 103, 815
- Peimbert, M., et al. 1993, *ApJ*, 414, 626
- Peimbert, M., et al. 2007, *RMxAC*, 29, 72
- Peletier, R., et al. 2007, *MNRAS*, 379, 445
- Pérez-González, P. G., et al. 2005, *ApJ*, 630, 82
- Pérez-González, P. G., et al. 2008a, *ApJ*, 675, 234
- Pérez-González, P. G., et al. 2008b, *ApJ*, 687, 50
- Pérez-González, P. G., et al. 2010, *A&A*, 518, 15
- Pérez-Montero, E., & Díaz, A. I., 2003, *MNRAS*, 346, 105
- Pérez-Montero, E., & Díaz, A. I., 2005, *MNRAS*, 361, 1063
- Pettini, M., & Pagel B. E. J., 2004, *MNRAS*, 348, 59
- Pilyugin, L. S., 2001, *A&A*, 369, 594
- Pilyugin, L. S., Vílchez, J. M., & Contini, T., 2004, *A&A*, 425, 849
- Pohlen, M., & Trujillo, I., 2006, *A&A*, 454, 759
- Przybilla, N., Nieva, M. F., & Butler, K., 2008, *ApJ*, 688, L103
- Puls, J., et al. 2005, *A&A*, 435, 669
- Puls, J., et al. 2006, *A&A*, 454, 625
- Putman, M. E., et al. 2009, *ApJ*, 703, 1486
- Quadri, R., et al. 2008, *ApJ*, 685, 1
- Quider, A., et al. 2009, *MNRAS*, 398, 1263
- Reach, W. T., et al. 2009, *ApJ*, 690, 683
- Robertson, B., et al. 2006, *ApJ*, 645, 986
- Rodríguez-Muñoz, L., 2009, Astrophysics Master thesis, Universidad Complutense Madrid
- Rodríguez, M., & Delgado-Inglada, G., 2011a, *ApJ*, 733, L50
- Rodríguez, M., & Delgado-Inglada, G. 2011b, *IAU Symp. 283, Planetary Nebulae: an Eye to the Future*
- Rodríguez, M., & García-Rojas, J., 2010, *ApJ*, 708, 1551
- Rosales-Ortega, F. F., et al. 2011, *MNRAS*, 415, 2439
- Roskar, R., et al. 2008, *ApJ*, 684, 79
- Rose, J.A., 1994, *AJ*, 107, 206



- Rossa, J., & Dettmar, R. J., 2003, *A&A*, 406, 493
- Roy, J. R., & Walsh, J. R., 1997, *MNRAS*, 288, 715
- Rudnick, G., et al., 2003, *ApJ*, 599, 847
- Sabalisk, N. S. P., et al. 1995, *ApJ*, 444, 200
- Sahai, R., & Trauger, J. T., 1998, *AJ*, 116, 1357
- Sahai, R., Morris, M., Sánchez Contreras, C., & Claussen, M., 2007, *AJ*, 134, 2200
- Sahai, R., et al. 2011, *ApJ*, 740, 39
- Salimbeni, S., et al. 2009, *A&A*, 501, 865
- Samland, M., et al. 1996, *RvMA*, 9, 227
- Samland, M., & Gerhard, O. E., 2003, *A&A*, 399, 961
- Sánchez, S. F., et al. 2004, *ApJ*, 614, 586
- Sánchez, S. F., et al. 2005, *A&A*, 429, 21
- Sánchez, S. F., et al. 2006, *AN*, 327, 850
- Sánchez, S. F., et al. 2007a, *A&A*, 465, 207
- Sánchez, S. F., et al. 2012, *A&A*, 538, 8
- Sánchez-Blázquez, P., et al. 2006, *A&A*, 457, 809
- Sánchez-Blázquez, P., et al. 2009, *MNRAS*, 398, 591
- Sánchez-Blázquez, P., et al. 2010, *IAUS*, 262, 188
- Sánchez-Blázquez, P., et al. 2011, *MNRAS*, 415, 709
- Sánchez-Blázquez, P., et al. 2012, in prep.
- Sánchez Contreras, C., Bujarrabal, V., Miranda, L.F., & Fernández-Figueroa, M.J., 2000, *A&A*, 355, 1103
- Sánchez Contreras, C., & Sahai R., 2001, *Apel*, 553, 173
- Sánchez Contreras, C., Sahai, R., & Gil de Paz, A., 2002, *ApJ*, 389, 271
- Sánchez Contreras, C., Le Mignant, D., Sahai, R., Chaffee, F.H., & Morris, M., 2006, *IAUS*, 234, 71
- Sánchez Contreras, C., Sahai, R., Gil de Paz, A., and Goodrich R., 2008, *ApJS* 179, 166
- Sandage, A., 1971, *ApJ*, 166, 13
- Sanders, D. B., 2003, *JKAS*, 36, 149
- Santiago-Cortés, M., et al. 2010, *MNRAS*, 405, 1293
- Satyapal, S., Vega, D., Dudik, R. P., Abel, N. P. & Heckman, T., 2008, *ApJ*, 677, 926
- Scannapieco, E., et al. 2002, *ApJ*, 574, 590



- Scorza, C., & van den Bosch, F., C., 1998, MNRAS, 300, 469
- Scoville, N., et al. 2007, ApJS, 172, 1
- Sellwood, J. A., & Binney, J. J., 2002, MNRAS, 336, 785
- Sheth, K., et al. 2010, PASP, 122, 1397
- Shaver, P. A., et al. 1983, MNRAS, 204, 53
- Shaviv, N. J., & Dekel, A., 2003, arXiv:0305527
- Sheth, K., et al. 2010, PASP, 122, 1397
- Shi, F., et al. 2007, A&A, 475, 409
- Shields, G. A., Searle, L., 1978, ApJ, 222, 821
- Silich, S., et al. 2003, ApJ, 590, 791
- Silich, S., et al. 2004, ApJ, 610, 226
- Silich, S., et al. 2007, ApJ, 669, 952
- Silich, S., et al. 2010, ApJ, 711, 25
- Simon, J., et al. 2006, ApJ, 649, 709
- Simon-Díaz, S., et al. 2010, ApJ, 720, 174
- Skillman, E., et al. 1989, ApJ, 347, 875
- Smale, A., et al. 1997, ApJ, 483, 119
- Smith, H. E., 1975, ApJ, 199, 591
- Smith, H. E., et al. 2007, AJ, 134, 836
- Snedden, C., 1973, ApJ, 184, 839
- Snedden, C., et al. 2009, ApJS, 182, 80
- Soderblom, D.R., 2010, ARA&A, 48, 581
- Sommer-Larsen, J., et al. 2003, ApJ, 596, 47
- Sommer-Larsen, J., & Yoshii, Y., 1990, MNRAS, 243, 468
- Springel, F., et al. 2005, Nature, 435, 629
- Stasińska, G., Tenorio-Tagle, G., Rodríguez, M., & Henney, W. J., 2007, A&A, 471, 193
- Stauffer, J. R., et al. 1998, ApJ, 504, 805
- Stauffer, J. R., et al. 1999, ApJ, 527, 219
- Stoklasova, I., et al. 2009, A&A, 500, 1287
- Storey, P. J. 1994, A&A, 282, 999
- Takeuchi, T., et al. 2005, A&A, 440, 17



- Talent, D. L., et al. 1980, BAAS, 12, 866
- Tautvaisiene, G., et al. 2007, AJ, 134, 2318
- Taylor, V., et al. 2005, ApJ, 630, 784
- Tenorio-Tagle, G., 1996, AJ, 111, 1641
- Tenorio-Tagle, G., et al. 2003, ApJ, 597, 279
- Tenorio-Tagle, G., et al. 2005, ApJ, 620, 217
- Tenorio-Tagle, G., et al. 2005, ApJ, 628, 13
- Tenorio-Tagle, G., et al. 2007, ApJ, 658, 1196
- Tenorio-Tagle, G., et al. 2007, NewAR, 51, 125
- Tenorio-Tagle, G., et al. 2010, ApJ, 708, 1621
- Tenorio-Tagle, G., & Muñoz-Tuñón, C., 1997, ApJ, 478, 134
- Tenorio-Tagle, G., & Muñoz-Tuñón, C., 1998, ApJ, 293, 299
- Tikhonov, N. A., & Galazoutdinova, O. A., 2002, A&A, 394, 33
- Thomas, D., et al. 2005, ApJ, 621, 673
- Thuan, T. X., & Martin, G. E., 1981, ApJ, 247, 823
- Tomisaka, K., & Ikeuchi, S., 1988, ApJ, 330, 695
- Trager, S. C., et al. 2000, 119, 1645
- Tremonti, C., et al. 2004, ApJ, 613, 898
- Trott, C., et al. 2010, MNRAS, 401, 1540
- Trujillo, I., et al. 2004, ApJ, 604, 521
- Trujillo, I., et al. 2006, ApJ, 650, 18
- Tsamis, Y. G., & Péquignot, D., 2005, MNRAS, 364, 687
- Tsamis, Y. G., & Walsh, J. R., 2011, MNRAS, 417, 2072
- Tsamis, Y. G., et al. 2003, MNRAS, 338, 687
- Tsamis, Y. G., et al. 2003, MNRAS, 345, 186
- Tsamis, Y. G., et al. 2008, MNRAS, 386, 22
- Tsamis, Y. G., et al. 2011, MNRAS, 412, 1367
- Tutukov, A. V., & Fedorova, A. V., 2006, Astronomy Reports 50, 785
- U, V., et al. 2009, ApJ, 704, 1120
- Urbaneja, M. A., et al. 2005a, ApJ, 622, 862



- Urbaneja, M. A., et al. 2005b, ApJ, 635, 311
- Valdez-Gutiérrez, M., et al. 2001, A&A, 366, 35
- Valenti, J.A., & Fischer, D.A., 2005, ApJS, 159, 141
- van Breukelen, C., et al. 2006, MNRAS, 373, 26
- van den Bergh, S., 1975, ARA&A, 13, 217
- van den Bergh, S., 1977, ApJ, 215, 103
- van den Bergh, S., 1980, tsup.work, 11
- van Winckel, H., 2003, ARA&A, 41, 391
- Vanzella, E., et al. 2005, A&A, 434, 53
- Vanzella, E., et al. 2006, A&A, 454, 423
- Vazdekis, A., 1999, ApJ, 513, 224
- Veilleux, S., Cecil, G., & Bland-Hawthorn, J., 2005, ARA&A, 43, 769
- Verheijen, M. A. W., et al. 2004, AN, 325, 151
- Vila-Costas, M. B., & Edmunds, M. G., 1992, MNRAS, 259, 121
- Vilchez, J. M., & Esteban, C., 1996, MNRAS, 280, 720
- Vilchez, J. M., et al. 1988, MNRAS, 235, 633
- Vilchez, J. M., & Iglesias-Páramo, J., 1998, ApJ, 508, 248
- Vink, J., & de Koter, A., 2002, A&A, 393, 543
- Vlajic, M., et al. 2009, ApJ, 697, 361
- Vorobyov, E. I., 2006, MNRAS, 370, 1046
- Walborn, N. R., et al. 2002, AJ, 124, 1601
- Weaver, R., et al. 1977, ApJ, 218, 377
- Westfall, K., et al. 2007, in Formation and Evolution of Galaxy Disks, ASP Conference Series, Vol. 396, p.41
- Whittet, D. C. B., 2010, ApJ, 710, 1009
- Williams, B., et al. 2009, AJ, 137, 419
- Wilson, T. L., et al. 2008, ApJ, 698, 1943
- Wirth, G. D., et al. 2004, AJ, 127, 3121
- Wolf, C., et al. 2005, ApJ, 630, 771
- Woosley, S. E., & Bloom, J. S., 2006, ARA&A, 44, 507
- Woosley, S. E., et al. 2002, Reviews of Modern Physics, 74, 1015



- Worthey, G., et al. 1994, ApJS, 94, 687
- Wu, X., et al. 2007, AJ, 133.1560
- Wunsch, R., et al. 2008, ApJ, 683, 683
- Wyithe, S., and Loeb, A., 2006, Nature, 441, 332
- Yin, S. Y., et al. 2007, A&A, 462, 535
- Yoachim, P., 2010, ApJ, 716, 4
- Young, L. M., et al. 2007, ApJ, 659, 331
- Zahid, H. J., & Bresolin, F., 2011, ApJ, 730, 137
- Zapatero Osorio, M. R., et al. 2000, Science, 290, 103
- Zaritsky, D., et al. 1989, AJ, 97, 97
- Zaritsky, D., et al. 1994, ApJ, 420, 87
- Zhang, Y., et al., 2005, A&A, 442, 249
- Zhu, G., et al 2009, ApJ ,701, 86